University of South-Eastern Norway

Changhun Jeong

Model Predictive Control for Energy Systems under Uncertainty

Dissertation for the degree of Ph.D
Process, Energy and Automation Engineering

Faculty of Technology, Natural Sciences and Maritime Studies

University of
South-Eastern Norway

Changhun Jeong

Model Predictive Control for Energy Systems under Uncertainty

A PhD dissertation in
Process, Energy and Automation Engineering

Faculty of Technology, Natural Sciences and Maritime Studies
University of South-Eastern Norway
Porsgrunn

Doctoral dissertations at the University of South-Eastern Norway no. 201

ISSN: 2535-5244 (print)
ISSN: 2535-5252 (online)

ISBN: 978-82-7206-872-0 (print)
ISBN: 978-82-7206-873-7 (online)

Print: University of South-Eastern Norway

Preface

This thesis is submitted to the University of South-Eastern Norway (USN) in partial fulfilment of the requirements of the degree of Philosophiae Doctor (PhD) in the Process, Energy and Automation Engineering program. The PhD project work has been conducted under the supervision of Associate Professor Roshan Sharma, with co-supervision by Professor Nils-Olav Skeie.

The thesis consists of seven scientific papers, four journal papers and three conference paper. The thesis is divided in two main parts. The first part presents the background and research objectives, an extensive literature review and some additional notes on the case studies. Further, a summary of relevant methods and a summary of the seven scientific papers is given. Finally, The work is concluded with some observations of what has been achieved towards the research objectives

Porsgrunn, 7th December 2023

Changhun Jeong

Contents

List of Figures

List of Tables

Nomenclature

Symbol	Explanation
APC	Advanced Process Control
BEMS	Building Energy Management System
DCS	Distributed Control System
DMC	Dynamic Matrix Control
DP	Dynamic Programming
GPC	Generalized Predictive Control
LP	Linear Programming
MPC	Model Predictive Control
NLP	Nonlinear Programming
NVE	The Norwegian Water Resources and Energy Directorate
OCP	Optimal Control Problem
PI control	Proportional-Integral control
PID control	Proportional-Integral-Derivative control
RTO	Real-Time Optimization

Part I

1 Introduction

1.1 Background

As human societies expand in size, affluence, and population, the demand for energy to sustain these developments increases proportionally [1]. Since the 1800s, there has been a substantial global population increase, approximately sevenfold, and a fourfold rise in per capita energy consumption. Consequently, global energy consumption has surged by a factor of 28. This surge can be primarily attributed to the widespread utilization of fossil fuels [2]. Notably, the growth rate of global energy consumption has remained consistent since 1850, hovering at approximately 2.4% annually with a deviation of only 0.08% [3].

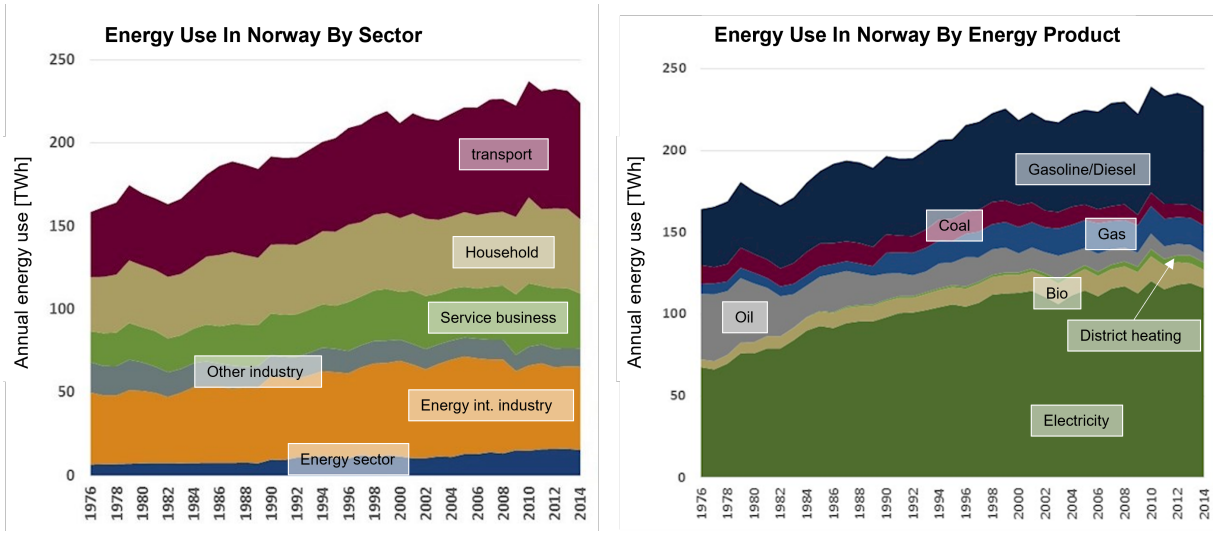

Figure 1.1: Energy consumption by sectors in mainland Norway[left] and Energy consumption by-products in mainland Norway[right][4]

This trend is not unique to the global stage; Norway also faces escalating energy consumption challenges, as indicated by a report from The Norwegian Water Resources and Energy Directorate (NVE) [4]. Over the span of 1976 to 2014, the total annual domestic energy consumption in Norway escalated by 40%. Electricity, as portrayed in Figure 1.1 [right], stands as the predominant energy product in Norway, exhibiting consistent growth. According to NVE's projections, this growth trajectory is set to persist due to factors like

expanding heating systems, increased electric vehicle adoption, and population growth [5].

To solve the emerging energy challenges in the future, both generation and consumption systems must be operated optimally by generating energy on demand and consuming the minimum possible energy.

Norway is known for abundant hydropower resources [6]. Hydropower is considered a mature and alluring green technology that generates electricity by utilizing the energy differentials from elevated to lower altitudes [7]. While various renewable sources like wind and solar energy are contingent on weather conditions for passive power generation, hydropower boasts distinct advantages: flood prevention and energy security. Empowered by reservoirs, hydropower stations flexibly produce electricity as long as water reservoirs hold, thus compensating for peak demand [8], [9]. Consequently, hydropower plays a pivotal role in the transition towards sustainability. In 2019, global hydropower capacity constituted 55.6% of global renewable energy capacity, with a remarkable 18.3% of global generation capacity [10], [11].

Despite its allure and popularity, operating hydropower systems is difficult due to strict regulations aimed at safeguarding surrounding ecosystems. Operational lapses, such as sudden water discharge from dams, can trigger destructive floods [12]. Consequently, regulations mandate consistent flow rates throughout watercourses and impose constraints like downstream minimum flow rates and seasonal reservoir water level fluctuations [13]. Furthermore, uncertainties in the system compound operational complexities, including inflow fluctuations, power production planning, and measurement errors [14].

Not only considering the generation of the electricity in the greener way but also the consumption of the energy must be reduced. The global energy landscape spotlights commercial and residential buildings as contributors to nearly 30% of total energy consumption, primarily attributed to heating and cooling needs [15]. Also, as illustrated in Figure 1.1 [left], a large portion of the energy is consumed in households in Norway. Despite the advances in construction techniques and insulations, the rate of building renovations remains low due to the investment cost and construction time. For example, the annual renewal in France is estimated at around 1% [16].

Here, without much investment or replacement of the equipment or materials, process control technology emerges as a potential immediate and effective solution to future energy challenges by generating energy more efficiently from hydropower and minimizing the energy consumption in building heating. Process control technology offers the means to optimize electricity generation given existing resources and enhance energy efficiency for heating living areas. Initially devised to streamline manufacturing processes by adhering to quality standards and environmental regulations while minimizing resource and energy usage, process control technology has evolved in tandem with advancements in computer technology [17].

These advancements have paved the way for intricate control algorithms, including optimal, adaptive, fuzzy, ratio, and feed-forward control algorithms. Moreover, the combination of hardware and software has established the foundation of Advanced Process Control (APC), which can solve complex multivariable control problems and mixed integer-discrete control problems, exemplified by Model Predictive Control (MPC) and distributed control systems (DCS). APC offers multifaceted benefits such as energy conservation, reduced resource consumption, time savings, cost reduction, and enhanced competitiveness in terms of both quality and costs [17].

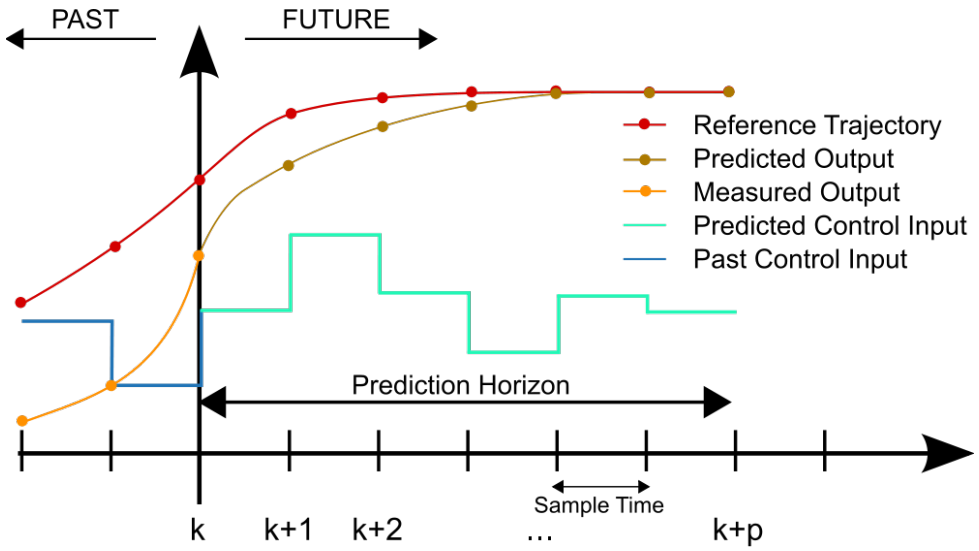

Figure 1.2: Model Predictive Control Scheme [18]

MPC, in particular, has gained attention across industries and research domains due to its capacity to manage control and state constraints in multi-input, multiple-output systems [19]. The core idea behind MPC is straightforward: it leverages a dynamic model to predict system behavior, solving an optimal control problem (OCP) to derive an optimal control sequence based on the projected system behavior. Subsequently, the first control input from this sequence is applied to the system. This process repeats at every time step [20], [21]. Figure 1.2 illustrates this MPC process, where predicted control inputs are optimized over a prediction horizon to steer the system towards a reference trajectory.

However, while MPC stands as an appealing control strategy, the presence of uncertainties in the system, such as model mismatch or exogenous disturbances, can undermine optimal operation and constraint robustness [22], [23]. To address these challenges within the MPC framework, researchers have introduced robust and stochastic MPC frameworks [24].

1.2 Research Objectives and Scope

This thesis undertakes the utilization and simulation of MPC frameworks across three case studies, accounting for the presence of uncertainties. These case studies hold significant implications for addressing energy challenges:

1. **Dalsfoss Hydropower System:** Operated by Skagerak Kraft AS in Telemark, Norway, the Dalsfoss hydropower system is a crucial contributor to energy production. The Dalsfoss hydropower station utilizes the reservoir. Implementing MPC in the systems can enhance their efficiency and performance. By considering disturbances such as the amount of water inflow forecast, this thesis explores how MPC can ensure optimal utilization of the water resource at the system, even amidst seasonally varying operational conditions and complex concession requirements.
2. **Hjartdøla Hydropower System:** The Hjartdøla hydropower system is also operated by Skagerak Kraft AS in Telemark, Norway. The Hjartdøla hydropower plant is operated intermittently. To make the water flow at downstream as constant as possible, the Hjartsdøla hydropower system includes a buffer reservoir, Hjartsjå. Considering the uncertain water inflow forecast from four different rivers, this thesis suggests an MPC framework that can control the system efficiently while adhering to the operational requirements such as the water level at the reservoir and minimum flowrates at downstream.
3. **Building Temperature Control System:** Heating systems in buildings are notorious energy consumers. Applying MPC to manage temperature inside a building can offer potential energy savings without compromising occupants' comfort. The thesis delves into the intricacies of this case study to demonstrate how MPC can optimize energy consumption while maintaining a conducive indoor environment, by considering uncertainties in the system parameters and the weather forecast.

Through these case studies, the thesis aims to investigate the efficacy of MPC frameworks under the presence of uncertainty, shedding light on their potential use as tools to tackle energy challenges. To achieve this overarching goal, the research pursues the following specific objectives:

1. **Formulation of Optimal Control Problems for Enhanced System Operation:** Previous research, such as the work conducted on the Dalsfoss hydropower plant system [14], [25], focused on applying MPC to maintain water levels within a moderate range for constraint satisfaction. However, recognizing the value of maximizing water levels as a resource for electricity generation, this study presents a new OCP formulation, for the Dalsfoss hydropower plant system, that aims to maximize the water level while still satisfying all the operational constraints. Also, the new OCPs for the Hjartdøla hydropower system and the building temperature control system are formulated.

2. **Implementation of Robust MPC Frameworks for Uncertain Systems:** After establishing the OCPs for three case studies, a series of simulations assess the performance of various MPC frameworks. These include deterministic (nominal) MPC, multistage MPC, and chance-constrained MPC. Through open-loop robustness analysis, the simulations expose potential constraint violations when deterministic MPC is used and illustrate how the existing MPC frameworks handle these uncertainties.

3. **Development of Novel Methods and MPC Frameworks:** While the multistage and chance-constrained MPC frameworks offer enhanced robustness in the presence of uncertainties, their application faces challenges such as computational demands or inadequate robustness. To address these limitations, novel techniques or entirely new MPC frameworks are imperative.

PAPER	CASESTUDY	OBJECTIVES		
		1 Formulation Of OCP	2 Existing Methods	3 Novel Methods
A	Dalsfoss	OCP, DMPC, RA		
B	Dalsfoss		MSMPC, RA	
C	Dalsfoss		MSMPC, Simple, RA	
D	Hjartdøla	OCP, DMPC, MSMPC, Simple, RA		
E	Hjartdøla		MSMPC, SSMPC, RA	
F	Dalsfoss		MSMPC, SSMPC, Simple, RA	
G	Building	OCP, DMPC, MSMPC, CCMPC, HMPC		

OCP: Formulation of optimal control problem, DMPC: Deterministic(nominal) MPC,
RA: Open-loop robustness analysis, MSMPC: Multistage MPC, Simple:Simplified Method,
SSMPC: Seqeuntial Stochastic MPC, CCMPC: Chance-constrained MPC, HMPC: Hybrid MPC
___ : newly suggested methods in this thesis work

Figure 1.3: Research scopes by papers

To accomplish these objectives across the three distinct case studies, this research is presented through a series of seven papers. The research scope is visually illustrated in Figure 1.3. The scope of the research can be summarized as follows:

Case Study 1: Dalsfoss Hydropower Station System

- Paper A: Reformulation of the OCP for the Dalsfoss system, deterministic MPC simulation, and open-loop robustness analysis.
- Paper B: Simulation of nominal MPC and multistage MPC for the Dalsfoss system. Comparative analysis demonstrates the advantages of the multistage MPC framework.
- Paper C: Introduction of the simplified method that reduces the size of OCP for the practical implementation of multistage MPC in the Dalsfoss system.
- Paper F: Introduction of sequential stochastic MPC combined with the simplified method for the further acceleration of the computational speed.

Case Study 2: Hjartdøla Hydropower System

- Paper D: OCP formulation for the Hjartdøla system, multistage MPC simulation with the simplified method, and verification of the method's effectiveness.
- Paper E: Implementation of sequential stochastic MPC for the Hjartdøla system, emphasizing computational efficiency and feasibility.

Case Study 3: Building Temperature Control System

- Paper G: OCP formulation for the building temperature control system, deterministic MPC, multistage MPC, and chance-constrained MPC simulations, and the proposal of a hybrid MPC framework.

The intricate web of research endeavors encapsulated within these papers ultimately contributes to a comprehensive understanding of the potential and limitations of MPC frameworks in the context of energy systems facing uncertainties. Through these contributions, the thesis not only enhances the theoretical underpinnings of MPC strategies but also offers practical insights into addressing energy challenges.

1.3 Contributions

This thesis serves as an invaluable resource by providing a comprehensive understanding of and practical strategies within the domain of Model Predictive Control (MPC) frameworks. These frameworks hold the potential to improve energy production and usage by offering enhanced efficiency. This is of paramount significance, especially in the context of Norway, where hydropower systems constitute a cornerstone of the nation's electricity generation. Additionally, the heightened energy demand for building heating during the extended cold winter months adds further impetus to the need for refined energy control strategies.

Notably, as of 2021, Norway operates a staggering 1681 domestic hydropower plants with approximately 1000 hydropower storage reservoirs, contributing to a production of 136.4 TWh of electricity. This substantial output translates to an impressive 90% of the country's total power generation. The intricate interplay of water inflow and installed capacity underscores the operational dynamics of hydropower stations. Yet, the inherent uncertainty in water inflow, varying both seasonally and annually, poses a challenge. A robust control system capable of navigating this uncertainty and effectively regulating water inflow into reservoirs is a necessity in this context [5].

Norway's energy landscape extends beyond its dominant hydropower presence; the country boasts an extensively electrified heating sector, with individual electric heating accounting for 63% of total heating demand. The result is a heightened demand for electricity during the harsh winter months. This demand surge could potentially strain both generation capacity and hydropower reservoir contents, which tend to be lowest during winter. As a result, the need for a cost-effective and smart control system for building temperature management becomes apparent.

This thesis makes significant contributions through three illuminating case studies, each addressing key challenges:

- **Hydropower Reservoir Control:** With two case studies, this work delves into the control of water levels under uncertain water inflow conditions. One case focuses on reservoir water level control for optimized power production, while the other centers on regulating a buffer reservoir to maintain steady downstream water flowrates post-turbine operation.

- **Building Temperature Control System:** Employing a grey-box modeling approach, this thesis presents a case study for building temperature control. The method's adaptability renders it suitable for various building types, offering a customized and efficient control solution.

The novel solutions to the challenges are introduced, such as the simplified method to multistage MPC, sequential stochastic MPC, and hybrid MPC. The suggested solutions to the uncertainties in the systems ensured faster computational time without degrading the performance compared to the other existing methods.

While this thesis showcases three case studies, the underlying methodologies and principles are poised to find application in a broader spectrum of contexts. The strategies proposed herein possess the potential to not only maximize profits but also minimize costs in diverse settings under uncertainty. The presented research thus lays the foundation for a more sustainable and efficient energy landscape, contributing significantly to the advancement of energy control systems.

1.4 Outline of Thesis

This research has produced seven self-contained, peer-reviewed scientific papers. Part I of this dissertation, titled 'Synopsis,' forms a unified framework that ties together these individual papers. Through six chapters, this framework clarifies how each paper addresses research questions and contributes to our primary objective.

Chapter 1 provides a succinct background to our research, underscoring the vital role of optimization in hydropower systems and building temperature control systems. Here, the research objectives and scope are defined to help readers grasp the study's boundaries. Additionally, the challenges and the distinct contributions of the research are outlined, providing readers with a clear roadmap for exploration.

In **Chapter 2**, an extensive literature review explores various approaches to addressing uncertainty in optimization problems, including robust and stochastic optimization methods. Furthermore, prior research within the domains of hydropower and building temperature control systems is covered.

Chapter 3 addresses the process description and mathematical models of two hydropower systems operated by Skagerak Kraft AS, along with the building system for temperature control. Associated mathematical models are presented, along with the introduction of operational requirements and descriptions of uncertainty within each case study.

Chapter 4 forms the theoretical foundation of the thesis, elucidating both established methods and unique contributions made during the research, ranging from open-loop optimal control to various robust and stochastic techniques.

Chapter 5 provides a summary of the research papers generated throughout the journey. The motivations, results, and conclusions of each paper are encapsulated, offering a concise yet informative overview of academic contributions and the development of research over the past three years.

Concluding the Synopsis, **Chapter 6** offers a final assessment of the findings and their implications. This chapter also looks forward, outlining potential directions for future research in the domain of optimizing hydropower and building temperature control systems amid prevailing uncertainties.

Part II, titled 'Scientific Papers,' comprises the complete research papers, forming the core of this thesis.

2 Literature Review

2.1 Process control

A complex control system can encompass a multitude of measurements and control loops, often numbering in the thousands. In practical implementation, such intricate systems are logically partitioned into distinct layers, organized by their respective time scales. This hierarchical structure, depicted in Figure 2.1, entails:

- **Scheduling (weeks):** Long-term planning that establishes the overall strategy and operational goals.
- **Site-wide optimization (day):** Optimizing large-scale operational decisions within a daily timeframe.
- **Local optimization (hour):** Focusing on finer-grained optimization within hourly intervals.
- **Supervisory (Predictive, advanced) control (minutes):** Employing advanced control strategies to guide the process within minute-scale intervals.
- **Regulatory control (seconds):** Ensuring rapid and precise adjustments to maintain stability and performance at the second-scale level.

In the domain of process control, the primary focus often centers on the lower three tiers of this hierarchy. The local optimization layer harnesses real-time optimization (RTO), where a defined metric, typically related to operating profit or cost, is optimized using up-to-date steady-state process models. These models are then used to determine optimal process set points. These set-points guide the feedback process control systems in the lower layers (i.e., supervisory and regulatory control), manipulating the process inputs to steer the system towards the optimized states [26].

While pursuing the objectives mentioned earlier, process control also grapples with disturbance rejection and the pursuit of an optimal trajectory for process dynamics. The supervisory control layer is the domain of advanced control algorithms, which accommodate process constraints, variable couplings, and unit interactions. Within this layer, model predictive control (MPC), a strategy rooted in optimal control concepts, has gained widespread adoption in the process industry [26].

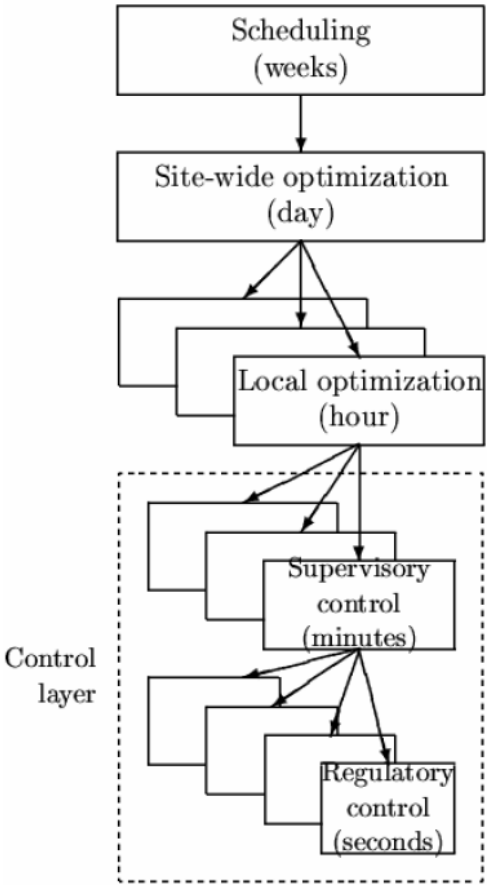

Figure 2.1: Typical control hierarchy in a complex system [26]

The regulatory control layer encompasses single-input single-output control loops, commonly exemplified by proportional-integral-derivative (PID) control. These loops work in tandem with the supervisory control layer to enact control actions that align with the directives set forth by higher layers [26], [27].

In the quest to seamlessly integrate economic process optimization with process control, as well as to harness the potential performance enhancements stemming from dynamic, transient, or time-varying operations, the concept of economic MPC has emerged. Economic MPC, based on general cost functions or performance indices, represents a synthesis of economic optimization and model-based control. This framework extends the traditional MPC paradigm, aligning the control strategy's objectives with broader economic goals [28]–[30].

2.2 Model Predictive control

The inception of Model Predictive Control (MPC) can be traced back to the 1960s, but it wasn't until the 1980s that significant interest ignited in this domain. The catalyst for this momentum was the publication of seminal works such as IDCOM [31], Dynamic Matrix Control (DMC) [32], and the comprehensive exposition of Generalized Predictive Control (GPC) [33], [34].

MPC has garnered significant attention in both academic and industrial circles, owing to its versatile framework capable of handling complex multiple-input, multiple-output systems with constraints [20], [21], [35].

MPC operates by optimizing the expected behavior of a dynamic system through the adjustment of its control inputs. This optimization relies on a predictive model of the process, making the choice of model a critical aspect of MPC design. While feedback mechanisms can mitigate some shortcomings in model quality, relying on a subpar model is akin to driving without headlights at night—feedback alone may prove insufficiently responsive [36].

In its early industrial applications, MPC predominantly employed models based on time-domain characteristics, input/output responses, and step or impulse responses [31], [32], [37]. This preference was partly due to the initial popularity of MPC in the process industries, where linear models offered clarity and ease of understanding. Furthermore, the abundant availability of linear systems theories, including linear quadratic regulator theory, Kalman filtering theory, and the internal model principle, made them readily applicable to MPC.

However, the integration of nonlinear models into MPC emerged as a pivotal advancement, driven by the potential for improved control performance through more accurate predictions. The inherent complexities of process control—such as conservation laws, momentum and energy considerations, phase equilibria, chemical kinetics, and product properties—all introduce nonlinearities into process descriptions [36].

MPC operates by repeatedly solving an online optimization problem to determine a control sequence that adheres to specified constraints. This approach is suitable for control applications where the optimal control problem can be resolved within a single sampling interval. The nominal stability of MPC, whether applied to linear or nonlinear systems with strict state and control constraints, can be achieved through the incorporation of terminal cost and constraints or by extending the horizon of the online optimization problem [20], [36], [38].

In practical MPC implementations, there are instances where no feasible solution exists to satisfy all constraints. Rather than declaring such situations as process exceptions, a common approach is to seek a solution that enforces some inequality constraints while relaxing others to ensure feasibility. Input constraints, often rooted in physical limitations

like valve saturation, must never be breached. In contrast, output constraints typically represent desired operational ranges that can be violated if necessary. To handle potential infeasibilities, output constraints are often treated as "soft" constraints in the MPC formulation. Several researchers have explored the formulation of output constraints as soft constraints to enhance the practicality of MPC [39]–[43].

2.3 Optimization under Uncertainty

While many aspects of nominal Model Predictive Control (MPC) have been thoroughly explored and understood, addressing the challenges posed by uncertainty remains a dynamic and active research frontier within MPC.

The presence of uncertainty, whether stemming from additive disturbances, state estimation errors, or model inaccuracies, presents a formidable challenge [36]. While nominal MPC inherently offers some degree of robustness due to its receding-horizon nature, its deterministic optimization formulation often falls short in effectively handling uncertainties, resulting in suboptimal performance [44], [45].

In response to this challenge, two pivotal MPC paradigms have emerged: Robust MPC and Stochastic MPC [24]. Robust MPC assumes known or bounded uncertainty and aims to ensure that system state and control constraints are satisfied for all possible realizations of this uncertainty. One notable approach within robust MPC is Min-Max MPC, which computes a control sequence that counteracts the worst-case scenario of uncertainty, often leading to conservative control inputs [46]. Multistage MPC evolved as a refinement of Min-Max MPC, incorporating a discrete-time scenario tree to capture the evolving nature of uncertainty. It computes multiple control trajectories across the scenario tree, effectively mitigating conservatism while maintaining constraint satisfaction [38], [47]. Multistage MPC has demonstrated its effectiveness across diverse domains, including chemical processes, autonomous vehicles, energy systems, and building climate control [47]–[52].

Conversely, when uncertainty follows a known probability distribution, it is more aptly described by probabilistic constraints. Stochastic MPC, in this context, ensures the satisfaction of such probabilistic constraints alongside any hard constraints, while concurrently stabilizing the system by driving the state toward a designated steady-state set [53]. Stochastic MPC has found wide-ranging applications in building climate control, power generation, chemical processes, and vehicle path planning [54]–[60], showcasing its adaptability in addressing uncertainty-related challenges across various fields.

Despite the successes of robust MPC and stochastic MPC, they face practical limitations. For example, multistage MPC, while promising, encounters challenges in industrial implementation due to the exponential growth in the size of the optimal control problem (OCP).

This growth is driven by factors such as the number of uncertain parameters or disturbances, the count of potential uncertainty realizations, and the length of the prediction horizon. Consequently, solving the OCP within reasonable time frames becomes computationally demanding, restricting its practical utility in industrial applications [47].

To tackle these challenges, various methods have been proposed to enhance the computational efficiency of multistage MPC. These include techniques like the robust horizon method [47], the primal decomposition algorithm [61], the adaptive horizon multistage MPC framework [62], and tube-enhanced multistage MPC [63]. These approaches strive to strike a balance between computational efficiency and control performance, rendering multistage MPC more practical and applicable in real-world industrial settings.

2.4 Control Strategies in Hydropower

Various control strategies, spanning from proportional-integral (PI) control to heuristic, predictive, and optimal controls, have been proposed for water system management [64]–[66]. The intricate nature of hydropower operation has spurred interest in optimization tools for practical application, given their capacity to solve high-dimensional problems. Reservoir operation models, aided by optimization techniques like linear programming (LP) and dynamic programming (DP), have demonstrated efficacy [67]. Nonlinear programming (NLP) has been employed for optimizing California's reservoir operations to maximize monthly energy economic value [68]. Subsequently, nonlinear model predictive control (MPC) was integrated with Kalman Filtering, marginally mitigating reservoir water level deviations [69]. Acknowledging uncertainties, adaptive multi-MPC has been proposed to account for uncertain inflows [70], while a multi-objective constrained optimal control under stochastic MPC framework considers both normal and rare scenarios [71]. Also, many Advanced Process Control (APC) systems for controlling levels of reservoirs or tanks are presented [72]–[77]. In [72], the use of A nonlinear MPC with an extended Kalman filter for water-level control in reservoirs through floodgate manipulation is investigated through simulations. In [73], five distributed MPC schemes on a hydropower plant benchmark are tested by simulation works. It aims to coordinate several subsystems to generate energy according to the demand while satisfying water levels and flow requirements. In [74], generalized predictive control (GPC) is simulated for a multivariable model of a pumped-storage hydroelectric power station. Then, It shows the benefits of using APC compared with an existing PI controller. In [75], a method for achieving optimal hydraulic-level tracking is introduced. This method utilizes an inverse optimal controller designed to control power generation rates within a particular hydropower facility. Additionally, a neural network is incorporated into the system to assist in predicting and handling external disturbances. The effectiveness of this proposed approach is evaluated through simulations, where data obtained from the plant over an entire year of operation serves as a reference for tracking performance. In [76],

an approach utilizing Multi-Objective MPC is presented for the real-time management of a multi-reservoir system. This strategy integrates the non-dominated sorting genetic algorithm II, multi-criteria decision-making, and the receding horizon principle to address a real-time multi-objective reservoir operation challenge. The primary control objectives encompass minimizing deviations in reservoir storage, reducing flood risks downstream at a vulnerable location, and maximizing hydropower generation. The efficacy of the developed control system is evaluated through simulations. In [77], they suggest a nonlinear predictive control method for a hydropower system. The approach involves choosing a performance index with a terminal penalty function, and the effectiveness of the developed control strategy is evaluated through numerical experiments.

Skagerak Kraft AS and the University of South-eastern Norway (USN) sought to implement MPC in hydropower operations as The proficiency of MPC frameworks in hydropower system management has matured through research. Model identification and tuning were performed for the Grønvollfoss run-of-river power plant system. The model's efficacy was demonstrated through simulations using PI control with a Smith predictor and deterministic MPC, with MPC displaying superior performance [78], [79]. Noteworthy case studies, including the Dalsfos plant, have employed deterministic MPC [80]. Expanding the scope, stochastic MPC was explored, assessing real and assumed values through Gaussian noise addition [81]. The stochastic MPC approach was tested with multi-objective-based algorithms and its performance is compared to the deterministic MPC. This study showed the potential for the use of stochastic MPC [14].

This thesis includes more research on further optimizing the performance of MPC on hydropower systems and how to deal with uncertainty such as the forecast of the water inflows into the reservoir systems.

2.5 Building Temperature Control

The integration of model predictive control (MPC) into building energy management systems (BEMS) has been a dynamic field of research, marked by significant activity [82], [83]. This approach has been explored in regulating indoor temperatures using both active heating systems and passive solar blinds [54]. In [84], a comprehensive building model is developed for MPC implementation. Their four-month evaluation showcased substantial energy savings, reducing thermal energy consumption by 63% and HVAC electric energy consumption by 29%. These findings underscore the transformative potential that MPC integration holds for BEMS.

A reliable prediction model is essential to maximize the benefits of implementing MPC. Diverse modeling strategies have emerged to capture building thermal behaviors [85]. White-box modeling, rooted in mass and energy balances, uses differential equations

tailored to specific buildings [86]. However, this approach struggles with parameter identification for complex models. Black-box models, reliant on measurement data, offer high prediction accuracy but lack generalized applicability [87], [88].

A balanced approach, grey-box modeling, combines aspects of white-box and black-box methodologies [16]. Leveraging cognitive understanding and physical insights, grey-box models often utilize thermal network representations, exemplified by resistor-capacitor circuit models [89]. This approach capitalizes on reduced-order models, although its parameters represent combinations of multiple properties, necessitating parameter estimation from measured data [90].

Recent research in USN focused on parameter estimation for grey-box models in BEMS. The resultant models displayed low parameter dispersion, yielding close alignment with measurements. The developed models demonstrated deviations of approximately 0.5-1.5°C [91], [92].

it seemed evident that the synergy of MPC and grey-box modeling holds substantial promise for elevating HVAC efficiency within BEMS, illuminating a path towards energy-conscious building management. Therefore, in this work, the grey-box model is used for the simulation of MPC and how to deal with both the model errors and the forecast uncertainty in the future.

3 Mathematical Model and Process Description

3.1 Dalsfoss Hydropower system: The floodgate control

3.1.1 Process Description

The Kragerø watercourse is one of Skagerak Kraft AS's operational hubs for hydropower systems. It encompasses a series of five hydropower stations and a dam, positioned along the watercourse between Lake Tokke and the sea, as depicted in Figure 3.1. Among these stations, the Dalsfoss hydropower system is the uppermost one next to the Lake Toke [93]. The Dalsfoss system utilizes the water from Lake Toke's reservoir for power generation. The system has three turbines and two floodgates [94].

Figure 3.1: Overview of the Kragerø watercourse

To ensure the safe and environmentally friendly operation of the Dalsfoss system, Skagerak Kraft bears full responsibility. In this endeavor, strict compliance with regulations from the Norwegian Water Resource and Energy Administration (NVE) is essential to uphold a secure and eco-friendly operation. Notably, a set of these regulations pertains to environmental considerations, aiming to protect both local communities and the ecosystem. For example, a requirement within this regulatory framework concerns the maintenance of water levels at Merkebekk within specified bounds. These bounds, however, are not static and undergo seasonal fluctuations throughout the year [95].

Meeting the operational requirements consistently during operations poses a challenge due to the presence of uncertainties in the system. The uncertainties come from two primary sources. First, the power production plan, tailored to meet energy demands, introduces variability. Second, the inflow of water into the lake or dam, a critical factor, is subject to prediction. Skagerak Kraft develops the power production plan based on the future demand, electricity price, and so on. Concurrently, water inflow forecasts rely on a complex hydrological model and weather forecasts, culminating in the presentation of 50 potential future scenarios for the subsequent 13 days.

3.1.2 Mathematical Model

Figure 3.6 provides a visual representation of Lake Toke, offering insight into its two significant sections: the upper stream, known as Merkebekk, on the left-hand side, and the lower stream situated near the Dalsfoss dam on the right. Additionally, Figure 3.3 presents a simplified schematic of the floodgates at the Dalsfoss dam. In the context of the Dalsfoss hydropower system, the system states are h_1 and h_2, representing the water level height above a specified minimal low regulated level, denoted as $x_{\mathrm{LRV}}^{\mathrm{min}}$, at Merkebekk and Dalsfoss, respectively. The control inputs for the system are the gate opening height of floodgates, designated as h_{g}.

Within this system, as displayed in Figure 3.6, several key factors come into play:

- $\dot{V}_{\mathrm{i}}$ is the time-varying volumetric inflow into Lake Toke originating from its catchment area. This inflow is distributed between Merkebekk and Dalsfoss, as depicted in Figure 3.6. Skagerak Kraft employs a hydrological model, utilizing subscribed weather forecast information, to estimate $\dot{V}_{\mathrm{i}}$. It serves as an input disturbance in the system.
- Another significant disturbance is the power demand, denoted as W_{e}, which is scheduled by experts at Skagerak Kraft. This demand is used to compute the turbine flow rate, $\dot{V}_{\mathrm{t}}$, representing the requisite water flow rate for electricity generation. Notably, $\dot{V}_{\mathrm{t}}$ is subject to an operational limitation of $36\mathrm{m}^3/\mathrm{s}$.

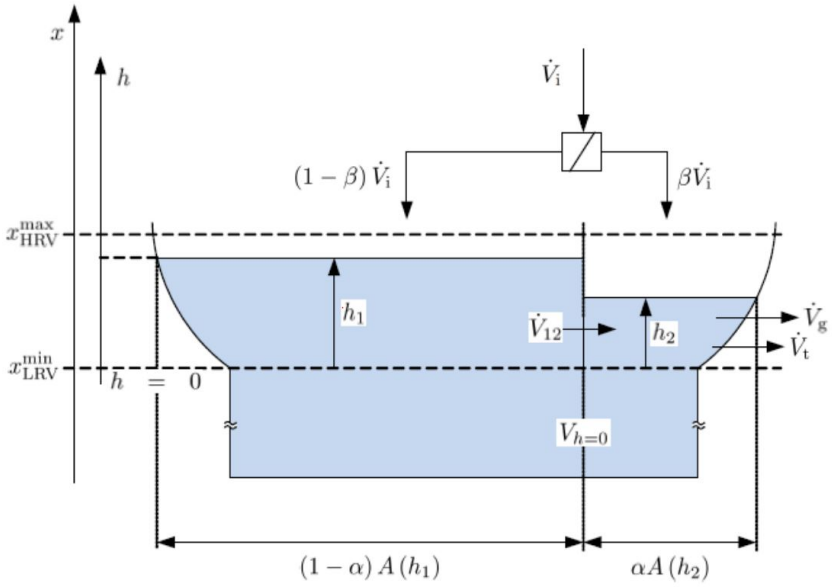

Figure 3.2: Schematic of lake Toke [25]

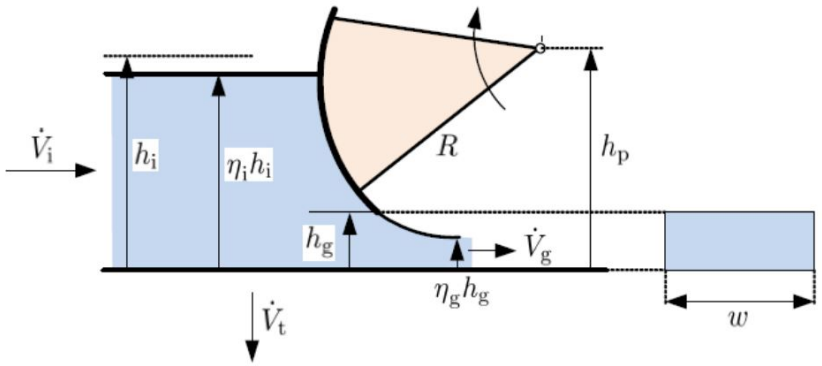

Figure 3.3: Structure of floodgate [25]

- $\dot{V}_g$ characterizes the flow rate through the floodgates. Water passing through these gates does not contribute to electrical power generation, as it bypasses the turbines and is merely released from the dam. Ideally, floodgate operations should prioritize keeping these gates closed to conserve water within the dam for energy production. Activation of floodgates is typically reserved for flood situations to fulfill regulatory requirements.

The model for Lake Toke has been initially developed and has subsequently undergone revisions, as suggested in related reports [25], [96]. A succinct summary of the model's key components and equations is provided below.

The heights of water level relative to sea level at Merkebekk and Dalsfoss denoted x_M and x_D, are given by:

$$x_{\mathrm{M}} = h_1 + x_{\mathrm{LRV}}^{\mathrm{min}} \tag{3.1}$$

$$x_{\mathrm{D}} = h_2 + x_{\mathrm{LRV}}^{\mathrm{min}} \tag{3.2}$$

The area of the surface curve at Lake Toke is calculated as:

$$A(h) = \max(28 \times 10^6 \cdot 1.1 \cdot h^{\frac{1}{10}}, 10^3) \tag{3.3}$$

Inter-compartment flow, $\dot{V}_{12}$, is expressed as:

$$\dot{V}_{12} = K_{12} \cdot (h_1 - h_2)\sqrt{|h_1 - h_2|} \tag{3.4}$$

where K_{12} is the inter-compartment flow coefficient.

The equation to calculate $\dot{V}_{\mathrm{t}}$ from the electrical power demand, W_{e}, is:

$$\dot{V}_{\mathrm{t}} = a\frac{\dot{W}_{\mathrm{e}}}{x_{\mathrm{D}} - x_{\mathrm{q}}} + b \tag{3.5}$$

where a and b are coefficients obtained from data fitting. x_{q} represents the downstream level after the turbine and can be obtained by solving the following cubic equation:

$$\begin{aligned} 0 = {} & c_1 x_{\mathrm{q}}^3 + (c_2 - c_1 x_{\mathrm{D}}) x_{\mathrm{q}}^2 \\ & + (c_3 - c_2 x_{\mathrm{D}} + c_4 \dot{V}_{\mathrm{g}}) x_{\mathrm{q}} \\ & + \dot{W}_{\mathrm{e}} - c_3 x_{\mathrm{D}} - c_4 \dot{V}_{\mathrm{g}} x_{\mathrm{D}} - c_5 \end{aligned} \tag{3.6}$$

where c_1, c_2, c_3, c_4, and c_5 are coefficients obtained from polynomial model fitting.

At the Dalsfoss power plant, there are two floodgates. The model for flow rate through floodgate j, $\dot{V}_{\mathrm{g},j}$, is given by:

$$\dot{V}_{\mathrm{g},j} = C_{\mathrm{d}} \cdot w_j \cdot \min(h_{\mathrm{g}}, h_2)\sqrt{2g \cdot \max(h_2, 0)} \tag{3.7}$$

where C_{d} is the discharge coefficient and g is the acceleration due to gravity.

The total water outflow from the Dalsfoss power station, $\dot{V}_{\mathrm{o}}$, is calculated as:

$$\dot{V}_{\mathrm{o}} = \dot{V}_{\mathrm{t}} + \sum^{j} \dot{V}_{\mathrm{g},j} \tag{3.8}$$

The dynamic models of the water levels, h_1 and h_2, are expressed as:

$$\frac{dh_1}{dt} = \frac{1}{(1-\alpha)A(h_1)}((1-\beta)\dot{V}_{\mathrm{i}} - \dot{V}_{12}) \tag{3.9}$$

$$\frac{dh_2}{dt} = \frac{1}{\alpha A(h_1)}(\beta \dot{V}_i + \dot{V}_{12} - \dot{V}_{\mathrm{t}} - \dot{V}_{\mathrm{g}}) \tag{3.10}$$

Parameters for the model are given in Table 3.3.

Table 3.1: Parameters for Lake Toke model

Parameter	Value	Unit	Comment
α	0.05	-	Fraction of surface area in compartment 2
β	0.02	-	Fraction of inflow to compartment 2
K_{12}	800	$\mathrm{m}^{\frac{3}{2}}/\mathrm{s}$	Inter compartment flow coefficient
C_{d}	0.7	-	Discharge coefficient, Dalsfoss gate
w_1	11.6	m	Width of Dalsfoss gate 1
w_2	11.0	m	Width of Dalsfoss gate 2
$x_{\mathrm{LRV}}^{\mathrm{min}}$	55.75	m MSL	Minimal low regulated level value
$x_{\mathrm{HRV}}^{\mathrm{max}}$	60.35	m MSL	Maximal high regulated level value
g	9.81	$\mathrm{m/s}^2$	Acceleration of gravity
a	124.69	Pa^{-1}	Coefficient in equation 3.5
b	3.161	m	Coefficient in equation 3.5
c_1	0.13152	$\mathrm{W/m}^{-3}$	Polynomial coefficient in equation 3.6
c_2	-9.5241	$\mathrm{W/m}^2$	Polynomial coefficient in equation **??**
c_3	$1.7234 \cdot 10^2$	W/m	Polynomial coefficient in equation 4.16a
c_4	$-7.7045 \cdot 10^{-3}$	Pa/m	Polynomial coefficient in equation 3.6
c_5	$-8.7359 \cdot 10^{-1}$	W	Polynomial coefficient in equation 3.6

3.1.3 Operational Requirements

The Dalsfoss hydropower plant operates under several requirements to ensure safe and efficient performance. These requirements include:

1. **The constant water flowrate:** Significant increases in water flow from the hydropower station can harm downstream ecosystems. To minimize these impacts, it is essential to maintain a relatively constant downstream flow rate ($\dot{V}_o$), especially during periods of high flow.
2. **Minimum downstream flowrate ($\dot{V}_o$):** To support the ecological balance of the watercourse and the movement of aquatic life, a minimum flow rate of $4\mathrm{m}^3/\mathrm{s}$ must be maintained downstream. This ensures that the watercourse remains viable and provides a suitable habitat for aquatic organisms.
3. **Water level regulation at Merkebekk:** The water level at the Merkebekk location, measured in meters above sea level (m MSL), must be kept within specific seasonal ranges defined by low regulated values (x_{LRV}) and high regulated values (x_{HRV}). These seasonal values are detailed in Table 3.2. The water level (x_{M}) at Merkebekk is calculated as the sum of h_1 and $x_{\mathrm{LRV}}^{\mathrm{min}}$.

Table 3.2: Seasonal level requirement

Date	x_{LRV}[m MSL]	x_{HRV}[m MSL]
Jan. 1 - Apr. 30	55.75	60.35
May. 1 - Aug. 30	58.10	59.85
Sept. 1 - Sept. 14	57.60	59.35
Sept. 15 - Oct. 27	55.75	59.35
Oct. 28 - Nov. 11	55.75	59.85
Nov. 12 - Dec. 31	55.75	60.35

4. **Maximum turbine flowrate ($\dot{V}_t$):** To ensure the safe and reliable operation of the turbine, the flow rate through it is capped at a maximum of $36\mathrm{m}^3/\mathrm{s}$. This limit prevents excessive stress on the equipment and guarantees its longevity.
5. **Floodgate opening height limitation:** The floodgate opening height is restricted to a maximum of $5.6\mathrm{m}$ for safety considerations. This limitation ensures that the floodgates can effectively control water flow without compromising their structural integrity or posing risks to personnel and infrastructure.

3.2 Hjartøla Hydropower system: The buffer reservoir control

3.2.1 Process Description

The Hjartdøla hydropower plant is also operated by Skagerak Kraft. It is located in Hjartdal municipality, Norway, as shown in Fig. 3.4. The Hjartdøla hydropower system, depicted in Fig. 3.5, consists of a buffer reservoir, Hjartsjå, which receives water from the

Hjartdøla hydropower plant and the Hjartsjå river. It subsequently releases this water downstream at Omnessfossen. The system also receives inflows from the Skorva, Skogsåa, and Mjella rivers.

Figure 3.4: Overview of the Hjartdola system

Unlike power plants that maintain relatively steady output levels, the Hjartdøla hydropower plant adapts its power production dramatically based on demand. This necessitates precise management of variations in discharged water flow rates to prevent adverse effects on downstream ecosystems [97].

The Hjartdøla system operates amidst various uncertainties, including fluctuations in power production and water inflows. Nevertheless, the system must adhere to stringent operational regulations, including the maintenance of water levels at Hjartsjå and controlled flow rates at both Hjartsjå and Omnessfossen. Downstream flow rates are managed through the manipulation of a floodgate at Hjartsjå. Water inflow predictions are generated using hydrological models and weather forecasts, providing 50 potential scenarios for the next 13 days (312 hours). Furthermore, the power production plan remains subject to changes influenced by factors such as electricity prices and demand [13].

Currently, the Hjartdøla system employs a manual PI controller with set point adjustments made by on-site personnel. However, this control approach is suboptimal due to its heavy reliance on human judgment and predictions of uncertainty, resulting in a high risk of constraint violations. Implementing Model Predictive Control (MPC) could enhance system performance and reduce risks. Specifically, Multistage MPC, which accounts for system uncertainties, may offer an even more robust control strategy, ensuring efficient and safe operation of the Hjartdøla hydropower plant.

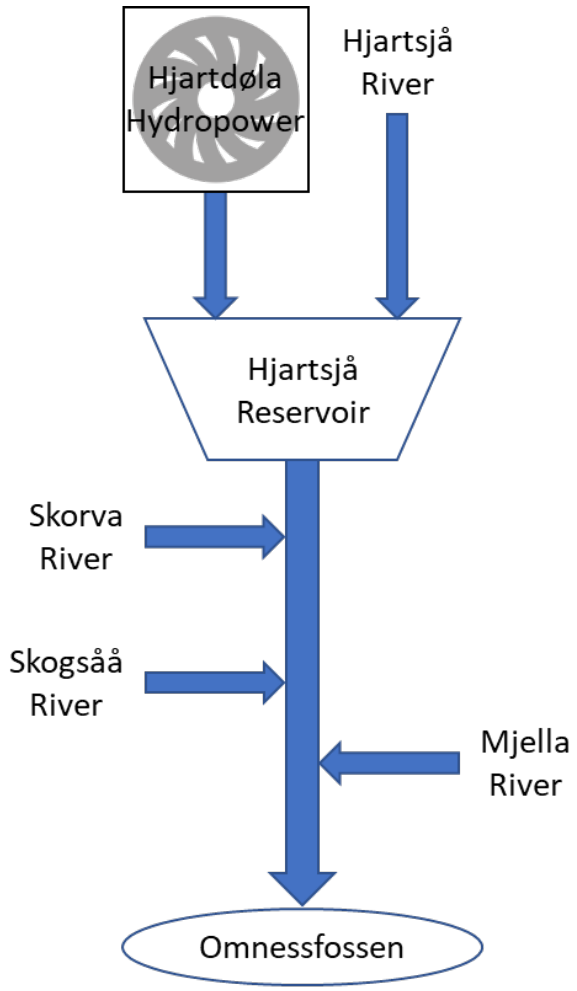

Figure 3.5: A simple plan showing the watercourses of the Hjartdøla hydropower system

3.2.2 Mathematical Model

The system state is denoted by the variable h, representing the water level in the reservoir relative to sea level. The control input is the opening of the floodgate, denoted as h_g. Figures 3.6 and 3.7 provide visual representations of the layout of the Hjartsjå reservoir and the structure of the floodgate at the reservoir, respectively. Water enters the reservoir from two sources: the Hjartsjå river, with a flow rate denoted as $\dot{V}_{i,H}$, and the turbines at the Hjartdøla hydropower plant, with a flow rate denoted as $\dot{V}_p$. The reservoir releases water through both a floodgate, represented by $\dot{V}_g$, and a flood threshold wall denoted as $\dot{V}_f$.

The water level in the reservoir, measured from its bottom and referred to as h_{in}, is described as follows:

Table 3.3: Parameters for Hjartdøla model

Parameter	Value	Unit	Comment
LRV	155.7	m MSL	Lower regulated value
HRV	157.5	m MSL	Higher regulated value
$h_{\text{in,max}}$	$HRV + 3 - LRV = 4.8$	m	Maximum water level of the reservoir
A_{min}	10^3	m^2	Minimum surface area of the reservoir
a	0.0474	-	Coefficient
b	1.6898	-	Coefficient
$h^{\text{msl}}_{\text{g,top}}$	157.37	m MSL	Top position of gate openning
L_1	12	m	Width of the gate
L_2	11	m	Width of the overflow channel
OFT^{msl}_1	157.5	m MSL	Overflow threshold 1
OFT^{msl}_2	158.5	m MSL	Overflow threshold 2

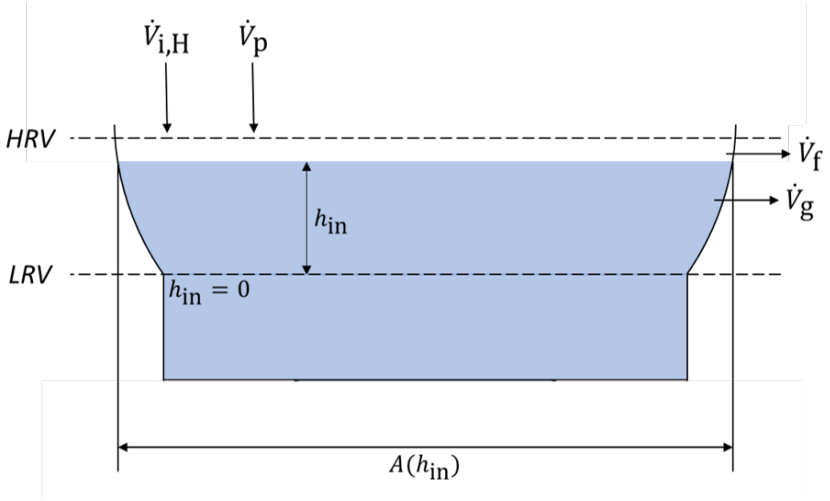

Figure 3.6: The simple layout of the Hjartsjå reservoir

$$h_{\text{in}} = \min(\max(0, h - LRV), h_{\text{in,max}}) \tag{3.11}$$

LRV is the low regulated value of the water level in the reservoir. The surface area of the reservoir is calculated as:

$$A = \max(A_{\text{min}}, 10^6 \cdot a \cdot b \cdot h_{\text{in}}^{(b-1)}) \tag{3.12}$$

The outflows from the reservoir are calculated as:

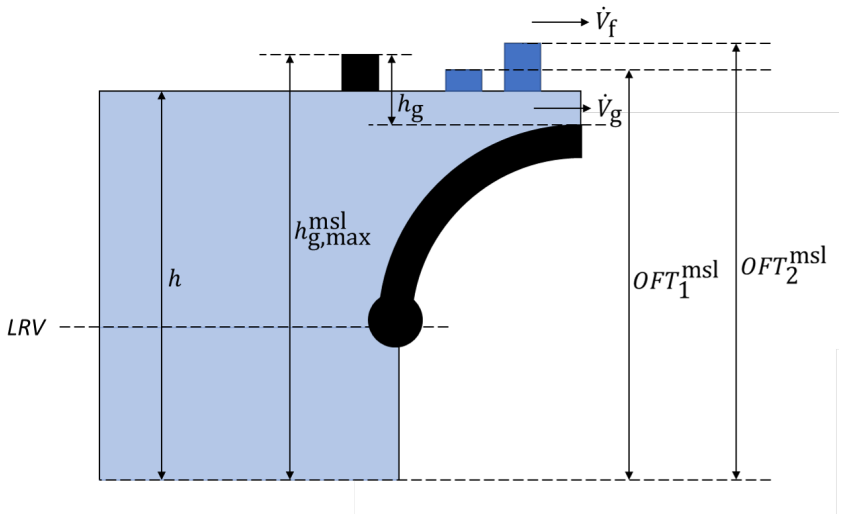

Figure 3.7: The simple layout of the floodgate at Hjartsjå reservoir

$$h_{out,g} = \max(0, h - (h_{g,top}^{msl} - h_g)) \tag{3.13}$$

where $h_{g,top}^{msl}$ and h_g denotes the top position of gate opening and the opening of the floodgate, respectively. The flowrate through floodgate, $\dot{V}_g$, is calculated as:

$$\dot{V}_g = 1.84 \cdot L_1 \cdot h_{out,g}^{1.5} \tag{3.14}$$

where L_1 represents the width of the gate. The flowrate through overflow channel, $\dot{V}_f$, can be expressed as:

$$\dot{V}_f = 1.8(L_1 \cdot h_{out,OF1}^{1.5} + L_2 \cdot h_{out,OF2}^{1.5}) \tag{3.15}$$

where $h_{out,OF1}$ and $h_{out,OF2}$ are calculated as followings:

$$h_{out,OF1} = \max(0, h - OFT_1^{msl}) \tag{3.16}$$

$$h_{out,OF2} = \max(0, h - OFT_2^{msl}) \tag{3.17}$$

where OFT_1^{msl} and OFT_2^{msl} mean the heights of the overflow thresholds. Therefore, the dynamic model of the reservoir is expressed as:

$$f = \frac{dh}{dt} = \frac{1}{A}(\dot{V}_{\mathrm{i,H}} + \dot{V}_{\mathrm{p}} - \dot{V}_{\mathrm{f}} - \dot{V}_{\mathrm{g}}) \tag{3.18}$$

The flowrate at downstream to Omnessfossen is:

$$\dot{V}_{\mathrm{O}} = \dot{V}_{\mathrm{g}} + \dot{V}_{\mathrm{f}} + \dot{V}_{\mathrm{i,SV}} + \dot{V}_{\mathrm{i,SS}} + \dot{V}_{\mathrm{i,M}} \tag{3.19}$$

$\dot{V}_{\mathrm{i,SV}}$, $\dot{V}_{\mathrm{i,SS}}$, and $\dot{V}_{\mathrm{i,M}}$ are flowrates of Skorva river, Skogsåa, and Mjella rivers, respectively. The parameters in the model are displayed in Table. 3.3.

3.2.3 Operational Requirements

The operational constraints governing the Hjartdøla reservoir system are imperative for ensuring operational safety and the protection of downstream ecosystems and habitats. These constraints encompass various facets, including but not limited to:

1. **Flowrate Stability at Downstream:** It is essential to maintain a consistent flowrate downstream to safeguard both fauna and human populations against abrupt alterations in flowrate or water level.
2. **Minimum Flowrates:** A minimum flowrate of 1.0 m^3/s must be maintained for water discharged from the Hjartsjå reservoir. A minimum flowrate of 2.5 m^3/s must be upheld at Omnessfossen (downstream) to facilitate the unimpeded movement of fish within the watercourse.
3. **Water Level Maintenance:** The water level within the Hjartsjå reservoir must be diligently managed within the boundaries defined by the High Regulated Value (HRV) and Low Regulated Value (LRV). This strict regulation is essential for preserving the ecological integrity of the surrounding ecosystem and habitat.

These operational requirements are instrumental in balancing the operational needs of the reservoir system with the imperative to protect and sustain the natural environment it interacts with.

3.3 Experimental building at USN: Temperature control

3.3.1 Process Description

The subject of this study is an experimental facility established in 2014 at the Porsgrunn campus of the University of South-eastern Norway [98]. Figure 3.8 illustrates both the

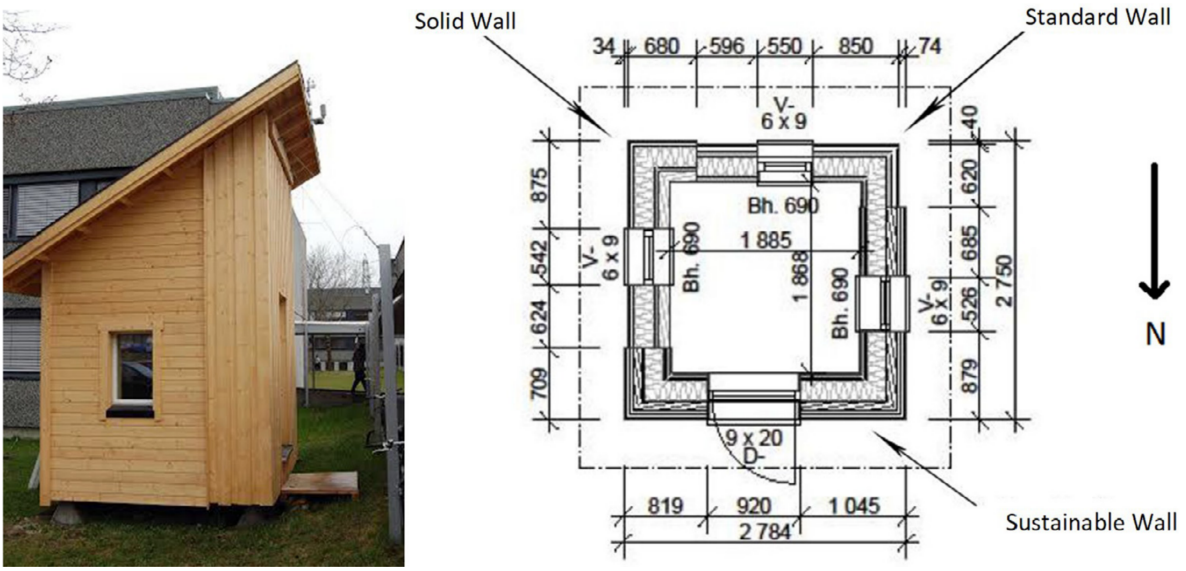

Figure 3.8: The picture of the experimental facility in USN [98]

exterior and floor plan of this test building. It has been meticulously designed with concrete support structures to ensure its separation from the ground. The internal volume of the building measures approximately 9.4 m^3, and it has been deliberately sealed, devoid of both natural and mechanical ventilation systems. To minimize solar radiation, three modestly-sized windows, each measuring 60 $\times$ 90 cm^2, have been strategically positioned in the south, east, and west orientations. Additionally, there is a door, measuring 90 $\times$ 120 cm^2, situated in the north direction. Furthermore, the presence of three adjacent buildings serves to further mitigate the penetration of solar radiation through the windows.

The building envelope has been constructed utilizing an amalgamation of diverse materials, including wooden cladding, glass wool, air-fill, polyethylene vapor barriers, wood, cement chipboard, particleboard, and cardboard. The composition of each type of wall is unique and is a result of the precise combination of these materials. Similarly, the roof and floor of the building also possess distinct compositions.

This experimental building incorporates an electrical heater with a power rating of 375 W. This heating system includes a thermostat controller, a comprehensive measurement system, and a logging computer that consumes approximately 100 W. The measurement system is equipped with a variety of sensors designed to monitor critical parameters such as indoor and outdoor temperatures, humidity levels, air pressures, rainfall, wind speed, wind direction, and the overall power consumption within the building.

In sum, the experimental building serves as a meticulously controlled environment, ideal for conducting in-depth studies and analyses of the thermal dynamics and energy performance of buildings across various operational conditions.

3.3.2 Mathematical Model

System Model

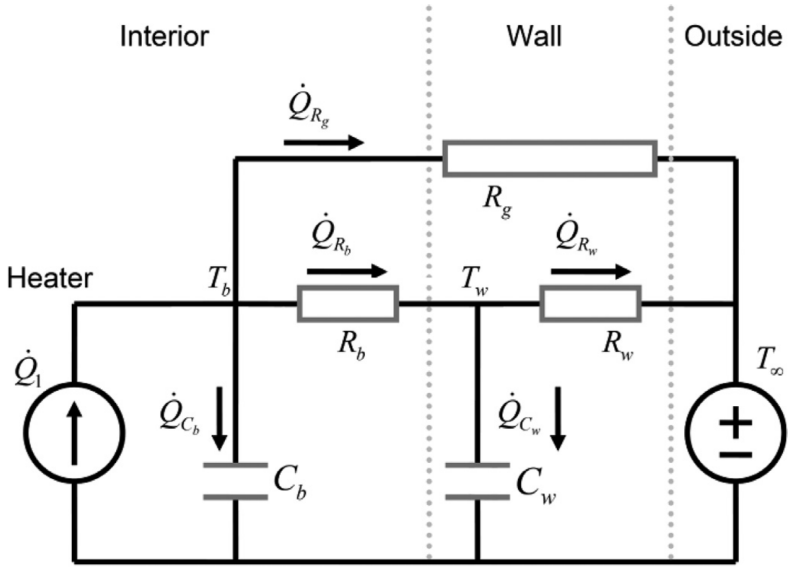

Figure 3.9: RC circuit model of the building [92]

The system model adopted in this study serves as a simplified representation of the experimental building and serves as the basis for obtaining calibration data. Illustrated in Figure 3.9, this model draws inspiration from the R3C2 model introduced in [16], albeit with the exclusion of the ventilation resistance component, as the test building lacks a ventilation system.

The model consists of two state variables, denoted as T_b and T_w, corresponding to the interior temperature of the building and the temperature of the inner surface of the walls, respectively. These state variables are associated with capacitors C_b and C_w, representing the thermal energy storage capacities within the building's interior and its envelope (including walls, floor, and ceiling). Additionally, the model incorporates three resistance components. R_b signifies the thermal resistance between the building's interior and its walls, while R_w represents the resistance to heat flow through the walls, linking state T_w with the external temperature. The third resistance, R_g, characterizes heat flow resistance through elements of the building envelope not encompassed by the state T_w, such as windows and the door. The driving forces of the system are represented by $\dot{Q}$ and T_∞, where $\dot{Q}$ denotes the heat flow source (e.g., an electric heater), and T_∞ models the external temperature as a potential influencing factor.

To derive equations from the thermal network model, Kirchhoff's node potential law is applied, wherein each state within the circuit, namely T_b and T_w, is assigned to a circuit

node, and the inflow and outflow of each node are meticulously balanced. The model is then formulated in state-space representation, comprising a set of ordinary differential equations (ODEs) [91], [92], [99].

$$\frac{dx}{dt} = Ax_t + Bu_t + w_t \tag{3.20}$$

where

$$x_t = \begin{bmatrix} T_\mathrm{b} \\ T_\mathrm{w} \end{bmatrix}, u_t = \begin{bmatrix} \dot{Q} \\ T_\infty \end{bmatrix}$$

$$A = \begin{bmatrix} -\frac{1}{C_\mathrm{b}R_\mathrm{b}} - \frac{1}{C_\mathrm{b}R_\mathrm{g}} & \frac{1}{C_\mathrm{b}R_\mathrm{b}} \\ \frac{1}{C_\mathrm{w}R_\mathrm{b}} & -\frac{1}{C_\mathrm{w}R_\mathrm{b}} - \frac{1}{C_\mathrm{w}R_\mathrm{w}} \end{bmatrix}$$

$$B = \begin{bmatrix} \frac{1}{C_\mathrm{b}} & \frac{1}{C_\mathrm{b}R_\mathrm{g}} \\ 0 & \frac{1}{C_\mathrm{w}R_\mathrm{w}} \end{bmatrix}$$

Parameter Estimation

The process of parameter estimation within the context of this construction project has been previously documented in references[91], [92]. Parameter estimation entails the crucial task of determining the precise values of model parameters based on empirical data. In the specific case examined in this study, the initial approximation for parameter estimation is achieved by establishing nominal parameter values. These nominal values are derived from a combination of empirical experimentation and prior knowledge about the expected parameter range. It is noteworthy that these nominal values are grounded in an approximate understanding of parameter magnitudes, typically attainable for most practical building scenarios. While the nominal values themselves may not serve as highly accurate predictive models for the building's behavior, they perform a pivotal role as normalization constants, thus facilitating parameter estimation on a standardized scale. Furthermore, these nominal values effectively narrow down the search space to a region of interest where reasonable parameter values can be more readily discerned [91], [92].

In Table 3.4, we present a comprehensive compilation of the nominal parameter values, ascertained through empirical measurements. These values are instrumental as initial approximations for the calibration of the model. Additionally, they delineate the minimum and maximum parameter boundaries, effectively constraining the parameter space [86].

The noise covariance matrix, denoted as $W = \mathbf{diag}(w_{\mathrm{b}}^2, w_{\mathrm{w}}^2)$, is meticulously estimated from empirical data and is assumed to possess a diagonal structure. The parameter vector, denoted as $\boldsymbol{\theta}$, is intricately defined to encompass the following components:

$$\boldsymbol{\theta} = [R_{\mathrm{g}}, R_{\mathrm{b}}, R_{\mathrm{w}}, C_{\mathrm{b}}, C_{\mathrm{w}}, w_{\mathrm{b}}, w_{\mathrm{w}}] \tag{3.21}$$

Table 3.4: Nominal parameter values and min./max. range.

	R_{g}[K/W]	R_{b}[K/W]	R_{w}[K/W]	C_{b}[J/W]	C_{w}[J/W]
Nominal value (θ_0)	0.160	0.060	0.100	1200k	1200k
Min value (θ_{min})	0.048	0.018	0.03	360k	360k
Max value (θ_{min})	0.272	0.102	0.170	2040k	2040k

To mitigate the risk of over-parameterization, particular attention is directed towards the parameter R_{g}, wherein its value is deliberately constrained to a constant. It is pivotal to acknowledge that R_{g} represents the thermal resistance exhibited by windows and doors, subject to the influence of both interior and exterior temperatures. Pertinently, the UA values associated with these components are meticulously specified in [86]. It is imperative to recognize that the UA values are rooted in the product of two fundamental components, namely U (denoting the reciprocal of thermal resistance per unit area) and A (indicating the surface area). Therefore, armed with knowledge about either the thermal resistance (R) or heat transfer coefficient (U) for all pertinent windows and doors, alongside their corresponding surface areas (A), it is conceivable to accurately compute R_{g} as $1/(U_{\mathrm{g}}A_{\mathrm{g}})$. Detailed specifications for U and A are explicitly elucidated in Table 3.5, with the value of R_{g} being definitively set at 0.24 [86], [92].

Table 3.5: Specification of R_{g}

	U[W/m^{2}K]	A[m^2]	UA [W/K]	R [K/W]
Door	1.2	1.76	2.1	0.48
Windows	1.3	1.57	2.0	0.50
Total	-	-	4.1	0.24

To elucidate, within the R3C2 model depicted in Figure 3.9, a prior probability distribution is judiciously assigned to the parameter R_{g}, characterized as $\mathcal{N}(0.24, 0.01^2)$. This is in contrast to all other parameters, which are endowed with uniform priors represented as $p(\boldsymbol{\theta}) = 1$. It is imperative to underline that these probability distributions play a pivotal role in the optimization procedures that hinge upon Equation (3.22) [91].

$$J = \sum_{i=1}^{N} \sum_{k=1}^{n_x} e_k^2 = \sum_{i=1}^{N} \sum_{k=1}^{n_x} (x_k^i - x_k^{i,ref})^2 \tag{3.22}$$

Table 3.6: Values and standard deviations of estimated parameters

	$\hat{\theta}$	$\sigma/\hat{\theta}$
R_g[K/W]	0.236	6.0%
R_b[K/W]	0.072	5.7%
R_w[K/W]	0.084	5.7%
C_b[J/W]	1444k	4.7%
C_w[J/W]	293k	8.8%
w_b	0.149	3.2%
w_w	0.137	3.7%

Table 3.6 meticulously tabulate both the estimated parameter values and their corresponding standard deviations. The estimation of the posterior distribution for the parameters is adeptly achieved through the utilization of the Markov Chain Monte Carlo (MCMC) methodology. Data from the experimental building are employed comprehensively, encompassing temperature measurements (T_b, T_w, T_∞), in conjunction with measurements of the input electrical power ($\dot{Q}$) supplied to an electric heater. It is noteworthy that the temperatures T_b and T_w are deemed as reference data for the model outputs, whereas T_∞ and $\dot{Q}$ assume the role of model inputs. It is imperative to highlight that two sets of the acquired data are effectively utilized as training data, with the third set being judiciously reserved for the exclusive purpose of evaluating the posterior predictive distribution, along with assessing the calibrated model's efficacy in forecasting future system behaviors. In Table 3.6, the estimated parameters are meticulously delineated, alongside their corresponding standard deviations. Notably, the standard deviations are scaled by the maximum a posteriori (MAP) estimates of the parameters, thus enabling a meaningful comparison among distinct parameters [91], [92].

For a more in-depth examination of the parameter estimation proceedings within this specific case study, we direct the interested reader to consult the comprehensive discussions presented in [91], [92].

3.3.3 Operational Requirements

The operation of building temperature control aims to maintain the temperature inside at a specific temperature range with the minimum cost spent.

- **Building Temperature Control:** The specified temperature range for the building's interior is set to maintain a comfortable and consistent environment. The interior temperature must remain within the range of 20°C to 22°C. One of the distinctive challenges in maintaining this desired temperature range is the dynamic nature of outdoor temperatures. The external temperature varies throughout the day and night, and the building's heating and cooling systems must be capable

of adapting to these external temperature fluctuations. This adaptability is particularly important to ensure that occupants are not subjected to uncomfortable temperature extremes

- **Cost-Efficient Heating:** Beyond the imperative of temperature control, the project is also driven by the necessity to optimize operational costs, particularly in the realm of heating. The economic landscape has seen a steady rise in energy prices, making efficient heating strategies a paramount concern.

4 Methods Overview

4.1 Deterministic Model Predictive Control (MPC)

MPC is a control strategy that employs a finite horizon open-loop Optimal Control Problem (OCP) to compute a sequence of control inputs. This sequence is determined by predicting the future behavior of a dynamic system through the utilization of a mathematical model. Subsequently, the first control input in the sequence is implemented, and this process is iteratively repeated at discrete time intervals in a receding horizon fashion. MPC can be conceptualized as a feedback control approach that combines model-based predictions with the optimization of future control inputs to achieve the desired system performance [20].

Consider a discrete-time nonlinear system of the form

$$\mathbf{x}_{k+1} = \mathbf{f}(\mathbf{x}_k, \mathbf{u}_k, \boldsymbol{\theta}_k) \tag{4.1}$$

where $\mathbf{x}$ represent the state variables, $\mathbf{u}$ denote the control inputs, $\boldsymbol{\theta}$ denotes the nominal value of the uncertainty and k denotes the time sample. The system model is represented by $\mathbf{f}$. Within the framework of Certainty Equivalent MPC, the inherent uncertainty is preconceived and treated as a nominal value. The OCP is then formulated over a prediction horizon of length N_p as follows:

$$\begin{aligned}
\text{minimize} \quad & \sum_{k=0}^{N_\mathrm{p}} \mathbf{J}(\mathbf{x}_k, \mathbf{u}_k) && \text{(4.2a)}\\
\text{subject to} \quad & \mathbf{x}_k = \hat{x}_0, && \text{(4.2b)}\\
& \mathbf{x}_{k+1} = \mathbf{f}(\mathbf{x}_k, \mathbf{u}_k, \boldsymbol{\theta}_k), && \text{(4.2c)}\\
& \mathbf{g}(\mathbf{x}_k, \mathbf{u}_k) \leq 0, && \text{(4.2d)}\\
& \mathbf{x}_\mathrm{lb} \leq \mathbf{x}_k \leq \mathbf{x}_\mathrm{ub}, && \text{(4.2e)}\\
& \mathbf{u}_\mathrm{lb} \leq \mathbf{u}_k \leq \mathbf{u}_\mathrm{ub} && \text{(4.2f)}
\end{aligned}$$

At time sample k, the cost function is formally defined as $\mathbf{J}(\mathbf{x}_k, \mathbf{u}_k)$, as outlined in (4.2a). The initial state of the system is explicitly provided in (4.2b). The system model and output constraints are meticulously integrated within (4.2c) and (4.2d), respectively, while

the respective limits on states and control inputs are systematically enforced through (4.2e) and (4.2f).

4.2 Open-loop Robustness Analysis

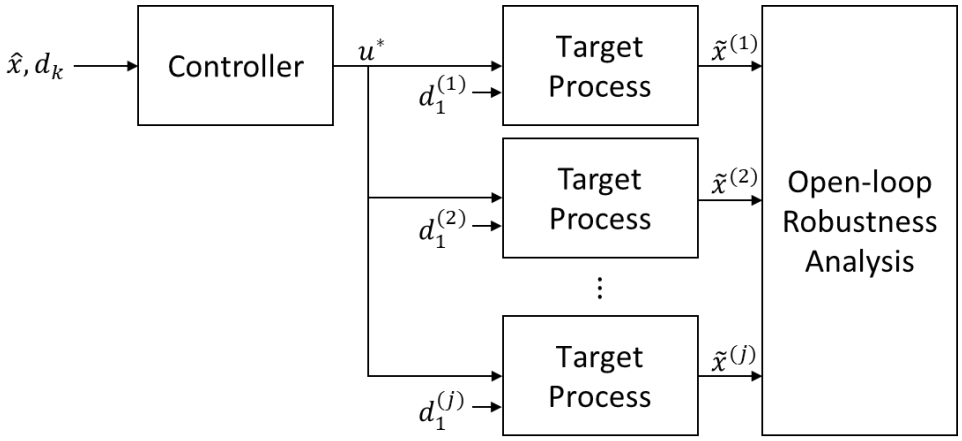

Figure 4.1: The procedure of open-loop robustness analysis

The objective of open-loop robustness analysis is to assess the extent of constraint violations resulting from uncertainties affecting the underlying process. The procedural steps for this analysis are visually depicted in Figure 4.1. After the MPC controller determines the control inputs, the initial element of these inputs is concurrently applied to the model while considering all potential sources of uncertainty. Subsequently, the assessment of constraint violations is conducted.

4.3 Multi-stage Model Predictive Control

Within the context of a multistage Model Predictive Control (MPC) framework, uncertainties, such as variations in model parameters or disturbances, can be effectively characterized using a discrete scenario tree, as exemplified in Figure 4.2. This tree delineates potential trajectories of uncertainty evolution in the future, and the corresponding control inputs are associated with branches stemming from a common node. The distinctive feature of multistage MPC lies in its capacity to adapt control inputs over time, thereby mitigating the impacts of uncertainties, as new information becomes available during the progressive traversal of the scenario tree.

[47].

the system can be written as:

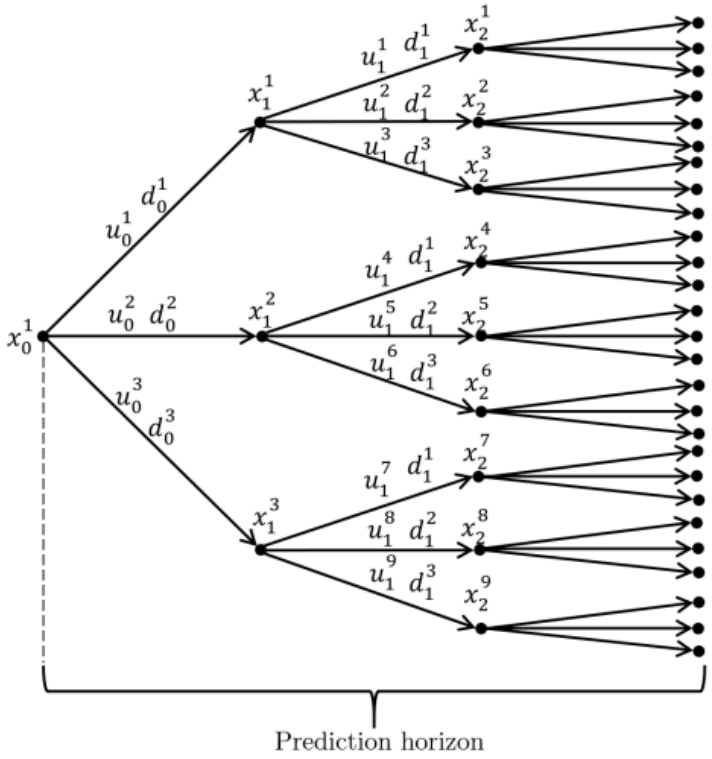

Figure 4.2: The structure of the scenario tree

$$x_{k+1}^{j} = f(x_k^{p(j)}, u_k^j, d_k^{r(j)}) \tag{4.3}$$

At time sample k, the variables $x_k^{p(j)}$, u_k^j, and $d_k^{r(j)}$ represent the state associated with a parent node, the control input, and the realization of uncertainty for scenario j.

Therefore, OCP for multistage MPC is formulated as:

$$\underset{u_k^j, \forall (j,k) \in I}{\text{minimize}} \quad \sum_{i=1}^{S} \omega_i \sum_{k=0}^{Np-1} L(x_{k+1}^j, u_k^j) \tag{4.4a}$$

$$\text{subject to} \quad x_{k+1}^j = f(x_k^{p(j)}, u_k^j, d_k^{r(j)}), \tag{4.4b}$$

$$x_k^j \in \mathbb{X}, \tag{4.4c}$$

$$u_k^j \in \mathbb{U}, \tag{4.4d}$$

$$u_k^j = u_k^l \quad \text{if} \quad x_k^{p(j)} = x_k^{p(l)} \tag{4.4e}$$

Equation (4.4a) defines the cost function, incorporating scenario probabilities denoted by ω_i. In this equation, $L(x_{k+1}, u_k)$ represents the stage cost, while N_p signifies the prediction

horizon. Equation (4.4b) characterizes the system model, while (4.4c) and (4.4d) establish boundaries for states and control inputs, respectively. Additionally, (4.4e) introduces non-anticipativity constraints, which require that control inputs u_k^k along branches stemming from the same parent node $x_k^{p(k)}$ must be identical. These constraints are essential because control inputs cannot anticipate the realization of uncertainty in future scenarios [47].

In practice, the industrial implementation of multistage MPC encounters challenges primarily stemming from the size of the Optimal Control Problem (OCP). The OCP's size experiences exponential growth due to factors such as the (a) multitude of uncertain parameters or disturbances, (b) numerous potential uncertainty realizations, and (c) an elongated prediction horizon. This exponential expansion imposes substantial computational demands, rendering the timely resolution of the OCP a challenging endeavor and limiting its practical applicability in industrial contexts [47].

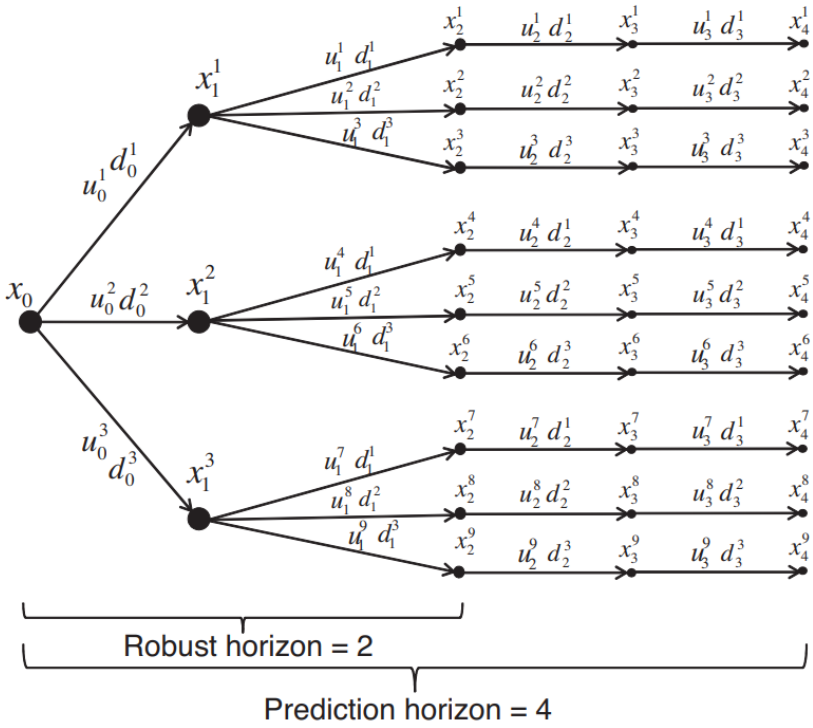

Figure 4.3: The structure of the scenario tree with a robust horizon

Effective implementation of multistage Model Predictive Control (MPC) necessitates careful design of the scenario tree to manage the size of the associated Optimal Control Problem (OCP). One strategy to mitigate the exponential growth of the scenario tree is the utilization of a robust horizon approach. This approach accounts for uncertainty evolution up to a certain time horizon and assumes its constancy for the remaining prediction horizon, as illustrated in Figure 4.3 [47].

4.4 Simplified Method for Multi-stage Model Predictive Control

The utilization of the simplified method in the multistage MPC framework significantly reduces S, the number of scenario ensembles, to just three. This substantial reduction results in a proportional decrease in the number of optimization variables, by a factor of $\frac{3}{S}$, and a corresponding reduction in constraints. As a consequence, the simplified method facilitates quicker and more efficient optimization problem-solving.

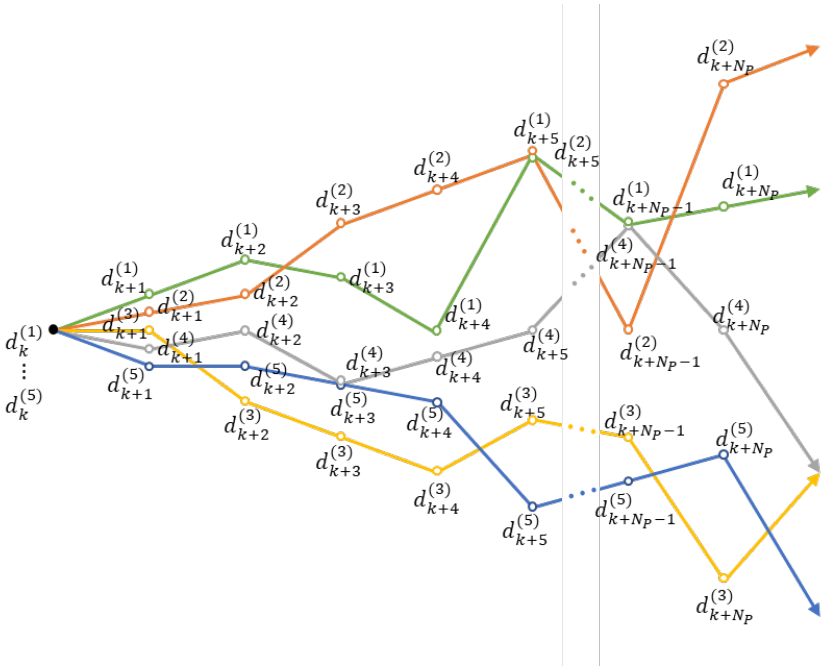

Figure 4.4: An example of scenario ensembles of uncertainty

Scenario ensembles constitute a collection of distinct scenarios representing various sources of unpredictability. They take on the structure of a scenario tree with a robust horizon of 1, although it's important to note that the values within these scenarios are not assumed to remain constant upon branching. Figure 4.4 showcases five representative scenario ensembles, each color-coded to denote a distinct scenario within the realm of uncertainty. The mathematical expression for the number of scenario ensembles, denoted as S, extending across the prediction horizon N_p at time sample k, is as follows:

$$\mathbf{d}_k = \begin{pmatrix} \mathbf{d}_k^{(1)} & \cdots & \mathbf{d}_k^{(S)} \\ \vdots & \ddots & \vdots \\ \mathbf{d}_{k+N_p}^{(1)} & \cdots & \mathbf{d}_{k+N_p}^{(S)} \end{pmatrix} \tag{4.5}$$

The simplified method encompasses the following two steps:

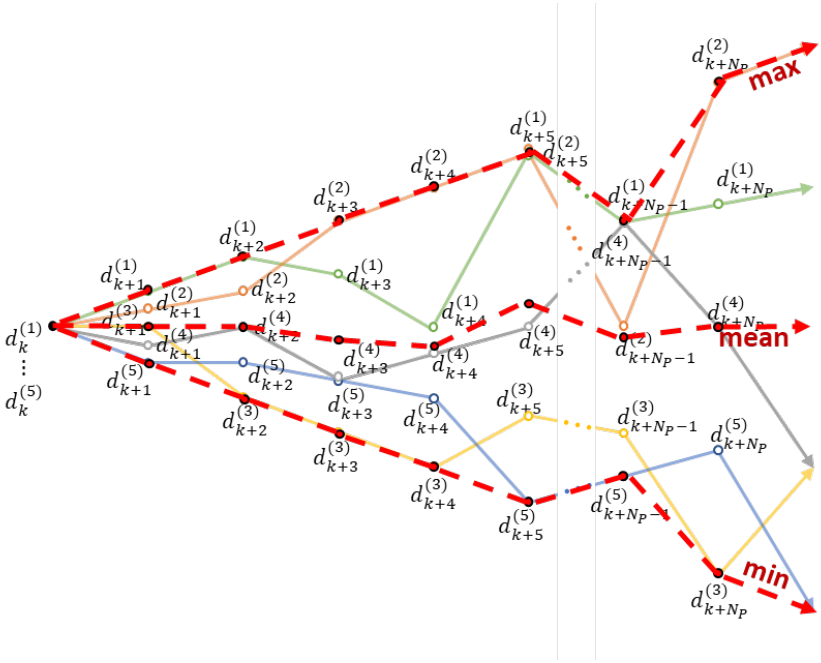

Figure 4.5: The three synthetic scenario ensembles of the uncertainty from the five example scenario ensembles

Step. 1: To generate synthetic scenario ensembles that represent the original ensembles, we utilize statistical data, including minimum, mean, and maximum values, for each time step across the forecasted horizon. As an example, consider the five uncertainty scenario ensembles illustrated in Figure 4.4. These ensembles can be transformed into three synthesized scenario ensembles, as indicated by the red dotted lines in Figure 4.5, by applying Equation (4.6), (4.7), and (4.8).

$$\mathbf{d}_{\max,k} = \begin{pmatrix} \max(\mathbf{d}_k^{(1)} & \cdots & \mathbf{d}_k^{(S)}) \\ \vdots & \ddots & \vdots \\ \max(\mathbf{d}_{k+N_p}^{(1)} & \cdots & \mathbf{d}_{k+N_p}^{(S)}) \end{pmatrix} \tag{4.6}$$

$$\mathbf{d}_{\text{mean},k} = \begin{pmatrix} \text{mean}(\mathbf{d}_k^{(1)} & \cdots & \mathbf{d}_k^{(S)}) \\ \vdots & \ddots & \vdots \\ \text{mean}(\mathbf{d}_{k+N_p}^{(1)} & \cdots & \mathbf{d}_{k+N_p}^{(S)}) \end{pmatrix} \tag{4.7}$$

$$\mathbf{d}_{\min,k} = \begin{pmatrix} \min(\mathbf{d}_k^{(1)} & \cdots & \mathbf{d}_k^{(S)}) \\ \vdots & \ddots & \vdots \\ \min(\mathbf{d}_{k+N_p}^{(1)} & \cdots & \mathbf{d}_{k+N_p}^{(S)}) \end{pmatrix} \tag{4.8}$$

A simplified scenario ensembles at each time sample k, denoted as $\mathbf{d}_{\text{syn},k}$, is formulated as follows:

$$\mathbf{d}_{\text{syn},k} = \begin{pmatrix} \mathbf{d}_{\max,k} & \mathbf{d}_{\text{mean},k} & \mathbf{d}_{\min,k} \end{pmatrix} \tag{4.9}$$

The three synthetic scenario ensembles, defined in Equation 4.9, comprehensively encapsulate the entire range of uncertainty portrayed by the original scenario ensembles in Equation 4.5.

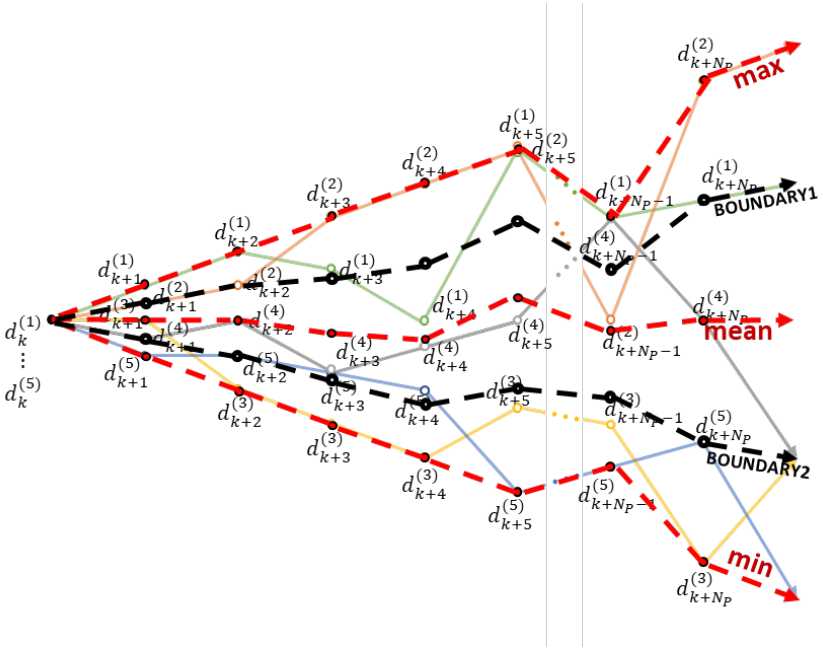

Figure 4.6: The defined boundary line, when s_1 and s_2 are set as 0.5

Step. 2: Utilizing synthetic scenario ensembles, each assigned its own probability of occurrence, offers a more accurate representation of the uncertainty originally depicted by the scenario ensembles. The probabilities associated with the three synthetic scenario ensembles are computed by quantifying the number of uncertainty data points from the original scenario ensembles that fall within predefined boundary regions. These boundaries can be established using either engineering expertise or statistical analysis. For instance, the statistically determined boundaries 1 and 2, denoted as B_1 and B_2, can be visualized in Figure 4.6 and are defined as follows:

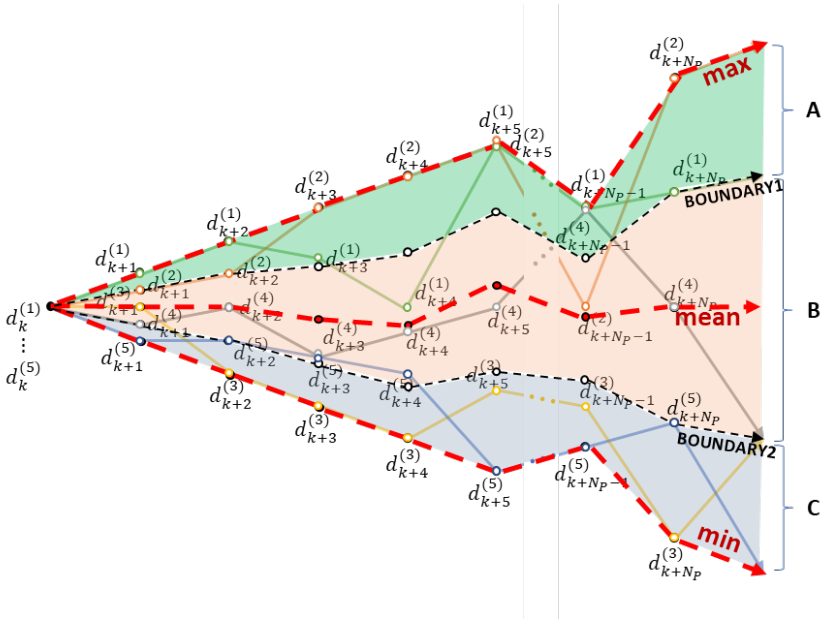

Figure 4.7: The defined boundary region to calculate the probabilities of occurrences of the synthesis scenario ensembles

$$B_1 = \mathbf{d}_{\text{mean},k} + s_1 \cdot (\mathbf{d}_{\text{max},k} - \mathbf{d}_{\text{mean},k})$$

$$B_2 = \mathbf{d}_{\text{mean},k} - s_2 \cdot (\mathbf{d}_{\text{mean},k} - \mathbf{d}_{\text{min},k})$$

where s_1 and s_2 are parameters that allow for the adjustment of the boundary ranges. As a result, the boundary regions as depicted in Figure 4.7 can be represented as follows:

$$\mathbf{A} \in (B_1, \mathbf{d}_{\text{max},k}]$$

$$\mathbf{B} \in [B_1, B_2]$$

$$\mathbf{C} \in [\mathbf{d}_{\text{min},k}, B_2)$$

Regions A, B, and C represent the likelihoods of occurrence for the maximum, mean, and minimum synthetic scenario ensembles, respectively. To illustrate, the computation of the likelihood of occurrence for the maximum synthetic scenario ensemble can be carried out in the following manner:

$$\omega_{\text{max}} = \frac{\sum_{j=1}^{S} \omega_j \cdot N_{\text{A}}^{(j)}}{\sum_{j=1}^{S} \omega_j \cdot N^{(j)}} \tag{4.10}$$

In this context, ω_j denotes the probability of the j^{th} original scenario ensemble occurring, while $N^{(j)}$ signifies the number of uncertainty points within the j^{th} original scenario ensemble. Additionally, $N_{\text{A}}^{(j)}$ specifically counts the number of uncertainty points belonging

to region A within the j^{th} original scenario ensemble. The probabilities for the mean and minimum synthetic scenario ensembles, denoted as ω_{mean} and ω_{min} respectively, can be computed in a similar manner.

4.5 Sequential Stochastic Model Predictive Control

The sequential stochastic MPC framework resembles a decision-making process akin to how humans formulate plans to attain long-term objectives. When confronted with a substantial goal, individuals typically begin by crafting a broad, high-level plan that outlines the general direction they intend to take. This initial plan does not delve into every potential uncertainty that might emerge in the distant future. As progress toward the long-term objective unfolds, more intricate short-term plans come into play. These plans are designed to accommodate immediate uncertainties, ensuring alignment with the overarching goal. They specify actions to be taken in the near future, such as those for the current day or the next sampling time, all while staying consistent with the broader long-term plan. Adjustments to the long-term plan are made as the situation evolves.

This concept finds reflection in the design of the sequential stochastic MPC framework, as illustrated in Figure 4.8. This framework integrates elements from both certainty-equivalent MPC and multistage MPC methodologies. The first optimizer, akin to certainty-equivalent MPC, functions as the high-level, long-term plan. It calculates the optimal reference control sequence over a prediction horizon of length $N_{\text{p}} = \phi_1$, taking into account nominal uncertainty values θ_k and initial state values $\mathbf{x}_0$. The second optimizer, a multistage MPC, intervenes to create a more detailed short-term plan for the near future. It does so by considering the reference control sequence $\mathbf{U}\text{ref}^*$ from the first optimizer and computing the optimal control sequence for a shorter period ($N\text{p} = \phi_2$), while incorporating the uncertainty d_k. The initial control input from the second optimizer is applied to the process, and this iterative process continues in a receding horizon fashion.

The first optimizer's formulation mirrors that of the OCP (4.2), which is employed in certainty equivalent MPC. The formulation of the second optimizer is akin to that of a multistage MPC framework and can be expressed as follows:

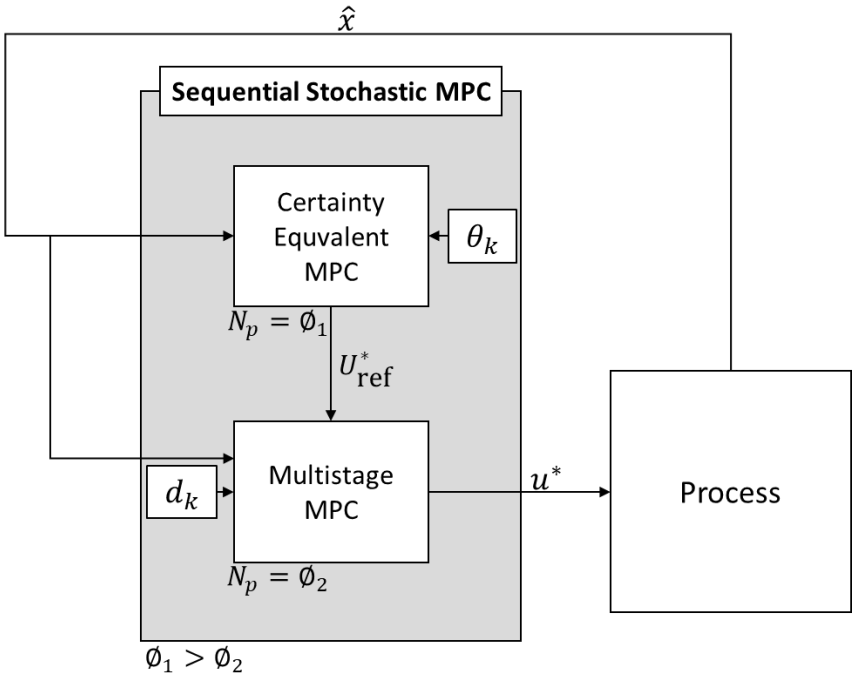

Figure 4.8: The framework of Sequential Robust MPC

$$\underset{\mathbf{x}_k,\,\mathbf{u}_k}{\text{minimize}} \quad \sum_{j=1}^{S} \omega_j \sum_{k=0}^{\phi_2} \mathbf{J}(\mathbf{x}_k^j, \mathbf{u}_k^j) + Q_u(\mathbf{u}_k^j - \mathbf{U}^*_{\text{ref},k})^2 \tag{4.11a}$$

$$\text{subject to} \quad \mathbf{x}_k^j = \hat{x}_0, \tag{4.11b}$$

$$\mathbf{x}_{k+1}^j = \mathbf{f}(\mathbf{x}_k^j, \mathbf{u}_k^j, \mathbf{d}_k^j), \tag{4.11c}$$

$$\mathbf{g}(\mathbf{x}_k^j, \mathbf{u}_k^j) \leq 0, \tag{4.11d}$$

$$\mathbf{x}_{\text{lb}} \leq \mathbf{x}_k^j \leq \mathbf{x}_{\text{ub}}, \tag{4.11e}$$

$$\mathbf{u}_{\text{lb}} \leq \mathbf{u}_k^j \leq \mathbf{u}_{\text{ub}}, \tag{4.11f}$$

$$\mathbf{u}_k^j = \mathbf{u}_k^l \quad \text{if} \quad \mathbf{x}_k^{p(j)} = \mathbf{x}_k^{p(l)} \tag{4.11g}$$

Consider a sequence indexed by $k = 0, 1, \ldots, \phi_2$, with ϕ_2 representing the length of the prediction horizon for the second optimizer. Within this context, the second optimizer calculates fresh optimal control sequences spanning the horizon of length ϕ_2. This calculation is enriched by the inclusion of the weight parameter Q_u, designed to facilitate tracking the reference control sequence from the first optimizer. Operating as a multistage MPC by design, this optimizer also integrates the system's uncertainties throughout the ϕ_2 horizon, employing a scenario tree structure to address them effectively.

Figure 4.9 presents control sequence trajectories for three different frameworks: certainty-

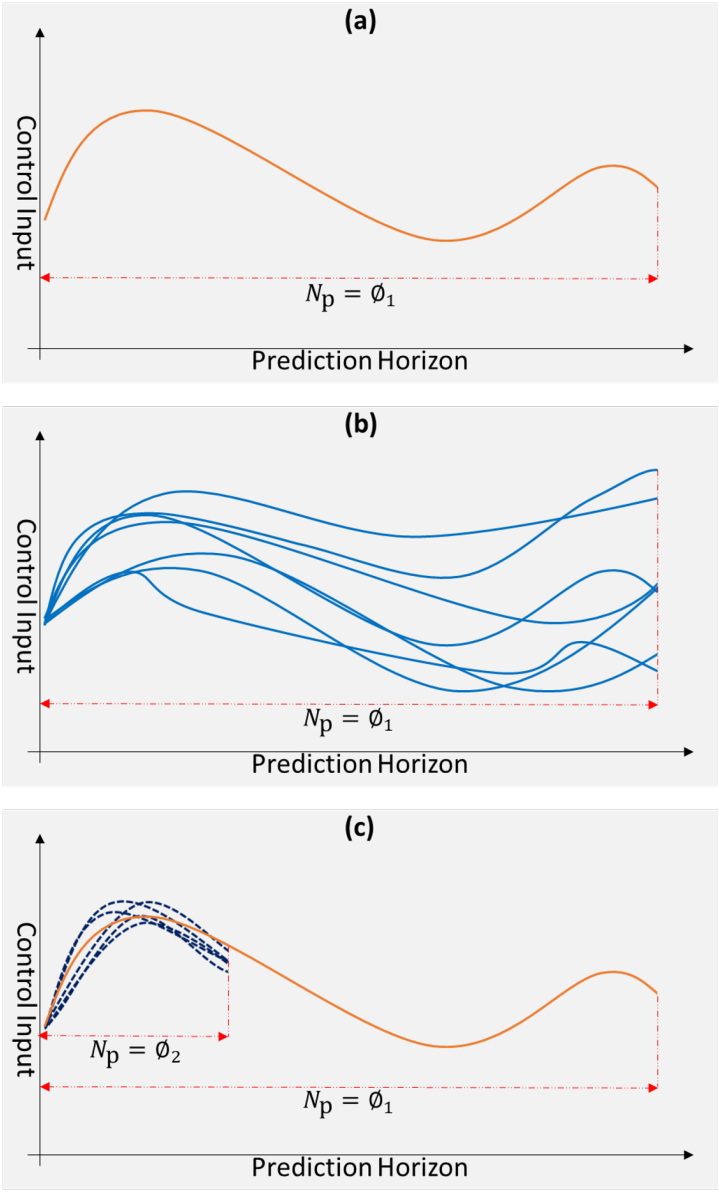

Figure 4.9: The example control trajectories: (a) Certainty-equivalent MPC (b) Multistage MPC (c) Sequential stochastic MPC

equivalent MPC, multistage MPC, and the proposed sequential stochastic MPC.

In Figure 4.9(a), the control sequence generated by certainty-equivalent MPC is displayed. This approach plans for a longer term using an extended prediction horizon ϕ_1 and considers nominal parameter values and input disturbances.

Figure 4.9(b) showcases control sequences produced by multistage MPC, operating under the same long-term plan with the extended prediction horizon ϕ_1. It handles uncertainties

using a scenario tree structure. For processes with extended prediction horizons where multistage MPC may struggle due to a large optimization problem.

The sequential stochastic MPC is depicted in Figure 4.9(c). It combines elements of both certainty-equivalent MPC and multistage MPC. In Figure 4.9(c), the orange line represents the long-term control sequence generated by the first optimizer, focusing solely on nominal process values over the extended prediction horizon ϕ_1. The blue dashed lines illustrate control trajectories produced by the second optimizer, working within a shorter prediction horizon ϕ_2 and considering system uncertainties through a scenario tree. Typically, when constraints are not a concern, the second optimizer yields a similar control solution to the first optimizer. However, if there's potential for constraint violations, the second optimizer takes a more conservative approach to ensure constraint adherence.

To illustrate the reduction in the size of the optimization problem, let's consider a system characterized by n_x states, n_u control inputs, and S uncertainty scenarios across a prediction horizon of length N_p. In a multistage MPC framework, the total number of decision variables to be optimized amounts to $(n_x+n_u)\cdot N_\mathrm{p}\cdot S$. In contrast, the sequential stochastic MPC approach tackles the problem through the sequential solving of two OCPs. The first OCP encompasses $(n_x+n_u)\cdot N_\mathrm{p}$ decision variables, while the second involves $(n_x+n_u)\cdot\phi_2\cdot S$ decision variables. This approach effectively reduces the problem size by a factor of $1/S$ and ϕ_2/N_p compared to the multistage MPC framework. This reduction in complexity carries significant computational benefits, particularly for systems entailing numerous uncertainty scenarios or extended prediction horizons. Furthermore, the convergence speed of the sequential stochastic MPC approach can be further accelerated when coupled with a simplified method on the second optimizer.

The sequential stochastic MPC scheme offers a significant advantage in terms of improved convergence during optimization problem-solving. As the prediction horizon extends further into the future, the uncertainty tends to become more variable. This heightened variability can potentially render the optimization problem infeasible when employing the multistage MPC framework. However, the sequential stochastic MPC scheme excels in effectively tackling this challenge and successfully resolves the optimization problem. This success stems from its ability to avoid considering uncertainties too far into the future, allowing for seamless system operation.

4.6 Chance-constrained Model Predictive Control

Chance-constrained MPC is a widely recognized stochastic MPC approach designed to accommodate uncertainties in system dynamics. Unlike nominal MPC, which assumes a deterministic evolution of the state x_k, real-world systems frequently demonstrate variations in model structure and parameters. To address these uncertainties, the system model is adjusted as follows:

$$x_{k+1} = Ax_k + Bu_k + G_{\mathrm{M}} w_{\mathrm{M},k} \tag{4.12}$$

In this context, the disturbances $w_{\mathrm{M},k}$ are taken to be sequences of independent and identically distributed variables with a known probability distribution denoted as p_w. Additionally, it is presumed that $\mathrm{E}[w_{\mathrm{M},k} \cdot w_{\mathrm{M},k}^{\top}] = Q_w$.

Chance-constrained MPC utilizes the information about the predicted state's mean and variance to maintain state constraint violations within acceptable limits. With the available system information at time k, its objective is to minimize the expected value of the cost function. This is achieved by considering a stochastic prediction model for the state, input constraints, and state chance constraints [57], [100]. The formulation of the Chance-constrained OCP is presented as follows [24]:

$$\begin{aligned}
\underset{u}{\text{minimize}} \quad & \mathrm{E}\left[\sum_{k=0}^{N} J_k\right] && \text{(4.13a)}\\
\text{subject to} \quad & x_{k+1} = Ax_k + Bu_k + G_{\mathrm{M}} w_{\mathrm{M},k}, && \text{(4.13b)}\\
& \Pr[H_c x_{k+1} \leq h_c] \geq 1 - \beta_j, && \text{(4.13c)}\\
& Du_k \leq d, && \text{(4.13d)}\\
& \mathrm{E}[x_0] = \hat{x}, \quad w_k \sim p_w && \text{(4.13e)}
\end{aligned}$$

In this OCP formulation, (4.13c) represents the state chance constraints, with a predefined threshold $\beta_j \in (0, 0.5]$ determining the probability of violating constraint h_c. It's important to note that the introduction of the stochastic variable $w_{\mathrm{M},k}$ in the model (4.13b) doesn't involve the use of specific realizations or sequences of disturbance values for prediction. Instead, it entails the propagation of the mean and variance of the stochastic state through the model equations (4.13b). This propagation is essential for evaluating the cost function (4.13a) and chance constraints (4.13c).

In cases where the model is linear and uncertainty follows a Gaussian distribution, the stochastic OCP can be reformulated into a format akin to deterministic MPC. This modified OCP takes on the following structure [101]:

$$\begin{aligned}
\underset{v}{\text{minimize}} \quad & \sum_{k=0}^{N} J_k^{\mathrm{SMPC}} && \text{(4.14a)}\\
\text{subject to} \quad & z_{k+1} = Az_k + Bv_k, && \text{(4.14b)}\\
& Hz_{k+1} \leq \eta_{k+1}, && \text{(4.14c)}\\
& Dv_k \leq d, && \text{(4.14d)}\\
& z_0 = \hat{x} && \text{(4.14e)}
\end{aligned}$$

where J_k^{SMPC} in Equation (4.14a) is expressed as:

$$J_k^{\text{SMPC}} = (z_{k+1}^\top Q_x z_{k+1} + v_k^\top R_u v_k) \tag{4.15}$$

In this context, key variables include z and v, which represent the deterministic state component and perturbations to a static feedback law, respectively. These are expressed as $x_k = z_k + e_k$ and $u_k = K_\text{p} e_k + v_k$, with e_k denoting the error at time k, and K_p as the feedback law constant. Additionally, (4.14c) introduces η_{k+1} as $H_j z_{k+1} \leq F^{-1} j, k+1(1-\beta)$, where $F^{-1} j, k+1$ signifies the inverse cumulative density function (CDF). The difference $h_j - \eta_{k+1}$ represents the constraint back-off magnitude, indicating the extent to which the predicted value $H_j z_{k+1}$ needs to deviate from the original bound h_c to satisfy the chance constraint (4.13c). When $w_{\text{M},k}$ follows a Gaussian distribution, computing η_{k+1} is straightforward by propagating state covariance over the prediction horizon. Consequently, both the predicted state x_{k+1} and the error e_{k+1} follow Gaussian distributions. As $He - h$ represents a linear transformation of the Gaussian random variable e, the CDFs $F_{j,k+1}$ and their inverses can be computed based on the probability distribution function of $He_{k+1} - h$ [101].

4.7 Hybrid Model Predictive Control

The hybrid MPC approach is designed to address two distinct sources of uncertainties: model mismatch and exogenous disturbances. To tackle model mismatch, a validation step is employed, where model predictions are compared with experimental data, allowing deviations to be characterized in probabilistic terms. In contrast, exogenous information is incorporated into the control framework via a scenario tree, constructed based on either expert opinions or provided prediction information. The model mismatch is managed through a chance-constrained framework, which relaxes associated state constraints by specifying an acceptable level of constraint violation. Meanwhile, the scenario tree is seamlessly integrated into the optimization problem using the multistage MPC framework to counteract the influence of exogenous disturbances. This integrated approach yields the following optimization problem formulation for hybrid MPC:

$$\underset{u}{\text{minimize}} \quad \sum_{j=1}^{S} \omega_j \mathrm{E}\left[\sum_{k=0}^{N} J_k\right] \tag{4.16a}$$

$$\text{subject to} \quad x_{k+1}^j = f(x_k^{p(j)}, Bu_k^j, Gw_k^{r(j)}), \tag{4.16b}$$

$$\Pr[H_c x_{k+1}^j \leq h_c] \geq 1-\beta_j, \tag{4.16c}$$

$$Du_k^j \leq d, \tag{4.16d}$$

$$u_k^j = u_k^l \quad \text{if} \quad x_k^{p(j)} = x_k^{p(l)}, \tag{4.16e}$$

$$\mathrm{E}[x_0^j] = \hat{x}, \quad wk \sim p_w \tag{4.16f}$$

In this formulation, the system dynamics are characterized by the state equation (4.16b). Here, $Gw_k^{r(j)}$ represents the uncertainty at time step k within the j^{th} scenario, defined as $Gw_k^{r(j)} = G_{\mathrm{M}} w_{\mathrm{M},k}^{r(j)} + G_{\mathrm{E}} w_{\mathrm{E},k}^{r(j)}$. The chance constraint (4.16c) ensures that the state complies with the hard constraint $H_c xk + 1^j \leq h_c$ with a probability of at least $1-\beta_j$. Control bounds are established by (4.16d), while the non-anticipativity constraint (4.16e) guarantees that control inputs are equal when corresponding states are equal. The initial state is specified by (4.16f), with $\hat{x}$ representing the measured or estimated initial state, and $w_{\mathrm{M},k}$ as a random variable following the distribution p_w. The objective is to minimize the expected cost across all scenarios, $\sum_{j=1}^{S} \omega_j \mathrm{E}\left[\sum_{i=0}^{N} J_k\right]$, achieved by selecting suitable control inputs u_k^j.

In summary, the hybrid MPC approach effectively addresses both model mismatch and exogenous disturbances, offering robust handling of uncertainties in real-world systems. If the model uncertainty adheres to a Gaussian distribution and the model is linear, the hybrid MPC OCP can be expressed as follows:

$$\underset{u}{\text{minimize}} \quad \sum_{j=1}^{S} \omega_j \sum_{k=0}^{N} J_k^{j,\mathrm{SMPC}} \tag{4.17a}$$

$$\text{subject to} \quad z_{k+1}^j = Az_k^j + Bv_k^j + Gw_k^{r(j)}, \tag{4.17b}$$

$$Hz_{k+1}^j \leq \eta_{k+1}, \tag{4.17c}$$

$$Dv_k^j \leq d, \tag{4.17d}$$

$$v_k^j = v_k^l \quad \text{if} \quad z_k^{p(j)} = z_k^{p(l)}, \tag{4.17e}$$

$$z_0^j = \hat{x} \tag{4.17f}$$

5 Summary of Papers

5.1 Paper A - MPC Operation with Improved Optimal Control Problem at Dalsfoss Power Plant

In Paper A, a new Optimal Control Problem (OCP) formulation is presented with the goal of maximizing the water level in the reservoir at the Dalsfoss hydropower station. Previous approaches, such as the reference region tracking OCP, were employed for its operation, as discussed in earlier studies [14], [96]. However, the reference region tracking OCP primarily focuses on maintaining the water level at an appropriate but not necessarily maximum level. This suboptimal operation can result in the loss of water in the reservoir, which could otherwise be used to generate electricity. The newly proposed OCP effectively addresses this issue while also being more operator-friendly.

Paper A conducts a series of simulations, comparing the outcomes of both the reference region tracking OCP and the new OCP when implementing deterministic Model Predictive Control (MPC) with various initial set points. The results demonstrate that the new OCP leads to more optimal operation by maximizing the water level, i.e., by keeping more water in the reservoir instead of throwing it out through floodgates. However, it's important to note that the robustness of the new OCP is observed to be lower than that of the reference region tracking OCP due to uncertainties in water inflow forecasts, as revealed by an open-loop robustness analysis. This discrepancy arises from the fact that the reference region tracking OCP does not aim to maintain the water level as high as possible, leaving more room for additional water. This robustness analysis underscores the importance of incorporating robust or stochastic MPC schemes to mitigate the impact of forecast uncertainties in reservoir water inflow.

5.2 Paper B - Stochastic MPC For Optimal Operation of Hydropower Station Under Uncertainty

Paper B proposes two strategies to mitigate the impact of uncertainty in water inflow to the reservoir for the Dalsfoss hydropower system. Firstly, it suggests introducing a 5cm safety margin to the operational constraint when applying deterministic Model Predictive

Control (MPC). Secondly, it advocates for the use of multistage MPC, considering all available scenario ensembles of water inflow forecasts with equal probabilities.

Both approaches exhibit robustness, as indicated by the results of the open-loop robustness analysis. The inclusion of a safety margin in deterministic MPC leads to a more conservative operation, while multistage MPC brings the system closer to optimal performance compared to deterministic MPC. However, the computational speed of multistage MPC is significantly slower, approximately 18 times, due to the larger size of the Optimization Control Problem (OCP).

To address the computational speed issue, Paper B employs a strategy of generating three synthesis scenario ensembles from the original set of 50 scenario ensembles for the water inflow forecast. These three synthesis scenario ensembles, with equal probabilities, are used for implementing multistage MPC instead of all 50 scenarios. This optimization results in a remarkable 11.5-fold reduction in computational time, with a slight degradation in operational performance.

5.3 Paper C - Multistage model predictive control with simplified scenario ensembles for robust control of hydropower station

In Paper C, a novel approach is proposed to simplify the complexity of original scenario ensembles for water inflow forecasts without compromising the effectiveness of the multistage model predictive control (MPC) scheme. This method is presented in two key steps. Firstly, it involves generating the three synthesis scenario ensembles based on statistical information derived from the structure of the original scenario ensembles. Secondly, probabilities or weights are assigned to these synthesis scenario ensembles in accordance with the original scenario ensembles. The application of this method significantly reduces the size of the optimal control problem (OCP) by a factor of 3 divided by the number of scenario ensembles. For example, in the case of the Dalsfoss hydropower system with 50 possible scenario ensembles for water inflow forecasts, the OCP can be effectively reduced by 3/50 through the utilization of this simplified approach.

To assess the efficacy of this proposed method, Paper C conducts simulation experiments involving multistage MPC under various scenarios, including situations with both moderate water inflow and flooding. The results reveal that when using the simplified scenario ensembles with equal probabilities, the operation tends to be more conservative compared to the utilization of all original scenario ensembles. However, the computational speed significantly improves. Importantly, these findings align with the slight degradation in operational performance mentioned in Paper B. Nevertheless, it is noteworthy that when

the simplified method is employed, the simulation results are almost identical in operational performance compared to multistage MPC using all original scenario ensembles, effectively demonstrating the method's effectiveness in achieving robust control while mitigating computational demands.

5.4 Paper D - Multistage Model Predictive Control with Simplified Method on Scenario Ensembles of Uncertainty for Hjartdøla Hydropower System

Paper D employs a simplified method to enhance the computational efficiency of multistage model predictive control (MPC) while preserving its performance quality. Although this method had been previously applied in Paper C, its effectiveness is further substantiated through testing on a different case study.

As illustrated in Section 3.2.1, the Hjartdøla hydropower system shares similarities with the Dalsfoss hydropower system. However, the Hjartdøla system features a smaller reservoir and involves interactions with four rivers. Each of these rivers has 50 scenario ensembles for water inflow forecasts, resulting in a staggering 6,250,000 possible combinations when considering all four rivers simultaneously. The computational complexity made it infeasible to employ multistage MPC while considering all possible scenario tree combinations, necessitating a reduction in the scenario ensembles.

To address this, the study focused on the minimum water inflow scenario ensembles of three rivers (Skorva, Skogsåå, and Mjella) situated at the system's base. This ensured the minimum downstream flow rate requirement was consistently met. Subsequently, attention was directed solely toward the water inflow into the reservoir (Hjartså River) and its 50 possible scenario ensembles.

The findings of this research highlight the effectiveness of the simplified method, significantly reducing computational time while maintaining performance levels nearly identical to those achieved when using all scenarios for multistage MPC. Nevertheless, during this case study, questions arose regarding the method's efficacy when dealing with systems featuring multiple uncertainties.

5.5 Paper E - Sequential Stochastic Model Predictive Control for Operating Buffer Reservoir in Hjartdøla Hydropower System under Uncertainty

When implementing multistage model predictive control (MPC) in hydropower systems, two key concerns emerge. The first pertains to the computational demands resulting from the extensive size of optimal control problem (OCP). The second involves the challenge of achieving convergence in the optimization process when utilizing all available information from water inflow forecasts. Research findings revealed that the OCP failed to converge when substantial deviations existed among different scenario ensembles.

In Paper E, the effectiveness of the sequential stochastic MPC framework in addressing both of these concerns is thoroughly demonstrated in the case study of the Hjardøla hydropower system. The paper includes simulations involving four distinct MPC frameworks: Certainty Equivalent MPC, two multistage MPCs with varying prediction horizon lengths (13 days and 6 hours), and the Sequential Stochastic MPC (1st optimizer - 13 days, 2nd optimizer - 6 hours). The open-loop robustness analysis was performed to evaluate their performance. The results indicate that the two multistage MPCs and the sequential stochastic method did not display potential violations. Conversely, Certainty Equivalent MPC failed to ensure constraint satisfaction.

Notably, the Multistage MPC with a 13-day prediction horizon consistently demonstrated reliable performance. It excelled in maximizing reservoir water levels when increased water release was required to meet downstream minimum flow rate requirements, all while maintaining a steady flow rate. However, the Multistage MPC with a 6-hour prediction horizon yielded less competitive simulation results. It was characterized by unstable downstream flow rates and suboptimal reservoir water level maximization for future use.

On the other hand, the sequential stochastic MPC framework consistently matched the performance of the Multistage MPC with a 13-day prediction horizon length. Additionally, it successfully resolved the convergence issue and substantially reduced computational time when a severe flooding situation is assumed. This underscores its effectiveness as an efficient and robust solution for managing buffer reservoir operations in the face of uncertainty within the Hjardøla hydropower system.

5.6 Paper F - Implementation of Simplified Sequential Stochastic Model Predictive Control for Operation of Hydropower System under Uncertainty

The primary objective of Paper F is to further enhance the computational efficiency of the sequential stochastic model predictive control (MPC) framework. This enhancement is achieved by introducing a simplified method in the second optimizer. Additionally, Paper F conducts an extensive evaluation of the sequential stochastic MPC framework by varying tuning parameters and the prediction horizon length within the second optimizer.

The findings of Paper F present three significant advantages of implementing the simplified sequential stochastic MPC framework. Firstly, it highlights that, when properly configured, the sequential stochastic MPC outperforms multistage MPC. Secondly, the incorporation of the simplified method in the sequential stochastic MPC leads to a remarkable 85-fold reduction in computational time compared to multistage MPC. Lastly, the framework exhibits more robust optimization convergence, particularly in scenarios involving severe flooding situations characterized by substantial deviations among scenario ensembles of the water inflow forecast.

Paper F encompasses a comprehensive exploration of various settings within the sequential stochastic MPC framework. Firstly, it investigates the impact of different sets of weight parameters in the second optimizer. Secondly, the paper examines the effects of varying the prediction horizon length in the second optimizer. Remarkably, the performance of the controller remains relatively consistent regardless of the prediction horizon length. Consequently, it emphasizes the importance of selecting an appropriate prediction horizon length that minimizes computational demands while satisfying performance criteria.

Additionally, the study assesses the framework's performance with different nominal scenario ensembles of the water inflow forecast in the first optimizer. The results indicate that choosing any one of the scenario ensembles or the ensemble average as the nominal scenario ensemble yields comparable controller performance. However, when a random constant value for water inflow is set as the nominal scenario ensemble in the first optimizer, it significantly degrades overall controller performance and leads to erratic behavior.

In summary, Paper F establishes the utility of the sequential stochastic MPC framework and delves deeper into its potential by exploring various settings and configurations.

5.7 Paper G - Hybrid MPC Scheme for Controlling Temperature in Building with Grey-Box Model under Uncertainties in Model and Weather Forecast

In Paper G, the Hybrid model predictive control (MPC) framework is introduced to effectively address two distinct forms of uncertainties. The first is model uncertainty, characterized by known probabilities, while the second involves future uncertainties, such as weather forecast scenarios. This Hybrid MPC framework seamlessly combines the chance-constrained MPC and the multi-stage MPC, allowing it to tackle both types of uncertainty.

The chosen case study in Paper G involves around temperature control within a building. A grey-box model for the building had been previously developed and validated, incorporating stochastic uncertainty [91], [92]. For controlling the system, another layer of uncertainty arises from external factors, particularly outdoor temperatures. Despite periodic weather forecasts, small discrepancies between forecasts and real-world conditions are common. To account for these uncertainties, the framework considers temperature forecast uncertainty, with the boundaries of this uncertainty gradually increasing from the present moment to 24 hours in the future. This approach yields three distinct temperature forecast scenarios. The primary objective is to maintain the building's temperature within a desired range while factoring in electricity costs associated with heater usage.

Paper G formulates an optimal control problem (OCP) to address these challenges. It seeks to keep the building's temperature within the desired range while considering fluctuations in electricity prices.

The paper conducts simulations involving four types of MPCs: deterministic MPC, chance-constrained MPC, multi-stage MPC, and the proposed hybrid MPC. The simulations aim to maintain the building's temperature within the range of 20 to 22 degrees Celsius. Deterministic MPC is successful in keeping the temperature closest to 22 degrees Celsius among all the MPCs. However, when accounting for uncertainties in both the model and the forecast, the potential for temperature violations within the desired range emerges.

The simulation results of chance-constrained MPC and multi-stage MPC demonstrate their effectiveness in handling uncertainties related to the model and the forecast, respectively. The hybrid MPC also effectively manages both uncertainties simultaneously. To enhance robustness against model uncertainty, one can reduce the permissible probability of state constraint violations, denoted as β.

Finally, Paper G explores the impact of different weight parameter settings within the hybrid MPC framework in the case study. Increasing the weight on the cost-minimization term for electricity consumption leads to reduced power consumption and lower costs.

In summary, Paper G introduces a Hybrid MPC framework that effectively addresses model and weather uncertainties, providing valuable insights into temperature control within buildings.

6 Conclusion and Perspective

This chapter sums up the research works that have been done so far and then lists the future works that can be performed.

6.1 Conclusion

In hindsight, the research objectives outlined in Section 1.2 have been successfully achieved through a comprehensive investigation involving various papers, namely A, B, C, D, E, F, and G.

The research journey commenced with an exploration of dynamic optimization under uncertainty, focusing on the Dalsfoss hydropower station system. In Paper A, a new formulation of the Optimal Control Problem (OCP) is introduced and compared with previously established methods by running simulations of model predictive control (MPC). the newly formulated OCP showed its superior efficiency in maximizing water resources for power generation. In Paper B, the challenges posed by uncertain water inflow forecasts are addressed by employing a multistage MPC approach. Paper C introduced a simplified method to significantly reduce computational time while maintaining the effectiveness and performance of multistage MPC. Additionally, Paper F introduced a novel stochastic Sequential MPC framework, which not only enhanced computational efficiency but also reduced the likelihood of infeasibility issues in OCP solutions.

The research expanded to encompass the Hjardøla hydropower system in Papers D and E. In Paper D, the OCP is successfully formulated for this system and multistage MPC is leveraged along with the simplified method to mitigate the impact of uncertain water inflow forecasts. In Paper E, the sequential stochastic MPC framework is rigorously tested, further confirming the efficacy of both the simplified method and the new framework.

Paper G focuses on the building temperature system. Building upon previous studies that established the system model, parameter estimation, and estimated model uncertainty, the Hybrid MPC framework is proposed in Paper G. This framework combines multistage MPC and chance-constrained MPC, effectively utilizing the previously established model. The chance-constrained MPC aspect helps mitigate violations arising from model uncertainty, while the multistage MPC component addresses uncertainties related to future weather forecasts.

In summary, this research has made significant strides in addressing dynamic optimization under uncertainty across various domains, from hydropower systems to building temperature control, offering valuable insights and practical solutions to real-world challenges regarding the uncertainties in the system.

In particular, the novel MPCs frameworks and techniques that come from this research aim to predict the long future of the dynamic system with uncertainties, within the minimum computational effort, but without compromising the performance of the controller. The application can be expanded to other various applications such as other kinds of renewables, other industries, and even finance.

6.2 Future Perspective

Looking ahead, there are several promising avenues for future research in this field, including:

- **Expanding Uncertainty Sources:** Exploring additional sources of uncertainty within the system for more rigorous simulation and research. In this research, many of possible disturbances such as sensor errors in measurements of levels and flowrates were not considered. Considering the uncertainties, A more rigorous simulation and control system can be built.
- **Enhancing System Modeling:** Improving the accuracy of system models to enhance predictive capabilities. The system model used is designed simply, for example, demonstrating only two places of level in the large reservoir, Lake Toke. If the model is well-described rigorously, better control performance may be achieved in the real implementation of the MPCs.
- **Machine Learning Integration:** Leveraging machine learning algorithms and reinforcement learning techniques to approximate the optimization problem. Solving optimization problems has the potential to face difficulties such as the infeasibility of the problem or the long computational time. Therefore, the utilization of machine learning techniques to approximate the solution of the OCP will give more smoother operation.
- **Implementing the introduced tools in other various fields:** The suggested methods in this research were only applied to hydropower systems or a building temperature control system. However, the methods can be useful for other applications such as renewables systems, other industry applications, and finance systems.

These directions represent exciting opportunities to further advance our understanding and application of dynamic optimization under uncertainty, paving the way for more robust and efficient solutions in a wide range of domains.

Bibliography

[1] J. A. Tainter, 'Energy, complexity, and sustainability: A historical perspective,' eng, *Environmental innovation and societal transitions*, vol. 1, no. 1, pp. 89–95, 2011, ISSN: 2210-4224.

[2] C. Wilson and A. Grubler, 'Lessons from the history of technology and global change for the emerging clean technology cluster,' 2011.

[3] A. Jarvis, D. Leedal and C. Hewitt, 'Climate-society feedbacks and the avoidance of dangerous climate change,' eng, *Nature climate change*, vol. 2, no. 9, pp. 668–671, 2012, ISSN: 1758-678X.

[4] NVE, *Energy consumption in norway*, 2023. [Online]. Available: https://www.nve.no/energy-consumption-and-efficiency/energy-consumption-in-norway/.

[5] NVE, *Electricity consumption in norway towards 2030*, 2023. [Online]. Available: https://www.nve.no/energy-consumption-and-efficiency/energy-consumption-in-norway/electricity-consumption-in-norway-towards-2030/.

[6] *Energifakta*, May 2021. [Online]. Available: https://energifaktanorge.no/en/norsk-energiforsyning/kraftproduksjon/.

[7] H. Locher, 'Sustainable hydropower – issues and approaches,' eng, in IntechOpen, 2012, ISBN: 9789535101642.

[8] IEA, *Hydropower special market report—analysis and forecast to 2030*, eng. Paris, France: IEA, 2021.

[9] A. Torabi Haghighi, F. B. Ashraf, J. Riml, J. Koskela, B. Kløve and H. Marttila, 'A power market-based operation support model for sub-daily hydropower regulation practices,' eng, *Applied energy*, vol. 255, p. 113 905, 2019, ISSN: 0306-2619.

[10] J. Li, S. Chen, Y. Wu *et al.*, 'How to make better use of intermittent and variable energy? a review of wind and photovoltaic power consumption in china,' *Renewable and Sustainable Energy Reviews*, vol. 137, p. 110 626, 2021, ISSN: 1364-0321. DOI: https://doi.org/10.1016/j.rser.2020.110626. [Online]. Available: https://www.sciencedirect.com/science/article/pii/S1364032120309102.

[11] REN21, *Renewables. global status report, 2020a, (accessed: 23.7.2022)*, https://www.ren21.net/gsr-2020/, 2022.

[12] D. O. Olukanni, 'Assessment of impact of hydropower dams reservoir outflow on the downstream river flood regime – nigeria's experience,' eng, in IntechOpen, 2012, ISBN: 9789535101642.

[13] NVE, *Supervision of dams*, Nov. 2021. [Online]. Available: https://www.nve.no/supervision-of-dams/?ref=mainmenu.

[14] I. Menchacatorre, R. Sharma, B. Furenes and B. Lie, 'Flood management of lake toke: Mpc operation under uncertainty,' eng, 2019, ISSN: 1650-3686. [Online]. Available: https://hdl.handle.net/11250/2645438.

[15] IEA, *Building*, https://www.iea.org/reports/buildings, Paris, 2022.

[16] T. Berthou, P. Stabat, R. Salvazet and D. Marchio, 'Development and validation of a gray box model to predict thermal behavior of occupied office buildings,' eng, *Energy and buildings*, vol. 74, pp. 91–100, 2014, ISSN: 0378-7788.

[17] P. Ș. Agachi, *Basic process engineering control*, eng, Berlin, Germany, 2014.

[18] P. Rawat, 'Model predictive Control 101 - Pallav Rawat - Medium,' Feb. 2023. [Online]. Available: https://pallavrawat.medium.com/model-predictive-control-101-28de17208c39.

[19] J. Lee and Z. Yu, 'Worst-case formulations of model predictive control for systems with bounded parameters,' *Automatica*, vol. 33, no. 5, pp. 763–781, 1997, ISSN: 0005-1098. DOI: https://doi.org/10.1016/S0005-1098(96)00255-5.

[20] D. Mayne, J. Rawlings, C. Rao and P. Scokaert, 'Constrained model predictive control: Stability and optimality,' eng, *Automatica (Oxford)*, vol. 36, no. 6, pp. 789–814, 2000, ISSN: 0005-1098.

[21] M. Morari and J. H. Lee, 'Model predictive control : Past, present and future: Special issue: Selected and extended papers from the symposium on pse'97/escape'7,' eng, *Computers chemical engineering*, vol. 23, no. 4-5, pp. 667–682, 1999, ISSN: 0098-1354.

[22] J. R. Birge, 'State-of-the-art-survey–stochastic programming: Computation and applications,' eng, *INFORMS Journal on Computing*, vol. 9, no. 2, pp. 111–133, 1997, ISSN: 1091-9856. DOI: 10.1287/ijoc.9.2.111.

[23] A. Shapiro, D. Dentcheva and A. Ruszczyński, *Lectures on stochastic programming: modeling and theory* (MOS-SIAM Series on Optimization), eng. Society for Industrial and Applied Mathematics, 2009, ISBN: 089871687X.

[24] A. Mesbah, 'Stochastic model predictive control: An overview and perspectives for future research,' eng, *IEEE control systems*, vol. 36, no. 6, pp. 30–44, 2016, ISSN: 1066-033X.

[25] B. Lie, 'Final report: Kontrakt nr inan-140122 optimal control of dalsfos flood gates- control algorithm,' 2014.

[26] S. Skogestad, 'Control structure design for complete chemical plants,' *Computers Chemical Engineering*, vol. 28, no. 1, pp. 219–234, 2004, Escape 12, ISSN: 0098-1354. DOI: https://doi.org/10.1016/j.compchemeng.2003.08.002. [Online]. Available: https://www.sciencedirect.com/science/article/pii/S0098135403001984.

[27] T. E. Marlin, A. N. Hrymak *et al.*, 'Real-time operations optimization of continuous processes,' in *AIChE Symposium Series*, New York, NY: American Institute of Chemical Engineers, 1971-c2002., vol. 93, 1997, pp. 156–164.

[28] A. Helbig, O. Abel and W. Marquardt, 'Structural concepts for optimization based control of transient processes,' in *Nonlinear Model Predictive Control*, F. Allgöwer and A. Zheng, Eds., Basel: Birkhäuser Basel, 2000, pp. 295–311, ISBN: 978-3-0348-8407-5.

[29] J. B. Rawlings and R. Amrit, 'Optimizing process economic performance using model predictive control,' in *Nonlinear Model Predictive Control: Towards New Challenging Applications*, L. Magni, D. M. Raimondo and F. Allgöwer, Eds. Berlin, Heidelberg: Springer Berlin Heidelberg, 2009, pp. 119–138, ISBN: 978-3-642-01094-1. DOI: 10.1007/978-3-642-01094-1_10. [Online]. Available: https://doi.org/10.1007/978-3-642-01094-1_10.

[30] S. Engell, 'Feedback control for optimal process operation,' *Journal of Process Control*, vol. 17, no. 3, pp. 203–219, 2007, Special Issue ADCHEM 2006 Symposium, ISSN: 0959-1524. DOI: https://doi.org/10.1016/j.jprocont.2006.10.011. [Online]. Available: https://www.sciencedirect.com/science/article/pii/S0959152406001326.

[31] J. Richalet, A. Rault, J. Testud and J. Papon, 'Model predictive heuristic control: Applications to industrial processes,' *Automatica*, vol. 14, no. 5, pp. 413–428, 1978, ISSN: 0005-1098. DOI: https://doi.org/10.1016/0005-1098(78)90001-8. [Online]. Available: https://www.sciencedirect.com/science/article/pii/0005109878900018.

[32] C. R. Cutler and B. L. Ramaker, 'Dynamic matrix control¿a computer control algorithm,' *IEEE Transactions on Automatic Control*, vol. 17, p. 72, 1979. [Online]. Available: https://api.semanticscholar.org/CorpusID:122480259.

[33] D. Clarke, C. Mohtadi and P. Tuffs, 'Generalized predictive control—part i. the basic algorithm,' *Automatica*, vol. 23, no. 2, pp. 137–148, 1987, ISSN: 0005-1098. DOI: https://doi.org/10.1016/0005-1098(87)90087-2. [Online]. Available: https://www.sciencedirect.com/science/article/pii/0005109887900872.

[34] D. Clarke, C. Mohtadi and P. Tuffs, 'Generalized predictive control—part ii extensions and interpretations,' *Automatica*, vol. 23, no. 2, pp. 149–160, 1987, ISSN: 0005-1098. DOI: https://doi.org/10.1016/0005-1098(87)90088-4. [Online]. Available: https://www.sciencedirect.com/science/article/pii/0005109887900884.

[35] S. Qin and T. A. Badgwell, 'A survey of industrial model predictive control technology,' *Control Engineering Practice*, vol. 11, no. 7, pp. 733–764, 2003, ISSN: 0967-0661. DOI: https://doi.org/10.1016/S0967-0661(02)00186-7.

[36] J. Rawlings, 'Tutorial overview of model predictive control,' eng, *IEEE control systems*, vol. 20, no. 3, pp. 38–52, 2000, ISSN: 1066-033X.

[37] D. M. Prett and R. Gillette, 'Optimization and constrained multivariable control of a catalytic cracking unit,' *IEEE Transactions on Automatic Control*, vol. 17, p. 73, 1980. [Online]. Available: https://api.semanticscholar.org/CorpusID:118416823.

[38] P. Scokaert and D. Mayne, 'Min-max feedback model predictive control for constrained linear systems,' eng, *IEEE transactions on automatic control*, vol. 43, no. 8, pp. 1136–1142, 1998, ISSN: 0018-9286.

[39] N. Ricker, T. Subrahmanian and T. Sim, 'Case studies of model-predictive control in pulp and paper production,' *IFAC Proceedings Volumes*, vol. 21, no. 4, pp. 13–22, 1988, IFAC Workshop on Model Based Process Control, Atlanta, GA, USA, 13-14 June, ISSN: 1474-6670. DOI: https://doi.org/10.1016/B978-0-08-035735-5.50007-3. [Online]. Available: https://www.sciencedirect.com/science/article/pii/B9780080357355500073.

[40] H. Genceli and M. Nikolaou, 'Robust stability analysis of constrained l1-norm model predictive control,' *AIChE Journal*, vol. 39, no. 12, pp. 1954–1965, 1993. DOI: https://doi.org/10.1002/aic.690391206. eprint: https://aiche.onlinelibrary.wiley.com/doi/pdf/10.1002/aic.690391206. [Online]. Available: https://aiche.onlinelibrary.wiley.com/doi/abs/10.1002/aic.690391206.

[41] N. M. C. de Oliveira and L. T. Biegler, 'Constraint handing and stability properties of model-predictive control,' *AIChE Journal*, vol. 40, no. 7, pp. 1138–1155, 1994. DOI: https://doi.org/10.1002/aic.690400706. eprint: https://aiche.onlinelibrary.wiley.com/doi/pdf/10.1002/aic.690400706. [Online]. Available: https://aiche.onlinelibrary.wiley.com/doi/abs/10.1002/aic.690400706.

[42] A. Zheng and M. Morari, 'Stability of model predictive control with mixed constraints,' *IEEE Transactions on Automatic Control*, vol. 40, no. 10, pp. 1818–1823, 1995. DOI: 10.1109/9.467664.

[43] P. O. M. Scokaert and J. B. Rawlings, 'Feasibility issues in linear model predictive control,' *AIChE Journal*, vol. 45, no. 8, pp. 1649–1659, 1999. DOI: https://doi.org/10.1002/aic.690450805. eprint: https://aiche.onlinelibrary.wiley.com/doi/pdf/10.1002/aic.690450805. [Online]. Available: https://aiche.onlinelibrary.wiley.com/doi/abs/10.1002/aic.690450805.

[44] R. J. Elliott, 'Stochastic optimal control: The discrete time case,' eng, *SIAM Review*, vol. 22, no. 2, pp. 237–238, 1980, ISSN: 0036-1445.

[45] D. P. Bertsekas, 'Dynamic programming and suboptimal control: A survey from adp to mpc,' eng, *European journal of control*, vol. 11, no. 4-5, pp. 310–334, 2005, ISSN: 0947-3580.

[46] P. J. Campo and M. Morari, 'Robust model predictive control,' in *1987 American Control Conference*, 1987, pp. 1021–1026. DOI: 10.23919/ACC.1987.4789462.

[47] S. Lucia, T. Finkler and S. Engell, 'Multi-stage nonlinear model predictive control applied to a semi-batch polymerization reactor under uncertainty,' eng, *Journal of Process Control*, vol. 23, no. 9, pp. 1306–1319, 2013, ISSN: 0959-1524.

[48] R. Martí, S. Lucia, D. Sarabia, R. Paulen, S. Engell and C. de Prada, 'Improving scenario decomposition algorithms for robust nonlinear model predictive control,' eng, *Computers chemical engineering*, vol. 79, pp. 30–45, 2015, ISSN: 0098-1354.

[49] E. Klintberg, J. Dahl, J. Fredriksson and S. Gros, 'An improved dual newton strategy for scenario-tree mpc,' *2016 IEEE 55th Conference on Decision and Control (CDC)*, pp. 3675–3681, 2016.

[50] C. Jeong and R. Sharma, 'Stochastic mpc for optimal operation of hydropower station under uncertainty,' eng, *IFAC PapersOnLine*, vol. 55, no. 7, pp. 155–160, 2022, ISSN: 2405-8963.

[51] N. Janatian and R. Sharma, 'Multi-stage scenario-based mpc for short term oil production optimization under the presence of uncertainty,' *Journal of Process Control*, vol. 118, pp. 95–105, 2022, ISSN: 0959-1524. DOI: https://doi.org/10.1016/j.jprocont.2022.08.012.

[52] M. Maiworm, T. Bäthge and R. Findeisen, 'Scenario-based model predictive control: Recursive feasibility and stability,' eng, in *IFAC-PapersOnLine*, vol. 48, 2015, pp. 50–56.

[53] B. Kouvaritakis and M. Cannon, 'Introduction,' in *Model Predictive Control: Classical, Robust and Stochastic*. Cham: Springer International Publishing, 2016, pp. 1–9, ISBN: 978-3-319-24853-0. DOI: 10.1007/978-3-319-24853-0_1. [Online]. Available: https://doi.org/10.1007/978-3-319-24853-0_1.

[54] F. Oldewurtel, A. Parisio, C. N. Jones *et al.*, 'Use of model predictive control and weather forecasts for energy efficient building climate control,' eng, *Energy and buildings*, vol. 45, pp. 15–27, 2012, ISSN: 0378-7788.

[55] Y. Ma, S. Vichik and F. Borrelli, 'Fast stochastic mpc with optimal risk allocation applied to building control systems,' eng, in *2012 IEEE 51st IEEE Conference on Decision and Control (CDC)*, IEEE, 2012, pp. 7559–7564, ISBN: 9781467320658.

[56] M. Cannon, B. Kouvaritakis and X. Wu, 'Probabilistic constrained mpc for multiplicative and additive stochastic uncertainty,' eng, *IEEE transactions on automatic control*, vol. 54, no. 7, pp. 1626–1632, 2009, ISSN: 0018-9286.

[57] P. Li, M. Wendt and G. Wozny, 'Robust model predictive control under chance constraints,' eng, *Computers chemical engineering*, vol. 24, no. 2, pp. 829–834, 2000, ISSN: 0098-1354.

[58] I. Jurado, P. Millán, D. Quevedo and F. Rubio, 'Stochastic mpc with applications to process control,' eng, *International journal of control*, vol. 88, no. 4, pp. 792–800, 2015, ISSN: 0020-7179.

[59] L. Blackmore, M. Ono and B. C. Williams, 'Chance-constrained optimal path planning with obstacles,' eng, *IEEE transactions on robotics*, vol. 27, no. 6, pp. 1080–1094, 2011, ISSN: 1552-3098.

[60] A. Gray, Y. Gao, T. Lin, J. K. Hedrick and F. Borrelli, 'Stochastic predictive control for semi-autonomous vehicles with an uncertain driver model,' eng, in *16th International IEEE Conference on Intelligent Transportation Systems (ITSC 2013)*, IEEE, 2013, pp. 2329–2334, ISBN: 9781479929146.

[61] D. Krishnamoorthy, B. A. Foss and S. Skogestad, 'A primal decomposition algorithm for distributed multistage scenario model predictive control,' eng, 2019, ISSN: 0959-1524.

[62] Z. Mdoe, D. Krishnamoorthy and J. Jaschke, 'Adaptive horizon multistage nonlinear model predictive control,' in *2021 American Control Conference (ACC)*, 2021, pp. 2088–2093. DOI: 10.23919/ACC50511.2021.9483183.

[63] S. Subramanian, S. Lucia, S. A. Baradaran Birjandi, R. Paulen and S. Engell, 'A combined multi-stage and tube-based mpc scheme for constrained linear systems the research leading to the results has received funding from the european commission under grant agreement number 291458 (mobocon).,' *IFAC-PapersOnLine*, vol. 51, no. 20, pp. 481–486, 2018, 6th IFAC Conference on Nonlinear Model Predictive Control NMPC 2018, ISSN: 2405-8963. DOI: https://doi.org/10.1016/j.ifacol.2018.11.043.

[64] C. M. Burt, R. S. Mills, R. D. Khalsa and V. R. C, 'Improved proportional-integral (pi) logic for canal automation,' eng, *Journal of irrigation and drainage engineering*, vol. 124, no. 1, pp. 53–57, 1998, ISSN: 0733-9437.

[65] P.-O. Malaterre, D. C. Rogers and J. Schuurmans, 'Classification of canal control algorithms,' eng, *Journal of irrigation and drainage engineering*, vol. 124, no. 1, pp. 3–10, 1998, ISSN: 0733-9437.

[66] P. J. van Overloop, J. Schuurmans, R. Brouwer and C. M. Burt, 'Multiple-model optimization of proportional integral controllers on canals,' eng, *Journal of irrigation and drainage engineering*, vol. 131, no. 2, pp. 190–196, 2005, ISSN: 0733-9437.

[67] W. W.-G. Yeh, 'Reservoir management and operations models: A state-of-the-art review,' *Water Resources Research*, vol. 21, no. 12, pp. 1797–1818, 1985. DOI: https://doi.org/10.1029/WR021i012p01797. eprint: https://agupubs.onlinelibrary.wiley.com/doi/pdf/10.1029/WR021i012p01797. [Online]. Available: https://agupubs.onlinelibrary.wiley.com/doi/abs/10.1029/WR021i012p01797.

[68] J. A. Tejada-Guibert, J. R. Stedinger and K. Staschus, 'Optimization of value of cvp's hydropower production,' *Journal of Water Resources Planning and Management*, vol. 116, no. 1, pp. 52–70, 1990. DOI: 10.1061/(ASCE)0733-9496(1990)116:1(52). eprint: https://ascelibrary.org/doi/pdf/10.1061/%28ASCE%290733-9496%281990%29116%3A1%2852%29. [Online]. Available: https://ascelibrary.org/doi/abs/10.1061/%28ASCE%290733-9496%281990%29116%3A1%2852%29.

[69] M. Breckpot, O. M. Agudelo and B. De Moor, 'Flood control with model predictive control for river systems with water reservoirs,' eng, *Journal of irrigation and drainage engineering*, vol. 139, no. 7, pp. 532–541, 2013, ISSN: 0733-9437.

[70] D. K. Delgoda, S. K. Saleem, M. N. Halgamuge and H. Malano, 'Multiple model predictive flood control in regulated river systems with uncertain inflows,' eng, *Water resources management*, vol. 27, no. 3, pp. 765–790, 2013, ISSN: 0920-4741.

[71] H. A. Nasir, A. Care and E. Weyer, 'A scenario-based stochastic mpc approach for problems with normal and rare operations with an application to rivers,' eng, *IEEE transactions on control systems technology*, vol. 27, no. 4, pp. 1397–1410, 2019, ISSN: 1063-6536.

[72] W. Zhou, H. M. Thoresen and B. Glemmstad, 'Application of kalman filter based nonlinear mpc for flood gate control of hydropower plant,' eng, in *2012 IEEE Power and Energy Society General Meeting*, IEEE, 2012, pp. 1–4, ISBN: 1467327271.

[73] J. M. Maestre, M. A. Ridao, A. Kozma *et al.*, 'A comparison of distributed mpc schemes on a hydro-power plant benchmark,' eng, *Optimal control applications methods*, vol. 36, no. 3, pp. 306–332, 2015, ISSN: 0143-2087.

[74] G. A. M. Munoz-Hernandez and D. Jones, 'Mimo generalized predictive control for a hydroelectric power station,' eng, *IEEE transactions on energy conversion*, vol. 21, no. 4, pp. 921–929, 2006, ISSN: 0885-8969.

[75] M. A. Perez-Villalpando, K. J. Gurubel Tun, C. A. Arellano-Muro and F. Fausto, 'Inverse optimal control using metaheuristics of hydropower plant model via forecasting based on the feature engineering,' eng, *Energies (Basel)*, vol. 14, no. 21, p. 7356, 2021, ISSN: 1996-1073.

[76] N. M. Lin, X. Tian, M. Rutten, E. Abraham, J. M. Maestre and N. van de Giesen, 'Multi-objective model predictive control for real-time operation of a multi-reservoir system,' eng, *Water (Basel)*, vol. 12, no. 7, p. 1898, 2020, ISSN: 2073-4441.

[77] R. Zhang, D. Chen and X. Ma, 'Nonlinear predictive control of a hydropower system model,' eng, *Entropy (Basel, Switzerland)*, vol. 17, no. 9, pp. 6129–6149, 2015, ISSN: 1099-4300.

[78] L. Vytvytskyi, R. Sharma and B. Lie, 'Model based control for run-of-river system. part 1: Model implementation and tuning,' eng, *Modeling, identification and control*, vol. 36, no. 4, pp. 237–249, 2015, ISSN: 0332-7353.

[79] L. Vytvytskyi, R. Sharma and B. Lie, 'Model based control for run-of-river system. part 2: Comparison of control structures,' eng, *Modeling, identification and control*, vol. 36, no. 4, pp. 251–263, 2015, ISSN: 0332-7353.

[80] R. Evensen, *Deterministic flood control using mpc on the kragerø waterways*, eng, 2015. [Online]. Available: `http://hdl.handle.net/11250/2439036`.

[81] B. Dhakal, *Stochastic flood control using mpc of kragerø waterways*, eng, 2015. [Online]. Available: `http://hdl.handle.net/11250/2439062`.

[82] C. A. Thilker, H. G. Bergsteinsson, P. Bacher, H. Madsen, D. Calì and R. G. Junker, 'Non-linear model predictive control for smart heating of buildings,' eng, in *E3S Web of Conferences*, vol. 246, Les Ulis: EDP Sciences, 2021, p. 9005.

[83] C. A. Thilker, H. Madsen and J. B. Jørgensen, 'Advanced forecasting and disturbance modelling for model predictive control of smart energy systems,' eng, *Applied energy*, vol. 292, p. 116 889, 2021, ISSN: 0306-2619.

[84] T. Hilliard, L. Swan and Z. Qin, 'Experimental implementation of whole building mpc with zone based thermal comfort adjustments,' eng, *Building and environment*, vol. 125, pp. 326–338, 2017, ISSN: 0360-1323.

[85] S. Prívara, J. Cigler, Z. Váňa, F. Oldewurtel, C. Sagerschnig and E. Žáčeková, 'Building modeling as a crucial part for building predictive control,' eng, *Energy and buildings*, vol. 56, pp. 8–22, 2013, ISSN: 0378-7788.

[86] D. Perera, C. F. Pfeiffer and N.-O. Skeie, 'Modelling the heat dynamics of a residential building unit: Application to norwegian buildings,' eng, *Modeling, identification and control*, vol. 35, no. 1, pp. 43–57, 2014, ISSN: 0332-7353.

[87] L. Ljung, 'Prediction error estimation methods,' eng, *Circuits, systems, and signal processing*, vol. 21, no. 1, pp. 11–21, 2002, ISSN: 0278-081X.

[88] M. Jiménez, H. Madsen and K. Andersen, 'Identification of the main thermal characteristics of building components using matlab,' eng, *Building and environment*, vol. 43, no. 2, pp. 170–180, 2008, ISSN: 0360-1323.

[89] K&KAssociates, *Thermal Network Modelling Handbook*, eng. Legacy CDMS, 1972.

[90] M. Jiménez, H. Madsen, J. Bloem and B. Dammann, 'Estimation of non-linear continuous time models for the heat exchange dynamics of building integrated photovoltaic modules,' eng, *Energy and buildings*, vol. 40, no. 2, pp. 157–167, 2008, ISSN: 0378-7788.

[91] O. Brastein, A. Ghaderi, C. Pfeiffer and N.-O. Skeie, 'Analysing uncertainty in parameter estimation and prediction for grey-box building thermal behaviour models,' eng, *Energy and buildings*, vol. 224, p. 110 236, 2020, ISSN: 0378-7788.

[92] O. Brastein, D. Perera, C. Pfeifer and N.-O. Skeie, 'Parameter estimation for grey-box models of building thermal behaviour,' eng, *Energy and buildings*, vol. 169, pp. 58–68, 2018, ISSN: 0378-7788.

[93] SkagerakKraft, *Kragerø watercourse system, (accessed: 22.10.2022)*, https://www.skagerakkraft.no/kragero-watercourse/category2391.html, 2022.

[94] SkagerakKraft, *Dalsfos, (accessed: 22.10.2022)*, https://www.skagerakkraft.no/dalsfos/category1277.html, 2022.

[95] NVE, *Supervision of dams, (accessed: 22.10.2022)*, https://www.nve.no/supervision-of-dams/?ref=mainmenu, 2022.

[96] K. D. Kvam, B. Furenes, Å. Hasaa, A. Z. Gjerseth, N.-O. Skeie and B. Lie, 'Flood control of lake toke: Model development and model fitting,' eng, 2017, ISSN: 1650-3686. [Online]. Available: http://hdl.handle.net/11250/2466966.

[97] S. Kraft, Nov. 2017. [Online]. Available: https://www.skagerakkraft.no/hjartdola/category1382.html.

[98] D. Perera and N.-O. Skeie, 'Estimation of the heating time of small-scale buildings using dynamic models,' eng, *Buildings (Basel)*, vol. 6, no. 1, p. 10, 2016, ISSN: 2075-5309.

[99] A. Simpkins, 'System identification: Theory for the user, 2nd edition (ljung, l.; 1999) [on the shelf],' eng, *IEEE Robotics Automation Magazine*, vol. 19, no. 2, pp. 95–96, 2012, ISSN: 1070-9932.

[100] A. T. Schwarm and M. Nikolaou, 'Chance-constrained model predictive control,' eng, *AIChE journal*, vol. 45, no. 8, pp. 1743–1752, 1999, ISSN: 0001-1541.

[101] T. A. N. Heirung, J. A. Paulson, J. O'Leary and A. Mesbah, 'Stochastic model predictive control — how does it work?' eng, *Computers chemical engineering*, vol. 114, pp. 158–170, 2018, ISSN: 0098-1354.

[102] D. Bernardini and A. Bemporad, 'Scenario-based model predictive control of stochastic constrained linear systems,' in *Proceedings of the 48h IEEE Conference on Decision and Control (CDC) held jointly with 2009 28th Chinese Control Conference*, 2009, pp. 6333–6338. DOI: 10.1109/CDC.2009.5399917.

[103] M. B. Saltık, L. Özkan, J. H. Ludlage, S. Weiland and P. M. Van den Hof, 'An outlook on robust model predictive control algorithms: Reflections on performance and computational aspects,' *Journal of Process Control*, vol. 61, pp. 77–102, 2018, ISSN: 0959-1524. DOI: https://doi.org/10.1016/j.jprocont.2017.10.006.

[104] C. Jeong, B. Furenes and R. Sharma, 'Multistage model predictive control with simplified scenario ensembles for robust control of hydropower station,' *Modeling, Identification and Control*, vol. 44, no. 2, pp. 43–54, 2023. DOI: 10.4173/mic.2023.2.1.

[105] C. Jeong and R. Sharma, 'Multistage model predictive control with simplified method on scenario ensembles of uncertainty for hjartdøla hydropower system,' eng, *The 7th IEEE Conference on Control Technology and Applications, Bridgetown, Barbados (Accepted)*, 2023.

[106] S. Schmutz and J. Sendzimir, *Riverine Ecosystem Management : Science For Governing Towards a Sustainable Future (Volume 8.0)* (Aquatic Ecology Series), eng. Cham: Springer Open, 2018, vol. 8, ISBN: 3319732498.

[107] R. J. Batalla, C. N. Gibbins, J. Alcázar *et al.*, 'Hydropeaked rivers need attention,' eng, *Environmental research letters*, vol. 16, no. 2, p. 21 001, 2021, ISSN: 1748-9318.

[108] S. D. Langhans, S. C. Jähnig, M. Lago, A. Schmidt-Kloiber and T. Hein, 'The potential of ecosystem-based management to integrate biodiversity conservation and ecosystem service provision in aquatic ecosystems,' eng, *The Science of the total environment*, vol. 672, pp. 1017–1020, 2019, ISSN: 0048-9697.

[109] C. Jeong, B. Furenes and R. Sharma, 'MPC operation with improved optimal control problem at dalsfoss power plant.,' *Proceedings of SIMS EUROSIM conference 2021*, vol. 11, no. 1, pp. 226–233, 2021. DOI: 10.3384/ecp21185226.

[110] C. Jeong and R. Sharma, 'Tuning model predictive control for rigorous operation of the dalsfoss hydropower plant,' eng, *Energies (Basel)*, vol. 15, no. 22, p. 8678, 2022, ISSN: 1996-1073.

[111] J. A. E. Andersson, J. Gillis, G. Horn, J. B. Rawlings and M. Diehl, 'CasADi – A software framework for nonlinear optimization and optimal control,' *Mathematical Programming Computation*, vol. 11, no. 1, pp. 1–36, 2019. DOI: 10.1007/s12532-018-0139-4.

[112] N. R. Kristensen, H. Madsen and S. B. Jørgensen, 'Parameter estimation in stochastic grey-box models,' eng, *Automatica (Oxford)*, vol. 40, no. 2, pp. 225–237, 2004, ISSN: 0005-1098.

[113] G. Reynders, J. Diriken and D. Saelens, 'Quality of grey-box models and identified parameters as function of the accuracy of input and observation signals,' eng, *Energy and buildings*, vol. 82, pp. 263–274, 2014, ISSN: 0378-7788.

[114] A. Afram and F. Janabi-Sharifi, 'Gray-box modeling and validation of residential hvac system for control system design,' eng, *Applied energy*, vol. 137, pp. 134–150, 2015, ISSN: 0306-2619.

[115] S. F. Fux, A. Ashouri, M. J. Benz and L. Guzzella, 'Ekf based self-adaptive thermal model for a passive house,' eng, *Energy and buildings*, vol. 68, pp. 811–817, 2014, ISSN: 0378-7788.

[116] D. Perera, M. Halstensen and N.-O. Skeie, 'Prediction of space heating energy consumption in cabins based on multivariate regression modelling,' *International Journal of Modeling and Optimization*, vol. 5, pp. 385–392, Jan. 2015. DOI: 10.7763/IJMO.2015.V5.493.

[117] K. H. Esbensen, *Multivariate data analysis - in practice : An introduction to multivariate data analysis and experimental design*, eng, Oslo, 2000.

[118] A. Harby and M. Noack, 'Rapid flow fluctuations and impacts on fish and the aquatic ecosystem,' eng, in *Ecohydraulics*, Chichester, UK: John Wiley Sons, Ltd, 2013, pp. 323–335, ISBN: 0470976004.

[119] T. Consulting, *Hvor godt utnytter norske magasinkraftverk potensial for effektkjøring?* https://publikasjoner.nve.no/eksternrapport/2022/eksternrapport2022_02.pdf, 2022.

[120] N. Janatian and R. Sharma, 'Multi-stage scenario-based mpc for short term oil production optimization under the presence of uncertainty,' eng, *Journal of process control*, vol. 118, pp. 95–105, 2022, ISSN: 0959-1524.

[121] S. M. Zanoli, C. Pepe, G. Astolfi and F. Luzi, 'Reservoir advanced process control for hydroelectric power production,' *Processes*, vol. 11, no. 2, 2023, ISSN: 2227-9717. DOI: 10.3390/pr11020300. [Online]. Available: https://www.mdpi.com/2227-9717/11/2/300.

[122] M. Morari, C. E. Garcia and D. M. Prett, 'Model predictive control: Theory and practice,' *IFAC Proceedings Volumes*, vol. 21, no. 4, pp. 1–12, 1988, IFAC Workshop on Model Based Process Control, Atlanta, GA, USA, 13-14 June, ISSN: 1474-6670. DOI: https://doi.org/10.1016/B978-0-08-035735-5.50006-1. [Online]. Available: https://www.sciencedirect.com/science/article/pii/B9780080357355500061.

[123] S. Qin and T. Badgwell, 'An overview of industrial model predictive control technology,' in *Chemical Process Control–V, CACHE, AIChE*, 1997, pp. 232–256.

[124] A. E. Bryson, Y.-C. Ho and G. M. Siouris, 'Applied optimal control: Optimization, estimation, and control,' eng, *IEEE transactions on systems, man, and cybernetics*, vol. 9, no. 6, pp. 366–367, 1979, ISSN: 0018-9472.

[125] E. Polak, 'Computational methods in optimization: A unified approach,' 1971, ISSN: 0076-5392. DOI: https://doi.org/10.1016/S0076-5392(08)63019-2. [Online]. Available: https://www.sciencedirect.com/science/article/pii/S0076539208630192.

[126] T. Barjas Blanco, P. Willems, P.-K. Chiang, N. Haverbeke, J. Berlamont and B. De Moor, 'Flood regulation using nonlinear model predictive control,' eng, *Control engineering practice*, vol. 18, no. 10, pp. 1147–1157, 2010, ISSN: 0967-0661.

[127] T. Binder, L. Blank, H. G. Bock *et al.*, 'Introduction to model based optimization of chemical processes on moving horizons,' in *Online Optimization of Large Scale Systems*, M. Grötschel, S. O. Krumke and J. Rambau, Eds. Berlin, Heidelberg: Springer Berlin Heidelberg, 2001, pp. 295–339, ISBN: 978-3-662-04331-8. DOI: 10.1007/978-3-662-04331-8_18. [Online]. Available: https://doi.org/10.1007/978-3-662-04331-8_18.

[128] C. Kirches, H. G. Bock, J. P. Schlöder and S. Sager, 'Block-structured quadratic programming for the direct multiple shooting method for optimal control,' eng, *Optimization methods software*, vol. 26, no. 2, pp. 239–257, 2011, ISSN: 1055-6788.

[129] C. Rao, S. Wright and J. Rawlings, 'Application of interior-point methods to model predictive control,' eng, *Journal of optimization theory and applications*, vol. 99, no. 3, pp. 723–757, 1998, ISSN: 0022-3239.

[130] Y. Nesterov, *Introductory Lectures on Convex Optimization: A Basic Course*, 1st ed. Springer Publishing Company, Incorporated, 2014, ISBN: 1461346916.

[131] S. Richter, M. Morari and C. N. Jones, 'Towards computational complexity certification for constrained mpc based on lagrange relaxation and the fast gradient method,' eng, in *2011 50th IEEE Conference on Decision and Control and European Control Conference*, IEEE, 2011, pp. 5223–5229, ISBN: 9781612848006.

[132] M. Korda and C. N. Jones, 'Certification of fixed computation time first-order optimization-based controllers for a class of nonlinear dynamical systems,' eng, in *2014 American Control Conference*, American Automatic Control Council, 2014, pp. 3602–3608, ISBN: 1479932728.

[133] A. Wächter and L. Biegler, 'On the implementation of an interior-point filter line-search algorithm for large-scale nonlinear programming,' English (US), *Mathematical Programming*, vol. 106, no. 1, pp. 25–57, May 2006, Copyright: Copyright 2008 Elsevier B.V., All rights reserved., ISSN: 0025-5610. DOI: 10.1007/s10107-004-0559-y.

[134] L. T. Biegler, 'A survey on sensitivity-based nonlinear model predictive control,' eng, *IFAC Proceedings Volumes*, vol. 46, no. 32, pp. 499–510, 2013, ISSN: 1474-6670.

[135] M. Namazov and A. Alili, 'Design of stable takagi sugeno fuzzy control system for three interconnected tank system via lmis with constraint on the output,' eng, *IFAC PapersOnLine*, vol. 51, no. 30, pp. 721–726, 2018, ISSN: 2405-8963.

[136] C. Arnold, T. Aissa and S. Lambeck, 'Implicit regulator calculation for regular mimo-systems with predictive functional control demonstrated at a three tank system,' eng, *IFAC Proceedings Volumes*, vol. 47, no. 3, pp. 5375–5380, 2014, ISSN: 1474-6670.

[137] M. Essahafi, 'Model predictive control (mpc) applied to coupled tank liquid level system,' eng, 2014.

Part II

Appendix A

MPC Operation with Improved Optimal Control Problem at Dalsfoss power

Published in *Proceeding of The First SIMS EUROSIM Conference on Modelling and Simulation, SIMS EUROSIM 2021, and 62nd International Conference of Scandinavian Simulation Society, SIMS 2021*, September 21-23, Virtual Conference, Finland, 2021.
Paper presented by Changhun Jeong.
Authors: Changhun Jeong, Beathe Furenes, and Roshan Sharma.
Authors' roles in the article:
Changhun Jeong: Main ideas, implementation, and writing.
Beathe Furenes: Discussions, comments
Roshan Sharma (Supervisor): Discussions, comments, and proofreading.

MPC Operation with Improved Optimal Control Problem at Dalsfoss Power Plant

Changhun Jeong[1] Beathe Furenes[2] Roshan Sharma[1]

[1]Natural Sciences and Maritime Sciences Department of Electrical engineering, Information Technology and Cybernetics, University of South-Eastern Norway, Porsgrunn, Norway
{Changhun.Jeong,Roshan.Sharma}@usn.no
[2]Skagerak Kraft AS, Norway

Abstract

The operational conditions at the Dalsfoss power station are complicated due to many requirements such as environmental regulations and safety constraints. Model predictive control (MPC) has been in use at this power station to control the floodgates at the Dalsfoss dam. However, the current formulation of MPC at the power plant does not have routines to explicitly handle output constraints. In this paper, a new improved optimal control problem (OCP) is formulated for the operation of the flood gates at the Dalsfoss power station. This new OCP formulation is thought to be relatively easier for the operators to understand and it is more flexible to the violation of constraints. The aim of this paper is to extend the current MPC used at the power plant so that the output constraints are systematically included in the new improved MPC formulation. Two alternatives are presented and their robustness to an uncertain disturbance is analyzed through robustness analysis.

Keywords: Model predictive control, optimal control problem, flood management, uncertainty, robustness analysis

1 Introduction

Kragerø watercourse is one of many watercourse systems that Skagerak Kraft operates. The watercourse contains one dam and five hydropower stations which are located between lake Toke and the sea sequentially along the watercourse as shown in Figure 1. Its catchment area is over 1200 square kilometres and lies mainly in Telemark, Norway. The uppermost power plant is the Dalsfoss power plant which is located next to the dam (SkagerakKraft, 2021b). The system has intakes to three turbines and two flood gates (SkagerakKraft, 2021a).

Skagerak Kraft is fully responsible for the safety of the operations at the Dalsfoss power station. Therefore, requirements by the Norwegian Water Resource and Energy Administration (NVE) must be complied with to ensure safe and environmental-friendly operation. Some of these requirements are environmental-related and are imposed to prevent damages to the inhabitants and the ecosystem

Figure 1. Overview of the Kragerø watercourse (SkagerakKraft, 2021b).

around the water system. One of the most important constraints is to maintain the level of water at Merkebekk within a specific range. The range is not constant and changes over the months within a year (NVE, 2021). It is not easy to satisfy the requirement all the time during the operation due to two uncertainties in the system. One is the power production plan to meet the energy demand. The other is the water inflow to the lake/dam. Skagerak Kraft creates the power production plan and uses it to operate the plant. Water inflow to the lake is predicted by using a complex hydrological model and weather forecast information. As the result, the predicted water inflow is given as 50 possible future scenarios for the next 13 days.

MPC is known as an attractive multivariable constrained control approach with its ability to effectively deal with the complex dynamics of systems with multiple inputs and outputs and constraints. (Morari and H. Lee, 1999; Mayne, 2014). Therefore, a reference region tracking MPC based on a mathematical model of the system was suggested for the operation of the Dalsfoss power station (Lie, 2014). More research has been conducted since the first MPC was suggested in 2014. A better parameter fitting on the model was suggested due to a poor description of the model during a severe flood in September 2015

(Kvam et al., 2017). To obtain optimal operation under the uncertainty of water inflow, the use of multi-objective optimization (MOO) MPC was investigated with the OCP used in the reference region tracking MPC (Menchacatorre et al., 2019).

However, in the works of Lie (2014) and Menchacatorre et al. (2019) the water level at the dam (which is an output of the system under consideration) has not been explicitly handled as an output constraint, but is rather dealt indirectly using a complex cost/objective function during the formulation of the control problem. In this paper, two alternatives have been proposed to handle the concession requirements of the level at the dam by explicitly considering them as output constraint. Pros and cons of these two alternatives are discussed thoroughly in Section 3.

2 System Description

2.1 System model

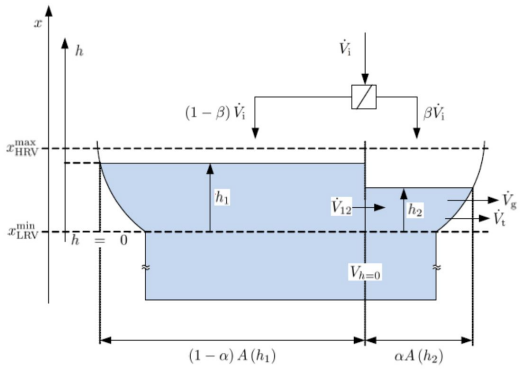

Figure 2. Schematic of lake Toke (Lie, 2014)

Figure 2 depicts a simplified layout of the lake Toke. The layout is divided into two parts. The left side of the layout represents the upper stream of lake Toke, Merkebekk. The right side describes the lower stream of lake Toke, near the Dalsfoss dam.

h_1 and h_2 are the height of water level above the minimal low regulated level value, $x^{\min}_{\mathrm{LRV}}$, at Merkebekk and Dalsfoss respectively. The water levels are states of the system. $\dot{V}_\mathrm{i}$ is the time-varying volumetric flow into Lake Toke from its catchment. $\dot{V}_\mathrm{i}$ is split to both Merkebekk and Dalsfoss as shown in Figure 2. Skagerak Kraft has a hydrological model to calculate $\dot{V}_\mathrm{i}$ with the weather forecast information they subscribe to. It is an input disturbance to the system. The other disturbance is the power demand denoted as W_e. It is scheduled by specialists in Skagerak Kraft. W_e is used to calculate the turbine flow, $\dot{V}_\mathrm{t}$, which means the required water flow rate to generate electrical power. $\dot{V}_\mathrm{t}$ is limited as operational condition by $36\mathrm{m}^3/\mathrm{s}$. $\dot{V}_\mathrm{g}$ is the flow rate through floodgates. Water that flows through flood gates does not produce any electrical power since they are not sent through turbines but simply discarded from the dam. Ideally, the flood gates should be kept closed as much as possible to conserve water in the dam for energy production and they should be activated only in a flood situation to satisfy concession requirements. Figure 3 shows the simplified schematic of the floodgate at the Dalsfoss dam. The gate opening height denoted h_g is the control input for the system.

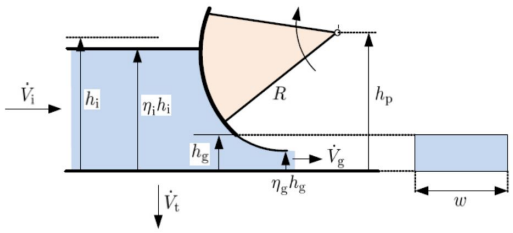

Figure 3. Structure of floodgate (Lie, 2014)

The model of lake Toke was developed and its update has been suggested (Lie, 2014; Kvam et al., 2017). A summary of the model follows:

The heights of water level relative to sea level at Merkebekk and Dalsfoss, denoted x_M and x_D, are given by:

$$x_\mathrm{M} = h_1 + x^{\min}_{\mathrm{LRV}} \tag{1}$$

$$x_\mathrm{D} = h_2 + x^{\min}_{\mathrm{LRV}} \tag{2}$$

The area of the surface curve at lake Toke is calculated as:

$$A(h) = \max(28\times 10^6 \cdot 1.1 \cdot h^{\frac{1}{10}}, 10^3) \tag{3}$$

Inter compartment flow $\dot{V}_{12}$ is expressed as:

$$\dot{V}_{12} = K_{12}\cdot(h_1 - h_2)\sqrt{|h_1 - h_2|} \tag{4}$$

where K_{12} is Inter compartment flow coefficient.
The equation to calculate $\dot{V}_\mathrm{t}$ from the electrical power demand W_e is:

$$\dot{V}_\mathrm{t} = a\frac{\dot{W}_\mathrm{e}}{x_\mathrm{D} - x_\mathrm{q}} + b \tag{5}$$

where a and b are coefficients from data fitting. x_q means downstream level after the turbine which can be obtained by solving the following cubic equation:

$$\begin{aligned} 0 = {} & c_1 x_\mathrm{q}^3 + (c_2 - c_1 x_\mathrm{D}) x_\mathrm{q}^2 \\ & + (c_3 - c_2 x_\mathrm{D} + c_4 \dot{V}_\mathrm{g}) x_\mathrm{q} \\ & + \dot{W}_\mathrm{e} - c_3 x_\mathrm{D} - c_4 \dot{V}_\mathrm{g} x_\mathrm{D} - c_5 \end{aligned} \tag{6}$$

where c_1, c_2, c_3, c_4, and c_5 are coefficient obtained from polynomial model fitting.
At Dalsfoss power plant there are two flood gates. The model for flow rate through floodgate j, $\dot{V}_{\mathrm{g},j}$, is:

$$\dot{V}_{\mathrm{g},j} = C_\mathrm{d} w_j \cdot \min(h_\mathrm{g}, h_2)\sqrt{2g\cdot\max(h_2, 0)} \tag{7}$$

where C_d is discharge coefficient and g is acceleration of gravity.
The total water outflow from the Dalsfoss power station, $\dot{V}_o$, is calculated as:

$$\dot{V}_o = \dot{V}_t + \sum^{j} \dot{V}_{g,j} \tag{8}$$

The dynamic model of states, h_1 and h_2, are expressed as:

$$\frac{dh_1}{dt} = \frac{1}{(1-\alpha)A(h_1)}((1-\beta)\dot{V}_i - \dot{V}_{12}) \tag{9}$$

$$\frac{dh_2}{dt} = \frac{1}{\alpha A(h_1)}(\beta\dot{V}_i + \dot{V}_{12} - \dot{V}_t - \dot{V}_g) \tag{10}$$

Parameters for the model are given in Table 1.

2.2 Operational constraints

Operational constraints on lake Toke are specified by NVE. They are designed to achieve (i) operational safety, (ii) securing ecological diversity, and (iii) avoiding property damage, e.g., by maintaining certain minimum and maximum levels at Merkebekk. The key constraints for a flood situation are:

1. The total water outflow from the Dalsfoss power station, V_o, should remain as steady as possible. This requirement is to keep people and animals safe from the sudden change of the water outflow and level at the downstream.

2. The minimum flow rate of the total water outflow should be bigger than $4\mathrm{m}^3/\mathrm{s}$. This restriction is not to disturb the ecosystem in the downstream, e.g to allow fishes to move freely, etc.

3. The water level at Merkebekk, x_M, must stay within a range:

$$x_M \in [x_{LRV}, x_{HRV}]$$

   where x_{LRV} and x_{HRV} denote the low regulated value and the high regulated value for the water level respectively. The seasonal change on level constraints throughout a year is briefly shown in Figure 4. This level constraint exists for not disturbing fauna along the shoreline, but also to prevent damages or inconvenience such as flooding properties or putting boats on dry land, etc. This constraint can be violated to satisfy the second constraint by going lower than x_{LRV} . However, the level of water at Merkebekk should never exceed the maximal high regulated value denoted as x_{HRV}^{max}.

4. When severe flooding occurs x_M can exceed x_{HRV}. However, after the culmination of flooding ends, x_M must reach x_{HRV} as soon as possible.

5. When the winter operation is terminated, the water level in the reservoir must reach x_{LRV}^{summer} quickly. However, the flow rate at the downstream, V_o, is limited to $20\mathrm{m}^3/\mathrm{s}$ until the water level is at the target level.

6. Although there is the minimum required flow rate at the downstream, $V_o \geq 4\mathrm{m}^3/\mathrm{s}$, it is more beneficial economically to have the flow rate larger than $10\mathrm{m}^3/\mathrm{s}$, which enables the operation of the four sequentially located power plants along the watercourse.

The fourth and fifth constraints mentioned above requires the judgement of the professional on sites such as when flooding begins and when the winter operation is completed. Therefore, in this paper, the two constraints are not considered.

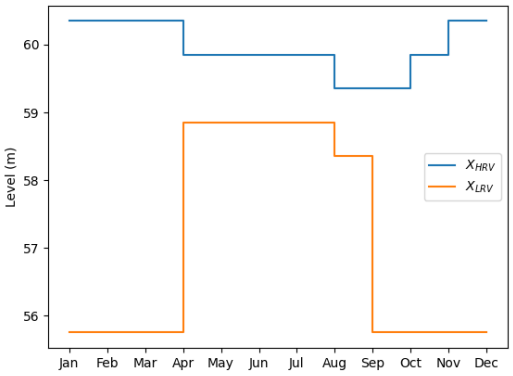

Figure 4. Water level constraint changes throughout year

3 Optimal Control Formulation

In this section, two alternative OCP formulations to improve the the current MPC used at Dalsfoss hydropower plant are presented. These two alternative MPC formulations can be regarded as extensions of the current MPC.

3.1 Reference region tracking OCP with output constraints

In the reference region tracking MPC currently being used at Dalsfoss, the water level at the dam is controlled to lie between the upper and the lower limits (see Figure 4) by formulating a complex objective function containing a reference region as,

$$\min \sum_{i=1}^{N} \omega_R R^2(x_{t+i}) + \omega_{\Delta u} \Delta u_{c,t+i-1}^2 + \omega_u u_{c,t+i-1}^2 \tag{11}$$

Here ω is a weight matrix and N is length of the prediction horizon. u is control input and it has operational constraint such as $u_{c,i} \in [0, h_{g,max}]$. $h_{g,max}$ means the maximal

Table 1. Parameters for Lake Toke model

Parameter	Value	Unit	Comment
α	0.05	-	Fraction of surface area in compartment 2
β	0.02	-	Fraction of inflow to compartment 2
K_{12}	800	$\mathrm{m}^{\frac{3}{2}}/\mathrm{s}$	Inter compartment flow coefficient
C_d	0.7	-	Discharge coefficient, Dalsfoss gate
w_1	11.6	m	Width of Dalsfoss gate 1
w_2	11.0	m	Width of Dalsfoss gate 2
$x_{\mathrm{LRV}}^{\min}$	55.75	m	Minimal low regulated level value
$x_{\mathrm{HRV}}^{\max}$	60.35	m	Maximal high regulated level value
g	9.81	$\mathrm{m/s}^2$	Acceleration of gravity

allowed opening height of the floodgate. Δu denotes the gate opening changes which is:

$$\Delta u_{\mathrm{c},t} = u_{\mathrm{c},t} - u_{\mathrm{c},t-1} \tag{12}$$

The level reference term in Equation 11, $R^2(x_{t+i})$, is expressed as:

$$R(x_{t+1}) = \min(x_{\mathrm{M},t+1} - \gamma_{t+i}^{\mathrm{l}}, 0) + \max(x_{\mathrm{M},t+1} - \gamma_{t+i}^{\mathrm{u}}, 0) \tag{13}$$

where $\gamma_{t+i}^{\mathrm{l}}$ and $\gamma_{t+i}^{\mathrm{u}}$ work as lower and upper boundaries of the reference region. They are calculated by:

$$\gamma_i^{\mathrm{l}} = (1 - X_\mathrm{R}) x_{\mathrm{LRV},i} + X_\mathrm{R} x_{\mathrm{HRV},i} \tag{14}$$

$$\gamma_i^{\mathrm{u}} = f(x_{\mathrm{HRV}}) - \delta_{\mathrm{HRV}} \tag{15}$$

where X_R and δ_{HRV} are the variable inputs that engineers can put their insight into. A typical value for X_R is 0.75. The purpose of δ_{HRV} is to have a slight margin wrt. the maximal allowed level for x_M. $f(x_{\mathrm{HRV}})$ is decided based on whether excessive flooding occurs or not as follow:

$$f(x_{\mathrm{HRV}}) = \begin{cases} x_{\mathrm{HRV}}^{\max}, & \text{for excessive flooding} \\ x_{\mathrm{HRV}} & \text{otherwise} \end{cases}$$

The reference level term in Equation 11 becomes zero when the water level at Merkebekk stays in the reference range defined by Equations 14 and 15. The reference term is only activated when the water level is outside of the reference range. Therefore, the weight on the use of floodgates (i.e. control inputs) and the rate of change of control inputs are more emphasized when the water level remains in the specified reference range. In this formulation, the only constraints are the input constraints, and the constraints on the water level are really only handled as a complex cost function. It is a well-known fact that only using a cost function does not guarantee constraint satisfaction. In this paper, the addition of output constraints on the water level at Merkebekk is suggested as,

$$x_{\mathrm{LRV}} \leq x_\mathrm{M} \leq f(x_{\mathrm{HRV}})$$

3.2 New OCP with constraint relaxation

When handling the flood gates, care should be taken that the water from the dam is not let out through flood gates unnecessarily. This would result in loss of water which otherwise could be used to produce electricity. In this sense, saving as much water as possible (i.e. having as high water level as possible) in the dam while still satisfying the concession requirements also becomes necessary. In this newly formulated OCP, the objective function is designed to maximize the water level at Merkebekk and is simpler compared to the objective function in the reference region tracking OCP, Equation 11 as:

$$\min \sum_{i=1}^{N} \omega_\mathrm{R} R_{\mathrm{new}}^2(x_{t+i}) + \omega_{\Delta\mathrm{u}} \Delta u_{\mathrm{c},t+i-1}^2 + \omega_\mathrm{u} u_{\mathrm{c},t+i-1}^2 + p^2 \omega_\mathrm{p} \tag{16}$$

The new reference term in Equation 16 is expressed as:

$$R_{\mathrm{new}}(x_{t+1}) = x_{\mathrm{M},t+1} - f(x_{\mathrm{HRV}}) v \tag{17}$$

Equation 17 is simpler than Equation 13. It is not only more effective to preserve the water as much as possible in the reservoir, but also easier for operators and engineers to understand.

The last term, $p^2\omega_p$ which is the penalty for violation of level constraints, is newly added. The variable p is the slack variable which is used to modify the level constraints as:

$$x_{\mathrm{LRV}} + p \leq x_\mathrm{M} \leq f(x_{\mathrm{HRV}})$$

The value of the slack variable is automatically decided by the optimizer since it is added to the list of the decision variable (Sharma, 2020). This term can offer more flexibility on optimization when the constraints are violated, for example when x_M goes lower than x_{LRV} to satisfy the minimum flow rate requirement on the total outflow, $V_\mathrm{o} = 4\mathrm{m}^3/\mathrm{s}$, the optimization would not fail (due to infeasibility) and cause the malfunction of the controllers in the system.

4 Simulation of Nominal MPC

This section presents the simulation results of nominal MPC using the two alternative OCP formulations as described in Section 3. For the simulation, the two disturbances, the power production plan and the water inflow to the lake Toke must be described.

For the simplicity of the simulation, the power production plan is assumed to generate maximum power. This can be achieved by setting a fixed value on V_t as $36\text{m}^3/\text{s}$. This is the maximum flow rate that can pass through the turbine at Dalsfoss hydropower station.

The actual data of water inflow prediction stored by Skagerak Kraft is applied for the simulation. The water inflow prediction is given each day as 50 possible future scenarios for the next 13 days. An example of the water inflow prediction is shown in Figure 5. It is the historical inflow prediction data recorded on 15th April 2020. The deviation of the inflow prediction tends to be bigger as time marches further into the future. The prediction data can be expressed in matrix form as Equation 18.

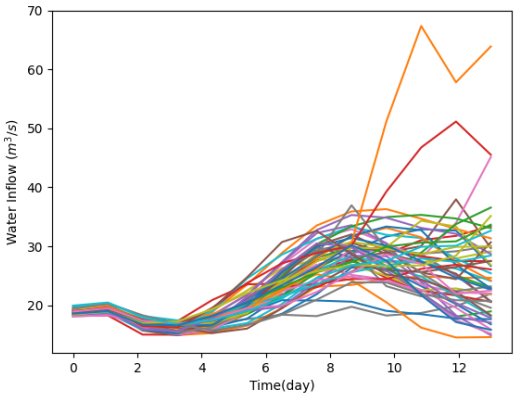

Figure 5. 50 ensembles of the water inflow prediction to lake Toke on April 15 2020

$$\dot{V}_{\text{i},t} = \begin{pmatrix} \dot{V}_{\text{i},t}^{(1)} & \dot{V}_{\text{i},t}^{(2)} & \cdots & \dot{V}_{\text{i},t}^{(50)} \\ \dot{V}_{\text{i},t+1}^{(1)} & \dot{V}_{\text{i},t+1}^{(2)} & \cdots & \dot{V}_{\text{i},t+1}^{(50)} \\ \vdots & \vdots & \ddots & \vdots \\ \dot{V}_{\text{i},t+12}^{(1)} & \dot{V}_{\text{i},t+12}^{(2)} & \cdots & \dot{V}_{\text{i},t+12}^{(50)} \end{pmatrix} \tag{18}$$

The rows in Equation 18 shows the time evolution of the water inflow prediction and the column represents the different 50 possible scenarios of water inflows. The prediction of the inflow to the lake is updated every 24 hours. For simulation of nominal MPC, the average value of the water inflow prediction is used. It is calculated as:

Table 2. Parameters for the simulations

Parameter	Value	Unit
X_{R}	0.75	-
δ_{HRV}	0.05	m
ω_{R}	10	-
$\omega_{\Delta\text{u}}$	1	-
ω_{u}	1	-
ω_{p}	100	-
$h_{\text{g,max}}$	5.6	m

$$\dot{V}_{\text{avg},t} = \begin{pmatrix} \text{Mean}(\dot{V}_{\text{i},t}^{(1)} & \dot{V}_{\text{i},t}^{(2)} & \cdots & \dot{V}_{\text{i},t}^{(50)}) \\ \text{Mean}(\dot{V}_{\text{i},t+1}^{(1)} & \dot{V}_{\text{i},t+1}^{(2)} & \cdots & \dot{V}_{\text{i},t+1}^{(50)}) \\ \vdots & \vdots & \ddots & \vdots \\ \text{Mean}(\dot{V}_{\text{i},t+12}^{(1)} & \dot{V}_{\text{i},t+12}^{(2)} & \cdots & \dot{V}_{\text{i},t+12}^{(50)}) \end{pmatrix} \tag{19}$$

The average is calculated on each time step with a new set of the water inflow prediction. The water inflow prediction based on the historical data is multiplied by a flood coefficient to simulate the flooding situations. The flood coefficient is set as 3 for the nominal MPC.

The period of simulation is set from April 15 to May 15 and includes a drastic change of the level constraints at Merkebekk. The simulation is performed with two different initial points for the water level to demonstrate two different situations. One initial point for the water level is located lower than the reference region and the other initial point is located in the reference region. Parameters for the OCPs are presented in Table 2. For the optimization, IPOPT in CasADi is used in Python (Andersson et al., 2019).

4.1 Simulation result: Initial water level below the reference region

Figure 6 shows the result of the simulation of nominal MPC at Dalsfoss power station using the reference region tracking MPC with output constraints when the initial water level at Merkebekk is below the reference region. The upper figure shows the level control and the lower figure shows the control actions during the simulation. The floodgate is supposed to remain closed to make the water level reach the reference region. However, floodgates are drastically opened several times and remain opened. It causes the water level to drop since the water is being thrown out from the reservoir. This abnormal action is due to the optimization problem becoming infeasible and the time-varying level constraints not being satisfied at such low water level. The optimizer then fails to find an optimal solution and produces incorrect and abnormal results.

Figure 7 shows the result of the simulation of nominal MPC using the newly formulated OCP with constraint relaxation as described in Section 3.2. The upper plot in Figure 7 represents the level changes and the lower plot shows the floodgate openings during the simulation. Thanks to

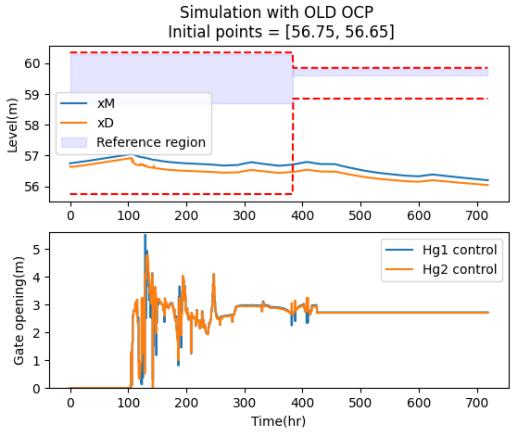

Figure 6. Simulation result of MPC at Dalsfoss station using the reference region tracking OCP with output constraints for initial water level lower than reference region. (upper plot - level control, lower plot - floodgate opening)

the penalty term, $p^2\omega_p$, in Equation 16, in the newly formulated OCP, output constraint (water level) relaxation is possible due to the use of slack variables. This does not cause any failures of optimization problem during the simulation. Therefore, as it is supposed to be, the floodgate stays closed. Despite the violation of the level constraint at around 380 hours, the water level is maximized and the level constraints are satisfied later at around 400 hours. The reason that the level constraint (lower constraint) is not fulfilled at ca. 380 hours is due to the control signals being saturated. The flood gates are completely closed and the inflow to the lake is not sufficiently large. Under this circumstance, this is the best the new OCP can perform without failing due to constraint relaxation.

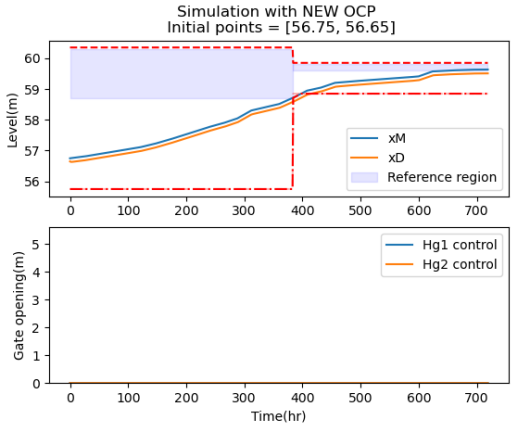

Figure 7. Simulation result of MPC at Dalsfoss station using the new OCP with constraint relaxation for initial water level lower than reference region. (upper plot - level control, lower plot - floodgate opening)

4.2 Simulation result: Initial water level in the reference region

Figure 8 shows the simulation result of nominal MPC using the reference region tracking MPC with output constraints. The initial point for the water level at Merkebekk is located inside of the reference region. The upper plot in Figure 8 shows the level change and the lower plot shows the gate openings during the simulation. The water level remains nearly constant but the water level is not maximized. The gate stays constantly opened and thus results in unnecessary loss of water through the flood gates.

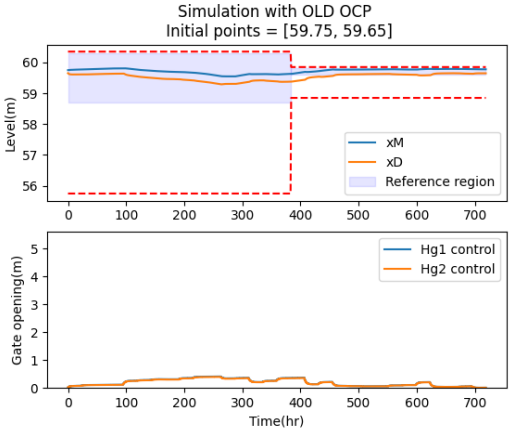

Figure 8. Simulation result of MPC at Dalsfoss station using the reference region tracking MPC with output constraints for initial water level in reference region. (upper plot - level control, lower plot - floodgate opening)

The simulation result of nominal MPC using the new OCP with constraint relaxation with an initial water level lying inside of the reference region is displayed in Figure 9. The upper plot shows the level change and the lower plot shows the gate openings during the simulation. The water level is maximized as intended to save as much useful water as possible in the dam. Achieving a higher level at the dam while still satisfying the concession requirement means more water is preserved in the reservoir, and this extra water can then be sent through the turbine later on to produce useful electric power (increased profit). This shows that the new OCP with constraint relaxation results in an improved operation of the hydropower plant.

5 Robustness Analysis

The realization of all possible water inflow, which means the first data of water inflow prediction on every update of the prediction every day, is presented in Figure 10.

With robustness analysis, the goal is to use the nominal MPC to all the individual 50 ensembles of the water inflow predictions. In order words, robustness analysis enables us to study the effect of applying a nominal/deterministic MPC to an uncertain system. Here uncertainty lies in the fact that any one of the 50 possible inflow forecasts can occur in the future in the real plant. The robustness analy-

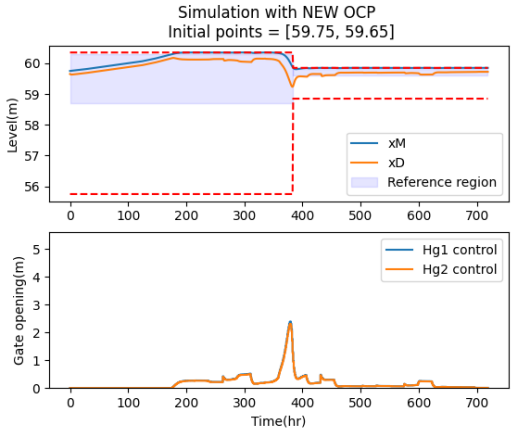

Figure 9. Simulation result of MPC at Dalsfoss station using the new OCP with constraint relaxation for initial water level in reference region. (upper plot - level control, lower plot - floodgate opening)

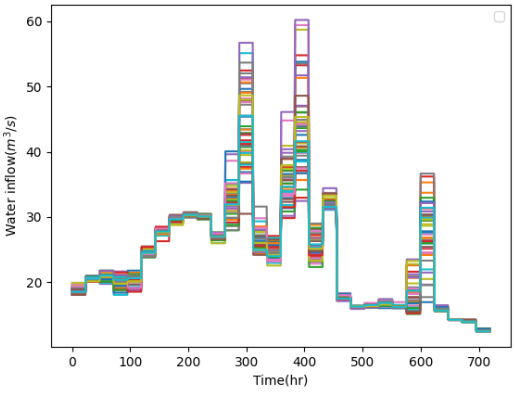

Figure 10. Plot of water inflow prediction

sis shows the possibility of constraint violation due to the influence of uncertainty. Since there are significant deviations in the realization of water inflow in each scenario, this section presents the result of the robustness analysis of nominal MPC using both OCPs as described in Section 3 at the Dalsfoss power station.

For robustness analysis, the nominal scenario must be chosen to get a sequence of the applied control input throughout the simulation time. Then, the sequence of the applied control input is used to evolve the states with different inflow forecast scenarios of the uncertainty by the system model as shown in Figure 11. The first scenario of water inflow prediction, $(\dot{V}^{(1)}_{\mathrm{i},t}, \cdots, \dot{V}^{(1)}_{\mathrm{i},t+12})$ in Equation 18, is chosen as the nominal prediction set and the other scenarios are considered as the possible future occurrences.

The flooding coefficient is set as 3 for the analysis. The initial water levels are located inside of the reference region so that the OCP for the reference region tracking MPC with output constraints does not fail to converge due to the violation of the time-varying level constraints (i.e., due to infeasibility).

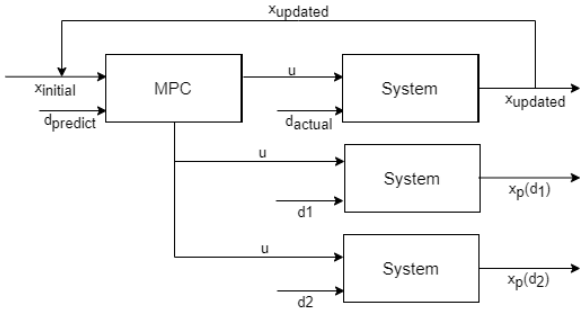

Figure 11. Scheme of robustness analysis

Figure 12 displays the result of the robustness analysis of nominal MPC with the reference region tracking OCP with output constraints. The violation of the level constraint does not occur. However, the water level is remained in the reference region instead of achieving the optimal states, i.e., maximizing the water level.

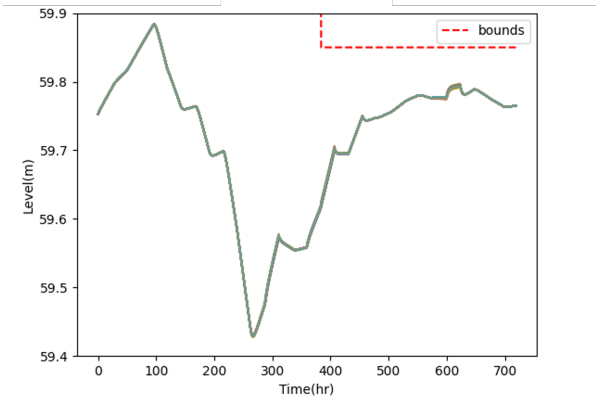

Figure 12. Robustness analysis on level control at Dalsfoss power station using the reference region tracking MPC with output constraints

The robustness analysis result with the new OCP with constraint relaxation is shown in Figure 13. The areas marked by blue and green colours in Figure 13 are displayed in Figure 14 and Figure 15 respectively. The potential violation of the level constraint is detected by 1384 times throughout the simulation period. when the nominal MPC with new OCP is applied to the uncertain system, the level constraints are not always satisfied for all the possible water inflows to the lake that can happen in the future. Some realizations can result in the violation of constraints. This reflects reality since in the real plant, water inflow to the lake can be dictated by one (or some other) of the possible forecast realizations.

6 Conclusion

The new OCP with constraint relaxation shows some improvements over the OCP for the reference region tracking MPC with output constraints. As presented in Section 4, it not only saves more water in the reservoir compared to the reference region tracking with output constraints but

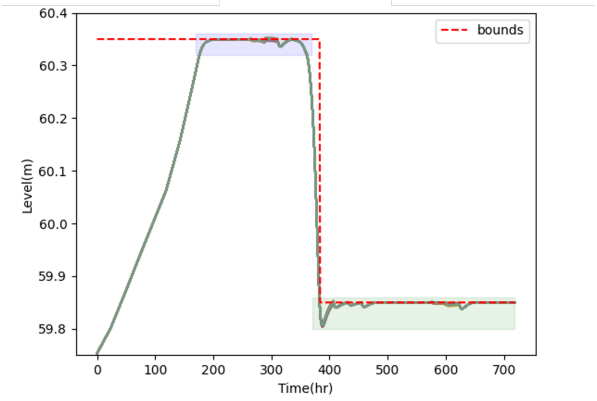

Figure 13. Robustness analysis on level control at Dalsfoss power station using the new OCP with constraint relaxation

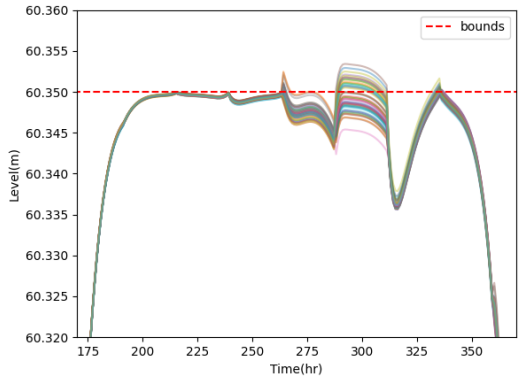

Figure 14. Enlarged robustness analysis on level control at Dalsfoss power station using the new OCP with constraint relaxation : time = [170,370]

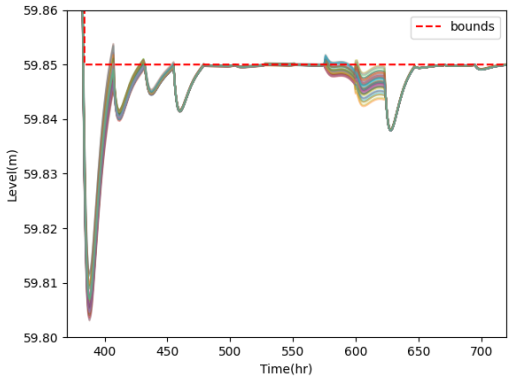

Figure 15. Enlarged robustness analysis on level control at Dalsfoss power station using the new OCP with constraint relaxation : time = [370,720]

also, did not cause any failure on optimization due to infeasibilities. Also, since the new OCP with constraint relaxation is simpler, it should be easier for the operators and engineers on the site to understand. More study should be performed with the new OCP with constraint relaxation by using more realistic operational scenarios including the use of power production plan in the future.

In robustness analysis, a flood situation is assumed by setting the flood coefficient as 3. The new OCP with constraint relaxation shows the vulnerability compared to the reference region tracking MPC in terms of the robustness of MPC. While the reference region tracking MPC has no potential violations on the level constraint, the MPC with new OCP displays 1384 times of the potential violation. However, this kind of possible constraint violation can be mitigated by employing a stochastic MPC or putting the safety margin. For the use of the stochastic MPC, the new OCP with constraint relaxation in this paper may be more beneficial to use due to its flexibility on output constrained optimization and its behaviour to save more water at the dam.

References

Joel A E Andersson, Joris Gillis, Greg Horn, James B Rawlings, and Moritz Diehl. CasADi – A software framework for nonlinear optimization and optimal control. *Mathematical Programming Computation*, 11(1):1–36, 2019. doi:10.1007/s12532-018-0139-4.

Kristian D. Kvam, Beathe Furenes, Åsmund Hasaa, Alexander Zhang Gjerseth, Nils-Olav Skeie, and Bernt Lie. Flood control of lake toke: Model development and model fitting. 2017. ISSN 1650-3686. URL `http://hdl.handle.net/11250/2466966`.

Bernt Lie. Final report: Kontrakt nr inan-140122 optimal control of dalsfos flood gates- control algorithm. 2014.

David Q Mayne. Model predictive control: Recent developments and future promise. *Automatica (Oxford)*, 50(12): 2967–2986, 2014. ISSN 0005-1098.

Itsaso Menchacatorre, Roshan Sharma, Beathe Furenes, and Bernt Lie. Flood management of lake toke: Mpc operation under uncertainty. 2019. ISSN 1650-3686.

Manfred Morari and Jay H. Lee. Model predictive control: past, present and future. *Computers chemical engineering*, 23(4): 667–682, 1999. ISSN 0098-1354.

NVE. Supervision of dams, (accessed: 24.05.2021). `https://www.nve.no/supervision-of-dams/?ref=mainmenu`, 2021.

Roshan Sharma. Lectures note for course iia 4117 : Model predictive control in university of south-eastern norway. 2020.

SkagerakKraft. Dalsfos, (accessed: 24.05.2021). `https://www.skagerakkraft.no/dalsfos/category1277.html`, 2021a.

SkagerakKraft. Kragerø watercourse system, (accessed: 24.05.2021). `https://www.skagerakkraft.no/kragero-watercourse/category2391.html`, 2021b.

Appendix B

Stochastic MPC For Optimal Operation of Hydropower Station Under Uncertainty

Published in *13th IFAC Symposium on Dynamics and Control of Process Systems, including Biosystems DYCOPS 2022* 14–17 June 2022, Busan, Republic of Korea
Paper presented by Changhun Jeong.
Authors: Changhun Jeong, and Roshan Sharma.
Authors' roles in the article:
Changhun Jeong: Main ideas, implementation, and writing.
Roshan Sharma (Supervisor): Discussions, comments, and proofreading.

Available online at www.sciencedirect.com

ScienceDirect

IFAC PapersOnline CONFERENCE PAPER ARCHIVE

IFAC PapersOnLine 55-7 (2022) 155–160

Stochastic MPC For Optimal Operation of Hydropower Station Under Uncertainty

Changhun Jeong * **Roshan Sharma** *

* *Department of Electrical engineering, Information Technology and Cybernetics, University of South-Eastern Norway, Porsgrunn, Norway (e-mail: changhun.jeong@usn.no / roshan.sharma@usn.no).*

Abstract: The operational condition at the Dalsfoss power station is complicated due to many requirements related to environmental regulations and safety constraints such as the seasonally varying water level requirement at the reservoir. However, the operation becomes more difficult due to uncertainties in the system. In this paper, at first a certainty equivalent MPC is applied to the uncertain hydro power system and it has been shown that its robustness property is poor. Secondly, to prevent the constraint violations due to the uncertainties in the system, two measures are taken. One measure is to introduce a safety margin for the constraints and further design a certainty equivalent MPC. The other measure is to implement a multi-stage MPC for robust constraint satisfaction. Two types of multi-stage MPC are considered in this paper. The first employs all of the possible 50 scenarios of the uncertainty of an input disturbance variable, and the latter generates and uses three synthetic scenarios to approximate all of the possible 50 scenarios. All of the simulation results are compared for their robust performances and computational time.

Keywords: Model predictive control, Multi stage model predictive control, Stochastic analysis, uncertainty, flood management

1. INTRODUCTION

The Kragerø watercourse is located in Telemark, Norway. The catchment area of the watercourse is over 1200 square kilometers. There are five hydropower plants along the watercourse. The locations of the five plants are shown in Figure 1. The uppermost hydro power plant is the Dalsfoss power plant. The plant is operated by Skagerak Kraft. The plant has two flood gates and one intake to a turbine (SkagerakKraft, 2021a,b).

Fig. 1. Overview of the Kragerø watercourse. (SkagerakKraft, 2021b).

For proper operation of the power plant concession requirements are imposed by the Norwegian Water Resource and Energy Administration (NVE). Some of the requirements are related to safety while others are related to the ecosystem around the watercourse (NVE, 2021). However, it is arduous to satisfy all of the requirements due to the presence of uncertainty in the system. The prediction of how much water will flow into the reservoir (lake Tokke) from the surrounding terrain is quite uncertain. The power production is decided by Skagerak Kraft from considering aspects such as the power demand and the electricity price change in the future. The prediction of water inflow is given as 50 possible scenarios for the next 13 days. The prediction is constructed based on the weather forecast and complex hydrological models. The water inflow prediction is updated every 24 hours.

Model predictive control (MPC) is an attractive multivariable constrained optimal control approach to deal with dynamic system with multiple inputs, outputs and constraints (Morari and H. Lee, 1999; Mayne et al., 2000). In a previous work, a reference region tracking deterministic MPC was suggested for the operation of the Dalsfoss power station. This MPC was designed to let the water level at the reservoir remain with in a specified region (Lie, 2014). As a further improvement, a stochastic MPC based on multi-objective optimization (MOO) was proposed (Menchacatorre et al., 2019) to consider the uncertainty on the water inflow. For the MOO based stochastic MPC, the optimal control problem (OCP) formulation was similar to the reference region tracking MPC. A new OCP, based on the maximization of the water level at the reservoir is

10.1016/j.ifacol.2022.07.437

formulated, simulated and compared to the OCP of the reference region tracking MPC. Although a deterministic MPC based on the new OCP maintains a higher level of water at the dam, it shows that robust constraint satisfaction cannot be guaranteed for all 50 possible inflow scenarios (Jeong et al., 2021).

In this paper, further works on Dalsfoss hydropower plant have been discussed with the aim to prevent the potential violation of constraints due to the uncertainties in the system, and to systematically handle large computational time associated with stochastic MPC. For this, a certainty equivalent MPC with a safety margin on the water level constraint, and a multi-stage MPC are proposed and discussed in detail in this paper.

The paper is organized as follows: In section 2, a brief introduction of the multi-stage MPC is presented. The system model, constraints and the optimal control problem are described in section 3. In sections 4 and 5, it discusses the simulation condition and the results of the simulation for certainty equivalent MPC and multi-stage MPC. Finally, the conclusion is written in section 6.

2. MULTI-STAGE MODEL PREDICTIVE CONTROL

A standard formulation of a deterministic MPC does not deal with uncertainty in the system. It is because the optimization technique does not consider uncertainty (Birge, 1997; Shapiro et al., 2009).

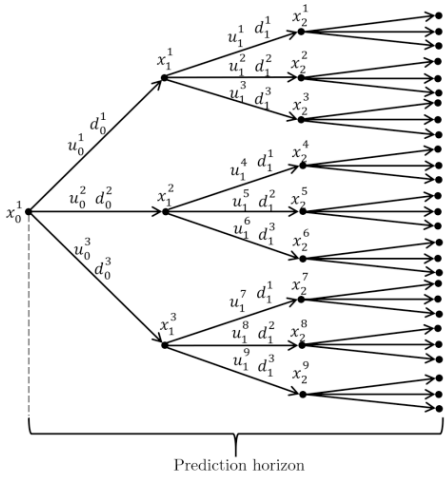

Fig. 2. Scenario tree representation of uncertainty evolution for multi-stage MPC (Lucia et al., 2013)

Multi-stage MPC includes the uncertainty of the system, as a form of scenario tree, into the optimization problem. A typical structure of a scenario tree is displayed in Fig. 2. The scenario tree describes the possible evolution of the uncertainty at each time step. It branches out at each node. Every node has expected states by branched uncertain events and control input from the events. For the Dalsfoss hydropower, the scenario tree will have 50 branches with each branch corresponding to each possible water inflow prediction. OCP for multi-stage MPC is described as follow:

$$\min_{x} \quad \sum_{j=1}^{S} \omega_j \sum_{i=1}^{N} J(x_{i,j}, u_{i,j}, p_{i,j}) \tag{1a}$$

$$\text{subject to} \quad g(x_{i,j}, u_{i,j}, p_{i,j}) \geq 0, \tag{1b}$$

$$h(x_{i,j}, u_{i,j}, p_{i,j}) = 0. \tag{1c}$$

$$\sum_{j=1}^{S} \bar{E}_j u_j = 0 \quad j \in 1, ..., S \tag{1d}$$

where ω denotes the probability or weight for each scenario, (1a) is the cost function, (1b) and (1c) are inequality and equality constraints. The last constraint, (1d), is the non-anticipativity constraint which guarantees to have the same control input for all branches arising from the same parent node (Lucia et al., 2013).

Since the future uncertainty is included in the optimization problem, the size of the OCP increases exponentially as the number of branches or scenarios increases. Therefore, when designing a scenario tree, it is critical to include the uncertainty in the future but also to have a tractable size of the OCP for feasible computational time. A good trade-off between robustness and computational cost can be achieved by constructing a simplified scenario tree that uses only the minimum, maximum and mean values of the scenarios, rather than using all possible scenarios. The simplified scenario tree will then have less number of branches but can still describe uncertainty of the system well. (Thangavel et al., 2018).

3. SYSTEM DESCRIPTION

3.1 System model

Lake Toke is located next to the Dalfoss power station and it works as a water reservoir for the hydro power plant. The simplified layout of the lake is displayed in Fig. 3. The lake is divided into two compartments described by two different water levels (h_1 and h_2) in Fig. 3. The left side is the upper part of the lake called Merkebekk and the right side is Dalsfoss which is the lower part of the lake near to the dam and the plant. The dynamic model of the lake Toke is described in Lie (2014)

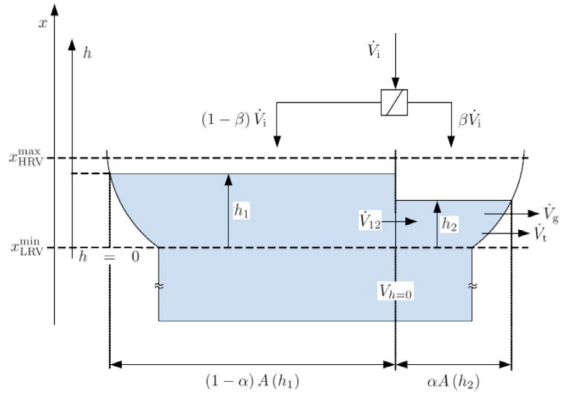

Fig. 3. Schematic of lake Toke (Lie, 2014)

The states of the systems are water levels at Merkebekk and Dalsfoss which are denoted as h_1 and h_2 respectively. The water levels above the sea level at Merkebekk and Dalsfoss, x_M and x_D, can be expressed as:

$$x_{\mathrm{M}} = h_1 + x_{\mathrm{LRV}}^{\min} \tag{2}$$

$$x_{\mathrm{D}} = h_2 + x_{\mathrm{LRV}}^{\min} \tag{3}$$

where $x_{\mathrm{LRV}}^{\min}$ means the low regulated value of the water level.

The area of the lake surface is calculated based on the water level as:

$$A(h_i) = \max(28 \times 10^6 \cdot 1.1 \cdot h_i^{\frac{1}{10}}, 10^3) \tag{4}$$

The inter compartment flow, $\dot{V}_{12}$, is defined based on the height difference of the water levels as follow:

$$\dot{V}_{12} = K_{12} \cdot (h_1 - h_2)\sqrt{|h_1 - h_2|} \tag{5}$$

where K_{12} is the inter compartment flow coefficient.

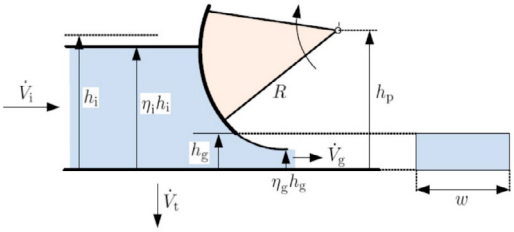

Fig. 4. Structure of floodgate (Lie, 2014)

The Dalsfoss dam has two flood gates. The height of the gate openings are denoted as h_{g1} and h_{g2}. The layout of floodgate structure is displayed in Fig. 4. The water flowrate through floodgate is expressed as:

$$\dot{V}_{\mathrm{g}} = C_{\mathrm{d}} w \cdot \min(h_{\mathrm{g}}, h_2)\sqrt{2g \cdot \max(h_2, 0)} \tag{6}$$

where C_{d} means the discharge coefficient and g represents the acceleration of gravity. The width of the floodgate is denoted as w. The maximum opening height of floodgates is up to 5.6m.

The water inflow to the lake and the power production are disturbances in the system. The water inflow is denoted as $\dot{V}_{\mathrm{i}}$. The water inflow prediction is updated everyday based on weather forecast data. The power produced is written as W_{e}. The water flowrate through a turbine, $\dot{V}_{\mathrm{t}}$, is given by:

$$\dot{V}_{\mathrm{t}} = a\frac{\dot{W}_{\mathrm{e}}}{x_{\mathrm{D}} - x_{\mathrm{q}}} + b \tag{7}$$

In (7), a and b are coefficients obtained from the data fitting method and x_{q} means the water level at quoy. The water level at quoy is calculated by solving the following cubic equation.

$$\begin{aligned} 0 = {} & c_1 x_{\mathrm{q}}^3 + (c_2 - c_1 x_{\mathrm{D}}) x_{\mathrm{q}}^2 \\ & + (c_3 - c_2 x_{\mathrm{D}} + c_4 \dot{V}_{\mathrm{g}}) x_{\mathrm{q}} \\ & + \dot{W}_{\mathrm{e}} - c_3 x_{\mathrm{D}} - c_4 \dot{V}_{\mathrm{g}} x_{\mathrm{D}} - c_5 \end{aligned} \tag{8}$$

where c_1, c_2, c_3, c_4, and c_5 are obtained by coefficient from polynomial data fitting.

The total water outflow from the Dalsfoss power station, $\dot{V}_{\mathrm{o}}$, is a summation of water flowrates through the floodgates and the turbines as follow:

$$\dot{V}_{\mathrm{o}} = \dot{V}_{\mathrm{t}} + \sum \dot{V}_{\mathrm{g}} \tag{9}$$

The dynamic model of states, h_1 and h_2, are described by the following equations:

$$\frac{dh_1}{dt} = \frac{1}{(1-\alpha)A(h_1)}((1-\beta)\dot{V}_{\mathrm{i}} - \dot{V}_{12}) \tag{10}$$

$$\frac{dh_2}{dt} = \frac{1}{\alpha A(h_2)}(\beta \dot{V}_{\mathrm{i}} + \dot{V}_{12} - \dot{V}_{\mathrm{o}}) \tag{11}$$

Parameters for the model are specified in Table 1.

3.2 Operational constraints

The operational requirements are decided by NVE. It is mandatory to satisfy those requirements for (i) operational safety, (ii) securing ecological diversity, and (iii) avoiding property damage. The constraints are:

(1) The flowrate of the total water outflow, $\dot{V}_{\mathrm{o}}$, should not change abruptly. This constraint ensures that people and animals downstream do not experience sudden large changes in the outflow.
(2) The flowrate of the total water outflow, $\dot{V}_{\mathrm{o}}$, must be kept bigger than $4\mathrm{m}^3/\mathrm{s}$. The ecosystem is not disturbed and fishes in downstream can move freely by satisfying this constraint.
(3) The water level at Merkebekk, x_{M}, must be maintained within a specified water level range:
$$x_{\mathrm{M}} \in [x_{\mathrm{LRV}}, x_{\mathrm{HRV}}]$$
where x_{LRV} and x_{HRV} mean the low and the high regulated value for the water level respectively. The seasonal level requirement changes are shown in Fig. 2.
(4) When severe flooding occurs, x_{HRV} can be extended to $x_{\mathrm{HRV}}^{\max}$. However, after the culmination of flooding ends, x_{M} must reach x_{HRV} as soon as possible.
(5) The flow rate through the turbine, V_{t}, is limited up to $36\mathrm{m}^3/\mathrm{s}$.

3.3 Optimal control problem

When handling the flood gates, care should be taken that the water from the dam is not thrown out through flood gates unnecessarily. This would result in loss of water which otherwise could be used to produce electricity. In this sense, saving as much water as possible (i.e. having as high water level as possible) in the dam while still satisfying the concession requirements becomes necessary. The objective function in the OCP is designed to maximize the water level at Merkebekk and to minimize the control action and its rate of change as: (Jeong et al., 2021)

$$\min_u \sum_{i=1}^{N} \omega_R R_{\mathrm{new}}^2(x_{t+i}) + \omega_{\Delta u} \Delta u_{\mathrm{c},t+i-1}^2 + \omega_u u_{\mathrm{c},t+i-1}^2 + p^2 \omega_p \tag{12}$$

Table 1. Parameters for Lake Toke model

Parameter	Value	Unit	Comment
α	0.05	-	Fraction of surface area in compartment 2
β	0.02	-	Fraction of inflow to compartment 2
K_{12}	800	$\mathrm{m}^{\frac{3}{2}}/s$	Inter compartment flow coefficient
C_d	0.7	-	Discharge coefficient, Dalsfoss gate
w_1	11.6	m	Width of Dalsfoss gate 1
w_2	11.0	m	Width of Dalsfoss gate 2
$x_{\mathrm{LRV}}^{\min}$	55.75	m	Minimal low regulated level value
$x_{\mathrm{HRV}}^{\max}$	60.35	m	Maximal high regulated level value
g	9.81	$\mathrm{m/s}^2$	Acceleration of gravity
a	124.69	Pa^{-1}	Coefficient in equation 7
b	3.161	m	Coefficient in equation 7
c_1	0.13152	$\mathrm{W/m}^{-3}$	Polynomial coefficient in equation 8
c_2	-9.5241	$\mathrm{W/m}^2$	Polynomial coefficient in equation 8
c_3	$1.7234 \cdot 10^2$	W/m	Polynomial coefficient in equation 8
c_4	$-7.7045 \cdot 10^{-3}$	Pa/m	Polynomial coefficient in equation 8
c_5	$-8.7359 \cdot 10^{-1}$	W	Polynomial coefficient in equation 8

Table 2. Seasonal level requirement

Date	x_{LRV}[m]	x_{HRV}[m]
Jan. 1 - Apr. 30	55.75	60.35
May. 1 - Aug. 30	58.85	59.85
Sept. 1 - Sept. 14	55.75	59.35
Oct. 28 - Nov. 11	55.75	59.85
Nov. 12 - Dec. 31	55.75	60.35

The first term in (12) is to maximize the water level at Merkebekk and expressed as:

$$R_{\mathrm{new}}(x_{t+1}) = x_{\mathrm{M},t+1} - x_{\mathrm{HRV}} \tag{13}$$

The last term, $p^2\omega_p$, is the penalty for violation of level constraints. The variable p is the slack variable which is automatically decided by the optimizer. It allows the violation on x_{LRV} to satisfy the minimum flowrate constraints.

4. SIMULATION

4.1 Simulation setup

To implement the simulations, the two disturbances, the power production and the water inflow to the lake Toke, must be defined.

The synthetic data of the power production plan used for the simulation is described on Fig. 5. In this paper it is assumed that the power production is perfectly known.

For the water inflow, the real data of the water inflow prediction stored by the plant operator as historical data is utilized. The water inflow prediction data is updated every 24 hours. The prediction consists of an averaged water inflow on each day for the next 13 days and there are 50 such prediction scenarios. Since the prediction does not reflect hourly changes in water inflow, the water inflow is assumed to be constant during each day. The real historical data is multiplied by 3 to simulate the flooding situation.

The period of the simulation is set from April 15 to May 15. This period involves the drastic change of the water level constraints at Merkebekk. The step size is set as 1 hour. The length of the prediction horizon is 3 days i.e. 72 hours. The weighting parameters for OCP are determinded from trial and error and are stated in Table 3. For the solution of multi-stage MPC, multiple shooting method and IPOPT solver in CasADi are used (Andersson et al., 2019).

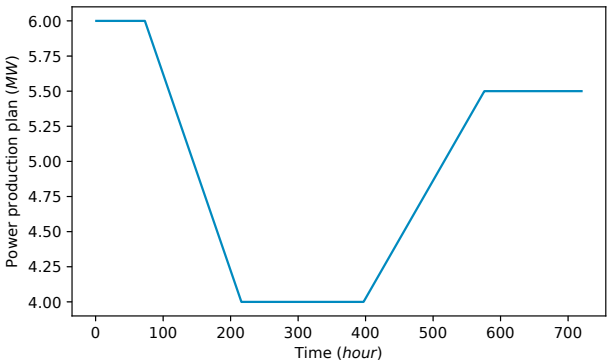

Fig. 5. Synthetic plan for power production during the simulation period

Table 3. Parameters for the simulations

Parameter	Value	Unit
ω_R	10	-
$\omega_{\Delta u}$	1	-
ω_u	1	-
ω_p	100	-

4.2 Robustness analysis

Robustness analysis is a tool that shows how the controller performs due to the influence of uncertainty. It is performed to show the number of potential violation of the constraints when the realized disturbance is different from the one that was used for prediction. The procedure of the robustness analysis is displayed in Fig. 6. When the optimal control input is calculated by the optimizer, it is applied not only to the nominal system but also to imaginary systems each having different realization of the input disturbance. However, the state is not updated through the imaginary systems but only stored for analysis.

4.3 Control strategies

In this subsection, MPC formulations which can handle the effect of future uncertainty is described. In this paper, 3 types of formulations have been studied as follow:

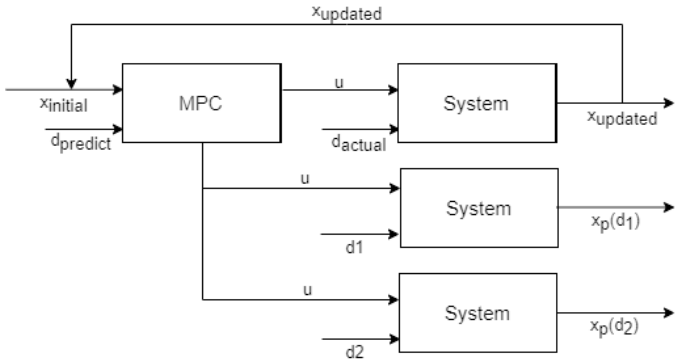

Fig. 6. The procedure of robustness analysis

- **Certainty-equivalent MPC with safety margin**: With this method, a virtual upper bound for the water level is created by subtracting a small value (safety margin) from the actual upper bound. This virtual upper bound of the water level is then used to formulate a certainty-equivalent MPC. The safety margin decreases the maximum allowed water level at the reservoir by a small value. The idea is that any fluctuations of the water level due to uncertainty will remain within the safety margin and will never go above the actual upper bound. In this study, the value of the safety margin is set as 5cm.
- **Multi-stage MPC using all the 50 scenarios**: The weight on each scenario is set as 1 for the implementation of the multi-stage MPC because every scenario has an equal probability of occurrence. However, using all 50 prediction scenarios increases the size of the OCP by 50 times, which increases the complexity of the problem and will therefore also require significantly larger computational time.
- **Multi-stage MPC using 3 synthetic scenarios**: To have the balance between the robustness and the computational demand, only three synthetic scenarios are generated from the all of the 50 possible scenarios by extracting maximum, minimum and mean values along the prediction horizon. Therefore, these 3 synthetic scenarios cover the whole range of the 50 possible scenarios.

5. RESULT

Fig. 7 shows the results of the robustness analysis when the certainty-equivalent MPC is used. There are 1287 cases of total possible violations counted by robustness analysis throughout the whole simulation period. Although certainty equivalent MPC maintains the water to the maximum possible level, it is shown that there is a danger that the constraints may be violated in the future. However, there were zero constraint violation counted by robustness analysis when the two multi-stage MPC techniques, and certainty equivalent MPC with safety margin are employed.

The level changes and the control input throughout the simulation period are displayed in Fig. 8 and Fig. 9. CE-MPC means the certainty equivalent MPC and CE-MPC(S) stands for the certainty equivalent MPC with a safety margin. MS-MPC shows the water level changes when multi-stage MPC with all of 50 possible scenarios

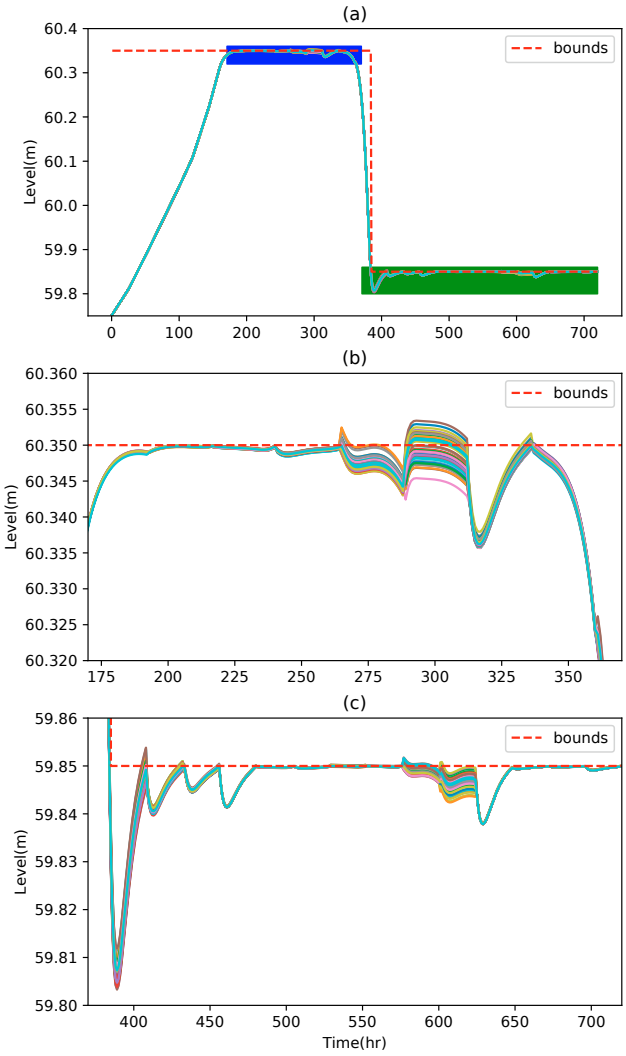

Fig. 7. The robustness analysis of certainty equivalent MPC: (a) robustness analysis through the whole simulation period, (b) detailed image of robustness analysis (blue color area in (a)), (c) detailed image of robustness analysis (green color area in (a))

are used. MS-MPC(R) shows the simulation result, using multi-stage MPC with only the three synthetic scenarios. Certainty equivalent MPC(CE-MPC) pursues the most maximized water level, but the robustness is proven to be vulnerable as shown in Fig. 6. The performance of the certainty equivalent MPC with the safety margin(CE-MPC(S)) is the worst compared to the other approaches, i.e. it maintains the lowest water level at the dam. Multi-stage MPC with all of 50 possible scenarios(MS-MPC) shows more conservative performance compared to the certainty equivalent MPC but better performance than the certainty equivalent MPC with a safety margin. Multi-stage MPC with the three synthetic scenarios(MS-MPC(R)) has similar (only negligible performance loss) compared with the MS-MPC. MS-MPC and MS-MPC(R) shows less drastic changes on control input through simulation period.

Table 4 is the summary of the computational time required to complete simulations. When CE-MPC is used for the simulation, it takes only 163s(avg. iteration time: 227ms).

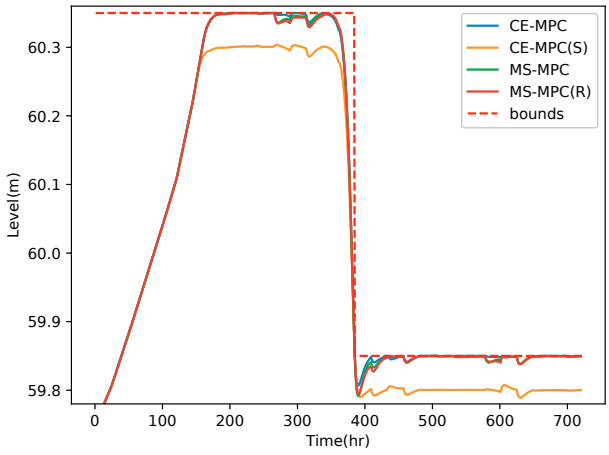

Fig. 8. The level changes throughout the simulation period

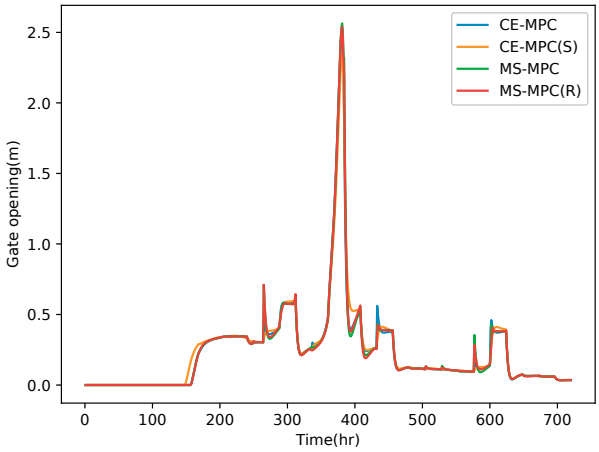

Fig. 9. The control input throughout the simulation period

Table 4. Computation time for simulations[s]

CE-MPC	MS-MPC	MS-MPC(R)
163	2977	257

However, it takes 18.2 times more, 2977s(avg. iteration time: 4135ms), when the MS-MPC is applied. The computational time decreases significantly to 257s(avg. iteration time: 358ms) when MS-MPC(R) is used.

6. CONCLUSION

Although with the certainty-equivalent MPC, constraint violations can occur, this paper presents three approaches to eliminate the influence of future uncertainty. One is to add a conservative safety margin on the certainty equivalent MPC. The other two is to employ multi-stage stochastic MPC. From the simulation results, all of approaches perform well. However, multi-stage MPC shows better performance compared to certainty equivalent MPC with safety margin. Therefore, the implementation of multi-stage MPC on the Dalfoss hydropower station seems beneficial because it gives strong robustness while it keeps the water level as maximum as possible. Also, The computation time for implementing multi-stage MPC can be significantly reduced without performance loss by selecting only the three synthetic scenarios instead of using all of the 50 scenarios. The performance is not significantly degraded when the three synthetic scenarios are used with the multi-stage MPC.

Although multi-stage MPC shows advantages compared to the other approaches, there is still more uncertainty to consider. Firstly, there may be a case that the actual water inflow might be out of the considered uncertainty range. Secondly, the water inflow may change every hour or every minute unlike how it is assumed in this paper. It may be necessary to investigate how to implement the multi-stage MPC under these conditions.

REFERENCES

Andersson, J.A.E., Gillis, J., Horn, G., Rawlings, J.B., and Diehl, M. (2019). CasADi – A software framework for nonlinear optimization and optimal control. *Mathematical Programming Computation*, 11(1), 1–36. doi: 10.1007/s12532-018-0139-4.

Birge, J.R. (1997). State-of-the-art-survey–stochastic programming: Computation and applications. *INFORMS Journal on Computing*, 9(2), 111–133.

Jeong, C., Furenes, B., and Sharma, R. (2021). MPC operation with improved optimal control problem at dalsfoss power plant. *Proceedings of SIMS EUROSIM conference 2021*, 11(1), 226–233. doi:10.3384/ecp21185226.

Lie, B. (2014). Final report: KONTRAKT NR INAN-140122 optimal control of dalsfos flood gates- control algorithm.

Lucia, S., Finkler, T., and Engell, S. (2013). Multi-stage nonlinear model predictive control applied to a semi-batch polymerization reactor under uncertainty. *Journal of Process Control*, 23(9), 1306–1319.

Mayne, D., Rawlings, J., Rao, C., and Scokaert, P. (2000). Constrained model predictive control: Stability and optimality. *Automatica (Oxford)*, 36(6), 789–814.

Menchacatorre, I., Sharma, R., Furenes, B., and Lie, B. (2019). Flood management of lake toke: MPC operation under uncertainty. *Proceedings of SIMS conference 2019*, 9–16. doi:10.3384/ecp201709.

Morari, M. and H. Lee, J. (1999). Model predictive control: past, present and future. *Computers chemical engineering*, 23(4), 667–682.

NVE (2021). Supervision of dams, (accessed: 24.05.2021). `https://www.nve.no/supervision-of-dams/?ref=mainmenu`.

Shapiro, A., Dentcheva, D., and Ruszczyński, A. (2009). *Lectures on stochastic programming: modeling and theory*. MOS-SIAM Series on Optimization. Society for Industrial and Applied Mathematics.

SkagerakKraft (2021a). Dalsfos, (accessed: 24.05.2021). `https://www.skagerakkraft.no/dalsfos/category1277.html`.

SkagerakKraft (2021b). Kragerø watercourse system, (accessed: 24.05.2021). `https://www.skagerakkraft.no/kragero-watercourse/category2391.html`.

Thangavel, S., Lucia, S., Paulen, R., and Engell, S. (2018). Dual robust nonlinear model predictive control: A multi-stage approach. *Journal of process control*, 72, 39–51.

Appendix C

Multistage Model Predictive Control with Simplified Scenario Ensembles for Robust Control of Hydropower Station

Published in *MIC Journal: Modeling, Identification and Control*, 2023.
Authors: Changhun Jeong, Beathe Furenes, and Roshan Sharma.
Authors' roles in the article:
Changhun Jeong: Main ideas, implementation, and writing.
Beathe Furenes: Discussions, comments, and proofreading.
Roshan Sharma (Supervisor): Discussions, comments, and proofreading.

Modeling, Identification and Control, Vol. 44, No. 2, 2023, pp. 43–54, ISSN 1890–1328

Multistage model predictive control with simplified scenario ensembles for robust control of hydropower station

Changhun Jeong [1] Beathe Furenes [2] Roshan Sharma [1]

[1] *Department of Electrical engineering, Information Technology and Cybernetics, University of South-Eastern Norway, Porsgrunn, Norway. E-mail:* changhun.jeong@usn.no / roshan.sharma@usn.no

[2] *Skagerak Kraft AS, Porsgrunn, Norway.*

Abstract

This paper proposes simplification of the scenario ensembles that describe the uncertainty present in a hydropower plant. The simplified scenario tree is further used with a multistage model predictive control for optimal operation of the hydropower station. The proposed method reduces the number of considered scenario ensembles of water inflow forecast into the reservoir in the Dalsfoss hydropower plant, which leads to less computational demand of the multistage MPC. The method takes two steps: the creation of three synthesis scenario ensembles and the estimation of the probability of occurrence of the three synthesis scenario ensembles. The simulation results of multistage MPC with 4 different types of scenario ensembles demonstrate that the proposed simplified method reduces the computation demand of the multistage MPC by 15 times approximately, without degrading its performance.

Keywords: Multistage model predictive control, Uncertainty, Simplified method, Renewable energy

1 Introduction

Hydropower is an attractive renewable energy with two significant benefits; flooding management and energy security. The presence of a reservoir in a hydropower system enables it to hold the water for generating power or ensure the steady water flow in downstream in the future (IEA, 2021; Torabi Haghighi et al., 2019). However, the operation of a hydropower system is challenging. Some operational constraints and requirements must comply when operating a hydropower system, for ensuring safety in the operation and preventing damage to the ecosystem (NVE, 2021). Furthermore, the presence of uncertainty, such as water inflow to a reservoir, exacerbates the difficulty of the operation of a hydropower system.

The operation of the Dalsfoss hydropower plant is not exceptional for the challenge because there are several operational constraints and requirements posed by NVE(NVE, 2021), and uncertainty of water inflow. Thus, Skagerak Kraft, the operator of the plant, has been considering the implementation of model predictive control (MPC). MPC is an appealing control strategy for a constrained multi-input and multi-output system and optimal operation (Morari and Lee, 1999). It aims to achieve optimal operation and satisfy the posed constraints. MPC computes the optimal control sequence by solving an optimal control problem (OCP) and applies the first element of the sequence to the system (Mayne et al., 2000).

The first attempt of utilizing MPC for the Dalsfoss hydropower plant was made internally in Skagerak Kraft AS. It suggested a system model of the Dalsfoss hydropower system and simulated the deterministic MPC with reference region tracking OCP that aims

doi:10.4173/mic.2023.2.1

to keep the water level in a specific range instead of maximizing it. Then, later, the model and the OCP are used to test the stochastic MPC in (Menchacatorre et al., 2019). However, because of the reference region tracking OCP, it is observed a large amount of water was thrown away through floodgates instead of being used for power generation in the future, despite the constraints on the water level being seldom activated.

To address this issue, the new OCP was formulated in (Jeong et al., 2021). The new objective function was designed to maximize the water level at the reservoir and explicit constraints on the water level bounds were posed. As the result, the water level was maximized during the simulations and the constraint of the maximum water level became activated. However, due to the activation of the constraint, the constraint was not satisfied when uncertainty was realized differently from the predicted value. Later, the newly proposed OCP was tested with various sets of weight parameters for finding preferred operational condition in Jeong and Sharma (2022b).

Uncertainty in the system, such as model mismatch and disturbances, can lead to the failure of the optimal operation and even to potential constraint violations during operation (Birge, 1997; Shapiro et al., 2009). There has been much research to counteract the influence of the uncertainty in the MPC framework (Mesbah, 2016). Firstly, Min-max MPC was introduced in (Campo and Morari, 1987). Min-max calculates the control sequence over a single trajectory that aims to counteract the influence of all possible realizations of uncertainty. In other words, it provides the control input for the worst-case scenario of uncertainty. This approach frequently yields a highly conservative control input, while ensuring the robust satisfaction of constraints. Later, multistage MPC appeared as the solution of the highly conservative solution of Min-max MPC in (Scokaert and Mayne, 1998; Lucia et al., 2013). The uncertain system behavior is described by a discrete-time scenario tree, which accounts for the future evolution of uncertainty. Multistage MPC computes many control trajectories over the scenario tree. The effectiveness and performance of the multistage MPC approach have been demonstrated in various industrial applications(Lucia et al., 2013; Klintberg et al., 2016; Maiworm et al., 2015).

Multistage MPC was effective in counteracting the uncertain water inflow in the operation of the Dalsfoss hydropower plant as well (Jeong and Sharma, 2022a). The 50 scenario ensembles of the water inflow forecast are used as the scenario tree for implementing the multistage MPC. As result, no violation was observed. To reduce the computational time, instead of the whole scenario ensembles, the three synthesis scenario ensembles were created and used for multistage MPC. Although the computational demand was significantly reduced and no violation of constraints was observed, the performance was degraded.

This paper proposes a solution, the simplified method, to compensate for the performance degradation when using the synthesis scenario ensembles to enhance the computation speed of the multistage MPC. The simplified method consists of two stages: (1) Generation of synthesis scenario ensembles and (2) estimation of the probability of each synthesis scenario ensemble. The synthesis scenario ensemble must encapsulate the original scenario ensembles and encompass all realizations of uncertainty. The probabilities add more information on uncertainty in the synthesis scenario ensembles. The implementation of this method significantly reduces the size of the optimization problem, yet does not degrade the performance of the multistage MPC framework. The mentioned advantage of the proposed method is demonstrated through a simulation of the Dalsfoss hydropower station system. The simulations of multistage MPCs with 4 different structures of scenario ensembles of water inflow prediction are performed under the moderate water inflow situation, and the flooding situation.

The organization of this paper is as follows: Section 2 provides overviews of multistage MPC, robust horizon, and open-loop robustness analysis. Section 3 introduces the method to simplify the scenario ensembles. The system model of the Dalsfoss hydropower plant system, its operational constraints, and the formulation of the OCP for multistage MPC are explained in Section 4. The simulation setup and the given data of water inflow forecasts and power production plan for running the simulations are described in Section 5. Section 6 presents the simulation results, and the conclusion is discussed in Section 7.

2 Preliminary

2.1 Multistage model predictive control

In a multistage MPC framework, the uncertainty, such as model parameters or disturbances, can be represented by a form of a discrete scenario tree as illustrated in Figure 1. The possible evolution of the uncertainty in the future and the corresponding control inputs are described by branches from a node. The control inputs from multistage MPC can counteract the effects of the uncertainties as new information will be available as the future sampling in the setting of the scenario tree (Lucia et al., 2013).

The system can be expressed as:

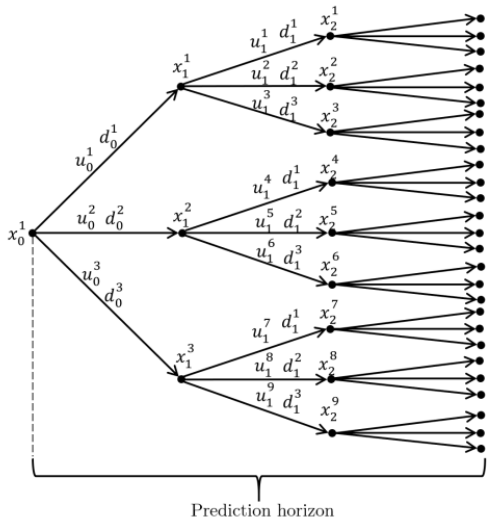

Figure 1: The structure of the scenario tree

$$x_{k+1}^j = f(x_k^{p(j)}, u_k^j, d_k^{r(j)}) \tag{1}$$

where $x_k^{p(j)}$, u_k^j, and $d_k^{r(j)}$ denote the parent state, the control input, and the realization of the uncertainty at time sample k.

It is possible to formulate OCP for multistage MPC as:

$$\begin{aligned}
\underset{u_k^j, \forall (j,k) \in I}{\text{minimize}} \quad & \sum_{i=1}^{S} \omega_i \sum_{k=0}^{Np-1} L(x_{k+1}^j, u_k^j) && \text{(2a)}\\
\text{subject to} \quad & x_{k+1}^j = f(x_k^{p(j)}, u_k^j, d_k^{r(j)}), && \text{(2b)}\\
& x_k^j \in \mathbb{X}, && \text{(2c)}\\
& u_k^j \in \mathbb{U}, && \text{(2d)}\\
& u_k^j = u_k^l \quad \text{if} \quad x_k^{p(j)} = x_k^{p(l)} && \text{(2e)}
\end{aligned}$$

Equation (2a) is the cost function which considers a probability of a scenario by ω_i, and where $L(x_{k+1}, u_k)$ is the stage cost and N_p is the prediction horizon. Equation (2b) is the system model. Equations (2c) and (2d) are bounds of states and control inputs. Equation (2e) denotes non-anticipativity constraints that all the control inputs u_k^k on branches from the same parent node $x_k^{p(k)}$ have to be equal. the non-anticipativity constraints are necessary because the control inputs cannot anticipate the realization of the uncertainty in the future (Lucia et al., 2013).

When implementing multistage MPC, the biggest challenge is to solve the OCP in a reasonable time. It is because of the large size of OCP. The size of the OCP grows exponentially with the prediction horizon and with the number of uncertainties and the number of branches in the scenario tree (Lucia et al., 2013).

2.2 Robust horizon

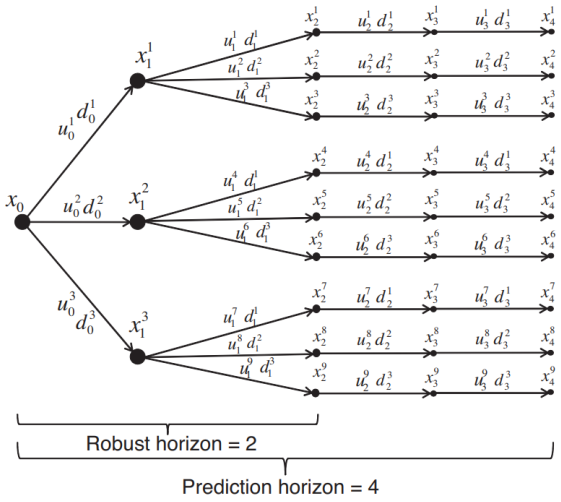

Figure 2: The structure of the scenario tree with a robust horizon

It is critical to have a proper size of OCP by designing the scenario tree properly when running the multistage MPC. One method to avoid the exponential growth of the scenario tree is to utilize a robust horizon. It considers the evolution of the uncertainty up to certain time steps and assumes that the uncertainty remains constant until the end of the prediction horizon, as depicted in Figure 2 (Lucia et al., 2013).

2.3 Open-loop robustness analysis

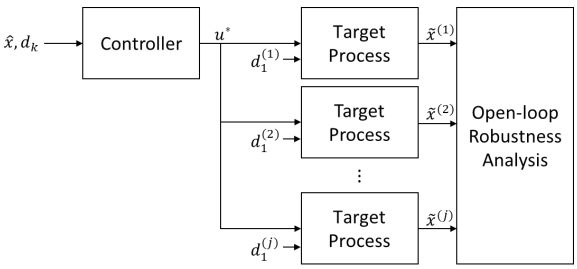

Figure 3: The procedure of open-loop robustness analysis

The open-loop robustness analysis aims to check the constraint violations due to the occurrence of uncertainties in the process. The analysis procedure is illustrated in Figure 3. Once the MPC controller computes

the control inputs, the first element of the control inputs is applied to the model with all possible uncertainties in parallel, and the violation of the constraints is accessed (Jeong et al., 2021).

3 Simplification of scenario ensembles

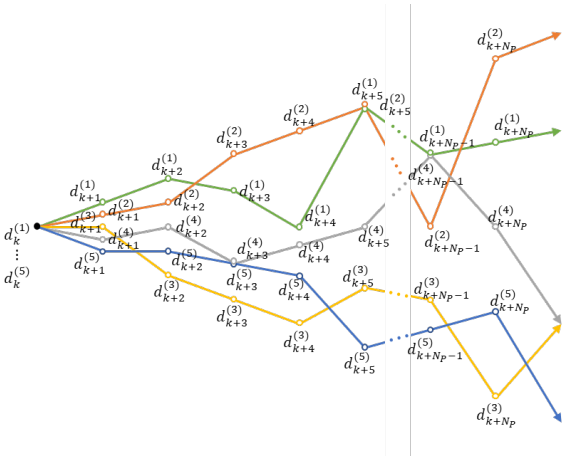

Figure 4: An example of scenario ensembles of uncertainty

The scenario ensembles consist of a collection of distinct scenarios of unpredictability. They resemble a scenario tree with a robust horizon of 1 for the hydro power case study, but the values are not assumed to remain constant after branching. Five example scenario ensembles are displayed in Figure 4. Each color represents one scenario in the ensemble of uncertainty. The number of scenario ensembles, S, over the prediction horizon, N_p, at time sample k can be mathematically expressed as follows:

$$\mathbf{d}_k = \begin{pmatrix} \mathbf{d}_k^{(1)} & \cdots & \mathbf{d}_k^{(S)} \\ \vdots & \ddots & \vdots \\ \mathbf{d}_{k+N_p}^{(1)} & \cdots & \mathbf{d}_{k+N_p}^{(S)} \end{pmatrix} \tag{3}$$

The simplified method streamlines the scenario ensembles to three when there are more than three scenario ensembles present. This is achieved through the following two steps:

Step. 1: The process of creating synthetic scenario ensembles, which represent the original ensembles, can be accomplished by using statistical data such as the minimum, mean, and maximum values of the ensembles at each time step throughout the predicted horizon. As an illustration, consider the five scenario ensembles of uncertainty depicted in Figure 4. These

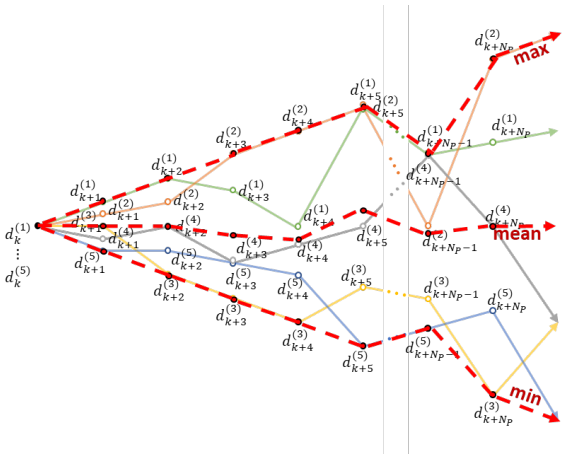

Figure 5: The three synthetic scenario ensembles of the uncertainty from the five example scenario ensembles

ensembles can be transformed into three synthesis scenario ensembles, as demonstrated in Figure 5 with red dotted lines, by using Equation (4),(5), and (6).

$$\mathbf{d}_{\max,k} = \begin{pmatrix} \max(\mathbf{d}_k^{(1)} & \cdots & \mathbf{d}_k^{(S)}) \\ \vdots & \ddots & \vdots \\ \max(\mathbf{d}_{k+N_p}^{(1)} & \cdots & \mathbf{d}_{k+N_p}^{(S)}) \end{pmatrix} \tag{4}$$

$$\mathbf{d}_{\text{mean},k} = \begin{pmatrix} \text{mean}(\mathbf{d}_k^{(1)} & \cdots & \mathbf{d}_k^{(S)}) \\ \vdots & \ddots & \vdots \\ \text{mean}(\mathbf{d}_{k+N_p}^{(1)} & \cdots & \mathbf{d}_{k+N_p}^{(S)}) \end{pmatrix} \tag{5}$$

$$\mathbf{d}_{\min,k} = \begin{pmatrix} \min(\mathbf{d}_k^{(1)} & \cdots & \mathbf{d}_k^{(S)}) \\ \vdots & \ddots & \vdots \\ \min(\mathbf{d}_{k+N_p}^{(1)} & \cdots & \mathbf{d}_{k+N_p}^{(S)}) \end{pmatrix} \tag{6}$$

A simplified scenario ensembles at each time sample k, represented as $\mathbf{d}_{\text{syn},k}$, is constructed as:

$$\mathbf{d}_{\text{syn},k} = \begin{pmatrix} \mathbf{d}_{\max,k} & \mathbf{d}_{\text{mean},k} & \mathbf{d}_{\min,k} \end{pmatrix} \tag{7}$$

The three synthetic scenario ensembles, as described in Equation 7, encompass the full extent of uncertainty represented by the original scenario ensembles in Equation 3.

Step. 2: The use of synthetic scenario ensembles, each with its own probability of occurrence, provides a better representation of uncertainty given by the original scenario ensembles. The probabilities of the three synthetic scenario ensembles are calculated by determining the number of uncertainty points from

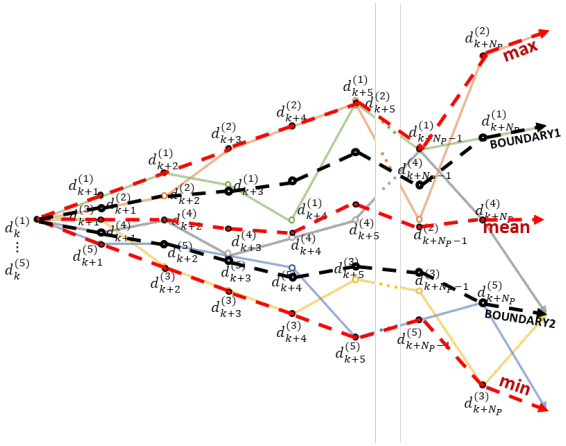

Figure 6: The defined boundary line, when s_1 and s_2 are set as 0.5

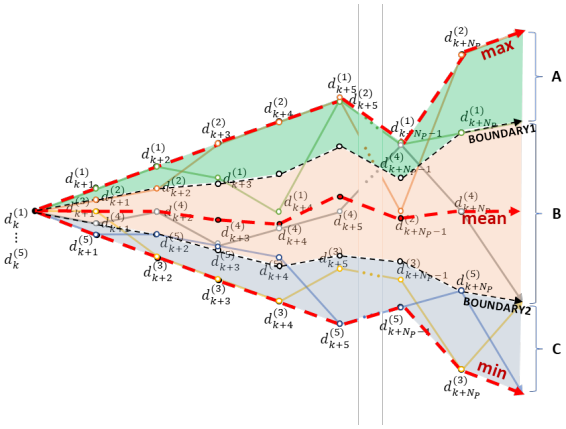

Figure 7: The defined boundary region to calculate the probabilities of occurrences of the synthesis scenario ensembles

the original scenario ensembles that fall within predefined boundary regions. These boundaries can be determined based on either engineering expertise or statistical analysis. For example, the boundaries 1 and 2, denoted by B_1 and B_2, can be established statistically as shown in Figure 6 and are described as follows:

$$B_1 = \mathbf{d}_{\text{mean},k} + s_1 \cdot (\mathbf{d}_{\max,k} - \mathbf{d}_{\text{mean},k})$$

$$B_2 = \mathbf{d}_{\text{mean},k} - s_2 \cdot (\mathbf{d}_{\text{mean},k} - \mathbf{d}_{\min,k})$$

where s_1 and s_2 are parameters that allow for the adjustment of the boundary ranges. As a result, the boundary regions as depicted in Figure 7 can be represented as follows:

$$\mathbf{A} \in (B_1, \mathbf{d}_{\max,k}]$$

$$\mathbf{B} \in [B_1, B_2]$$

$$\mathbf{C} \in [\mathbf{d}_{\min,k}, B_2)$$

Regions A, B, and C encompass the probabilities of occurrence for the maximum, mean, and minimum synthetic scenario ensembles, respectively. For instance, the calculation of the probability of occurrence for the maximum synthetic scenario ensemble can be performed as follows:

$$\omega_{\max} = \frac{\sum_{j=1}^{S} \omega_j \cdot N_{\text{A}}^{(j)}}{\sum_{j=1}^{S} \omega_j \cdot N^{(j)}} \tag{8}$$

where ω_j is the possibility of occurence of the j^{th} original scenario ensemble, and $N^{(j)}$ represents the number of uncertainty points in the j^{th} original scenario ensemble, and $N_{\text{A}}^{(j)}$ refers to the number of uncertainty points that belong to region A in the j^{th} original scenario ensemble. The probabilities of occurrence for the mean and minimum synthetic scenario ensembles, ω_{mean} and $\omega_{\min}$, can be calculated in a similar fashion.

3.1 Multistage MPC with simplified scenario ensembles

By utilizing the simplified method, the number of scenario ensembles in the multistage MPC framework is significantly reduced to three. This leads to a substantial decrease in the number of optimization variables by a factor of $\frac{3}{S}$ and also reduces the number of constraints. As a result, the simplified method makes it easier and faster to solve the optimization problem.

4 System description

The Dalsfoss hydropower plant, located in Telemark, Norway along the Kragerø watercourse, consists of a reservoir called Lake Toke and a dam for its power production. Maintaining control over the water level in the reservoir is essential for safe and flexible operation (SkagerakKraft, 2021a,b). However, uncertainty in the water inflow system presents a challenge in controlling the water level. The water inflow to the reservoir is impacted by various factors, such as ice melt, precipitation, and streams. To address this issue, the operation of the Dalsfoss hydropower plant is guided by the forecast which has 50 possible scenario ensembles of water inflow to the reservoir, each with an equal chance of occurrence. These scenarios are generated every 24 hours through the use of complex hydrological models and weather forecast information, providing a 13-day forecast of water inflow into the reservoir.

4.1 System model

A simplified layout of Lake Toke can be seen in Figure 8, which separates the lake into two areas: the

upper region known as Merkebekk, situated on the left side, and the lower region, known as Dalsfoss, located near the dam and hydropower plant on the right side.

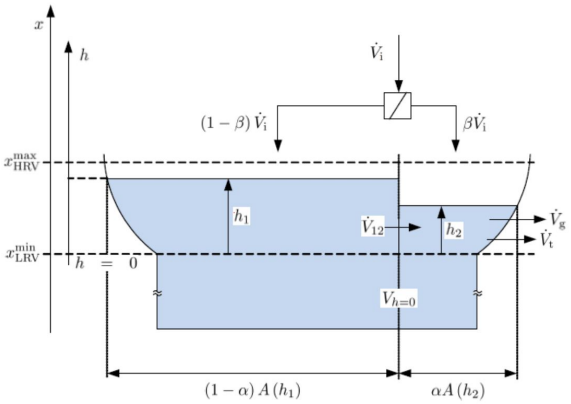

Figure 8: Simplified layout of lake Toke

The water levels in Merkebekk and Dalsfoss, denoted by h_1 and h_2 respectively, act as the states of the system. The flow between the two regions, $\dot{V}_{12}$, is dependent on the difference in water levels. The surface area of Lake Toke, represented as $A(h_i)$, is calculated based on the water level and its unique curvature structure. The fraction of the surface area located in Dalsfoss, denoted by α, must also be considered. The water inflow, $\dot{V}_i$, which comes from various sources such as rivers, precipitation, and ice melting, is described by a coefficient β that represents the ratio of water flowing into Dalsfoss. The operational guidelines must include the consideration of level constraints, such as the minimum low regulated level value (LRV), $x_{\text{LRV}}^{\min}$, and the maximum high regulated level value (HRV), $x_{\text{HRV}}^{\max}$. The flow rates through the floodgate, $\dot{V}_g$, and the turbine, $\dot{V}_t$, combine to make up the total outflow, $\dot{V}_o$, towards the downstream.

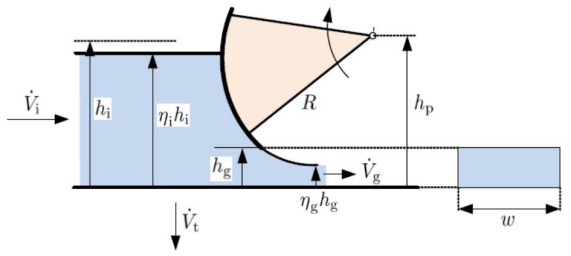

Figure 9: Structure of floodgate

The dynamic model of Lake Toke features two floodgates for regulating the water level within the reservoir, as depicted in Figure 9. The opening heights of these floodgates, represented by h_g, serve as controllable variables that impact the flow rate of water released from the reservoir, $\dot{V}g$. The model is also used in previous works (Menchacatorre et al., 2019; Jeong et al., 2021; Jeong and Sharma, 2022a,b). A summary of the dynamic model, along with its relevant parameters in Table 1, is provided as:

$$\frac{dh_1}{dt} = \frac{1}{(1-\alpha)A(h_1)}((1-\beta)\dot{V}_i - \dot{V}_{12}) \tag{9}$$

$$\frac{dh_2}{dt} = \frac{1}{\alpha A(h_2)}(\beta\dot{V}_i + \dot{V}_{12} - \dot{V}_o) \tag{10}$$

$$A(h_i) = \max(28\times10^6 \cdot 1.1 \cdot h_i^{\frac{1}{10}}, 10^3) \tag{11}$$

$$\dot{V}_{12} = K_{12}\cdot(h_1 - h_2)\sqrt{|h_1 - h_2|} \tag{12}$$

$$\dot{V}_g = C_d \cdot w \cdot \min(h_g, h_2)\sqrt{2g\cdot\max(h_2, 0)} \tag{13}$$

$$\dot{V}_t = a\frac{\dot{W}_e}{x_D - x_q} + b \tag{14}$$

In equation (14), the variable x_q represents the water level at the quay, and it is obtained through the resolution of the following cubic equation.

$$\begin{aligned} 0 = {} & c_1 x_q^3 + (c_2 - c_1 x_D)x_q^2 \\ & + (c_3 - c_2 x_D + c_4\dot{V}_g)x_q \\ & + \dot{W}_e - c_3 x_D - c_4\dot{V}_g x_D - c_5 \end{aligned} \tag{15}$$

The water levels above sea level at Merkebekk, x_M, and Dalsfoss, x_D, are calculated as follows:

$$x_M = h_1 + x_{\text{LRV}}^{\min} \tag{16}$$

$$x_D = h_2 + x_{\text{LRV}}^{\min} \tag{17}$$

4.2 Operational constraints

To ensure safe operation, protect the local wildlife, and prevent damage to nearby properties, the hydropower plant must comply with a set of established constraints:

1. To ensure the safety of individuals and wildlife along the watercourse, it's crucial to avoid abrupt changes in the downstream flow rate, $\dot{V}_o$. Maintaining a consistent flow rate is of utmost importance.

2. To facilitate the free migration of fish and preserve the watercourse, it's vital to maintain the downstream flow rate, $\dot{V}_o$, at a minimum of $4\text{m}^3/\text{s}$.

Table 1: Parameters for Lake Toke model

Parameter	Value	Unit	Comment
α	0.05	-	Fraction of surface area in compartment 2
β	0.02	-	Fraction of inflow to compartment 2
K_{12}	800	$m^{\frac{3}{2}}/s$	Inter compartment flow coefficient
C_d	0.7	-	Discharge coefficient, Dalsfoss gate
w_1	11.6	m	Width of Dalsfoss gate 1
w_2	11.0	m	Width of Dalsfoss gate 2
$x_{\text{LRV}}^{\min}$	55.75	m MSL	Minimal low regulated level value
$x_{\text{HRV}}^{\max}$	60.35	m MSL	Maximal high regulated level value
g	9.81	m/s^2	Acceleration of gravity
a	124.69	Pa^{-1}	Coefficient in equation (14)
b	3.161	m	Coefficient in equation (14)
c_1	0.13152	W/m^{-3}	Polynomial coefficient in (15)
c_2	-9.5241	W/m^2	Polynomial coefficient in (15)
c_3	$1.7234 \cdot 10^2$	W/m	Polynomial coefficient in equation (15)
c_4	$-7.7045 \cdot 10^{-3}$	Pa/m	Polynomial coefficient in equation (15)
c_5	$-8.7359 \cdot 10^{-1}$	W	Polynomial coefficient in equation (15)

3. The water level at Merkebekk must be maintained within specified bounds, as indicated by:

$$x_{\text{M}} \in [x_{\text{LRV}}, x_{\text{HRV}}]$$

These bounds vary based on the season, as outlined in Table. 2.

4. The maximum flow rate through the turbine, $\dot{V}_t$, is capped at $36m^3/s$.

5. The maximum opening height of the floodgates is restricted to 5.6m.

Table 2: Seasonal level requirement

Date	x_{LRV}[m MSL]	x_{HRV}[m MSL]
Jan. 1 - Apr. 30	55.75	60.35
May. 1 - Aug. 30	58.85	59.85
Sept. 1 - Sept. 14	55.75	59.35
Oct. 28 - Nov. 11	55.75	59.85
Nov. 12 - Dec. 31	55.75	60.35

4.3 Optimal control problem

The objective of MPC for the hydropower system is to maximize the utilization of water resources in the generation of electricity, and in satisfying the steady flow and the minimum water flow at downstream. The cost function of the OCP is defined as:

$$J_k = \omega_{x_{\text{M}}} L^2(x_{\text{M},k+i}) + \omega_{\Delta h_g} \Delta h_{g,k}^2 + \omega_{h_g} h_{g,k}^2 + \omega_p p_k^2 \tag{18}$$

The parameters affecting the objective function are listed in Table 3. The first component of the objective function, in Equation (18), aims to maximize the water level at Merkebekk by setting the reference target as the high regulated value (HRV):

$$L(x_k) = x_{\text{M},k} - x_{\text{HRV}} \tag{19}$$

The second term, $\omega_{\Delta h_g} \Delta h_{g,k}^2$, serves to minimize variations in the height of the floodgate opening, thus reducing wear and tear on the floodgate and maintaining a stable flow rate downstream. The third term, $\omega_{h_g} h_{g,k}^2$, aims to minimize the utilization of the floodgate. The final term in the objective function, $\omega_p p^2$, is a penalty term in the event of a violation of the water level constraints. This penalty term allows for a degree of slack from the lower regulated value (x_{LRV}) to prioritize the satisfaction of the minimum flow rate constraint when there is not enough water in the reservoir for both constraints. The slack variable is denoted as p_k. The level constraint is formed as: $x_M \in [x_{LRV} - p, x_{HRV}]$. The value of p_k is determined by solving OCP (Jeong et al., 2021).

Table 3: Parameters for objective function

Parameter	Value	Unit
ω_R	10	-
$\omega_{\Delta u}$	1	-
ω_u	1	-
ω_p	10000	-

Therefore, the optimal control problem for the mul-

tistage MPC is formulated as:

$$\underset{u_k^j, \forall (j,k) \in I}{\text{minimize}} \quad \sum_{i=1}^{S} \omega_i \sum_{k=0}^{Np-1} J_k \tag{20a}$$

$$\text{subject to} \quad x_{k+1}^j = f(x_k^{p(j)}, u_k^j, \dot{V}_{\mathrm{i},k}^{r(j)}, \dot{W}_{\mathrm{e},k}), \tag{20b}$$

$$x_{\mathrm{LRV}} \leq x_{\mathrm{M},k}^j \leq x_{\mathrm{HRV}}, \tag{20c}$$

$$0 \leq u_k^j \leq 5.6m, \tag{20d}$$

$$0 \leq \dot{V}_{\mathrm{t}} \leq 36m^3/s, \tag{20e}$$

$$4m^3/s \leq \dot{V}_{\mathrm{O}} \leq \inf, \tag{20f}$$

$$u_k^j = u_k^l \quad \text{if} \quad x_k^{p(j)} = x_k^{p(l)} \tag{20g}$$

where the system state, x_k^j, is defined as $[h_{1,k}^j, h_{2,k}^j]$, and the control input, u_k^j, is defined as $[h_{\mathrm{g1},k}^j, h_{\mathrm{g2},k}^j]$.

5 Simulation setup

5.1 General setting

The simulation period is set for a duration of one month, from April 15th to May 15th. This period includes a significant change in the required water level. The prediction horizon is determined as 13 days (312 hours). The simulations are executed utilizing the IPOPT solver in CasADi (Andersson et al., 2019).

5.2 Uncertainties in the system

The Dalsfoss hydropower plant faces two main sources of uncertainty: the water inflow and the power production plan. To simulate the system more realistically, historical data on power production and the stored scenario ensembles of the water inflow prediction from the real hydropower plant are utilized. A perfect prediction is assumed on the power production plan.

5.2.1 Power production plan

The power production plan for the period of April 15th to May 15th, 2020 is depicted in Figure 10. The data for this plan is obtained from Skagerak Kraft who is the operator of the hydropower plant..

5.2.2 Water inflow forecast

The water inflow forecast is obtained by updating it every 24 hours in the form of 50 scenario ensembles for the next 13 days (312 hours). The 50 scenario ensembles, which were obtained on April 15th, 2020 from Skagerak Kraft, are graphically represented as an example in Figure 11. These ensembles are mathematically represented in a matrix form as follows:

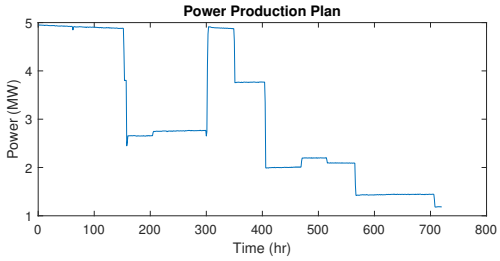

Figure 10: Actual power production history from April 15th, 2020 to May 15th, 2020

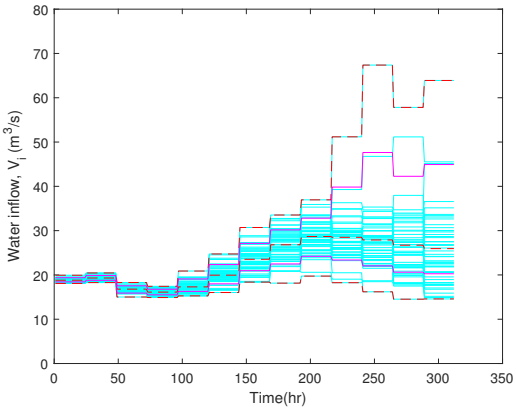

Figure 11: Example of the water inflow forecast obtained on April 15th, 2020 from Skagerak. The cyan color lines are the original 50 scenario ensembles, the red dotted lines represent the three synthesis scenario ensembles, and the pink lines are boundaries with s_1 and s_2 set as 0.5.

$$\dot{V}_{\mathrm{i},k} = f \cdot \begin{pmatrix} \dot{V}_{\mathrm{i},k}^{(1)} & \dot{V}_{\mathrm{i},k}^{(2)} & \cdots & \dot{V}_{\mathrm{i},k}^{(50)} \\ \dot{V}_{\mathrm{i},k+1}^{(1)} & \dot{V}_{\mathrm{i},k+1}^{(2)} & \cdots & \dot{V}_{\mathrm{i},k+1}^{(50)} \\ \vdots & \vdots & \ddots & \vdots \\ \dot{V}_{\mathrm{i},k+312}^{(1)} & \dot{V}_{\mathrm{i},k+312}^{(2)} & \cdots & \dot{V}_{\mathrm{i},k+312}^{(50)} \end{pmatrix}, \tag{21}$$

Where the columns in the matrix represent individual water inflow scenarios. The severity of flooding conditions is described through the use of a flooding coefficient, f, which is set to values of 1 and 2 to represent the moderate water inflow situation and the flooding situation, respectively. For an example, with f = 2, the original real water inflow ensembles are all multiplied by 2 to represent a flood situation.

In this paper, the scenario ensembles of the water inflow prediction are chosen for implementing multistage MPC with notations as described below:

- **MS** contains the original 50 scenario ensembles of the water inflow forecast without any simplification.

- **OS** has the original three scenario ensembles of the water inflow forecast. They are ensembles that have maximum, median, and minimum accumulated amounts of water inflow over the forecast period among all ensembles. The scenario ensemble numbers i, l, and m are chosen as:

$$\sum \dot{V}^{(i)}_{\mathrm{i},k} = \max(\sum \dot{V}^{(1)}_{\mathrm{i},k}, \sum \dot{V}^{(2)}_{\mathrm{i},k}, \ldots, \sum \dot{V}^{(50)}_{\mathrm{i},k})$$

$$\sum \dot{V}^{(l)}_{\mathrm{i},k} = \mathrm{median}(\sum \dot{V}^{(1)}_{\mathrm{i},k}, \sum \dot{V}^{(2)}_{\mathrm{i},k}, \ldots, \sum \dot{V}^{(50)}_{\mathrm{i},k})$$

$$\sum \dot{V}^{(m)}_{\mathrm{i},k} = \min(\sum \dot{V}^{(1)}_{\mathrm{i},k}, \sum \dot{V}^{(2)}_{\mathrm{i},k}, \ldots, \sum \dot{V}^{(50)}_{\mathrm{i},k})$$

  where

$$\sum \dot{V}^{(j)}_{\mathrm{i},k} = \dot{V}^{(j)}_{\mathrm{i},k+1} + \dot{V}^{(j)}_{\mathrm{i},k+2} + \cdots + \dot{V}^{(j)}_{\mathrm{i},k+312}$$

- **Syn(p)** contains three synthetic scenario ensembles with probability distribution information, which is the proposed method in this paper. To set boundary, values of s_1 and s_2 are set as 0.5.

- **Syn(e)** has three synthetic scenario ensembles with equal probability. The synthetic scenario ensembles are constructed by applying the first step of the simplification, Equations (4), (5), and (6). Then, the equal probability is given to the scenario ensembles without using the second step of the simplification.

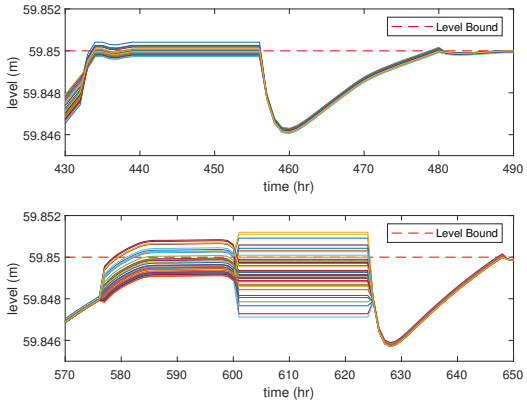

Figure 12: The potential constraint violations caused by implementing multistage MPC using three original scenarios (OS)

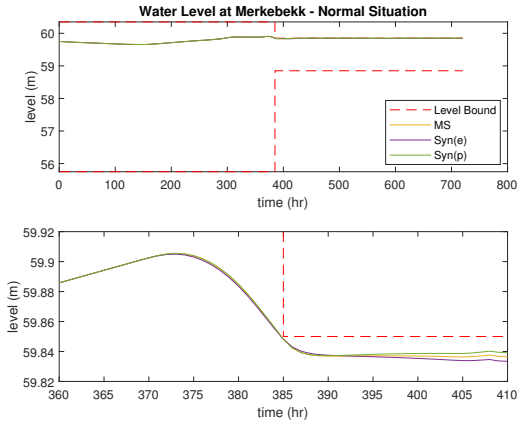

Figure 13: The water level at Merkebekk during the simulation under the moderate water inflow situation

6 Result

6.1 Open-loop Robustness anaylsis

Multistage MPCs with **MS**, **Syn(e)**, and **Syn(p)** show good robustness against constraint violations caused by water inflow uncertainty. This is not the case for multistage MPC with **OS**, as demonstrated by simulations that reveal potential constraint violations (depicted in Figure 12). The figure illustrates possible water level trajectories at Merkebekk from the open-loop robustness analysis, with each line representing a distinct scenario. The analysis shows that under the moderate water inflow situation, there are 283 potential violations, and this number increases to 567 in the flooding situation. As multistage MPC with **OS** is not robust to constraint violations, the simulation results from this method will not be discussed further in this paper.

6.2 Simulation result

The simulation results of the water level at Merkebekk under the moderate water inflow situation ($f = 1$) are presented in Figure 13. The upper plot of the figure provides an overview of the water level through the entire simulation period, while the lower plot provides a closer examination of the water level during the sharp fluctuations in the level bounds.

The simulation results of the flooding situation ($f = 2$) are presented in Figure 14. The topmost plot in this figure illustrates the variation of the water level at Merkebekk over the entire simulation duration. The two lower plots in the figure serve to provide a more detailed view of the water level changes during selected periods, effectively being the magnified sections of the topmost plot.

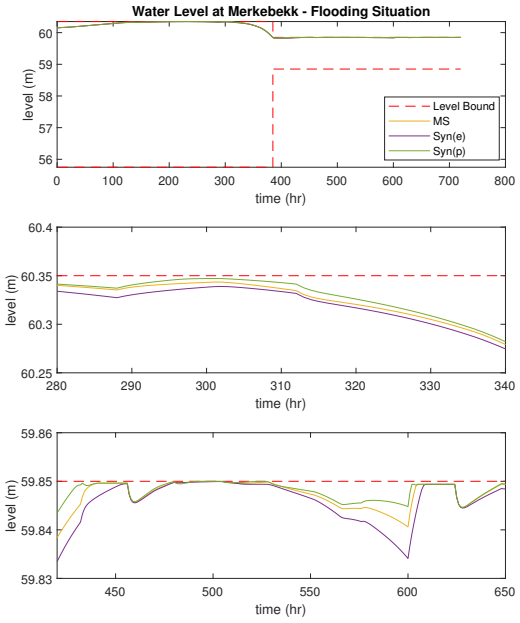

Figure 14: The water level at Merkebekk during the simulation under the flooding situation

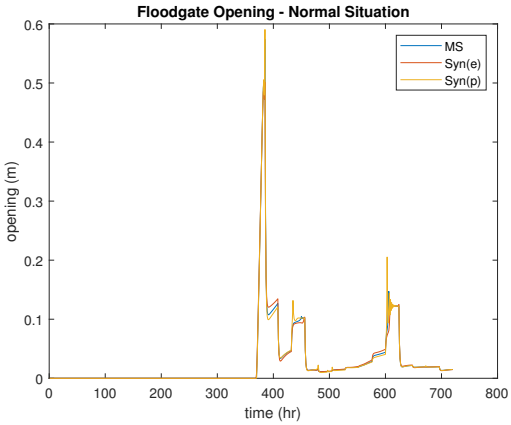

Figure 15: Floodgate opening height through simulations in moderate water inflow situation

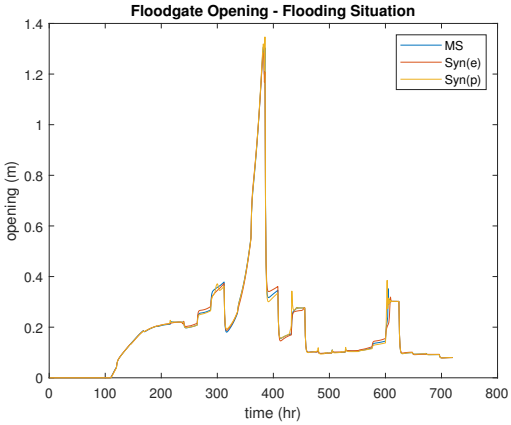

Figure 16: Floodgate opening height through simulations in flooding water inflow situation

The representation of the water level changes in both Figure 13 and Figure 14 are depicted by several lines, each of which corresponds to different simulation scenarios. The red dotted lines indicate the boundaries of the level constraints, represented by x_{LRV} and x_{HRV}. The water level simulated by multistage MPC with **MS** is indicated by the yellow line, while the result of the simulation of multistage MPC with **Syn(e)** is depicted by the purple line. The green line represents the water level changes simulated by multistage MPC with **Syn(p)**.

The opening heights of one floodgate gate with different multistage MPCs(with **MS**, **Syn(e)**, and **Syn(p)**) during the simulation are depicted in Figures 15 and 16. The opening heights of the other floodgate are almost identical to the illustrated figures. Figure 15 represents the opening height of the floodgate under the moderate water inflow situation. Figure 16 presents the opening height of the floodgate during the flooding situation. The opening heights of the floodgate, are indicated by yellow, purple, and green lines, corresponding to the results generated by multistage MPCs with **MS**, **Syn(e)**, and **Syn(p)**, respectively.

Under the moderate water inflow situation, the water level constraints are rarely activated, as the amount of water flowing into the reservoir is not large. Therefore, three multistage MPCs with **MS**, **Syn(e)**, and **Syn(p)** control the system almost identically. During the early stages of the simulation, until around 370 hours, the water levels are controlled by all MPC types and remain relatively unchanged as shown in the upper plot of Figure 13. This period, seen in the left half of the upper plot in Figures 15 and 16, exhibits no significant control actions. However, when the level constraint change, the floodgates start opening, from around 360 hours, to ensure the water level does not exceed the constraint. After 395 hours, subtle differences in the water levels are observed for each multistage MPC, with the highest water level being demonstrated by multistage MPC with **Syn(p)**, the middle water level by multistage MPC with **MS**, and the lowest water level by multistage MPC with **Syn(e)**.

For the flooding situation, the inflow of water into the reservoir is much larger, resulting in a rapid in-

crease in the water level. No control action is taken on the floodgates until 100 hours because the water level does not reach the maximum water level as depicted in Figure 16. As soon as the water level reaches the maximum level, the floodgates are opened to maintain the water level within the constraints. All of the multistage MPCs effectively manage to maintain the water level while satisfying all constraints, but there are slight differences in the water levels among the different multistage MPCs. In line with the simulation result of the moderate water inflow situation, multistage MPC with **Syn(p)** has the highest water level, multistage MPC with **MS** has the middle water level, and multistage MPC with **Syn(e)** has the lowest water level in the flooding scenario.

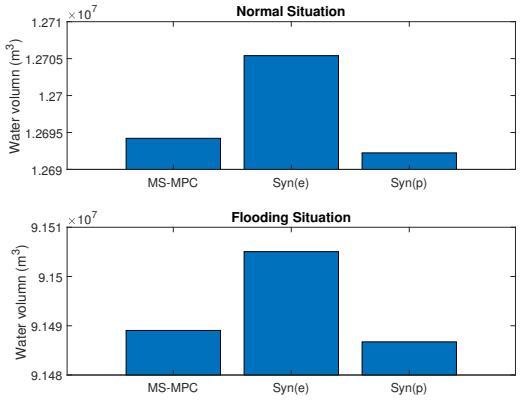

Figure 17: The total amount of water thrown out through floodgates during the simulation period

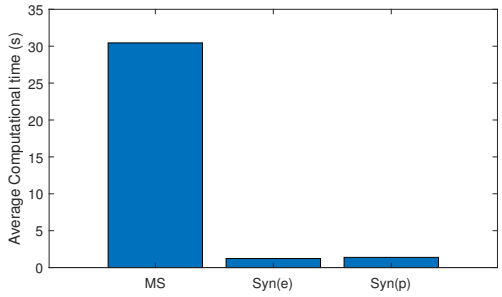

Figure 18: Average computation time for optimization on each time sample

Figure 17 illustrates the total amount of discharged water through the floodgates during the simulation period. As depicted in the figure, multistage MPC with **Syn(p)** exhibits a slightly lower flow rate compared to multistage MPC with **MS**. On the other hand, multistage MPC with **Syn(e)** displays the highest amount of water discharge through the floodgates over the simulation period.

The computational speed of each multistage MPC is presented in Figure 18. Multistage MPC with **MS** requires the longest computation time, with an average of approximately 30 seconds per time sample. In contrast, multistage MPCs with **Syn(p)** and **Syn(e)** have significantly lower computation time, with an average of approximately 2.5 seconds per time sample.

7 Conclusion

In conclusion, this paper presents a practical and efficient method for simplifying the scenario ensembles for multistage MPC applied to the Dalsfoss hydropower station. By using the proposed method, the size of the OCP was reduced by 94%, and the computational speed for solving the OCP was accelerated by 15 times. The simulation results indicate that the performance of multistage MPC with the simplified method (**Syn(p)**) is better or competitive with multistage MPC without using the simplified method (**MS**), and show the improvement in the performance from multistage MPC with (**Syn(e)**), while satisfying all the level constraints. The proposed method in this paper probably cannot be generalized as the simplification of multistage MPC for all types of processes. However, for processes where the uncertainty is already described by scenario ensembles, the proposed method can be effectively used to make the multistage MPC, which a dynamic optimizer for robust control, much more faster and real time implementable.

References

Andersson, J. A. E., Gillis, J., Horn, G., Rawlings, J. B., and Diehl, M. CasADi – A software framework for nonlinear optimization and optimal control. *Mathematical Programming Computation*, 2019. 11(1):1–36. doi:10.1007/s12532-018-0139-4.

Birge, J. R. State-of-the-art-survey–stochastic programming: Computation and applications. *INFORMS Journal on Computing*, 1997. 9(2):111–133. doi:10.1287/ijoc.9.2.111.

Campo, P. J. and Morari, M. Robust model predictive control. In *1987 American Control Conference*. pages 1021–1026, 1987. doi:10.23919/ACC.1987.4789462.

IEA. Hydropower special market report—analysis and forecast to 2030. https://www.iea.org/reports/

hydropower-special-market-report,License:CCBY4.0, 2021.

Jeong, C., Furenes, B., and Sharma, R. MPC operation with improved optimal control problem at dalsfoss power plant. *Proceedings of SIMS EUROSIM conference 2021*, 2021. 11(1):226–233. doi:10.3384/ecp21185226.

Jeong, C. and Sharma, R. Stochastic mpc for optimal operation of hydropower station under uncertainty. *IFAC PapersOnLine*, 2022a. 55(7):155–160. doi:10.1016/j.ifacol.2022.07.437.

Jeong, C. and Sharma, R. Tuning model predictive control for rigorous operation of the dalsfoss hydropower plant. *Energies (Basel)*, 2022b. 15(22):8678. doi:10.3390/en15228678.

Klintberg, E., Dahl, J., Fredriksson, J., and Gros, S. An improved dual newton strategy for scenario-tree mpc. *2016 IEEE 55th Conference on Decision and Control (CDC)*, 2016. pages 3675–3681. doi:10.1109/CDC.2016.7798822.

Lucia, S., Finkler, T., and Engell, S. Multi-stage nonlinear model predictive control applied to a semi-batch polymerization reactor under uncertainty. *Journal of Process Control*, 2013. 23(9):1306–1319. doi:10.1016/j.jprocont.2013.08.008.

Maiworm, M., Bäthge, T., and Findeisen, R. Scenario-based model predictive control: Recursive feasibility and stability. In *IFAC-PapersOnLine*, volume 48. pages 50–56, 2015. doi:10.1016/j.ifacol.2015.08.156.

Mayne, D., Rawlings, J., Rao, C., and Scokaert, P. Constrained model predictive control: Stability and optimality. *Automatica (Oxford)*, 2000. 36(6):789–814. doi:10.1016/S0005-1098(99)00214-9.

Menchacatorre, I., Sharma, R., Furenes, B., and Lie, B. Flood management of lake toke: Mpc operation under uncertainty. 2019. doi:10.3384/ecp20179.

Mesbah, A. Stochastic model predictive control: An overview and perspectives for future research. *IEEE control systems*, 2016. 36(6):30–44. doi:10.1109/MCS.2016.2602087.

Morari, M. and Lee, J. H. Model predictive control : past, present and future. *Computers chemical engineering*, 1999. 23(4-5):667–682. doi:10.1016/S0098-1354(98)00301-9.

NVE. Supervision of dams, (accessed: 24.05.2021). https://www.nve.no/supervision-of-dams/?ref=mainmenu, 2021.

Scokaert, P. and Mayne, D. Min-max feedback model predictive control for constrained linear systems. *IEEE transactions on automatic control*, 1998. 43(8):1136–1142. doi:10.1109/9.704989.

Shapiro, A., Dentcheva, D., and Ruszczyński, A. *Lectures on stochastic programming: modeling and theory*. MOS-SIAM Series on Optimization. Society for Industrial and Applied Mathematics, 2009.

SkagerakKraft. Dalsfos, (accessed: 24.05.2021). https://www.skagerakkraft.no/dalsfos/category1277.html, 2021a.

SkagerakKraft. Kragerø watercourse system, (accessed: 24.05.2021). https://www.skagerakkraft.no/kragero-watercourse/category2391.html, 2021b.

Torabi Haghighi, A., Ashraf, F. B., Riml, J., Koskela, J., Kløve, B., and Marttila, H. A power market-based operation support model for sub-daily hydropower regulation practices. *Applied Energy*, 2019. 255:113905. doi:https://doi.org/10.1016/j.apenergy.2019.113905.

Appendix D

Multistage Model Predictive Control with Simplified Method on Scenario Ensembles of Uncertainty for Hjartdøla Hydropower System

Published in *7th IEEE Conference on Control Technology and Applications (CCTA) 2023*, August 16-18 2023, Bridgetown, Barbados.
Paper presented by Changhun Jeong.
Authors: Changhun Jeong, and Roshan Sharma.
Authors' roles in the article:
Changhun Jeong: Main ideas, implementation, and writing.
Roshan Sharma (Supervisor): Discussions, comments, and proofreading.

Not available online

Appendix E

Stochastic Sequential Model Predictive Control for Operating Buffer Reservoir in Hjartdøla Hydropower System under Uncertainty

Under review in *MIC Journal: Modeling, Identification and Control*.
Authors: Changhun Jeong, Beathe Furenes, and Roshan Sharma.
Authors' roles in the article:
Changhun Jeong: Main ideas, implementation, and writing.
Beathe Furenes: Discussions, comments, and proofreading.
Roshan Sharma (Supervisor): Discussions, comments, and proofreading.

Modeling, Identification and Control, Vol. 31, No. 1, 2023, pp. 1–10, ISSN 1890–1328

Stochastic Sequential Model Predictive Control for Operating Buffer Reservoir in Hjartdøla Hydropower System under Uncertainty

Changhun Jeong [1] Beathe Furenes [2] Roshan Sharma [1]

[1] *Department of Electrical engineering, Information Technology and Cybernetics, University of South-Eastern Norway, Porsgrunn, Norway. E-mail:* changhun.jeong@usn.no / roshan.sharma@usn.no

[2] *Skagerak Kraft AS, Porsgrunn, Norway.*

Abstract

This study focuses on demonstrating the effectiveness and efficiency of the Stochastic Sequential Model Predictive Control (MPC) framework within the context of the Hjartdøla hydropower system. Multistage MPC, while effective in managing uncertainty, poses challenges due to its high computational demands and complex optimal control problems, particularly in applications requiring long-term forecasting, such as hydropower systems. Through a comparative simulation study with multistage MPC, this paper highlights the superior feasibility and computational speed of the Stochastic Sequential MPC framework. This work contributes to the broader understanding of MPC applications in hydropower systems

Keywords: Model predictive control, Stochastic MPC, Uncertainty, Flood management

1 Introduction

Hydropower, esteemed for its environmental benefits[IEA, 2021], confronts challenges that can adversely impact aquatic ecosystems within watercourses[Schmutz and Sendzimir, 2018]. Among these challenges, hydropeaking, characterized by abrupt fluctuations in discharged water flow rates from hydropower turbines, poses a significant threat. Hydropeaking incidents often result from operating hydropower stations in response to fluctuating power demand and can have devastating consequences on downstream fauna [Batalla et al., 2021].

To mitigate the ecological harm caused by hydropeaking, the deployment of buffer reservoirs has emerged as a viable solution. The primary objective of buffer reservoirs is to regulate downstream flow rates in a stable manner by temporarily storing or releasing water [Langhans et al., 2019]. However, managing these buffer reservoirs is a formidable task due to the presence of stringent operational regulations and inherent uncertainties. These uncertainties encompass factors such as variations in power production plans and fluctuations in water inflow originating from diverse streams and rivers.

The Hjartdøla hydropower system, situated in the Hjartdal municipality of Norway and operated by Skagerak Kraft, encounters similar challenges. This hydropower facility, equipped with two Pelton turbines and a buffer reservoir known as Hjartsjå, is specifically designed to control downstream water flow rates. The operational parameters of the Hjartdøla hydropower plant entail constraints related to the water level at Hjartsjå, flow rates through a floodgate, and downstream conditions. Furthermore, the system contends with multiple sources of uncertainty, including variations in power production plans, uncertainties in water inflow forecasts, and model-related uncertainties [SkagerakKraft, 2022].

Currently, the Hjartdøla system employs a Proportional-Integral (PI) controller for system control, supplemented by manual adjustments of setpoints conducted by on-site per-

http://dx.doi.org/10.4173/doi:10.4173/

sonnel. However, this control approach is suboptimal, as it heavily relies on human judgment and predictive assessments of uncertainty, thereby elevating the risk of violating operational constraints. Consequently, Skagerak Kraft AS is actively exploring the application of Model Predictive Control (MPC) frameworks to enhance the precision and efficiency of system control.

Model Predictive Control (MPC) has garnered substantial popularity across both industrial and research domains, particularly for optimizing the operation of constrained multiple-input multiple-output processes. Its efficacy in managing multivariable systems subject to constraints has led to successful implementations in various industrial applications [Morari and Lee, 1999]. MPC involves computing an optimal control sequence for the future by solving a finite horizon open-loop Optimal Control Problem (OCP) based on available system information. Subsequently, the first control input in the sequence is applied, and this procedure repeats at regular sampling intervals [Mayne et al., 2000]. Notably, MPC has demonstrated utility in addressing the operational constraints of hydropower systems [Jeong et al., 2021, Jeong and Sharma, 2022a], although challenges arise due to the inherent uncertainty associated with water inflow to the reservoir, potentially leading to constraint violations[Jeong et al., 2021].

To mitigate these constraint violations, addressing uncertainty becomes imperative when designing and implementing MPC. One prominent approach is Stochastic MPC, exemplified by the multistage MPC or scenario-based MPC framework [Mesbah, 2016]. The genesis of this framework can be traced back to the min-max feedback MPC concept introduced in [Scokaert and Mayne, 1998] and later formalized as multistage MPC by [Lucia et al., 2013]. This framework portrays future uncertainty evolution through a discrete-time scenario tree and employs feedback mechanisms, facilitating closed-loop optimization. It tackles the OCP across multiple control trajectories to account for all plausible realizations of uncertainty. Multistage MPC's versatility has been showcased across diverse domains, including chemical process systems[Lucia et al., 2013, Martí et al., 2015], autonomous vehicles[Klintberg et al., 2016], building climate control[Maiworm et al., 2015], and notably, the management of hydropower systems operating under uncertain water inflow conditions [Jeong and Sharma, 2022b, Jeong et al., 2023a, **?**]. However, challenges persist in terms of computational demands and the intricacy of the OCP structure.

To address these challenges inherent in multistage MPC, the Stochastic Sequential MPC framework was introduced in a prior study. This framework orchestrates two sequential optimizations: an initial optimizer akin to the certainty-equivalent MPC framework, followed by a subsequent optimizer that aligns closely with multistage MPC principles. Previous research demonstrated the advantages of enhanced feasibility and expedited computational efficiency in solving OCP, highlighting the benefits of employing the Stochastic Sequential MPC framework over traditional multistage MPC approaches[Jeong et al., 2023b].

This paper endeavors to apply the Sequential Stochastic Model Predictive Control (MPC) framework to the Hjartdøla hydropower system and subsequently assess its efficacy and efficiency in this context.

The paper's organizational structure is as follows: Section 2 offers an introduction to the Sequential Stochastic MPC framework. In Section 3, the study delves into the particulars of the case study and outlines the simulation configurations. Subsequently, Section 4 is dedicated to the presentation of simulation results, accompanied by a comprehensive discussion of the findings. Finally, Section 5 encapsulates the study's conclusions.

2 STOCHASTIC SEQUENTIAL MPC

The stochastic sequential MPC framework bears resemblance to human decision-making processes within the context of long-term project management. In such scenarios, an initial long-term plan is formulated based on available resources, skills, and information, without explicit consideration of future uncertainties. This long-term plan serves as a foundational blueprint for developing short-term action plans on a daily or weekly basis. While the short-term plans align with the long-term strategy, they also incorporate provisions for potential issues or uncertainties that might arise. In essence, the short-term plans strive to adhere as closely as possible to the long-term plan, while concurrently integrating contingency plans for unforeseen events. This iterative planning approach facilitates the effective and efficient management of long-term projects [Jeong et al., 2023b].

The framework of stochastic sequential MPC, as depicted in Figure 1, amalgamates characteristics from both the certainty-equivalent MPC framework and the multistage MPC framework. In this framework, the first optimizer functions akin to the certainty-equivalent MPC framework, generating a long-term reference control sequence denoted as $\mathbf{U}^*_{\mathrm{ref}}$. This reference control sequence is computed over a prediction horizon of length $N\mathrm{p} = \phi_1$, predicated on nominal values of uncertainty denoted as θ_k, and the measured or estimated system states denoted as $\hat{\mathbf{x}}$. Conversely, the second optimizer resembles the multistage MPC framework, producing short-term optimal control sequences by considering presently available scenarios of uncertainty in the future, denoted as $\mathbf{d}_k$, while also aiming to track the long-term reference control sequence, $\mathbf{U}^*_{\mathrm{ref}}$, generated by the first optimizer. The optimal control sequence within the second optimizer is computed over a shorter prediction horizon of length $N_{\mathrm{p}} = \phi_2$, where ϕ_2 is significantly shorter than ϕ_1

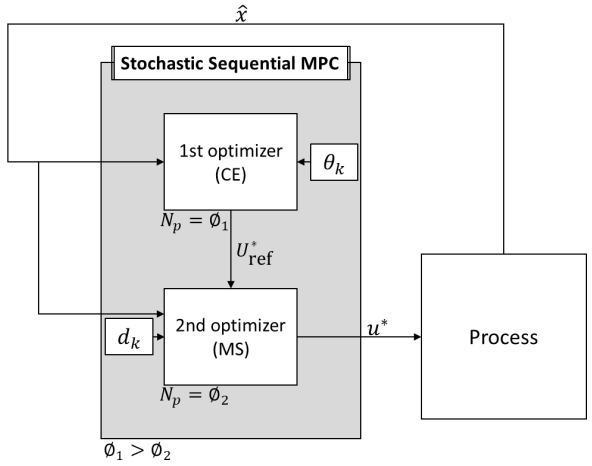

Figure 1: The framework of Stochastic Sequential MPC [Jeong et al., 2023b]

[Jeong et al., 2023b].

Despite not explicitly addressing uncertainty in the distant future, the stochastic sequential MPC framework incorporates future uncertainty information by by the second optimizer. Consequently, stochastic sequential MPC can achieve control performance akin to multistage MPC, while demanding less computational resources and enhancing the feasibility of the optimal control problem [Jeong et al., 2023b].

Let's consider a discrete-time nonlinear system, described by the following equation

$$\mathbf{x}_{k+1} = \mathbf{f}(\mathbf{x}_k, \mathbf{u}_k, \mathbf{d}_k) \tag{1}$$

In this equation, $\mathbf{x}_k \in \mathbb{R}^{n_x}$ represents the system states at time step k, $\mathbf{u}_k \in \mathbb{R}^{n_u}$ represents the control inputs at the same time step, and $\mathbf{d}_k$ denotes the ensemble of scenarios representing uncertainty over the prediction horizon, available at time step k. This relationship can be expressed as:

$$\mathbf{d}_k = \begin{pmatrix} \mathbf{d}_k^{(1)} & \cdots & \mathbf{d}_k^{(S)} \\ \vdots & \ddots & \vdots \\ \mathbf{d}_{k+N_\text{p}}^{(1)} & \cdots & \mathbf{d}_{k+N_\text{p}}^{(S)} \end{pmatrix} \tag{2}$$

Here, S represents the number of scenario ensembles, with each column representing a distinct scenario ensemble. The formulation of the first optimizer mirrors that of the certainty-equivalent MPC, taking the following form:

$$\begin{aligned}
\text{minimize} \quad & \sum_{k=0}^{\phi_1} \mathbf{J}(\mathbf{x}_k, \mathbf{u}_k, \theta_k) && \text{(3a)}\\
\text{subject to} \quad & \mathbf{x}_0 = \hat{\mathbf{x}}, && \text{(3b)}\\
& \mathbf{x}_{k+1} = \mathbf{f}(\mathbf{x}_k, \mathbf{u}_k, \theta_k), && \text{(3c)}\\
& \mathbf{g}(\mathbf{x}_k, \mathbf{u}_k, \theta_k) \leq 0, && \text{(3d)}\\
& \mathbf{x}_\text{lb} \leq \mathbf{x}_k \leq \mathbf{x}_\text{ub}, && \text{(3e)}\\
& \mathbf{u}_\text{lb} \leq \mathbf{u}_k \leq \mathbf{u}_\text{ub} && \text{(3f)}
\end{aligned}$$

Where θ_k represents the nominal value of the uncertainty d_k, and $\hat{\mathbf{x}}$ denotes the measured or estimated states. The initial state for the optimization problem is provided in equation (3b). The system model and output constraints are integrated into equations (3c) and (3d), respectively. The bounds on states and control inputs are enforced through equations (3e) and (3f). The prediction horizon length, denoted as N_p, is set to ϕ_1 with $k = 0, 1, \ldots, \phi_1$ [Jeong et al., 2023b].

As a result of the first optimization, the reference control sequence is derived as $\mathbf{U}^*_\text{ref} = [\mathbf{U}^*_{\text{ref},1}, \ldots, \mathbf{U}^*_{\text{ref},\phi_2}, \ldots, \mathbf{U}^*_{\text{ref},\phi_1}]$. A portion of this reference control sequence, specifically $[\mathbf{U}^*_{\text{ref},1}, \ldots, \mathbf{U}^*_{\text{ref},\phi_2}]$, is passed to the second optimizer. The formulation of the second optimizer closely resembles that of the multistage MPC framework, taking the following form:

$$\begin{aligned}
\text{minimize} \quad & \sum_{j=1}^{S} \omega_j \sum_{k=0}^{\phi_2} \mathbf{J}(\mathbf{x}_k^j, \mathbf{u}_k^j, \mathbf{d}_k^j) + Q_u(\mathbf{u}_k^j - \mathbf{U}^*_{\text{ref},k})^2 && \text{(4a)}\\
\text{subject to} \quad & \mathbf{x}_0^j = \hat{\mathbf{x}}, && \text{(4b)}\\
& \mathbf{x}_{k+1}^j = \mathbf{f}(\mathbf{x}_k^j, \mathbf{u}_k^j, \mathbf{d}_k^j), && \text{(4c)}\\
& \mathbf{g}(\mathbf{x}_k^j, \mathbf{u}_k^j, \mathbf{d}_k^j) \leq 0, && \text{(4d)}\\
& \mathbf{x}_\text{lb} \leq \mathbf{x}_k^j \leq \mathbf{x}_\text{ub}, && \text{(4e)}\\
& \mathbf{u}_\text{lb} \leq \mathbf{u}_k^j \leq \mathbf{u}_\text{ub}, && \text{(4f)}\\
& \mathbf{u}_k^j = \mathbf{u}_k^l \quad \text{if} \quad \mathbf{x}_k^{p(j)} = \mathbf{x}_k^{p(l)} && \text{(4g)}
\end{aligned}$$

In this context, Q_u serves as a weight parameter governing the tracking of the reference control sequence, while ω_j represents the weight or probability associated with the j^{th} scenario ensemble [Jeong et al., 2023b].

The initial states for all scenario ensembles in the optimization problem are provided by equation (4b). The system model and output constraints are integrated into equations (4c) and (4d), respectively. Bounds on states and control inputs are enforced through equations (4e) and (4f) [Jeong et al., 2023b].

The non-anticipativity constraint, as articulated in (4g), ensures that the same control inputs are applied at parent nodes where scenarios branch out. Here, l represents a scenario number distinct from j. The prediction horizon N_p is

set as ϕ_2, which is shorter than ϕ_1, with $k = 0, 1, \ldots, \phi_2$. Consequently, a new optimal control sequence is computed over the horizon length ϕ_2 and its first control input is applied to the system [Jeong et al., 2023b].

For a system characterized by n_x states and n_u control inputs, the multistage MPC framework necessitates solving an Optimization Control Problem (OCP) with $(n_x + n_u) \cdot N_\mathrm{p} \cdot S$ variables. Here, S denotes the number of available scenarios of uncertainty over the prediction horizon length N_p. In contrast, the stochastic sequential MPC framework addresses two OCPs sequentially. The first OCP involves $(n_x + n_u) \cdot N_\mathrm{p}$ variables, while the second OCP encompasses $(n_x + n_u) \cdot \phi_2 \cdot S$ variables. Consequently, the sizes of the OCPs in stochastic sequential MPC are reduced by factors of $1/S$ and ϕ_2/N_p compared to one in multistage MPC, resulting in decreased computational demands [Jeong et al., 2023b].

3 CASE STUDY

3.1 System description

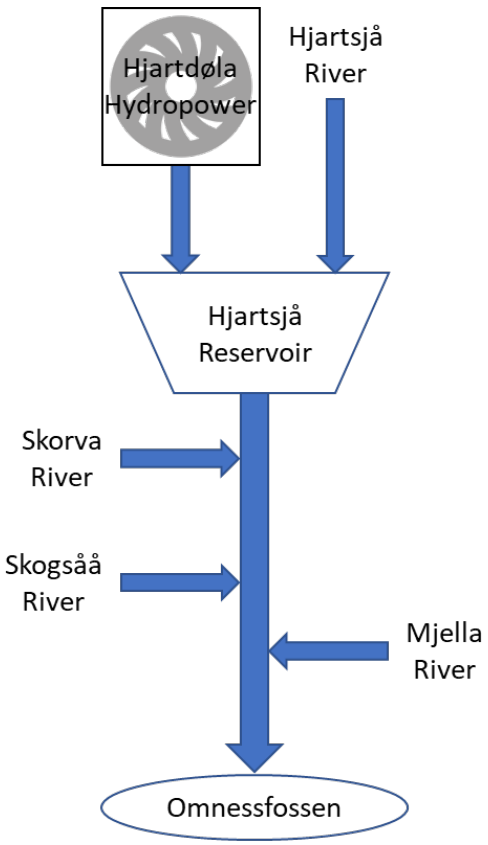

Figure 2: The simple layout of the watercourse system at Hjartdøla hydropower plant

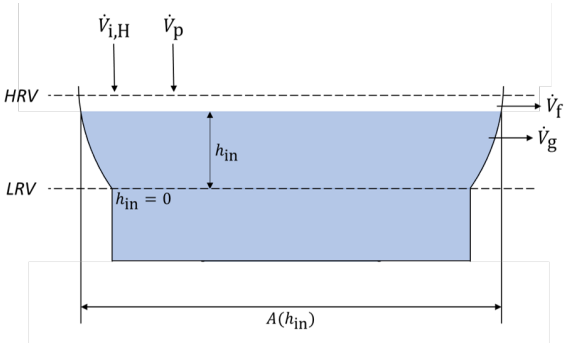

Figure 3: The structure of the Hjartsjå reservoir

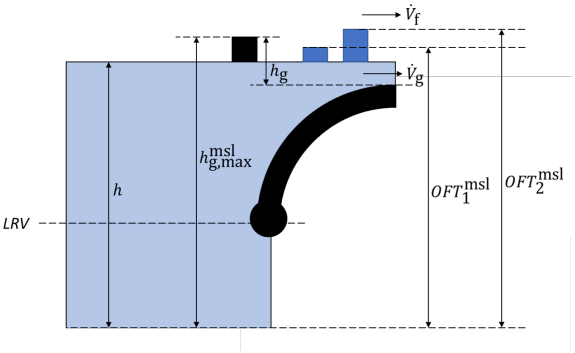

Figure 4: The structure of the floodgate at Hjartsjå reservoir

Hjardøla hydropower plant has two Pelton turbines of 60MW each. After the turbines, there is a buffer reservoir, called Hjartsjå, which is used to control the water flow rate at downstream SkagerakKraft [2022]. Figure. 2 displays a layout of the Hjartdøla hydropower system and Figure. 3 shows the structure of the Hjartsjå buffer reservoir. The water flows into Hjartsjå from two places: the Hjartdøla hydropower turbines $\dot{V}_\mathrm{p}$ and Hjartsjå river $\dot{V}_{\mathrm{i,H}}$. The water flows out from Hjartsjå through a floodgate $\dot{V}_\mathrm{g}$ and flood threshold walls $\dot{V}_\mathrm{f}$. Figure. 4 shows the structure of the floodgate at the reservoir. The water flows toward Omnessfossen located in downstream. Between Hjartsjå and Omnessfossen, three main rivers flow into the watercourse: Skorva river $\dot{V}_{\mathrm{i,SV}}$, Skogsåå river $\dot{V}_{\mathrm{i,SS}}$, and Mjella river $\dot{V}_{\mathrm{i,M}}$. The system has two types of uncertainties: the power production plan and the water inflow forecasts from all four rivers. The flow rate forecasts of all rivers are computed based on hydrological models of the rivers and weather forecast information. Each forecast has 50 possible scenario ensembles for the next 13 days (312 hours). The power production plan is the result of the optimization of factors such as electricity price, demand, etc. During the operation, it is important to consider all forecast information to avoid drastic changes in flow rates.

In the model, the state is the water level at the reservoir h, and the control input is the gate opening h_g. The parameters

Table 1: Parameters for Lake Toke model

Parameter	Value	Unit	Comment
LRV	155.7	m MSL	Lower regulated value
HRV	157.5	m MSL	Higher regulated value
$h_{\mathrm{in,max}}$	$HRV + 3 - LRV = 4.8$	m	Maximum water level of the buffer reservoir (Hjartsjå)
A_{min}	10^3	m^2	Minimum surface area of water in the buffer reservoir (Hjartsjå)
a	0.0474	-	Coefficient
b	1.6898	-	Coefficient
$h^{\mathrm{msl}}_{\mathrm{g,top}}$	157.37	m MSL	Top position of gate opening
L_1	12	m	Width of the gate
L_2	11	m	Width of the overflow channel
OFT^{msl}_1	157.5	m MSL	Overflow threshold 1
OFT^{msl}_2	158.5	m MSL	Overflow threshold 2

of the model are specified in Table. 1 and the model is as follows:

$$h_{\mathrm{in}} = \min(\max(0, h - LRV), h_{\mathrm{in,max}}) \tag{5}$$

$$A(h_{\mathrm{in}}) = \max(A_{\mathrm{min}}, 10^6 \cdot a \cdot b \cdot h_{\mathrm{in}}^{(b-1)}) \tag{6}$$

$$h_{\mathrm{out,g}} = \max(0, h - (h^{\mathrm{msl}}_{\mathrm{g,top}} - h_{\mathrm{g}})) \tag{7}$$

$$\dot{V}_{\mathrm{g}} = 1.84 \cdot L_1 \cdot h^{1.5}_{\mathrm{out,g}} \tag{8}$$

$$h_{\mathrm{out,OF1}} = \max(0, h - OFT^{\mathrm{msl}}_1) \tag{9}$$

$$h_{\mathrm{out,OF2}} = \max(0, h - OFT^{\mathrm{msl}}_2) \tag{10}$$

$$\dot{V}_{\mathrm{f}} = 1.8(L_1 \cdot h^{1.5}_{\mathrm{out,OF1}} + L_2 \cdot h^{1.5}_{\mathrm{out,OF2}}) \tag{11}$$

$$\dot{V}_{\mathrm{O}} = \dot{V}_{\mathrm{g}} + \dot{V}_{\mathrm{f}} + \dot{V}_{\mathrm{i,SV}} + \dot{V}_{\mathrm{i,SS}} + \dot{V}_{\mathrm{i,M}} \tag{12}$$

$$\frac{dh}{dt} = \frac{1}{A(h_{\mathrm{in}})}(\dot{V}_{\mathrm{i,H}} + \dot{V}_{\mathrm{p}} - \dot{V}_{\mathrm{f}} - \dot{V}_{\mathrm{g}}) \tag{13}$$

Operational constraints are designed to achieve (i) operational safety and (ii) prevention of damage to the environment at downstream. The constraints are regulated by the Norwegian Water Resource and Energy Administration (NVE). The violation of the constraints can cause an enormous fine and other sorts of penalties NVE [2022]. Therefore, the constraints must be satisfied. The essential constraints are:

1. The flow rate of the water at downstream(Omnessfossen) must be as steady as possible. This requirement is to keep the fauna and people at downstream safe from hydropeaking or the sudden change in the flow rates or levels at downstream.
2. The water flowing out from the Hjartsjå reservoir should be more than 1.0 m^3/s and more than 2.5 m^3/s at Omnessfossen. This ensures that fish can move freely in the watercourse.
3. The water level at the Hjartsjå reservoir must be maintained between HRV and LRV.

3.2 Optimal control problems

The main purpose of the buffer reservoir is to keep the water flow at downstream as constant as possible. Also, it may be beneficial to keep the water level in the reservoir as high as possible because it gives flexibility to the operation. For example, during the dry season, the reservoir can supply enough water for a longer period to satisfy the required minimum flow rate. The first optimizer computes the reference control sequence with the nominal value of the water inflows. The objective function for the first optimizer is formulated as:

$$J_{1,k} = L_k + \Delta R_k + \Delta VO_k \tag{14}$$

$$L_k = (h_k - HRV) \cdot Q_{\mathrm{h}} \cdot (h_k - HRV)^{\intercal} \tag{15}$$

$$\Delta R_k = (u_k - u_{k-1}) \cdot Q_{\Delta \mathrm{u}} \cdot (u_k - u_{k-1})^{\intercal} \tag{16}$$

$$\Delta VO_k = \Delta \dot{V}^k_{\mathrm{O}} \cdot Q_{\mathrm{V}} \cdot \Delta \dot{V}^{k\intercal}_{\mathrm{O}} \tag{17}$$

Equation (15) aims to maximize the water level in the buffer reservoir. Equations (16) and (17) inhibit the changes in the floodgate opening and the flow rate at downstream(Omnessfossen). The OCP of the first optimizer is

formed as:

$$\begin{aligned}
\text{minimize} \quad & \sum_{k=0}^{\phi_1} J_{1,k} && \text{(18a)}\\
\text{subject to} \quad & h_0 = \hat{h}, && \text{(18b)}\\
& h_{k+1} = f(h_k, h_{\mathrm{g},k}, \mathrm{mean}(\dot{V}^j_{\mathrm{i,H}})), && \text{(18c)}\\
& 1.0m^3/s \leq \dot{V}_{\mathrm{g},k}, && \text{(18d)}\\
& 2.5m^3/s \leq \dot{V}_{\mathrm{O},k}, && \text{(18e)}\\
& LRV \leq h_k \leq HRV, && \text{(18f)}\\
& 0 \leq h_{\mathrm{g},k} \leq 1.5m && \text{(18g)}
\end{aligned}$$

In the second optimizer, the uncertainty of water inflow is included in the optimization and the tracking term to the reference control sequence is added. The objective function of the second optimizer is formulated as:

$$J_{2,k} = J^j_{1,k} + Q_u(\mathbf{u}^j_k - \mathbf{U}^*_{\mathrm{ref},k})^2 \quad \text{(19)}$$

OCP for the second optimizer is formulated as:

$$\begin{aligned}
\text{minimize} \quad & \sum_{j=1}^{S} \omega_j \sum_{k=0}^{\phi_2} J_{2,k} && \text{(20a)}\\
\text{subject to} \quad & h^j_0 = \hat{h}, && \text{(20b)}\\
& h^j_{k+1} = f(h^j_k, h^j_{\mathrm{g},k}, \dot{V}^j_{\mathrm{i,H}}), && \text{(20c)}\\
& 1.0m^3/s \leq \dot{V}_{\mathrm{g},k}, && \text{(20d)}\\
& 2.5m^3/s \leq \dot{V}_{\mathrm{O},k}, && \text{(20e)}\\
& LRV \leq h^j_k \leq HRV, && \text{(20f)}\\
& 0 \leq h^j_{\mathrm{g},k} \leq 1.5m, && \text{(20g)}\\
& h^1_{\mathrm{g},1} = h^2_{\mathrm{g},1} = \cdots = h^S_{\mathrm{g},1} = 0 && \text{(20h)}
\end{aligned}$$

The non-anticipative constraint, (20h), stands only in the first time step, $k = 1$. It is because the given scenario ensembles of the water inflow are independent of each other. Therefore, the only initial state is a parent node. The weighting parameters in the objective function are set as shown in Table 2.

Table 2: Weight parameters in objective function

Parameter	1st optimizer	2nd optimizer
Q_{h}	1	1
$Q_{\Delta \mathrm{u}}$	100	0
Q_{V}	1000	0
Q_u	-	100

3.3 Simulation setup

For the simulation, the actual water inflow prediction and the historical power production plan data, stored by Skagerak Kraft, are used. Figure. 5 and Figure. 6 show the structure of the water inflow forecast and the historical power production plan. While all 50 scenario ensembles of inflow of Hjartsjå river are considered, the water inflow predictions of the three rivers between the reservoir and Omnessfossen(downstream) are simplified by considering the possible scenario of minimum flow rates.

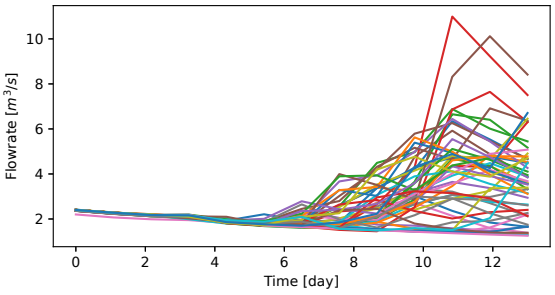

Figure 5: One example of the water inflow forecast

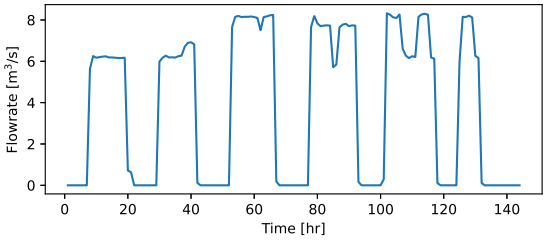

Figure 6: Historical water flow rate through the turbines for power production

For the simulation, the perfect model and the perfect prediction in power production are assumed. The simulation period is 5 days (144 hours) and the time step is set as 1 hour. The simulation is performed on CasAdi in Python Andersson et al. [2019]. In the simulation, four different MPCs are tested as follows:

1. **Certainty-equivalent MPC**: the prediction horizon length is set as 13 days (312 hours) and utilizes the mean value of the water inflow forecast for the prediction of water inflow.

2. **Multistage MPC (MS13d)**: the prediction horizon length is set as 13 days (312 hours) and considers all the scenario ensembles for the optimization.

3. **Multistage MPC (MS6h)**; the prediction horizon length is set as 6 hours and considers all the scenario ensembles for the optimization.

4. **Stochastic Sequential MPC (Seq)**: the first optimizer has 13 days (312 hours) of the prediction horizon

length and utilizes the mean value of the water inflow forecast to compute the reference control sequence. The second optimizer has 6 hours of the prediction horizon and considers all the possible scenarios of the water inflow for the optimization.

To assess the potential violations of the constraints by the realization of the different scenarios from the prediction, the open-loop robustness analysis is conducted. The process of the analysis is shown in Figure. 7. In the open-loop robustness analysis, the model is updated with the computed optimal control input and different water inflow from all the scenarios in an open-loop manner and checks whether the constraints are violated or not in the subsequent time step.

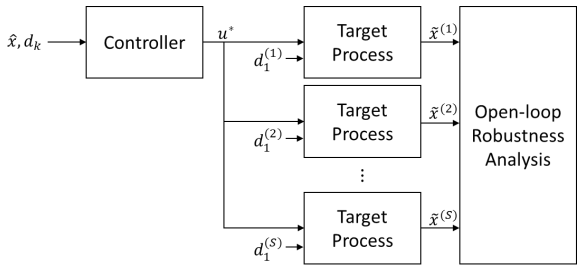

Figure 7: The procedure of open-loop robustness analysis

4 Simulation results and Discussion

Figure. 8 depicts the time-varying flow rate at the downstream location during the simulation period when the buffer reservoir is assumed to be absent. The figure highlights the occurrence of multiple hydropeaking events during the relatively short simulation period. To mitigate the potential damage caused by hydropeaking, it is imperative to optimize the operation of the buffer reservoir.

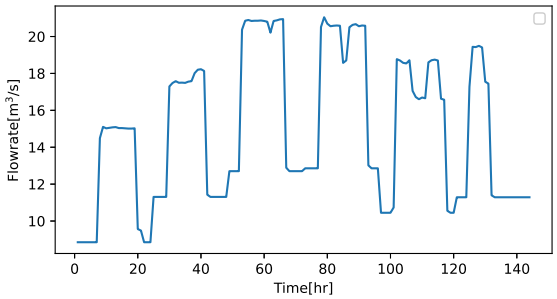

Figure 8: The flow rate at downstream under the assumption that a buffer reservoir does not exist

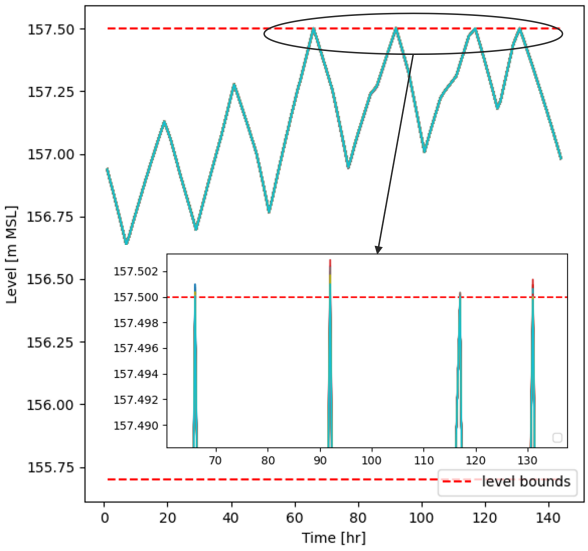

Figure 9: The result of the open-loop robustness analysis when the certainty equivalent MPC is implemented with the nominal values of the water inflow forecast

The simulation result of the certainty equivalent MPC and the open-loop robustness analysis is illustrated in Figure. 9, exhibiting the potential constraint violations at certain instances during the simulation period. It shows all the possible water level changes from all 50 possible scenario ensembles of water inflow. There are potential dangers of the constraint violations at 65 hours, 92 hours, 117 hours, and 131 hours during the simulation period. Although the water level surpasses the bound by small amounts, it is intolerable. However, these potential constraint violations are eliminated in the implementation of both the multistage MPC framework and the stochastic sequential MPC framework.

Figure. 10 shows the simulation results of three other MPC frameworks: the stochastic sequential MPC framework(**Seq**), the multistage MPC with 13 days of the prediction horizon length(**MS13d**), and the multistage MPC with 6 hours of the prediction horizon length (**MS6h**). Figure. 10(a) displays how the water level changes throughout the simulation period, Figure. 10(b) displays the gate openings (control input) throughout the simulation period, and Figure. 10(c) displays the flow rate at the downstream(Omnesfossen) during the simulation. The results of the sequential stochastic MPC are almost identical to that of the multistage MPC with 13 days of the prediction horizon length. For a fair comparison, the multistage MPC with 6 hours of the prediction horizon length (which is also equal to the prediction horizon length of the second optimizer for the sequential stochastic MPC) is displayed but it shows poor management of the water level, and the flow rate at

downstream. The water level is unnecessarily lowered and the flow rate at downstream is not controlled constantly. It shows the importance of tracking the reference control sequence.

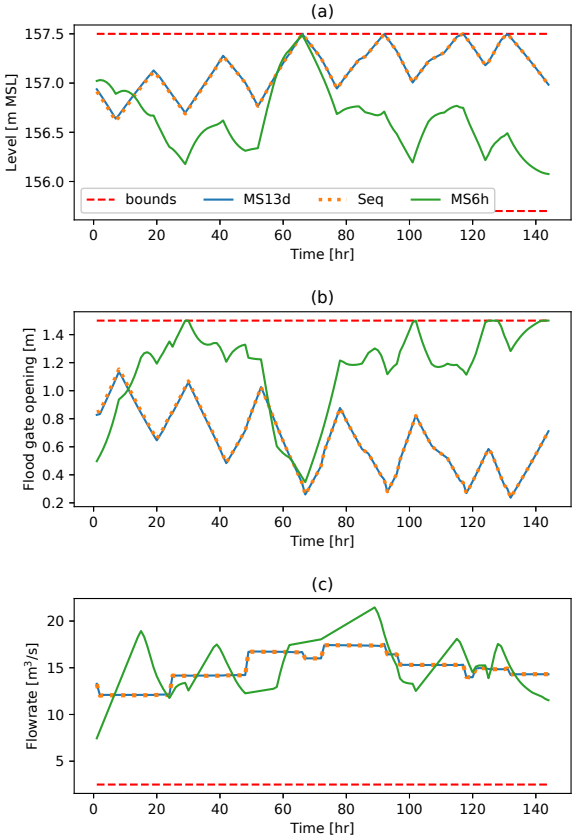

Figure 10: The comparison of the simulation results among the stochastic sequential MPC (**Seq**), the multistage MPC with different prediction horizon lengths of 6 hours (**MS6h**) and 13 days(**MS13d**): (a)The level changes throughout the simulation period, (b)The gate openings throughout the simulation period, and (c)The flow rate of the water at the downstream(Omnessfossen)

Table 3: The detail of computational time for each framework

MPC	Mean	Max	Min
Certainty Equivalent	0.2804	0.6006	0.2128
Stochastic Sequential	0.3081	0.6246	0.2513
Multistage 13 days	27.09	68.65	13.87
Multistage 6 hours	0.1439	0.6497	0.0812

Table. 3 presents a comparison of the computational time required by the multistage MPC and stochastic sequential MPC for the buffer reservoir operation problem. It is observed that the stochastic sequential MPC reduces the computational time by 87 times compared to the multistage MPC with the prediction horizon length set to 13 days. Moreover, despite considering all 50 possible scenario ensembles, the computation time of the stochastic sequential MPC is found to be comparable to that of the certainty equivalent MPC.

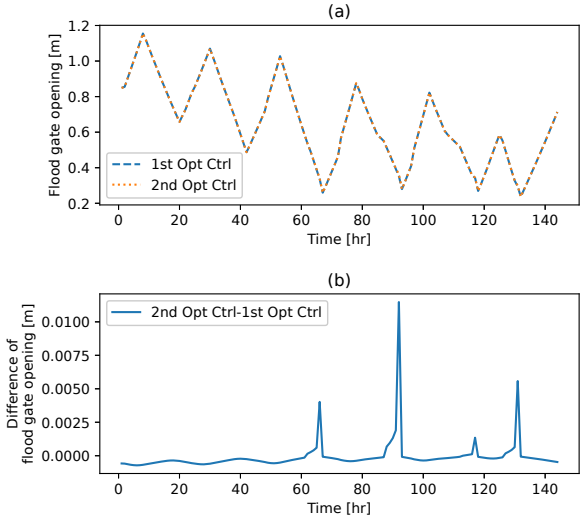

Figure 11: (a)The first control input from the first optimization and the second optimization of the stochastic sequential MPC framework, and (b)The difference of the first control input between the first and second optimization (The second optimization - the first optimization)

Figure.11 demonstrates how the second optimization mitigates the impact of uncertainty. Specifically, Figure.11(a) displays the first control inputs of the control sequences from the first optimizer and the second optimizer of the stochastic sequential MPC framework during the simulation period. It reveals that there is no significant difference between the two control sequences, which is reasonable since the second optimizer is designed to track the reference control sequence from the first optimizer. However, when the first control inputs of the second optimizer are subtracted from the first optimizer's first control inputs, as shown in Figure.11(b), it becomes apparent that the second optimizer increases the gate opening in certain instances. Notably, these instances align with the moments when the open-loop robustness analysis of the certainty equivalent MPC, shown in Fig9, detects potential constraint violations. This finding confirms that the second optimizer adjusts the control sequence slightly to mitigate the impact of uncertainty effectively when required and when there is a possibility of violating constraints.

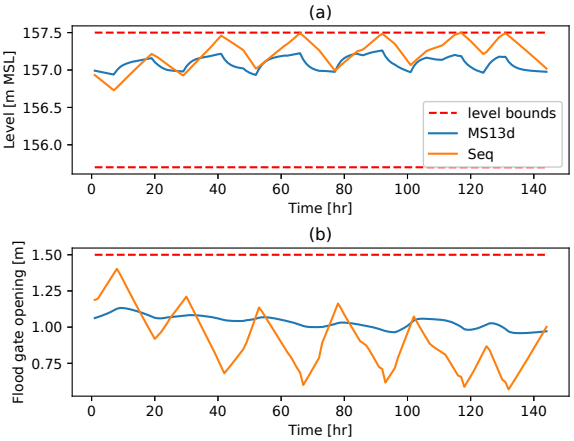

Figure 12: Simulation results of the stochastic sequential MPC(Prediction horizon: 1st optimizer:13days, 2nd optimizer:6hr) and multistage MPC(Prediction horizon: 13days) under assumption of the severe flooding situation. (a)The water level at the reservoir throughout the simulation period, and (b)The applied control inputs throughout the simulation period

In flooding situations, the deviation of water inflow from one scenario to another increase significantly in the further future over the prediction horizon, leading to the potential infeasibility of OCP and, consequently, unreasonable control actions. The simulation results of the stochastic sequential MPC and multistage MPC under severe flooding conditions are presented in Figure. 12. The results indicate that the multistage MPC fails to find an optimal solution, as the computation of OCP becomes infeasible, resulting in an inability to maximize the water level as desired. In contrast, the stochastic sequential MPC manages to find the optimal solution of OCP and effectively control the system in the desired manner. This highlights the better feasibility of the stochastic sequential MPC in solving OCP as it does not consider the deviations of the water inflow in the long-term future, which can be compensated by the feedback control concept.

5 Conclusion

This study utilizes the stochastic sequential MPC framework for controlling the buffer reservoir in the Hjartdøla hydropower system under uncertainty. Compared to the certainty equivalent MPC, which fails to account for uncertainty, and the multistage MPC, which has slower computation time, the stochastic sequential MPC effectively handles uncertainty and ensures that no constraint violations occur. The second optimizer in the stochastic sequential MPC framework is shown to counteract the influence of uncertainty by slightly adjusting the control sequence when necessary, as evidenced by simulation results. Moreover, the stochastic sequential MPC demonstrates significantly faster computation time and better feasibility in solving OCP, particularly under severe flooding conditions. These advantages are attributed to the first optimizer providing a reference control sequence to the second optimizer, which reduces computational demand while reflecting the trend of future uncertainty information. Overall, the results suggest that the stochastic sequential MPC framework is a promising approach for real-time control of hydropower systems under uncertainty.

References

IEA. Hydropower special market report—analysis and forecast to 2030. https://www.iea.org/reports/hydropower-special-market-report, License:CCBY4.0, 2021.

Stefan Schmutz and Jan Sendzimir. *Riverine Ecosystem Management : Science For Governing Towards a Sustainable Future (Volume 8.0)*, volume 8 of *Aquatic Ecology Series*. Springer Open, Cham, 2018. ISBN 3319732498. doi: 10.1007/978-3-319-73250-3.

R J Batalla, C N Gibbins, J Alcázar, J Brasington, C Buendia, C Garcia, M Llena, R López, A Palau, C Rennie, J M Wheaton, and D Vericat. Hydropeaked rivers need attention. *Environmental research letters*, 16(2):21001, 2021. ISSN 1748-9318. doi: 10.1088/1748-9326/abce26.

Simone D. Langhans, Sonja C. Jähnig, Manuel Lago, Astrid Schmidt-Kloiber, and Thomas Hein. The potential of ecosystem-based management to integrate biodiversity conservation and ecosystem service provision in aquatic ecosystems. *The Science of the total environment*, 672: 1017–1020, 2019. ISSN 0048-9697. doi: 10.1016/j.scitotenv.2019.04.025.

SkagerakKraft. Kraftverk - kraftverksoversikt - hjartdøla, (accessed: 24.10.2022). https://www.skagerakkraft.no/hjartdola/category1382.html, 2022.

M. Morari and J. H Lee. Model predictive control : past, present and future. *Computers chemical engineering*, 23 (4-5):667–682, 1999. ISSN 0098-1354. doi: 10.1016/S0098-1354(98)00301-9.

D.Q Mayne, J.B Rawlings, C.V Rao, and P.O.M Scokaert. Constrained model predictive control: Stability and optimality. *Automatica (Oxford)*, 36(6):789–814, 2000. ISSN 0005-1098. doi: 10.1016/S0005-1098(99)00214-9.

Changhun Jeong, Beathe Furenes, and Roshan Sharma. MPC operation with improved optimal control problem at dalsfoss power plant. *Proceedings of SIMS EUROSIM conference 2021*, 11(1):226–233, 2021. doi: 10.3384/ecp21185226.

Changhun Jeong and Roshan Sharma. Tuning model predictive control for rigorous operation of the dalsfoss hydropower plant. *Energies (Basel)*, 15(22):8678, 2022a. ISSN 1996-1073. doi: 10.3390/en15228678.

Ali Mesbah. Stochastic model predictive control: An overview and perspectives for future research. *IEEE control systems*, 36(6):30–44, 2016. ISSN 1066-033X. doi: 10.1109/MCS.2016.2602087.

P.O.M Scokaert and D.Q Mayne. Min-max feedback model predictive control for constrained linear systems. *IEEE transactions on automatic control*, 43(8):1136–1142, 1998. ISSN 0018-9286. doi: 10.1109/9.704989.

Sergio Lucia, Tiago Finkler, and Sebastian Engell. Multi-stage nonlinear model predictive control applied to a semi-batch polymerization reactor under uncertainty. *Journal of Process Control*, 23(9):1306–1319, 2013. ISSN 0959-1524. doi: 10.1016/j.jprocont.2013.08.008.

Rubén Martí, Sergio Lucia, Daniel Sarabia, Radoslav Paulen, Sebastian Engell, and César de Prada. Improving scenario decomposition algorithms for robust nonlinear model predictive control. *Computers chemical engineering*, 79:30–45, 2015. ISSN 0098-1354. doi: 10.1016/j.compchemeng.2015.04.024.

Emil Klintberg, John Dahl, Jonas Fredriksson, and Sébastien Gros. An improved dual newton strategy for scenario-tree mpc. *2016 IEEE 55th Conference on Decision and Control (CDC)*, pages 3675–3681, 2016. doi: 10.1109/CDC.2016.7798822.

Michael Maiworm, Tobias Bäthge, and Rolf Findeisen. Scenario-based model predictive control: Recursive feasibility and stability. In *IFAC-PapersOnLine*, volume 48, pages 50–56, 2015. doi: 10.1016/j.ifacol.2015.08.156.

Changhun Jeong and Roshan Sharma. Stochastic mpc for optimal operation of hydropower station under uncertainty. *IFAC PapersOnLine*, 55(7):155–160, 2022b. ISSN 2405-8963. doi: 10.1016/j.ifacol.2022.07.437.

Changhun Jeong, Beathe Furenes, and Roshan Sharma. Multistage Model Predictive Control with Simplified Scenario Ensembles for Robust Control of Hydropower Station. *Modeling, Identification and Control*, 44(2):43–54, 2023a. doi: 10.4173/mic.2023.2.1.

Changhun Jeong, Beathe Furenes, and Roshan Sharma. Implementation of simplified sequential stochastic model predictive control for operation of hydropower system under uncertainty. *Computers Chemical Engineering*, page 108409, 2023b. ISSN 0098-1354. doi: 10.1016/j.compchemeng.2023.108409.

NVE. Supervision of dams, (accessed: 24.10.2022). `https://www.nve.no/supervision-of-dams/?ref=mainmenu`, 2022.

Joel A E Andersson, Joris Gillis, Greg Horn, James B Rawlings, and Moritz Diehl. CasADi – A software framework for nonlinear optimization and optimal control. *Mathematical Programming Computation*, 11(1):1–36, 2019. doi: 10.1007/s12532-018-0139-4.

Appendix F

Implementation of simplified sequential stochastic model predictive control for operation of hydropower system under uncertainty

Published in *Computers & Chemical Engineering*, 2023.
Authors: Changhun Jeong, Beathe Furenes, and Roshan Sharma.
Authors' roles in the article:
Changhun Jeong: Main ideas, implementation, and writing.
Beathe Furenes: Discussions, comments, and proofreading.
Roshan Sharma (Supervisor): Discussions, comments, and proofreading.

Computers and Chemical Engineering 179 (2023) 108409

Contents lists available at ScienceDirect

Computers and Chemical Engineering

journal homepage: www.elsevier.com/locate/cace

Implementation of simplified sequential stochastic model predictive control for operation of hydropower system under uncertainty

Changhun Jeong [a,*], Beathe Furenes [b], Roshan Sharma [a]

[a] Department of Electrical engineering, Information Technology and Cybernetics, University of South-Eastern Norway, Campus Porsgrunn, Norway
[b] Skagerak Kraft, Porsgrunn, Norway

ARTICLE INFO

Keywords:
Model predictive control
Uncertainty
Sequential optimization
Energy system

ABSTRACT

Sequential stochastic model predictive control (MPC) is a control framework that sequentially employs two optimizers. The high-level optimizer generates a coarse long-term plan based on nominal uncertainty values, while the low-level optimizer refines the short-term plan by considering all possible realizations of these uncertainties. This paper highlights the advantages of the sequential stochastic MPC framework over the traditional multistage MPC approach. It offers faster computation times, improved feasibility of the optimal control problem (OCP), less conservative solutions, and enhanced flexibility in framework tuning. These advantages of sequential stochastic MPC are demonstrated through a case study on flood control in a hydropower station. Additionally, computational efficiency is further boosted with the simplified method which was proposed previously. The results reveal a remarkable performance improvement with an approximately 85 times faster computation time than the standard multistage MPC. These findings establish sequential stochastic MPC framework with the potential for practical implementation.

1. Introduction

Model Predictive Control (MPC) is a widely used control strategy for optimizing the operation of constrained multiple-input multiple-output processes. While MPC has demonstrated success in various industrial applications (Morari and Lee, 1999; Qin and Badgwell, 2003), it faces challenges when uncertainties or disturbances are present in the system, leading to constraint violations. Consequently, addressing uncertainty becomes crucial during the design and implementation of MPC, prompting the development of stochastic or robust MPC approaches (Mesbah, 2016; Saltık et al., 2018).

Robust MPC schemes aim to ensure the satisfaction of constraints and the achievement of closed-loop stability while maintaining computational efficiency and avoiding excessive conservatism. However, striking a balance between non-conservatism and low complexity poses a significant challenge in the field of robust MPC, often necessitating trade-offs.

One of the initial attempts to counteract the uncertainty in MPC scheme was the open-loop min–max MPC (Campo and Morari, 1987). In min–max MPC, the control inputs are chosen in a way that minimizes the maximum predicted cost or error over a finite prediction horizon, considering all possible scenarios of disturbance within a certain bounded set. This ensures that the controller is designed to handle the worst-case situation, providing a certain level of robustness against disturbances. However, the open-loop min–max MPC overlooks the incorporation of feedback in the predictions. To address this limitation, feedback min–max MPC has been introduced, explicitly incorporating feedback information in the predictions to reduce conservatism (Lee and Yu, 1997). General feedback min–max MPC optimizes the worst-case cost function value over a sequence of control inputs, leading to optimization problems with infinite dimensions. To overcome this, a tree structure can be utilized to represent uncertainty evolution, enabling a finite-dimensional optimization problem (Scokaert and Mayne, 1998). By considering various possibilities for adapting inputs in the predictions at each stage, this approach provides increased flexibility. However, the exponential growth of the tree structure with respect to the prediction horizon length limits its practicality for longer horizons.

Alternative robust MPC approaches optimize either the expected cost function's value (as demonstrated in Bernardini and Bemporad (2009)) or a weighted sum of all anticipated scenarios, a characteristic shared with multistage MPC (Lucia et al., 2013). Multistage MPC exhibits a less conservative performance compared to feedback-based min–max MPC, achieved by generating numerous control trajectories across the scenario tree. The tuning parameters allocated to scenarios within multistage MPC offer additional flexibility for refining closed-loop performance, contrasting with feedback min–max MPC strategies.

* Corresponding author.
E-mail addresses: changhun.jeong@usn.no (C. Jeong), roshan.sharma@usn.no (R. Sharma).

https://doi.org/10.1016/j.compchemeng.2023.108409
Received 5 April 2023; Received in revised form 19 August 2023; Accepted 5 September 2023
Available online 9 September 2023

Although the multistage MPC framework has shown promising applications in various fields such as chemical processes (Lucia et al., 2013; Martí et al., 2015), autonomous vehicles (Klintberg et al., 2016), energy systems (Jeong and Sharma, 2022a; Janatian and Sharma, 2022), and building climate control (Maiworm et al., 2015), its practical implementation in the industry poses challenges due to the size of the optimal control problem (OCP). The size of the OCP increases exponentially with (a) the number of uncertain parameters or disturbances, (b) the number of possible realizations of the uncertainty, and (c) the length of the prediction horizon. This exponential growth makes it computationally demanding and difficult to solve the OCP within reasonable time frames, limiting its industrial applicability.

To address this issues, various methods have been proposed to improve the computational efficiency of multistage MPC, such as robust horizon technique (Lucia et al., 2013), primal decomposition algorithm (Krishnamoorthy et al., 2019), simplified method for scenario ensembles (Jeong et al., 2023), adaptive horizon multistage MPC framework (Mdoe et al., 2021), and tube-enhanced multistage MPC (Subramanian et al., 2018). These methods aim to solve computational efficiency and control performance, making multistage MPC more practical and applicable in real-world industries.

Despite the advancements in multistage MPC, certain applications, such as hydropower systems, pose additional challenges due to seasonally changing constraints and uncertain weather forecast information. To effectively operate such case studies, there is a need for a new scheme that considers a long prediction horizon with low computational demand, to operate the system both smoothly and robustly.

Therefore, the sequential stochastic MPC method is proposed in this paper. This control framework utilizes a two-step optimization routine sequentially. The first optimization step generates a control sequence based on nominal values of uncertainty and a longer prediction horizon, which in this paper is referred to as a long-term control sequence. The second optimizer takes in the long-term control sequence as a base guide and refines the control sequences by considering the whole scenario tree of multistage MPC representing the uncertainty but with a relatively shorter prediction horizon. In this paper, the control sequence generated by the second optimizer under the presence of uncertainty is termed a short-term control sequence. The second optimizer aims to track the long-term sequence obtained from the initial optimization step but introduces necessary adjustments to the control sequences to handle the uncertainties. Then, the first control input from the second optimization step is applied to the system in a receding horizon fashion. This process when repeated gives rise to the sequential stochastic MPC framework. More details about the framework are provided in Section 3.

In this paper, the Dalsfoss hydropower station is used as a case study to implement the sequential stochastic MPC and to discuss the usefulness of this control framework. The hydropower station is located in Telemark, Norway, and is operated by Skagerak Kraft. For optimal operation, the hydropower system has to overcome some operational challenges such as seasonally changing water level requirements in its reservoir and uncertainty in the water inflow forecast to the reservoir. A more detailed description of the hydropower process is provided in Section 4. The sequential stochastic MPC framework is tested in the case study to demonstrate its better performance and better convergence of OCP compared to the multistage MPC framework (with a single optimizer), under the flooding situation. Then, to accelerate the computational speed of solving the OCP, the simplification of the scenario ensembles of the uncertainty, which was introduced in Jeong et al. (2023), is applied. Further, the simulations with different settings on the sequential stochastic MPC are performed to demonstrate the limitations and capabilities of the proposed control framework.

The remainder of the paper is organized as follows: Section 2 provides a quick overview of the certainty-equivalent MPC framework and multistage MPC framework. In Section 3, the sequential stochastic MPC framework is introduced. Section 4 presents the case study, the simplification of scenario ensembles, and simulation setups, and the results are presented in Section 5. A discussion of the findings is provided in Section 6. the Conclusion is given in Section 7.

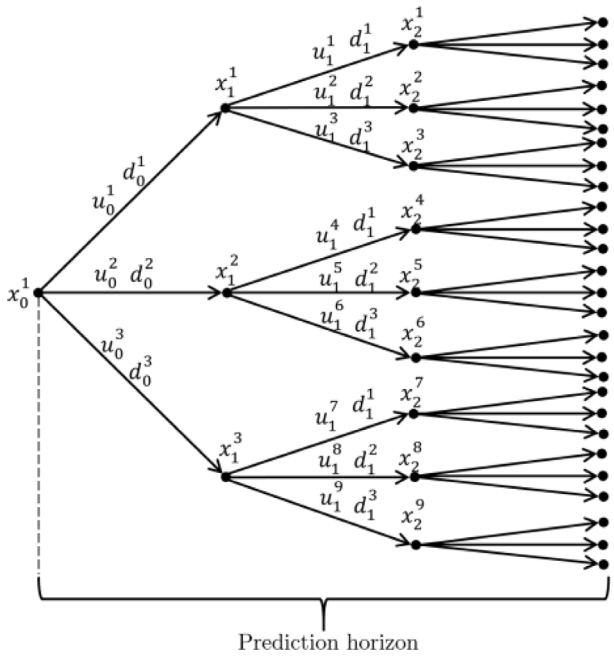

Fig. 1. An example of the structure of a scenario tree (Lucia et al., 2013).

2. Preliminary

2.1. Certainty-equivalent MPC

MPC is a control strategy that generates a control input sequence as a solution of a finite horizon open-loop OCP. The future behavior of the process is predicted by using a mathematical model of the system. The first control input in the sequence is then applied and the process is repeated at each sampling time in a receding horizon fashion. MPC can be considered as a feedback control approach that incorporates model-based predictions and optimizes future control inputs to achieve the desired system behavior (Mayne et al., 2000).

Consider a discrete-time nonlinear system of the form

$$\mathbf{x}_{k+1} = \mathbf{f}(\mathbf{x}_k, \mathbf{u}_k, \theta_k) \tag{1}$$

where $\mathbf{x}$ denotes the states, $\mathbf{u}$ denotes the control inputs, θ denotes the nominal value of the uncertainty and k denotes the time sample. The system model is presented by $\mathbf{f}$. In the certainty equivalent MPC, the uncertainty is predetermined as a nominal value. OCP is formulated over the prediction horizon with the length N_p as,

$$\begin{aligned}
\text{minimize} \quad & \sum_{k=0}^{N_\mathrm{p}} \mathbf{J}(\mathbf{x}_k, \mathbf{u}_k) && \text{(2a)}\\
\text{subject to} \quad & \mathbf{x}_k = \hat{x}_0, && \text{(2b)}\\
& \mathbf{x}_{k+1} = \mathbf{f}(\mathbf{x}_k, \mathbf{u}_k, \theta_k), && \text{(2c)}\\
& \mathbf{g}(\mathbf{x}_k, \mathbf{u}_k) \le 0, && \text{(2d)}\\
& \mathbf{x}_{\mathrm{lb}} \le \mathbf{x}_k \le \mathbf{x}_{\mathrm{ub}}, && \text{(2e)}\\
& \mathbf{u}_{\mathrm{lb}} \le \mathbf{u}_k \le \mathbf{u}_{\mathrm{ub}} && \text{(2f)}
\end{aligned}$$

The cost function at time sample k is defined as $\mathbf{J}(\mathbf{x}_k, \mathbf{u}_k)$ in (2a). The initial state of the system is given as (2b). System model and output constraints are incorporated in (2c) and (2d) and the bounds on states and control inputs are imposed in (2e) and (2f).

2.2. Multistage MPC

Multistage MPC is a well-known framework where the uncertainty affecting the process is often described in the form of a scenario tree

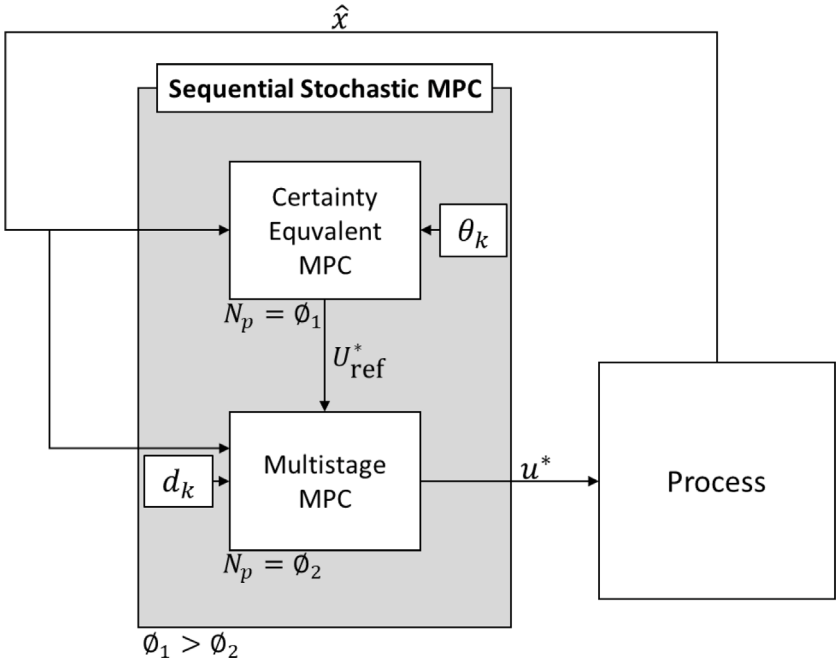

Fig. 2. The framework of sequential stochastic MPC.

as shown in Fig. 1. $(x)^j_k$, $(u)^j_k$, and $(d)^j_k$ indicate state, control input, and uncertain variable in jth scenario at time sample k respectively. Only a brief introduction to multistage MPC is provided here. For details, the readers are referred to (Lucia et al., 2013). A discrete-time nonlinear system can be expressed as:

$$\mathbf{x}^j_{k+1} = \mathbf{f}(\mathbf{x}^j_k, \mathbf{u}^j_k, \mathbf{d}^j_k) \tag{3}$$

As shown in Fig. 1, in the framework of multistage MPC, the control and state trajectories are computed for a range of different scenario ensembles. The optimization problem is formulated over a prediction horizon N_p and a finite number of scenarios S, to find the optimal control inputs to satisfy the system's constraints and objectives. The OCP is expressed mathematically as:

$$\text{minimize} \quad \sum_{j=1}^{S} \omega_j \sum_{k=0}^{N_\text{p}} \mathbf{J}(\mathbf{x}^j_k, \mathbf{u}^j_k) \tag{4a}$$

$$\text{subject to} \quad \mathbf{x}^j_k = \hat{x}_0, \tag{4b}$$

$$\mathbf{x}^j_{k+1} = \mathbf{f}(\mathbf{x}^j_k, \mathbf{u}^j_k, \mathbf{d}^j_k), \tag{4c}$$

$$\mathbf{g}(\mathbf{x}^j_k, \mathbf{u}^j_k) \le 0, \tag{4d}$$

$$\mathbf{x}_\text{lb} \le \mathbf{x}^j_k \le \mathbf{x}_\text{ub}, \tag{4e}$$

$$\mathbf{u}_\text{lb} \le \mathbf{u}^j_k \le \mathbf{u}_\text{ub}, \tag{4f}$$

$$\mathbf{u}^j_k = \mathbf{u}^l_k \quad \text{if} \quad \mathbf{x}^{p(j)}_k = \mathbf{x}^{p(l)}_k \tag{4g}$$

where ω_j is the weight or probability of jth scenario ensemble and $\mathbf{x}^{p(j)}_k$ is the parent state at node. The initial states of the process are given as (4b). System model and output constraints are incorporated in (4c) and (4d) and the bounds on states and control inputs are imposed in (4e) and (4f). The non-anticipativity constraint, (4g), ensures that the same control inputs are used for each branch of the same parent node in the scenario tree, here l denotes another scenario number than j. For example, in Fig. 1, u^1_0, u^2_0, and u^3_0 have the same value as the control input. Similarly, u^1_1, u^2_1, and u^3_1 have the same values and so on for all branches Lucia et al. (2013).

3. Sequential stochastic MPC

The sequential stochastic MPC framework can be thought of as a decision-making process akin to how humans set a plan to achieve a long-term goal. When faced with a significant objective, individuals will first devise a general, broad-spectrum plan that accounts for the overall direction in which they aim to move, while not necessarily accounting for every uncertainty that may arise in the future during the long term.

Subsequently, as the plan to achieve a long-term goal progresses, more detailed short-term plans are made to take into account near-future uncertainties in order to achieve the overarching goal. These plans, such as what actions to take in the near future like the current day or next sampling time, are developed concerning the general long-term plan, and any necessary adjustments to the latter are made as the situation evolves.

This idea is reflected in the design of the sequential stochastic MPC framework, as shown in Fig. 2. The scheme is a combination of the certainty-equivalent MPC and multistage MPC frameworks. The first optimizer, similar to the certainty equivalent MPC framework, serves as the general long-term plan by computing the optimal reference control sequence over the prediction horizon length $N_\text{p} = \phi_1$, based on nominal values of uncertainty θ_k and initial state values $\mathbf{x}_0$. The second optimizer which is a multi-stage MPC then generates a more detailed short-term plan for the near future by taking into account the reference control sequence $\mathbf{U}^*_\text{ref}$ from the first optimizer and computing the optimal control sequence for a shorter period $N_\text{p} = \phi_2$, while considering uncertainty d_k. The first control input from the second optimizer is applied to the process, and this process repeats iteratively in a receding horizon fashion.

The formulation of the first optimizer is the same as the OCP (2) which is for certainty equivalent MPC. The formulation of the second optimizer is similar to a multistage MPC framework and is expressed as:

$$\underset{\mathbf{x}_k, \mathbf{u}_k}{\text{minimize}} \quad \sum_{j=1}^{S} \omega_j \sum_{k=0}^{\phi_2} \mathbf{J}(\mathbf{x}^j_k, \mathbf{u}^j_k) + Q_u(\mathbf{u}^j_k - \mathbf{U}^*_{\text{ref},k})^2 \tag{5a}$$

$$\text{subject to} \quad \mathbf{x}^j_k = \hat{x}_0, \tag{5b}$$

$$\mathbf{x}^j_{k+1} = \mathbf{f}(\mathbf{x}^j_k, \mathbf{u}^j_k, \mathbf{d}^j_k), \tag{5c}$$

$$\mathbf{g}(\mathbf{x}^j_k, \mathbf{u}^j_k) \le 0, \tag{5d}$$

$$\mathbf{x}_\text{lb} \le \mathbf{x}^j_k \le \mathbf{x}_\text{ub}, \tag{5e}$$

$$\mathbf{u}_\text{lb} \le \mathbf{u}^j_k \le \mathbf{u}_\text{ub}, \tag{5f}$$

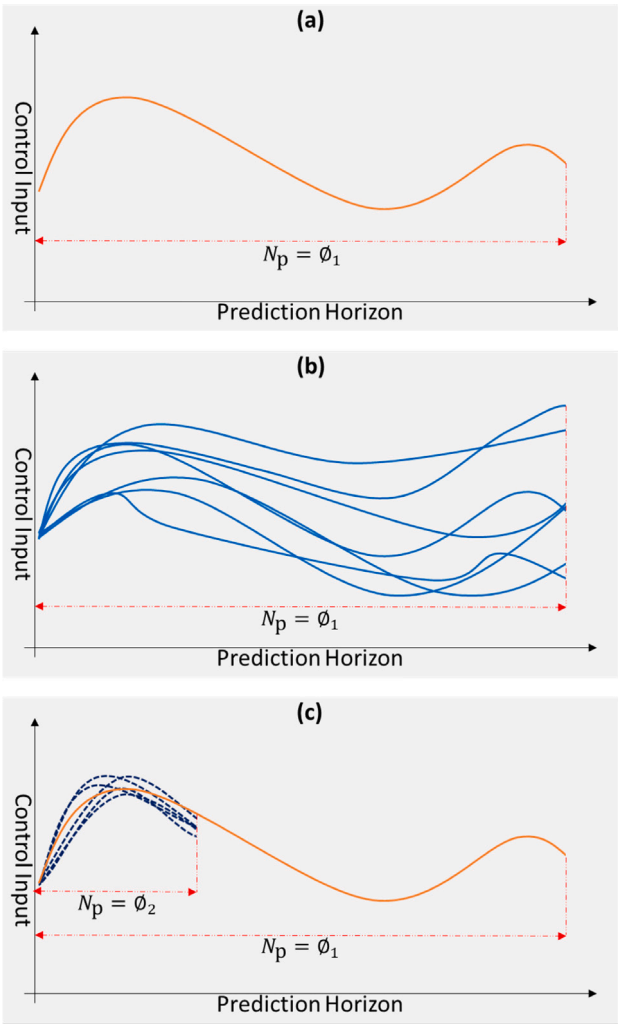

Fig. 3. The example control trajectories: (a) Certainty-equivalent MPC (b) Multistage MPC (c) Sequential stochastic MPC.

$$\mathbf{u}_k^j = \mathbf{u}_k^l \quad \text{if} \quad \mathbf{x}_k^{p(j)} = \mathbf{x}_k^{p(l)} \tag{5g}$$

Let $k = 0, 1, \ldots, \phi_2$, where ϕ_2 denotes the length of the prediction horizon for the second optimizer. The second optimizer computes new optimal control sequences over the horizon length ϕ_2 by taking into account the weight parameter Q_u for tracking the reference control sequence. This optimizer being a multistage MPC by its design also takes into account the uncertainties present in the system for the horizon ϕ_2 using a scenario tree structure.

An illustration of the control sequence trajectories for the certainty-equivalent MPC, multistage MPC, and the proposed sequential stochastic MPC frameworks is shown in Fig. 3. Fig. 3(a) illustrates the control sequence generated by the certainty-equivalent MPC for a long-term plan taking into account a longer prediction horizon ϕ_1 and considering nominal values of the parameters and input disturbances. Fig. 3(b) illustrates the control sequences of a multi-stage MPC for the same long-term plan, i.e. considering the longer prediction horizon ϕ_1 but also taking into account the scenario tree structure for handling uncertainties.

For processes where the prediction horizon ϕ_1 can be very long, the size of the OCP for the multi-stage MPC can become large, which makes the practical implementation of multistage MPC very difficult. To deal with this, the proposed sequential stochastic MPC combines the effort of both the certainty-equivalent MPC and the multistage MPC in a unified framework as illustrated in Fig. 3(c). The orange colored line shows the long-term control sequence (over a longer prediction horizon ϕ_1)generated by the first optimizer of Fig. 2. This control sequence considers only the nominal values of the process. The blue dash colored lines show the control trajectories generated by the second optimizer over a shorter prediction horizon ϕ_2 by taking into account uncertainty present in the system represented by a scenario tree by the multi-stage framework. In general, when constraints are not activated, the second optimizer offers a similar or identical control solution to the first optimizer. However, once there is the potential for the constraint violation, the second optimizer circumvents the violation of the constraint by giving a necessary conservative control action.

To explain the reduction of the size of the OCP, assume a system with n_x states and n_u control inputs and S scenarios of uncertainty over prediction horizon N_p. The number of decision variables to optimize with a multi-stage MPC framework becomes $(n_x + n_u) \cdot N_p \cdot S$ variables. However, with the sequential stochastic MPC framework, two OCPs are solved sequentially. The first OCP has $(n_x + n_u) \cdot N_p$ number of decision variables, and the second OCP has $(n_x + n_u) \cdot \phi_2 \cdot S$ number of decision variables. Although this approach requires solving two OCPs, the sizes of the OCPs are reduced by $1/S$ and ϕ_2/N_p, respectively, compared to the multistage MPC's framework. This feature provides a computational advantage and it allows the sequential stochastic MPC approach to be more efficient for systems with a larger number of scenarios of uncertainty or a longer prediction horizon.

In this paper, it has been shown that the performance of the proposed sequential stochastic MPC is similar to the multi-stage MPC, however, with a much smaller computational footprint. This is one step closer to realizing a stochastic controller with an MPC framework in a practical sense for processes, under uncertainty, that need a longer prediction horizon. The usefulness of the proposed method has been demonstrated through simulations for the case study of the flood gate control of a hydropower station as described in Section 6.

4. Case study

Hydropower is widely recognized as a green technology for electricity generation and is known for its ability to supply power in response to demand. This energy system utilizes water from a reservoir to drive a turbine-generator system, thereby producing clean electricity while allowing for control over the water flow in the watercourse (IEA, 2021). Although hydropower plants are relatively straightforward systems, they are subject to various regulations and operational constraints. In Norway, the Norwegian Water Resource and Energy Administration (NVE) imposes operational requirements on hydropower stations, including seasonally changing water level constraints, to minimize environmental damage and ensure safe operation (NVE, 2022). The Dalfoss hydropower station, operated by Skagerak Kraft in southeastern Norway, is also obligated to comply with these requirements.

The Dalfoss hydropower plant features a reservoir, Lake Toke, with a catchment area of approximately 1150 km^2. The inflow of water into the lake, resulting from precipitation or snow melting, is not uniform and varies throughout the year. Therefore, the actual amount of water flowing into the reservoir remains uncertain. However, Skagerak possesses the ability to forecast water inflow using hydrological models and weather forecasts, enabling the generation of multiple scenarios. The water inflow forecast, encompassing 50 scenario ensembles for the next 13 days, considers all sources of water entering the reservoir, such as precipitation, ice melting, and inflow from various streams. Similarly, the power production plan can be adjusted, as it is determined by Skagerak Kraft's experts based on expected demand and energy prices in the future. The operation of the hydropower plant is challenging due to the presence of uncertainty and adherence to operational requirements (SkagerakKraft, 2022a,b).

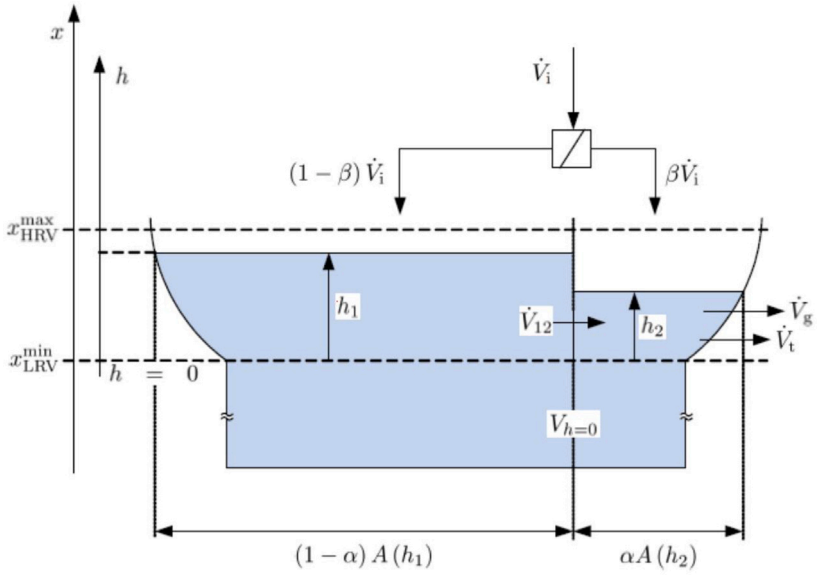

Fig. 4. Schematic representation of Lake Toke.

4.1. System model

The dynamic model of the Dalsfoss hydropower plant, which has been utilized for simulation purposes in previous works (Jeong and Sharma, 2022a; Jeong et al., 2021; Jeong and Sharma, 2022b; Menchacatorre et al., 2019), is employed in this study. Fig. 4 illustrates a simplified representation of Lake Toke, which consists of two sections: Merkebekk, located in the upper part of the lake, and Dalsfoss, situated in the lower part where the hydropower dam and power plant are situated.

In Fig. 4, the water levels at Merkebekk and Dalsfoss are denoted by the states h_1 and h_2, respectively. The inter-compartment flow, represented by $\dot{V}_{12}$, describes the water flow between the two compartments of the lake and is dependent on the difference in water levels. The surface area of Lake Toke, denoted as $A(h_i)$, is determined based on the water level and its curvature structure. The parameter α represents the fraction of the total surface area of the lake in the Dalsfoss compartment.

Water inflow, $\dot{V}_i$, originates from various sources such as rivers, precipitation, and ice melting, and the coefficient β represents the ratio of water inflow to the Dalsfoss compartment. Constraints on the water level are defined by x^{min}_{LRV} and x^{max}_{HRV}, which correspond to the minimal low regulated level value and the maximal high regulated level value, respectively.

The Dalsfoss hydropower station is equipped with two floodgates that allow water to be released from the reservoir. There are two ways water can flow out of the reservoir: through the turbines for electricity generation and by regulating the floodgates during flood situations. The flowrates through the floodgates and turbines denoted as $\dot{V}_g$ and $\dot{V}_t$, play a crucial role in the system. The total water outflow from the hydropower station, denoted as $\dot{V}_o$, is the sum of these flowrates. The flowrates through the floodgates and turbines, in conjunction with the inter-compartment flow, water inflow, and surface area of the lake, are essential factors that govern the dynamics of the Dalsfoss hydropower plant.

The structure of the floodgates at Dalsfoss is shown in Fig. 5. The opening height of the floodgate, h_g, determines the amount of water released.

The details of the dynamic model of the lake Toke are described in Table 1 and the followings:

$$\frac{dh_1}{dt} = \frac{1}{(1-\alpha)A(h_1)}((1-\beta)\dot{V}_i - \dot{V}_{12}) \tag{6}$$

Table 1
Parameters for Lake Toke model.

Parameter	Value	Unit	Comment
α	0.05	–	Fraction of surface area in compartment 2
β	0.02	–	Fraction of inflow to compartment 2
K_{12}	800	$m^{\frac{3}{2}}/s$	Inter compartment flow coefficient
C_d	0.7	–	Discharge coefficient, Dalsfoss gate
w_1	11.6	m	Width of Dalsfoss gate 1
w_2	11.0	m	Width of Dalsfoss gate 2
x^{min}_{LRV}	55.75	m MSL	Minimal low regulated level value
x^{max}_{HRV}	60.35	m MSL	Maximal high regulated level value
g	9.81	m/s^2	Acceleration of gravity
a	124.69	Pa^{-1}	Coefficient in Eq. (12)
b	3.161	m	Coefficient in Eq. (12)
c_1	0.13152	W/m^{-3}	Polynomial coefficient in Eq. (13)
c_2	−9.5241	W/m^2	Polynomial coefficient in Eq. (13)
c_3	$1.7234 \cdot 10^2$	W/m	Polynomial coefficient in Eq. (13)
c_4	$-7.7045 \cdot 10^{-3}$	Pa/m	Polynomial coefficient in Eq. (13)
c_5	$-8.7359 \cdot 10^{-1}$	W	Polynomial coefficient in Eq. (13)

$$\frac{dh_2}{dt} = \frac{1}{\alpha A(h_2)}(\beta\dot{V}_i + \dot{V}_{12} - \dot{V}_o) \tag{7}$$

$$A(h_i) = \max(28 \times 10^6 \cdot 1.1 \cdot h_i^{\frac{1}{10}}, 10^3) \tag{8}$$

$$\dot{V}_{12} = K_{12} \cdot (h_1 - h_2)\sqrt{|h_1 - h_2|} \tag{9}$$

$$\dot{V}_o = \dot{V}_g + \dot{V}_t \tag{10}$$

$$\dot{V}_g = C_d \cdot w \cdot \min(h_g, h_2)\sqrt{2g \cdot \max(h_2, 0)} \tag{11}$$

$$\dot{V}_t = a\frac{\dot{W}_e}{x_D - x_q} + b \tag{12}$$

In (12), x_q denotes the water level at quoy and is obtained by solving the following cubic equation:

$$\begin{aligned} 0 = {} & c_1 x_q^3 + (c_2 - c_1 x_D)x_q^2 \\ & + (c_3 - c_2 x_D + c_4 \dot{V}_g)x_q \\ & + \dot{W}_e - c_3 x_D - c_4 \dot{V}_g x_D - c_5 \end{aligned} \tag{13}$$

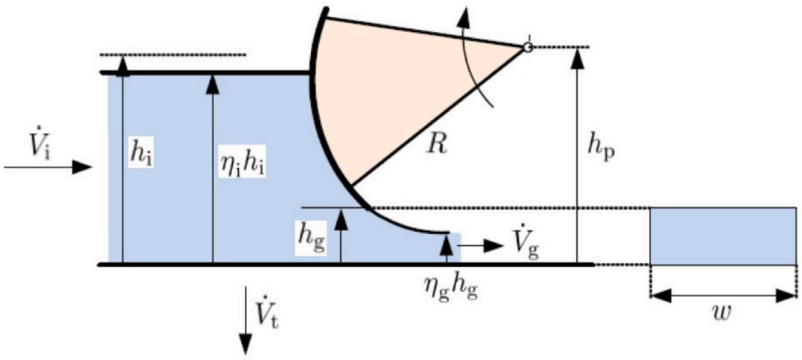

Fig. 5. Structure of floodgate.

Table 2
Seasonal level requirement.

Date	x_{LRV} [m MSL]	x_{HRV} [m MSL]
Jan. 1–Apr. 30	55.75	60.35
May. 1–Aug. 30	58.10	59.85
Sept. 1–Sept. 14	57.60	59.35
Sept. 15–Oct. 27	55.75	59.35
Oct. 28–Nov. 11	55.75	59.85
Nov. 12–Dec. 31	55.75	60.35

4.2. Operational requirements

The Dalsfoss hydropower plant is subject to several operational requirements to ensure safe and efficient operation. Some of important requirements are as follows:

1. **Mitigation of Hydropeaking Phenomenon:** Hydropeaking refers to the abrupt and significant increase in water flowrate discharged from a hydropower station, resulting in adverse impacts on downstream fauna and environmental conditions. To mitigate the detrimental effects of hydropeaking, it is imperative to maintain a relatively constant flowrate at downstream $\dot{V}_o$, particularly during periods of increased flowrate.
2. **Minimum downstream flowrate ($\dot{V}_\mathrm{o}$):** To preserve the ecological balance of the watercourse and facilitate the movement of fish species, it is necessary to maintain a minimum flowrate of $4, \mathrm{m}^3/\mathrm{s}$ downstream. This ensures that the watercourse does not dry up and provides sufficient habitat for aquatic organisms.
3. **Water level regulation at Merkebekk:** The water level at the Merkebekk location, measured above sea level (m MSL), must be kept within specific ranges defined by the low regulated value (x_{LRV}) and high regulated value (x_{HRV}). These values vary seasonally and are listed in Table 2. The water level is calculated as $x_\mathrm{M} = h_1 + x_{\mathrm{LRV}}^{\mathrm{min}}$, where x_M is the water level at Merkebekk above sea level (m MSL).
4. **Maximum turbine flowrate ($\dot{V}_\mathrm{t}$):** The flowrate through the turbine is limited to a maximum of $36, \mathrm{m}^3/\mathrm{s}$ to ensure the safe and reliable operation of the turbine. This limit prevents excessive strain on the equipment and guarantees the longevity of the turbine.
5. **Floodgate opening height limitation:** The opening height of the floodgates is restricted to a maximum of $5.6, \mathrm{m}$ for safety reasons. This limitation ensures that the floodgates can effectively regulate the water flow without compromising the structural integrity of the gates or posing a risk to personnel and infrastructure.

4.3. Optimal control problem

The OCP for the hydropower plant system involves the states of water levels at Dalsfoss and Merkebekk, denoted as $x = [h_1, h_2]$, respectively, and the control inputs are the opening heights of two floodgates, represented by $h_\mathrm{g} = [h_{\mathrm{g}1}, h_{\mathrm{g}2}]$. In the context of hydropower plants, water is a crucial resource for electricity production, emphasizing the importance of minimizing unnecessary water release through floodgates while maximizing reservoir storage. To address this objective, the OCP incorporates an objective function that reflects the control strategy's overall goal (Jeong et al., 2021).

The objective function at time sample k, denoted as J_k, is defined as follows:

$$J_k = \omega_R \cdot R^2(x_k) + h_{\mathrm{g},k} \cdot \omega_u \cdot h_{\mathrm{g},k}^\top + \Delta h_{\mathrm{g},k} \cdot \omega_{\Delta u} \cdot \Delta h_{\mathrm{g},k}^\top + \omega_p \cdot p_k^2 \tag{14}$$

In Eq. (14), ω_R, ω_u, $\omega_{\Delta u}$, and ω_p are weight parameters associated with the different components of the objective function. The first term aims to maximize the water level at Merkebekk by setting the reference target as the high regulated value (HRV), represented as $R(x_k) = x_{\mathrm{M},k} - x_{\mathrm{HRV},k}$.

The second term seeks to minimize the floodgate openings, while the third term discourages abrupt changes in the floodgate openings. Here, $\Delta h_{\mathrm{g},k} = h_{\mathrm{g},k} - h_{\mathrm{g},k-1}$.

The last term in Eq. (14), $\omega_p \cdot p_k^2$, introduces a penalty for violating the low water level constraint when the reservoir's water level is so low that it becomes infeasible to simultaneously satisfy the constraints for the required minimum downstream flowrate and the water level requirement. The slack variable p allows for slight deviations from the low regulated value (LRV) to meet the minimum flowrate constraint (Jeong et al., 2021).

The objective function (14) serves as the objective function in the multistage MPC and the first optimizer in the sequential stochastic MPC scheme. In the sequential stochastic MPC scheme, the second optimizer utilizes the following objective function:

$$J_{\mathrm{2nd},k} = J_k + (h_{\mathrm{g},k}^j - h_{\mathrm{g,ref},k}^*) \cdot Q_u \cdot (h_{\mathrm{g},k}^j - h_{\mathrm{g,ref},k}^*)^\top \tag{15}$$

Here, Q_u is a weight parameter that emphasizes control tracking. The objective function encourages the gate openings to closely follow the reference openings determined by the first optimizer.

An OCP for the certainty equivalent MPC or the first OCP in the sequential stochastic MPC is formulated as follow:

$$\text{minimize} \quad \sum_{k=0}^{N_\mathrm{p}} L_k \tag{16a}$$

$$\text{subject to} \quad x_{k+1} = f(x_k, h_{\mathrm{g},k}, \mathrm{E}(\dot{V}_{\mathrm{i},k}^{r(j)}), \dot{W}_{\mathrm{e},k}), \tag{16b}$$

$$x_{\mathrm{LRV}} + p_k \le x_{\mathrm{M},k} \le x_{\mathrm{HRV}}, \tag{16c}$$

$$0 \le h_{\mathrm{g},k} \le 5.6 \text{ m}, \tag{16d}$$

$$0 \le \dot{V}_\mathrm{t} \le 36 \text{ m}^3/\mathrm{s}, \tag{16e}$$

Table 3
Parameters for objective functions.

	ω_R	ω_u	$\omega_{\Delta u}$	Q_u	ω_p
Multistage MPC	10	1	1	0	10^4
Sequential stochastic MPC (1st Opt)	10	1	1	0	10^4
Sequential stochastic MPC (2nd Opt)	30	0	0	1	10^4

$$4\ \mathrm{m}^3/\mathrm{s} \le \dot{V}_\mathrm{O} \le \infty, \tag{16f}$$

$$x_0 = \hat{x} \tag{16g}$$

In Eq. (16), the cost function is represented by (16a), and the system model is described by (16b). The system model (16b) incorporates the nominal value of the realized water inflow forecast as $\mathrm{E}(\dot{V}^{r(j)}_{\mathrm{i},k})$. The seasonal constraints on the water level at Merkebekk are presented in (16c), and the minimum flowrate requirement is specified in (16f). The introduction of the slack variable in (16c) allows for violations to satisfy (16f) in cases where the water level is low in the reservoir. The gate opening is bounded by (16d), the turbine capacity is determined by (16e), and the measured water level at the current time serves as the initial point for the OCP, as stated in (16g). The L_k in the cost function (16a) is formulated as (14).

The formulation of the OCP for the multistage MPC or the second optimizer in the sequential stochastic MPC is presented as follows:

$$\text{minimize} \quad \sum_{i=1}^{S} \omega_j \sum_{k=0}^{N_\mathrm{p}} L^j_k \tag{17a}$$

$$\text{subject to} \quad x^j_{k+1} = f(x^{p(j)}_k, h^j_{\mathrm{g},k}, \dot{V}^{r(j)}_{\mathrm{i},k}, \dot{W}_{\mathrm{e},k}), \tag{17b}$$

$$x_\mathrm{LRV} + p^j_k \le x^j_{\mathrm{M},k} \le x_\mathrm{HRV}, \tag{17c}$$

$$0 \le h^j_{\mathrm{g},k} \le 5.6\ \mathrm{m}, \tag{17d}$$

$$0 \le \dot{V}^j_\mathrm{t} \le 36\ \mathrm{m}^3/\mathrm{s}, \tag{17e}$$

$$4\ \mathrm{m}^3/\mathrm{s} \le \dot{V}^j_\mathrm{O} \le \infty, \tag{17f}$$

$$h^j_{\mathrm{g},k} = h^l_{\mathrm{g},k} \quad \text{if} \quad x^{p(j)}_k = x^{p(l)}_k, \tag{17g}$$

$$x^j_0 = \hat{x} \tag{17h}$$

In Eq. (17), the cost function is represented by (17a), and the system model is described by (17b). The system model (17b) incorporates the seasonally changing constraints on the water level at Merkebekk, including a slack variable (17c). The gate opening is bounded by (17d), the turbine capacity is determined by (17e), and the required minimum flowrate at the downstream is specified in (17f). The non-anticipativity constraint is introduced in (17g). The measured water level at the current time serves as the initial point for the OCP, as stated in (17h). When the OCP (17) is used for the multistage MPC framework, the objective function (17a) is formed as (14). However, when the OCP (17) is used as the second optimizer in the sequential stochastic MPC framework, the objective function (17a) is formed as (15).

The weight parameters of the objective functions (14) and (15) are specified in Table 3. The determination of these parameters for the objective function in the certainty equivalent MPC involves numerous simulations and a trial-and-error process (Jeong and Sharma, 2022b). In addition to the parameters listed in Table 3, various sets of weight parameters are used for the second optimizer in the sequential stochastic MPC scheme in this work.

4.4. Simplification of scenario ensembles

A method for simplifying a large set of scenario ensembles for a single uncertainty was introduced and tested in previous research (Jeong et al., 2023; Jeong and Sharma, 2023). The purpose of this simplification method is to reduce the number of considered scenario ensembles to improve the efficiency of implementing the multistage MPC framework while maintaining satisfactory performance. The method consists of two steps: (1) the creation of synthetic scenario ensembles and (2) the calculation of the probability for each synthetic scenario ensemble.

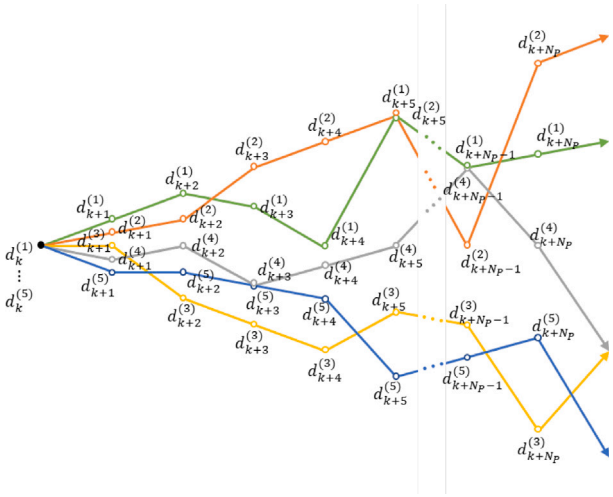

Fig. 6. An example of scenario ensembles of uncertainty.

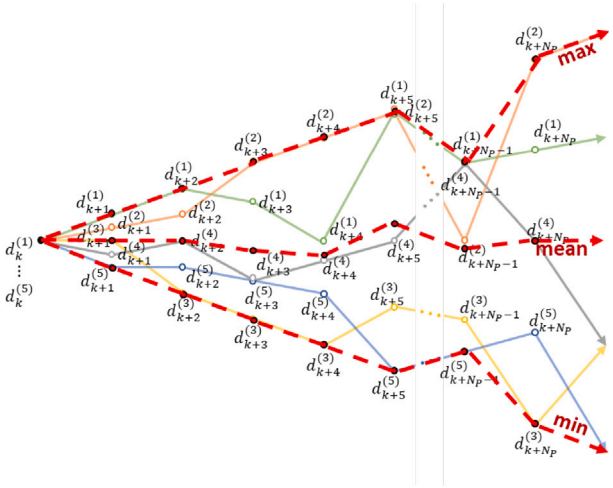

Fig. 7. The three synthetic scenario ensembles of the uncertainty from the five example scenario ensembles.

Fig. 6 illustrates an example of scenario ensembles for a hydropower station's water inflow uncertainty. In this example, 5 independent scenario ensembles are generated, forming a structure similar to a scenario tree with a robust horizon set to 1. However, the uncertainty after branching is not assumed to be constant. To simplify the structure of scenario ensembles, three synthetic scenarios are created by extracting the maximum, mean, and minimum values of the forecasted water inflow for each time step over the prediction horizon, as shown in Fig. 7. Mathematically, the synthetic scenario ensembles at time k can be represented as $d_{\mathrm{syn},k} = [d_{\mathrm{max},k}, d_{\mathrm{mean},k}, d_{\mathrm{min},k}]$. Here, $d_{\mathrm{i},k} = [d_{\mathrm{i},k}, d_{\mathrm{i},k+1}, \ldots, d_{\mathrm{i},k+N_\mathrm{p}}]$ denotes the maximum, mean, and minimum synthetic scenario ensembles, respectively, where $\mathrm{i} \in \{\mathrm{max}, \mathrm{mean}, \mathrm{min}\}$.

To calculate the probabilities of each synthetic scenario ensemble, boundary regions need to be defined. Fig. 8 shows the defined boundary 1 and boundary 2, as well as regions A, B, and C. Boundary 1 and boundary 2 are determined as $\mathbf{d}_{\mathrm{mean},k} + s_1 \cdot (\mathbf{d}_{\mathrm{max},k} - \mathbf{d}_{\mathrm{mean},k})$ and $\mathbf{d}_{\mathrm{mean},k} - s_2 \cdot (\mathbf{d}_{\mathrm{mean},k} - \mathbf{d}_{\mathrm{min},k})$, respectively, with s_1 and s_2 set to 0.5. Regions A, B, and C are defined as $\mathrm{A} \in (\mathrm{Boundary1}, d_{\mathrm{max},k}]$, $\mathrm{B} \in [\mathrm{Boundary1}, \mathrm{Boundary2}]$, and $\mathrm{C} \in [d_{\mathrm{min},k}, \mathrm{Boundary2})$, respectively.

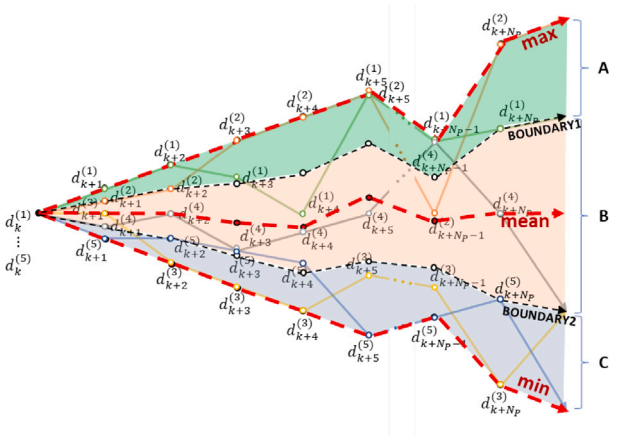

Fig. 8. The defined boundary region to calculate the probabilities of occurrences of the synthesis scenario ensembles.

Regions A, B, and C are utilized to determine the probabilities of occurrence for the maximum, mean, and minimum synthetic scenario ensembles, respectively. For instance, the probability of the maximum synthetic scenario ensemble $\omega_{\max}$ can be calculated as:

$$\omega_{\max} = \frac{\sum_{j=1}^{S} \omega_j \cdot N_{\mathrm{A}}^{(j)}}{\sum_{j=1}^{S} \omega_j \cdot N^{(j)}} \tag{18}$$

where ω_j represents the probability of occurrence of the jth original scenario ensemble, $N^{(j)}$ denotes the number of uncertainty points in the jth original scenario ensemble, and $N_{\mathrm{A}}^{(j)}$ refers to the number of uncertainty points that fall within region A for the jth original scenario ensemble. The probabilities for the mean and minimum synthetic scenario ensembles, ω_{mean} and $\omega_{\min}$, can be estimated using the same approach.

4.5. Simulation setup

The simulation setup for this case study encompasses one month from April 15th to May 15th. This timeframe was chosen because this period includes a transition in the water level requirements, posing a more challenging problem to be addressed. A prediction horizon of 13 days is employed to utilize the entire dataset of water inflow forecasts. The simulations are implemented using the IPOPT solver in CasADi (Andersson et al., 2019), which offers efficient optimization capabilities.

As previously mentioned, the Dalsfoss hydropower plant system is influenced by two sources of uncertainty: the power production plan and water inflow forecasts. For this case study, both uncertainties are defined based on historical data obtained from the actual hydropower plant, provided by Skagerak Kraft. Fig. 9 illustrates the actual power production plan spanning from April 15th, 2020, to May 15th, 2020. It is assumed that the power production plan can be accurately predicted during the simulation, as the feedback feature of MPC can effectively handle most changes in the power production plan in practice. Regarding water inflow forecasts, they are updated at every time step. Fig. 10 displays an example set of scenario ensembles stored from April 15th, 2020. The original scenario ensembles are represented by cyan lines. The simplified synthesis scenarios are depicted by red dotted lines, while the corresponding boundaries for the synthesis scenarios are indicated by pink lines.

In the simulation, the water inflow is multiplied by a flooding coefficient of 2 to simulate a flooding situation. This coefficient serves as an indicator of flood severity and allows for the investigation of system behavior under extreme conditions. By employing this approach, the performance of the proposed control scheme can be evaluated effectively. Furthermore, this study assumes a perfect model, obviating the need for state estimation. In the actual hydropower station, level sensors directly provide measurements for both states h_1 and h_2.

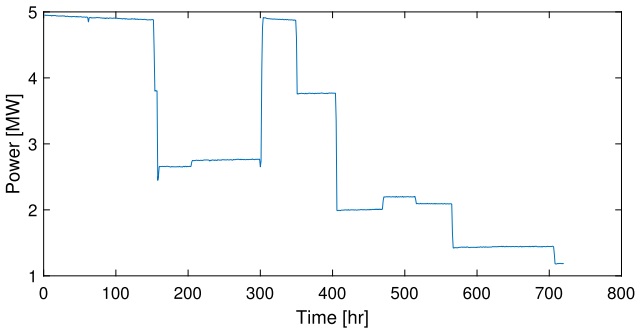

Fig. 9. Historical power production plan during the simulation period.

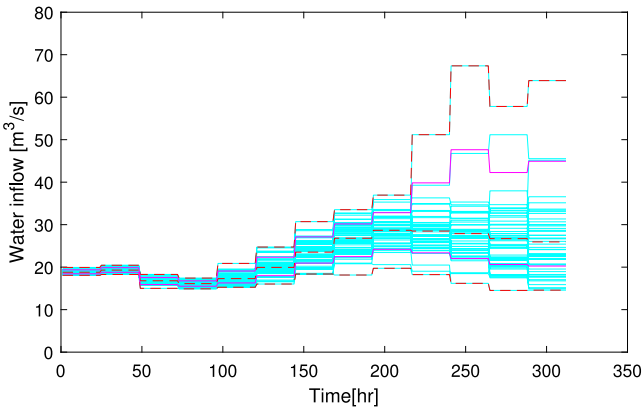

Fig. 10. Example of the water inflow forecast, April 15th, 2020, and its simplified synthesis inflow forecast.

Table 4
Simulated MPC frameworks.

Name	Control framework	N_{p} [day]	S
MS312	Multistage MPC	13	50
MS24	Multistage MPC	1	50
SS	Sequential stochastic MPC	1st opt:13, 2nd opt:1	50
SS(S)	Simplified sequential stochastic MPC	1st opt:13, 2nd opt:1	3

In this paper, four MPCs are simulated for comparison with given conditions in Table 4.

5. Simulation results

This section provides an analysis of the simulation study results. The performance of the sequential stochastic MPC scheme is compared with two multi-stage MPC schemes, each having different prediction horizon lengths of 24 h and 13 days. Additionally, the effectiveness and efficiency of a scenario simplification technique applied to the sequential stochastic MPC scheme are assessed. The section also includes relevant metrics such as computational time. Then, other features of the sequential stochastic MPC are introduced.

Figs. 11 and 12 present the comparison of simulation results for three MPC frameworks: Multistage MPC with 13 days of prediction horizon (**MS312**), multistage MPC with 24 h of prediction horizon (**MS24**), and sequential stochastic MPC with 13 days of the prediction horizon in the first optimizer and 24 h of the prediction horizon in the second optimizer (**SS**). Fig. 11(a) and (b) depict the changes in water level and floodgate opening, respectively, while Fig. 12 shows the variations in flowrate at different locations. In Fig. 11(a), the

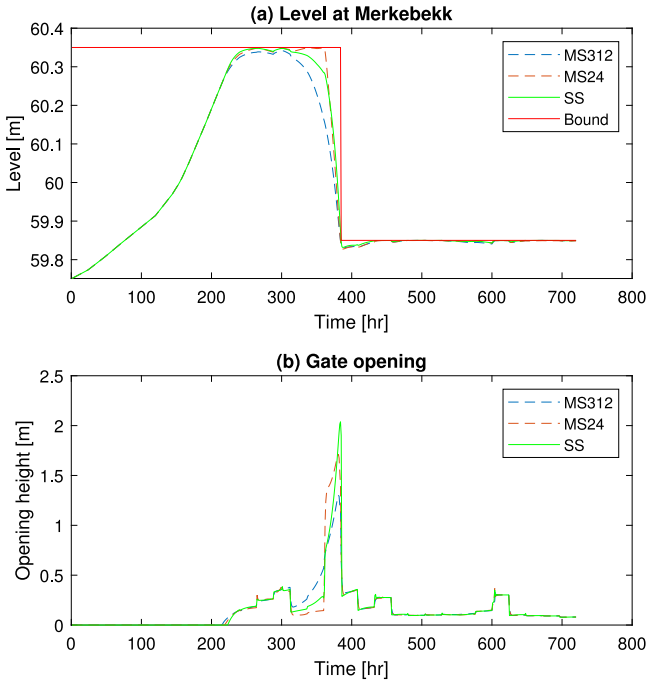

Fig. 11. The comparison of simulations results of Multistage MPC (13 days), Multistage MPC (1 day), and Sequential Stochastic MPC (1st opt:13 days and 2nd opt:1 day) on the water level and the floodgate opening.

red line indicates the upper bound of the water level constraint, and other lines show the water level changes at Merkebekk through the simulation period. Among the three MPCs, **MS24** keeps the highest water level. However, since **MS24** can predict only 24 h, it does not show good predictability in the seasonally changing water level constraint, which leads to drastic water level drops. It can be seen more in detail in Fig. 13. Fig. 13 illustrate the part of Fig. 11(a) in more detail approximately during the simulation period from 260 h to 380 h. In Fig. 13, the water level started decrease approximately from 320 h due to the constraint change in the near future, around at 385 h, when **MS312** or **SS** controls the system. However, **MS24** try to maximize the water level until 365 h and decrease the water level drastically almost from the highest possible water level, which means **MS24** has the poor predictability compared to **MS312** and **SS**. Therefore, **MS24** is not a suitable control algorithm in the hydropower case study. Meanwhile, **MS312** and **SS** maintain the proper predictability by decreasing the water level earlier than **MS24** and show robustness in the satisfaction of the constraints. Furthermore, **SS** maintained a water level higher than **MS312**.

Figs. 14 and 15 illustrate the effectiveness of the simplification method applied to the sequential stochastic MPC scheme. These figures compare the simulation results of the sequential stochastic MPC scheme using all 50 scenarios (**SS**) with the simplified sequential stochastic MPC scheme (**SS(S)**) using three synthesis scenarios. Fig. 14(a) shows the comparison of water level changes, while Fig. 14(b) presents the comparison of floodgate opening. Fig. 15 compares the flowrate changes at different locations. The results demonstrate that the simulation results of **SS(S)** and **SS** are almost identical, indicating the effectiveness of the simplification method.

Table 5 presents the reduction in computational time achieved by the simplified sequential stochastic MPC scheme. The average computational time of **SS(S)** is significantly faster than both **SS** without the simplified method and **MS312**. The computational time of **SS(S)** is approximately 3.5 times faster than **SS** and 85 times faster than **MS312**. **SS** is 24 times faster than **MS312**. These findings highlight the

Table 5
Computational time for each framework.

MPC	Mean [s]	Max [s]	Min [s]
SS(S)	0.2857	0.4293	0.2427
SS	0.9964	2.3132	0.6077
MS312	24.2222	42.4864	17.5488

computational efficiency of the sequential stochastic MPC scheme compared to the multi-stage MPC scheme. Moreover, the simplified method effectively enhances the computational efficiency of the sequential stochastic MPC scheme without compromising its performance.

The control actions generated by the first and second optimizers of the sequential stochastic MPC scheme are presented in Fig. 16(a). The difference in control actions between the two optimizers is also illustrated in Fig. 16(b). The results indicate that the control actions taken by the second optimizer are opening the floodgates less or more, to maintain a higher water level or avoid violation of level constraints.

The results depicted in Fig. 17 highlight a significant advantage of the sequential stochastic MPC scheme in terms of improved convergence when solving optimization problems. As evidenced by Fig. 10, the variation in water inflow predictions increases as the prediction horizon extends further into the future. This variation is particularly pronounced in scenarios where flooding is predicted. These variations can result in infeasibility of the optimization problem, as demonstrated by the simulation utilizing multistage MPC with a flood coefficient of 3 (MS.f3 in Fig. 17). The infeasibility is evident at around 150 h, at which point the MPC unreasonably opens the gate, resulting in a significant decrease in water level. The infeasibility of OCP occurs because a few water inflow scenario ensembles show the realization of unmanageable flooding situations in further future on the forecast. In contrast to the multistage MPC, the sequential stochastic MPC scheme demonstrates an ability to effectively solve the optimization problem and smoothly operate the system even when severe flooding happens as the flood coefficient is set as high as 3, 4, and 5.

The simulation results presented above demonstrate the superiority of the sequential stochastic MPC scheme compared to multistage MPC. The performance of the scheme can be adjusted by tuning its parameters. Figs. 18, and 19 illustrate the impact of different settings on the simulation results in the simplified sequential stochastic MPC scheme, which is used for faster computation and better performance.

In Fig. 18, the effect of different settings for the water level parameter in the objective function of the second optimizer is evaluated. The parameter is denoted as “L1”, “L10”, and so on, corresponding to values of 1, 10, and so forth in ω_R in the second optimizer, shown in Table 3. According to the figure, “L10” shows a similar performance with multistage MPC with 13 days of prediction horizon(MS). In general, as the parameter value increases, the water level is maintained at a higher level.

Fig. 19 illustrates the simulation results for different lengths of the prediction horizon on the second optimizer, while the first optimizer is set with a prediction horizon of 13 days. Specifically, the simulation results are shown for the cases where the prediction horizon is set to 12 h (N12), 24 h (N24), and so on. From the figure, it can be observed that the simulation results do not differ significantly for the different lengths of the prediction horizon.

This observation is supported by the computational time results presented in Table 6, which shows that the computational time for solving the optimization problem increases as the length of the prediction horizon on the second optimizer gets longer. Overall, this suggests that the choice of prediction horizon length for the second optimizer may not have a large impact on the performance of the sequential stochastic MPC scheme.

The simulation results presented in this study utilize the nominal value, or mean value, of water inflow prediction scenarios as input for the first optimizer, as depicted in Fig. 20. This figure illustrates the

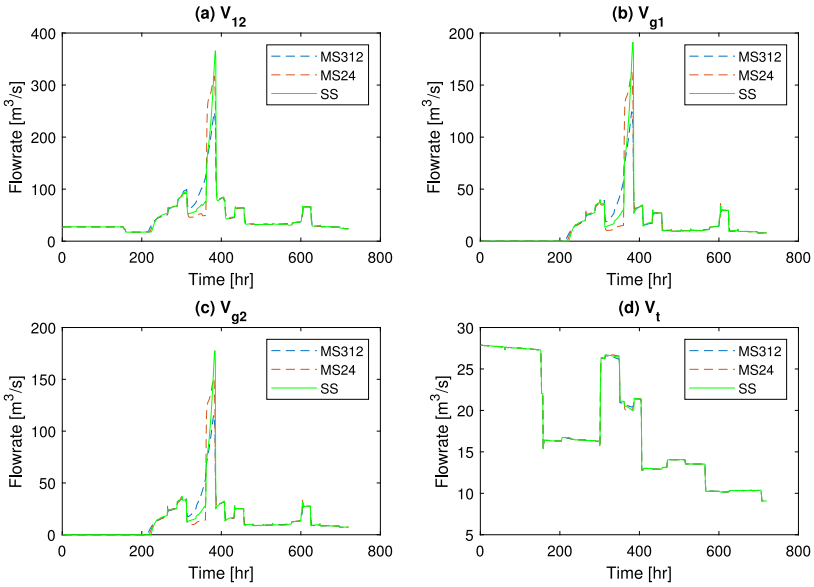

Fig. 12. Flowrates at the various location during the simulations of Multistage MPC (13 days), Multistage MPC (1 day), and Sequential Stochastic MPC (13 days and 1 day).

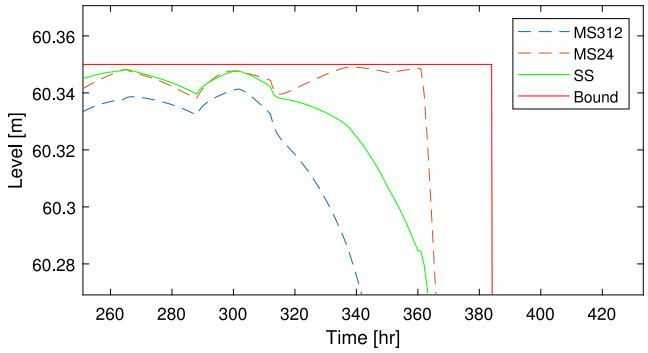

Fig. 13. The detailed comparison of simulations results of Multistage MPC (13 days), Multistage MPC (1 day), and Sequential Stochastic MPC (1st opt:13 days and 2nd opt:1 day) on the water level.

Table 6
The computational time for different length of the prediction horizon on the simplified sequential stochastic MPC scheme.

Np2 [day]	Mean [s]	Max [s]	Min [s]
12	0.2868	0.4953	0.2372
24	0.2996	0.4233	0.2491
72	0.3959	0.6179	0.3055
120	0.5102	1.0728	0.3822
168	0.6363	1.1258	0.4847
240	0.8844	1.3514	0.6315
312	1.1363	1.7379	0.9081

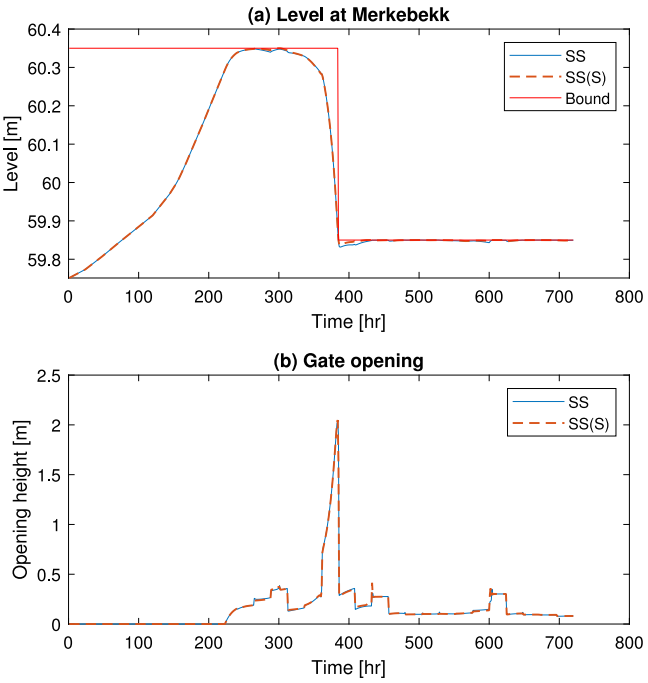

Fig. 14. The comparison of simulations results of Sequential Stochastic MPC (13 days and 1 day), and simplified Sequential Stochastic MPC (13 days and 1 day) on the water level and the floodgate opening.

performance of the sequential stochastic MPC when utilizing various values of water inflow prediction in the first optimizer. The label "Rand" in Fig. 20 corresponds to simulation results in which the water inflow prediction for the first optimizer is chosen randomly from the prediction ensemble. Conversely, "OP.max", "OP.med", and "OP.min" correspond to simulation results in which the first optimizer utilizes the scenario with the maximum, median, and minimum accumulated amount of water inflow prediction, respectively. The label "Const" represents the simulation results when the water inflow prediction is held constant at 200 m^3/s for the entire simulation period. The results demonstrate that the sequential stochastic MPC scheme performs well when utilizing scenarios from the water inflow prediction ensemble. However, when the water inflow prediction utilized in the first optimizer deviates significantly from the actual prediction, such as in the case of a constant prediction, the performance of the sequential stochastic MPC system decreases significantly, despite the second optimizer utilizing the correct ensemble of water inflow predictions.

6. Discussion

The presented simulation results provide compelling evidence regarding the superior optimality of the sequential stochastic MPC scheme compared to the traditional multistage MPC approach in controlling hydropower stations. The sequential stochastic MPC scheme

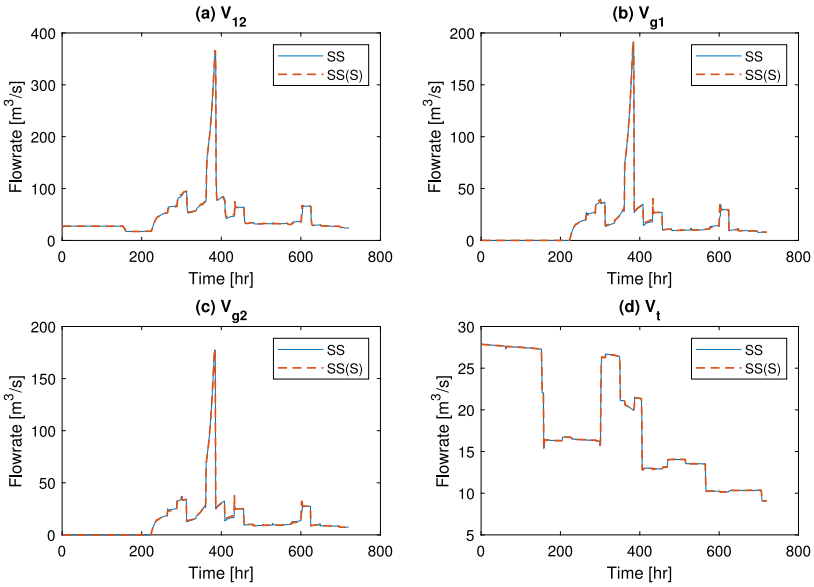

Fig. 15. Flowrates at the various location during the simulations of Sequential Stochastic MPC (13 days and 1 day) and Simplified Sequential Stochastic MPC (13 days and 1 day.

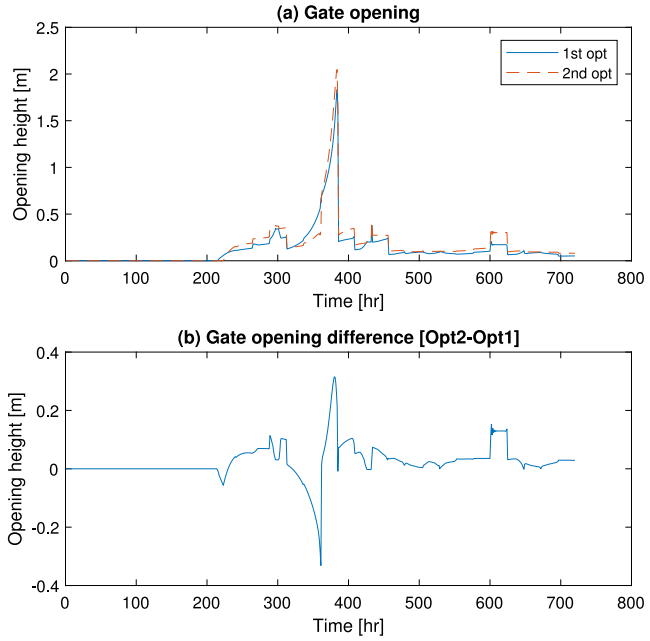

Fig. 16. (a)The first control input from the first optimization and the second optimization of the stochastic sequential MPC framework, and (b)The difference of the first control input between the first and second optimization (The second optimization - the first optimization).

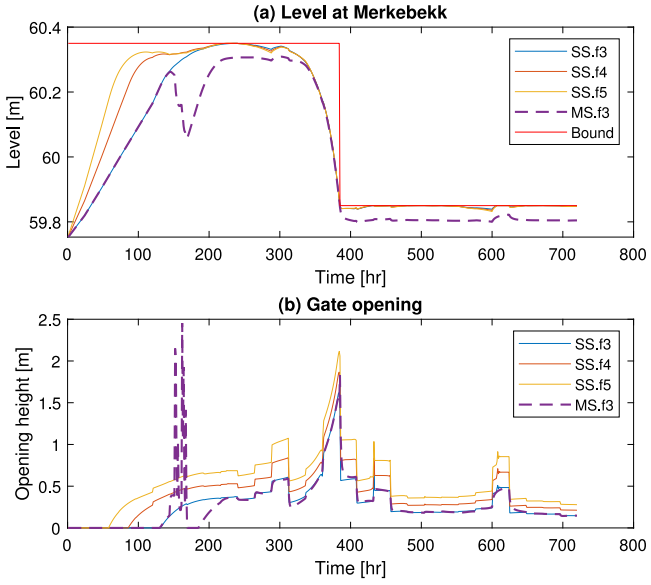

Fig. 17. Simulations under severe flooding situations by Multistage MPC(MS) and Sequential Stochastic MPC(SS).

exhibits comparable performance to the multistage MPC scheme while requiring significantly shorter computational times and ensuring better feasibility in solving the OCP.

Some readers may argue that the normal multistage MPC approach with a 13-day prediction horizon already converges rapidly enough for this particular hydropower system case study, considering the one-hour time step. However, as Skagerak continues to refine its hydrology models and gather more information from the area, it is anticipated that the time steps will be further shortened in the near future, which leads to the need of solving the bigger size of OCP in the shorter time. Therefore, the faster convergence achieved by employing the sequential stochastic MPC scheme holds promise as an algorithm for future applications.

Moreover, the sequential stochastic MPC scheme allows for fine-tuning, enabling the attainment of better optimality compared to the multistage MPC approach, depending on specific settings such as the weight parameter of the second optimizer in the scheme.

The convergence speed of the sequential stochastic MPC approach is further accelerated when combined with a simplified method. It is important to highlight that altering the length of the prediction horizon in the second optimizer does not lead to significant differences in the results. However, it increases the computational time and may render the optimization problem infeasible. Therefore, it is recommended to keep the length of the prediction horizon in the second optimizer as short as possible to ensure efficient computation. Additionally, it was observed that the choice of a scenario ensemble in the first optimizer does not have a substantial impact on the optimization process. However, if the forecast significantly deviates from the forecast, the system may not achieve optimal control.

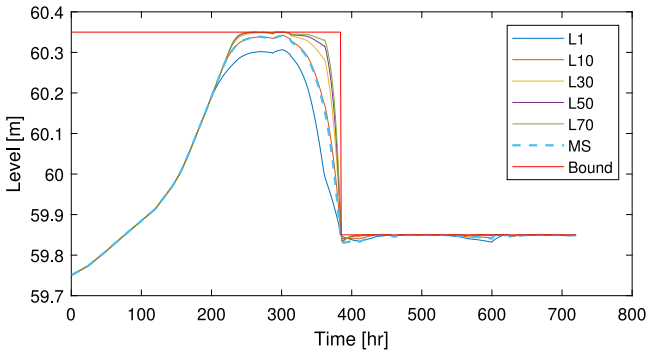

Fig. 18. Simulation results from different level parameter tuning on the second optimizer of the sequential stochastic MPC scheme.

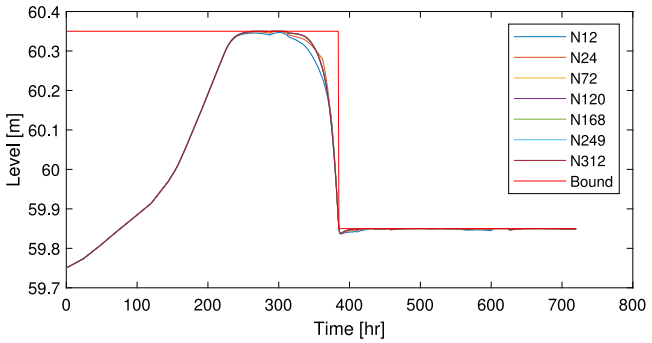

Fig. 19. Simulation results with different lengths of prediction horizon on the second optimizier of sequential stochastic MPC.

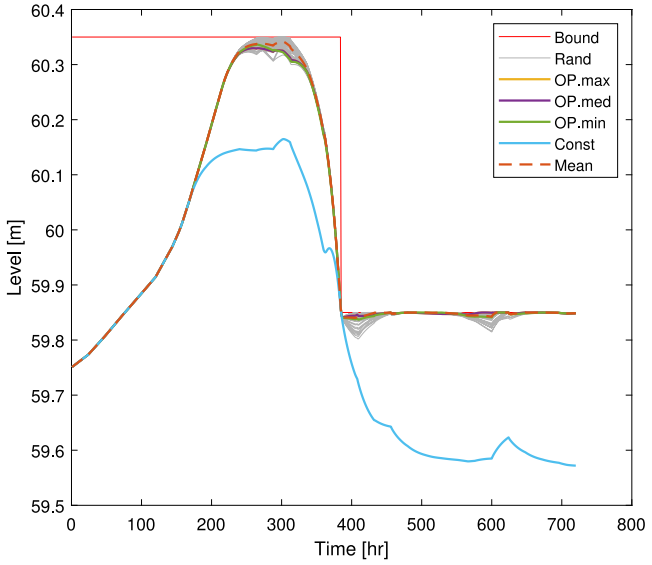

Fig. 20. Simulations of the sequential stochastic MPC scheme with different scenarios of water inflow prediction in the first optimizer.

While the current study primarily focuses on controlling the water level in the system, practical applications necessitate considering other constraints such as maintaining a constant flowrate downstream in the operation of a hydropower station. These constraints can be effectively addressed by adjusting the parameters of floodgate opening or by explicitly incorporating constraints on the flowrate change at the downstream location.

7. Conclusion

In conclusion, this study has proposed a novel sequential stochastic MPC scheme and conducted a comprehensive performance comparison with the traditional multistage MPC scheme. The findings demonstrate the superiority of the sequential stochastic MPC scheme in effectively and efficiently controlling water levels and floodgate openings in a river system, outperforming the multistage MPC scheme. Furthermore, the effectiveness of the simplified method is proven in the sequential stochastic MPC scheme. It accelerates the computational time without degrading the performance of the sequential stochastic MPC.

The research outcomes provide significant contributions to the field of water level and floodgate control. However, several avenues for future investigation remain open. One potential direction is to explore the incorporation of additional sources of uncertainty, such as measurement errors, into the MPC framework to enhance its robustness. Furthermore, it would be beneficial to implement and validate the proposed sequential stochastic MPC scheme in real-world settings to assess its practical applicability and performance under realistic conditions.

By addressing these future research directions, it is anticipated that further advancements can be made in the control of water levels and floodgate openings, ultimately enhancing the operational efficiency and resilience of hydropower systems.

CRediT authorship contribution statement

Changhun Jeong: Conceived and designed the analysis, Collected the data, Contributed data or analysis tools, Performed the analysis, Wrote the paper. **Beathe Furenes:** Collected the data, Giving the tips of how the real industry works, Proof-reading. **Roshan Sharma:** Supervising, advises, proof-reading.

Declaration of competing interest

The authors declare that they have no known competing financial interests or personal relationships that could have appeared to influence the work reported in this paper.

Data availability

Data will be made available on request.

References

Andersson, J.A.E., Gillis, J., Horn, G., Rawlings, J.B., Diehl, M., 2019. CasADi – A software framework for nonlinear optimization and optimal control. Math. Program. Comput. 11 (1), 1–36. http://dx.doi.org/10.1007/s12532-018-0139-4.

Bernardini, D., Bemporad, A., 2009. Scenario-based model predictive control of stochastic constrained linear systems. In: Proceedings of the 48h IEEE Conference on Decision and Control (CDC) Held Jointly with 2009 28th Chinese Control Conference. pp. 6333–6338. http://dx.doi.org/10.1109/CDC.2009.5399917.

Campo, P.J., Morari, M., 1987. Robust model predictive control. In: 1987 American Control Conference. pp. 1021–1026. http://dx.doi.org/10.23919/ACC.1987.4789462.

IEA, 2021. Hydropower Special Market Report—Analysis and Forecast to 2030. IEA, Paris, France.

Janatian, N., Sharma, R., 2022. Multi-stage scenario-based MPC for short term oil production optimization under the presence of uncertainty. J. Process Control 118, 95–105. http://dx.doi.org/10.1016/j.jprocont.2022.08.012.

Jeong, C., Furenes, B., Sharma, R., 2021. MPC operation with improved optimal control problem at Dalsfoss power plant. In: Proceedings of SIMS EUROSIM Conference 2021, Vol. 11. pp. 226–233. http://dx.doi.org/10.3384/ecp21185226, (1).

Jeong, C., Furenes, B., Sharma, R., 2023. Multistage model predictive control with simplified scenario ensembles for robust control of hydropower station. Model. Identif. Control 44 (2), 43–54. http://dx.doi.org/10.4173/mic.2023.2.1.

Jeong, C., Sharma, R., 2022a. Stochastic MPC for optimal operation of hydropower station under uncertainty. IFAC PapersOnLine 55 (7), 155–160.

Jeong, C., Sharma, R., 2022b. Tuning model predictive control for rigorous operation of the Dalsfoss hydropower plant. Energies (Basel) 15 (22), 8678.

Jeong, C., Sharma, R., 2023. Multistage model predictive control with simplified method on scenario ensembles of uncertainty for Hjartdøla hydropower system. In: The 7th IEEE Conference on Control Technology and Applications, Bridgetown, Barbados (Accepted). IEEE.

Klintberg, E., Dahl, J., Fredriksson, J., Gros, S., 2016. An improved dual Newton strategy for scenario-tree MPC. In: 2016 IEEE 55th Conference on Decision and Control (CDC). pp. 3675–3681.

Krishnamoorthy, D., Foss, B.A., Skogestad, S., 2019. A Primal decomposition algorithm for distributed multistage scenario model predictive control.

Lee, J., Yu, Z., 1997. Worst-case formulations of model predictive control for systems with bounded parameters. Automatica 33 (5), 763–781. http://dx.doi.org/10.1016/S0005-1098(96)00255-5.

Lucia, S., Finkler, T., Engell, S., 2013. Multi-stage nonlinear model predictive control applied to a semi-batch polymerization reactor under uncertainty. J. Process Control 23 (9), 1306–1319.

Maiworm, M., Bäthge, T., Findeisen, R., 2015. Scenario-based Model Predictive Control: recursive feasibility and stability. IFAC-PapersOnLine 48 (8), 50–56.

Martí, R., Lucia, S., Sarabia, D., Paulen, R., Engell, S., de Prada, C., 2015. Improving scenario decomposition algorithms for robust nonlinear model predictive control. Comput. Chem. Eng. 79, 30–45.

Mayne, D., Rawlings, J., Rao, C., Scokaert, P., 2000. Constrained model predictive control: stability and optimality. Automatica (Oxford) 36 (6), 789–814.

Mdoe, Z., Krishnamoorthy, D., Jaschke, J., 2021. Adaptive horizon multistage nonlinear model predictive control. In: 2021 American Control Conference (ACC). pp. 2088–2093. http://dx.doi.org/10.23919/ACC50511.2021.9483183.

Menchacatorre, I., Sharma, R., Furenes, B., Lie, B., 2019. Flood management of lake Toke: MPC operation under uncertainty. URL https://hdl.handle.net/11250/2645438.

Mesbah, A., 2016. Stochastic Model Predictive Control: an overview and perspectives for future research. IEEE Control Syst. 36 (6), 30–44.

Morari, M., Lee, J.H., 1999. Model predictive control : past, present and future: Special Issue: Selected and extended papers from the Symposium on PSE'97/ESCAPE'7. Comput. Chem. Eng. 23 (4–5), 667–682.

NVE, 2022. Supervision of dams. (accessed: 22.10.2022), https://www.nve.no/supervision-of-dams/?ref=mainmenu.

Qin, S., Badgwell, T.A., 2003. A survey of industrial model predictive control technology. Control Eng. Pract. 11 (7), 733–764. http://dx.doi.org/10.1016/S0967-0661(02)00186-7.

Saltık, M.B., Özkan, L., Ludlage, J.H., Weiland, S., Van den Hof, P.M., 2018. An outlook on robust model predictive control algorithms: reflections on performance and computational aspects. J. Process Control 61, 77–102. http://dx.doi.org/10.1016/j.jprocont.2017.10.006.

Scokaert, P., Mayne, D., 1998. Min-max feedback model predictive control for constrained linear systems. IEEE Trans. Automat. Control 43 (8), 1136–1142.

SkagerakKraft, 2022a. Dalsfos. (accessed: 22.10.2022), https://www.skagerakkraft.no/dalsfos/category1277.html.

SkagerakKraft, 2022b. Kragerø watercourse system. (accessed: 22.10.2022), https://www.skagerakkraft.no/kragero-watercourse/category2391.html.

Subramanian, S., Lucia, S., Baradaran Birjandi, S.A., Paulen, R., Engell, S., 2018. A combined multi-stage and tube-based MPC scheme for constrained linear systems. IFAC-PapersOnLine 51 (20), 481–486. http://dx.doi.org/10.1016/j.ifacol.2018.11.043, 6th IFAC Conference on Nonlinear Model Predictive Control NMPC 2018.

Appendix G

Hybrid Model Predictive Control Scheme for Controlling Temperature in Building Under Uncertainties

Published in *IEEE Access*, 2023.
Authors: Changhun Jeong, Ole Magnus Brastein, Nils-Olav Skeie, and Roshan Sharma.
Authors' roles in the article:
Changhun Jeong: Main ideas, implementation, and writing.
Ole Magnus Brastein: Discussions, and proofreading.
Nils-Olav Skeie (Co-Supervisor): proofreading.
Roshan Sharma (Supervisor): Discussions, comments, and proofreading.

IEEE Access
Multidisciplinary ⋮ Rapid Review ⋮ Open Access Journal

Received 15 September 2023, accepted 11 October 2023, date of publication 16 October 2023, date of current version 26 October 2023.

Digital Object Identifier 10.1109/ACCESS.2023.3324691

RESEARCH ARTICLE

Hybrid Model Predictive Control Scheme for Controlling Temperature in Building Under Uncertainties

CHANGHUN JEONG, OLE MAGNUS BRASTEIN, NILS-OLAV SKEIE, AND ROSHAN SHARMA
University of South-Eastern Norway, 3918 Porsgrunn, Norway
Corresponding author: Changhun Jeong (changhun.jeong@usn.no)

ABSTRACT This paper presents a study on temperature control with a heater in a building using Model Predictive Control (MPC) with a focus on addressing two uncertainties: in model and the weather forecast. In previous works, a grey-box model of the building system was developed, and the values of parameters were estimated by the estimation techniques. In this work, based on the model, simulations are conducted comparing four types of MPC controllers: Deterministic MPC, Multistage MPC, Chance-constrained MPC, and hybrid MPC. The hybrid framework integrates the strengths of the multistage and chance-constrained MPCs to achieve conservative performance and increased robustness in constraint satisfaction. The simulations demonstrate that while deterministic MPC may not always guarantee constraint satisfaction, the hybrid framework offers improved robustness by considering uncertainties in model mismatch and uncertain weather forecasts. The 95% confidence region of model uncertainty is used to assess the robustness of simulations. The results show that the hybrid MPC approach is effective in maintaining temperature in the desired range and ensuring constraint satisfaction in controlling the temperature in a building.

INDEX TERMS Chance-constrained MPC, HVAC system, model predictive control, multistage MPC, optimal control, optimization, stochastic MPC, temperature control, uncertain parameter, uncertainty.

I. INTRODUCTION

Commercial and residential buildings account for approximately 30% of the global energy consumption, with a major portion attributed to heating and cooling utilities [1].

While modern construction techniques and insulation materials have significantly reduced energy consumption for heating and cooling purposes, the rate of building renewal remains considerably low. For instance, in France, the annual renewal rate is estimated to be around 1% [2]. Consequently, the importance of effective building energy management systems (BEMS) has increased, as they offer a more feasible solution compared to modifying the building structure using modern construction techniques. Among the various solutions available, model predictive control (MPC) has garnered attention. At each time step, the control input for heating in a building is determined by solving an optimal control problem (OCP). The OCP consists of a predictive model used to forecast future behavior and constraints that must be satisfied during operation. Solving the OCP yields the optimal control input based on the current knowledge. The first control input from the sequence is then applied to the system, and this process is repeated at the next time step [3], [4]. In the context of BEMS, the utilization of MPC provides benefits in terms of both temperature set point tracking and energy consumption minimization [2].

The research focused on employing MPC in BEMS has witnessed substantial activity [5], [6]. The application of MPC for regulating indoor tempeature using both active heating systems and passive solar blinds were investigated [7]. In [8], a comprehensive building model composed of layered models, which they utilized in conjunction with MPC, was developed. Notably, their four-month experimental evaluation demonstrated remarkable energy savings, with thermal energy consumption reduced by 63% and HVAC electric energy consumption reduced by 29%. These findings

The associate editor coordinating the review of this manuscript and approving it for publication was Feiqi Deng.

highlight the significant potential benefits associated with the integration of MPC into BEMS.

The presence of a reliable prediction model is essential for maximizing the benefits derived from MPC. Various modeling approaches have been proposed to capture the thermal behavior of buildings [9]. For instance, a white-box model based on mass and energy balance was developed, incorporating a system of ordinary and partial differential equations specific to a particular building [10]. However, when dealing with complex models, it becomes challenging to identify a large number of required parameters accurately.

An alternative approach for constructing thermal behavior models is the black box approach, which relies solely on measurement data without prior knowledge of the building. Black box models tend to exhibit high prediction accuracy. However, the drawback lies in the difficulty of generalizing such models, as they do not incorporate physical knowledge to define the model structure. Numerous studies have employed the black box approach, utilizing methods such as ARMAX [11], [12] and PLS-R method [13], [14].

Another modeling approach commonly employed is the grey-box modeling method, which combines aspects of both white-box and black-box models [2], [15], [16], [17], [18]. Grey-box models leverage the cognitive understanding of the underlying physics of the system. In the context of building heating, the structure of the model can be represented using thermal networks. Notably, resistor-capacitor circuit models serve as exemplary thermal network models [19]. The grey-box modeling approach offers certain advantages over the white-box approach, such as reduced-order models. However, a notable characteristic of grey-box models is that their parameters are lumped, meaning each parameter represents a combination of multiple physical properties. Consequently, the estimation of these parameters must be based on measured data [20].

Hence, the formulation of grey-box models offers a more streamlined and comprehensive approach to modeling BEMS. Notably, previous research, in [21] and [22], focused on parameter estimation for grey-box models in the context of BEMS. The outcomes of these study yielded a model characterized by low parameter dispersion. Consequently, the developed model exhibited good agreement with measured data, displaying small deviations, approximately 0.5-1.5°C for the most case.

To address the inherent uncertainties and mismatches in system dynamics, stochastic approaches prove to be valuable. Stochastic MPC leverages probabilistic descriptions of uncertainties to establish chance constraints. These chance constraints require that state and output constraints are satisfied with a predefined level of probability. By incorporating chance constraints, stochastic MPC enables systematic utilization of stochastic uncertainty characterization, allowing for permissible levels of probabilistic violation of constraints. This approach facilitates the systematic exploration of trade-offs between achieving control objectives and ensuring probabilistic constraint satisfaction in the presence of uncertainty [23]. Stochastic MPC has found wide-ranging applications in various domains, including building climate control [7], [24], power generation and distribution [25], chemical processes [26], [27], and vehicle path planning [28], [29]. These applications highlight the versatility and effectiveness of stochastic approaches in addressing uncertainty-related challenges across diverse fields.

However, the epistemic error, which is the mismatch between the model and reality, is not the sole source of uncertainty. Various other uncertainties exist, including exogenous disturbances such as external temperature variations from the forecast information. In order to address this uncertainty in the forecast, multistage MPC has emerged as a viable solution [30].

In multistage MPC, the uncertainty is captured through a discrete-time scenario tree that incorporates the future evolution of uncertainty. By considering multiple control trajectories over the scenario tree, multistage MPC accounts for the uncertainty in a robust and proactive manner [32], [33]. The effectiveness and performance of the multistage MPC approach have been demonstrated in various industrial applications, highlighting its applicability and value in practice [30], [31], [33], [34].

Hence, this paper proposes a hybrid MPC framework which incorporates both stochastic MPC and multistage MPC approaches to address two distinct sources of uncertainty: the model uncertainty and the uncertain weather forecast information.

This paper aims to implement the proposed hybrid MPC framework, utilizing a grey box model of the building, to effectively control and regulate indoor temperature. By integrating both stochastic MPC and multistage MPC strategies, this framework provides a comprehensive solution to counteract the uncertainties arising from model mismatch and weather forecast discrepancies. The objective is to achieve robust and reliable temperature control inside the building, considering both sources of uncertainty simultaneously.

The paper is organized as follows: Section II provides brief introductions to several key concepts, including MPC, chance-constrained MPC, multistage MPC, and the parameter estimation method for a grey-box model. Section III presents the proposed hybrid MPC approach. In Section IV, the system description, system model, the parameter estimation process, and the formulation of OCPs for the four types of MPC are discussed. Section V covers the simulation setup conditions and presents the corresponding results. Finally, Sections VI and VII offer discussion and conclusion, respectively.

II. PRELIMINARY

In this section, three types of MPC approaches and the parameter estimation technique are briefly described. The description in this section is for general use. More specific use of these approaches for the indoor temperature management

of the building is described later in Section IV-C. The state variable is denoted as x, the control input as u, the exogenous disturbance as w_{E}, and the model uncertainty as w_{M}. The notation $(\cdot)_k^{(j)}$ represents the state, control input, and uncertainty at time sample k and on the j^{th} scenario. The notation $\mathrm{E}[\cdot]$ denotes an expected value. The system matrices are denoted as A and B. The system matrices for model uncertainty and exogenous disturbance are denoted as G_{M} and G_{E}, respectively.

A. MODEL PREDICTIVE CONTROL

MPC, also known as receding-horizon control, is widely employed for advanced control of multi-variable systems with state and control input constraints [3], [4]. Consider a time-invariant linear system in the discrete-time form:

$$x_{k+1} = Ax_k + Bu_k \tag{1}$$

When perfect knowledge of the system is available, MPC involves solving the following OCP at each sampling time k:

$$\begin{aligned}
\underset{}{\text{minimize}} \quad & \sum_{k=0}^{N} J_k && \text{(2a)}\\
\text{subject to} \quad & x_{k+1} = Ax_k + Bu_k && \text{(2b)}\\
& Hx_{k+1} \le h && \text{(2c)}\\
& Du_k \le d && \text{(2d)}\\
& x_0 = \hat{x} && \text{(2e)}
\end{aligned}$$

In OCP (2), N represents the length of the prediction horizon. The system model is written in (2b). The state and control inputs are posed in (2c) and (2d). The matrices H and D correspond to the state and input constraint matrices, respectively, with h and d representing the corresponding constraint values. The initial state is given from measurement or estimation as posed in (2e). In the cost function (2a), J_k is commonly chosen as a regularization cost to drive the state and input to zero:

$$J_k = (x_{k+1}^\top Q_x x_{k+1} + u_k^\top R_u u_k) \tag{3}$$

here, $u := \{u_0, u_1, \ldots, u_N\}$ is a sequence of control inputs, and the matrices $Q_x \ge 0$, and $R_u \ge 0$ are weight matrices.

B. CHANCE-CONSTRAINED MPC

Chance-constrained MPC is a well-known stochastic MPC approach that accounts for uncertainties in system dynamics. While the nominal MPC assumes a deterministic evolution of the state x_k, real systems often exhibit uncertainties in model structure and parameters. To incorporate these uncertainties, the system model (1) is modified as follows:

$$x_{k+1} = Ax_k + Bu_k + G_{\mathrm{M}} w_{\mathrm{M},k} \tag{4}$$

here, the disturbances $w_{\mathrm{M},k}$ is assumed to be sequences of independent and identically distributed variables with known probability distribution p_w. Additionally, it is assumed that $\mathrm{E}[w_{\mathrm{M},k} \cdot w_{\mathrm{M},k}^\top] = Q_w$.

Chance-constrained MPC leverages the knowledge of the mean and variance of the predicted state to ensure that state constraint violations remain within acceptable bounds. Given the available system information at time k, chance-constrained MPC aims to minimize the expected value of the cost function (3) while considering a stochastic prediction model for the state, input constraints, and state chance constraints [26], [35]. The Chance-constrained OCP can be formulated as follows [23]:

$$\begin{aligned}
\underset{u}{\text{minimize}} \quad & \mathrm{E}\left[\sum_{k=0}^{N} J_k\right] && \text{(5a)}\\
\text{subject to} \quad & x_{k+1} = Ax_k + Bu_k + G_{\mathrm{M}} w_{\mathrm{M},k} && \text{(5b)}\\
& \Pr[H_c x_{k+1} \le h_c] \ge 1 - \beta_j && \text{(5c)}\\
& Du_k \le d && \text{(5d)}\\
& \mathrm{E}[x_0] = \hat{x}, \quad w_k \sim p_w && \text{(5e)}
\end{aligned}$$

In this OCP formulation, (5c) represents the state chance constraints, where the probability of violating constraint h_c is set by a predefined threshold $\beta_j \in (0, 0.5]$. Notably, the inclusion of the stochastic variable $w_{\mathrm{M},k}$ in the model (5b) does not imply using specific realizations or sequences of disturbance values for prediction. Instead, it involves propagating the mean and variance of the stochastic state through the model equations (5b), which are necessary for evaluating the cost function (5a) and chance constraints (5d).

When the model is linear and the uncertainty follows a Gaussian distribution, the stochastic OCP can be transformed into a similar form to the deterministic MPC. The modified OCP takes the following form [36]:

$$\begin{aligned}
\underset{v}{\text{minimize}} \quad & \sum_{k=0}^{N} J_k^{\mathrm{SMPC}} && \text{(6a)}\\
\text{subject to} \quad & z_{k+1} = Az_k + Bv_k && \text{(6b)}\\
& Hz_{k+1} \le \eta_{k+1} && \text{(6c)}\\
& Dv_k \le d && \text{(6d)}\\
& z_0 = \hat{x} && \text{(6e)}
\end{aligned}$$

where J_k^{SMPC} in Equation (6a) is expressed as:

$$J_k^{\mathrm{SMPC}} = (z_{k+1}^\top Q_x z_{k+1} + v_k^\top R_u v_k) \tag{7}$$

here, z and v represent the deterministic term of the state and perturbations to a static feedback law, respectively. They can be expressed as $x_k = z_k + e_k$ and $u_k = K_{\mathrm{p}} e_k + v_k$, where e_k represents the error at time k and K_{p} is the feedback law constant. In (6c), η_{k+1} is defined as $H_j z_{k+1} \le F_{j,k+1}^{-1}(1-\beta)$, where $F_{j,k+1}^{-1}$ is the inverse cumulative density function (CDF). The difference $h_j - \eta_{k+1}$ represents the constraint back-off magnitude, indicating how much the predicted value $H_j z_{k+1}$ needs to back off from the original bound h_c to satisfy the chance constraint (5c). When $w_{\mathrm{M},k}$ is Gaussian, computing η_{k+1} is straightforward. Given $x_k \sim \mathcal{N}(z_k, \Sigma_k)$, the state covariance can be propagated over the prediction horizon as $\Sigma_{k+1} = A\Sigma_k A^\top + GQ_w G^\top$ for $k = 0, 1, \ldots, N-1$.

Consequently, the predicted state x_{k+1} and error e_{k+1} follow Gaussian distributions $x_{k+1} \sim \mathcal{N}(z_{k+1}, \Sigma_{k+1})$ and $e_{k+1} \sim \mathcal{N}(0, \Sigma_{k+1})$, respectively. Since $He - h$ is a linear transformation of the Gaussian random variable e, the CDFs $F_{j,k+1}$ and their inverses can be computed from the probability distribution function of $He_{k+1} - h$. For further details, refer to [36].

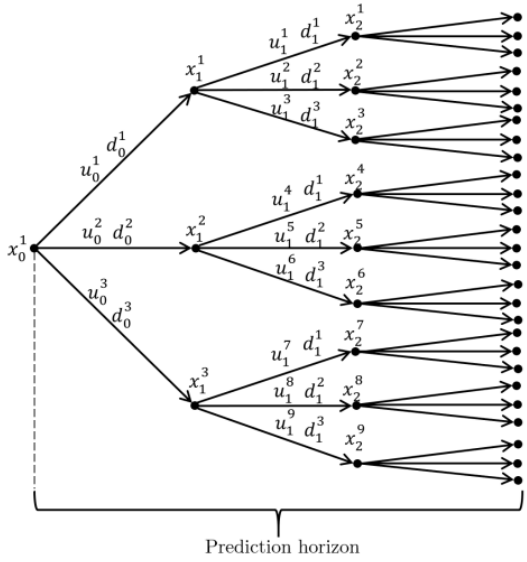

FIGURE 1. The structure of the scenario tree [33].

C. MULTISTAGE MPC

Multistage MPC employs a form of scenario tree, as shown in Figure 1, to describe the uncertainty. The control inputs are optimized to counteract uncertainties in the tree. When implementing multistage MPC, all control inputs branching at the same node must be equal. These equal control inputs are imposed by non-anticipativity constraints [33].

The time-invariant linear system model with exogenous disturbance can be written as:

$$x_{k+1} = Ax_k + Bu_k + G_{\mathrm{E}} w_{\mathrm{E},k} \tag{8}$$

The OCP of multistage MPC can be formulated as follows:

$$\underset{u}{\text{minimize}} \sum_{j=1}^{S} \omega_j \sum_{k=0}^{N} J_k^j \tag{9a}$$

$$\text{subject to} \quad x_{k+1}^j = Ax_k^{p(j)} + Bu_k^j + G_{\mathrm{E}} w_{\mathrm{E},k}^{r(j)} \tag{9b}$$

$$Hx_{k+1}^j \leq h \tag{9c}$$

$$Du_k^j \leq d \tag{9d}$$

$$u_k^j = u_k^l, \quad \text{if} \quad x_k^{p(j)} = x_k^{p(l)} \tag{9e}$$

$$x_0^j = \hat{x} \tag{9f}$$

In this formulation, ω_j represents the weight or importance of the j^{th} scenario. The system model is given in (9b). Here, $x_k^{p(j)}$ means the parent node state where the scenario is branching out, and $w_{\mathrm{E},k}^{r(j)}$ is the realization of the uncertainty scenarios on current time. The state and the control bounds are posed in (9c) and (9d), respectively. The non-anticipativity constraint is given in (9e). Here, j and l denote different scenarios. The initial condition is set in (9f).

In multistage MPC, the size of the optimization problem can grow exponentially with the length of the prediction horizon, the number of uncertainties, and the number of branches from each parent node. To address this challenge, a technique called robust horizon is often employed, which limits the branching of scenarios up to a certain stage while assuming the later uncertainties to be constant. This approach provides a compromise between handling uncertainties and computational efficiency [33].

D. GREY-BOX MODEL AND PARAMETER ESTIMATION

The process of parameter identification through numerical optimization has been extensively studied in the literatures [2], [18], [37]. Optimization algorithms are commonly employed to minimize an objective function, which in the context of parameter estimation, typically represents the discrepancy between model predictions and reference data. The objective function is based on the simulation error computed over the entire calibration period, as opposed to the traditional one-step-ahead prediction errors commonly used in statistical approaches [12], [38]. This approach can be seen as a least squares curve fitting procedure. Consequently, the objective function is defined as the mean square error (MSE) between simulated and measured states over the entire dataset. The chosen error function is a standard quadratic norm [39], expressed as:

$$J = \sum_{i=1}^{N} \sum_{k=1}^{n_x} e_k^2 = \sum_{i=1}^{N} \sum_{k=1}^{n_x} (x_k^i - x_k^{i,ref})^2 \tag{10}$$

where n_x denotes the number of states and N is the number of samples in the dataset. The sum of squared errors for each temperature state is accumulated, with equal weighting assigned to all states. Alternatively, it is possible to assign weights based on the uncertainties associated with the measurements, such as the covariance of the measurements, as commonly practiced in statistical approaches to parameter estimation [38].

III. HYBRID MPC

The hybrid MPC approach is developed to address two sources of uncertainties separately: model mismatch and exogenous disturbance. The model mismatch is quantified during the validation step by comparing the model predictions with experimental data, allowing for the characterization of deviations in probabilistic terms. On the other hand, exogenous information is incorporated into the control framework through a scenario tree, which can be constructed based on expert opinions or provided prediction information. The model mismatch is handled using a chance-constrained

framework, which relaxes the associated state constraints by specifying an acceptable level of constraint violation. The scenario tree, on the other hand, is integrated into the optimization problem using the multistage MPC framework to counteract the influence of the exogenous disturbance. By combining these two frameworks, the following OCP for the hybrid MPC is formulated:

$$\underset{u}{\text{minimize}} \quad \sum_{j=1}^{S} \omega_j \mathrm{E}\left[\sum_{k=0}^{N} J_k\right] \tag{11a}$$

$$\text{subject to} \quad x_{k+1}^{j} = A x_k^{p(j)} + B u_k^{j} + G w_k^{r(j)} \tag{11b}$$

$$\Pr[H_c x_{k+1}^{j} \le h_c] \ge 1 - \beta_j \tag{11c}$$

$$D u_k^{j} \le d \tag{11d}$$

$$u_k^{j} = u_k^{l} \quad \text{if} \quad x_k^{p(j)} = x_k^{p(l)} \tag{11e}$$

$$\mathrm{E}[x_0^{j}] = \hat{x}, \quad wk \sim p_w \tag{11f}$$

In this formulation, the system dynamics are captured by the state equation (11b), where $Gw_k^{r(j)}$ describes the uncertainty at time step k on j^{th} scenario as $Gw_k^{r(j)} = G_{\mathrm{M}} w_{\mathrm{M},k}^{r(j)} + G_{\mathrm{E}} w_{\mathrm{E},k}^{r(j)}$. The chance constraint (11c) ensures that the state satisfies the hard constraint $H_c xk + 1^j \le h_c$ with a probability of at least $1 - \beta_j$. The control bounds are given by (11d). The non-anticipativity constraint (11e) ensures that the control inputs are equal if the corresponding states are equal. The initial state is specified by (11f), where $\hat{x}$ represents the measured or estimated initial state and $w_{\mathrm{M},k}$ is a random variable following the distribution p_w. The objective is to minimize the expected cost over the entire scenario $\sum_{j=1}^{S} \omega_j \mathrm{E}\left[\sum_{i=0}^{N} J_k\right]$ by selecting appropriate control inputs u_k^{j}.

Overall, the hybrid MPC approach counteracts both model mismatch and exogenous disturbance effectively, providing an ability to handle uncertainties in real-world systems.

If the model uncertainty is expressed in the form of a Gaussian distribution and the model is linear, the OCP for hybrid MPC can be written as:

$$\underset{u}{\text{minimize}} \quad \sum_{j=1}^{S} \omega_j \sum_{k=0}^{N} J_k^{j,\mathrm{SMPC}} \tag{12a}$$

$$\text{subject to} \quad z_{k+1}^{j} = A z_k^{j} + B v_k^{j} + G w_k^{r(j)} \tag{12b}$$

$$H z_{k+1}^{j} \le \eta_{k+1} \tag{12c}$$

$$D v_k^{j} \le d \tag{12d}$$

$$v_k^{j} = v_k^{l} \quad \text{if} \quad z_k^{p(j)} = z_k^{p(l)} \tag{12e}$$

$$z_0^{j} = \hat{x} \tag{12f}$$

IV. SYSTEM DESCRIPTION

The building in this study is an experimental setup constructed in 2014 at the Porsgrunn campus of the University of South-eastern Norway [40]. The exterior and floor plan of the test building is depicted in Figure 2. The building is designed with concrete support structures, ensuring that it remains detached from the ground. The internal volume of the building is approximately 9.4 m^3, and it is sealed without both natural and mechanical ventilation systems. To limit solar irradiation, three small windows measuring 60×90 cm^2 are positioned in the south, east, and west directions, while a 90×120 cm^2 door is located in the north direction. Additionally, the presence of three surrounding buildings further restricts the amount of solar radiation entering through the windows.

The building envelope is constructed using a combination of different materials, including wooden cladding, glass wool, air-fill, polyethylene vapor barriers, wood, cement chipboard, particleboard, and cardboard. Each type of wall exhibits a unique construction, resulting from the combination of these materials. Similarly, the roof and floor of the building have distinct compositions.

The experimental building features an electrical heater with a power rating of 375 W, comprising a thermostat controller, a measurement system, and a logging computer consuming approximately 100 W. The measurement system incorporates various sensors to monitor parameters such as indoor and outdoor temperatures and humidity, air pressures, rainfall, wind speed, wind direction, and total power usage.

Overall, the experimental building serves as a controlled environment for studying and analyzing the thermal dynamics and energy performance of buildings under different operating conditions.

A. SYSTEM MODEL

The chosen system model in this study offers a simplified representation of the experimental building, serving as the source of calibration data. Illustrated in Figure 3, the model is founded on the R3C2 model employed in a previous study [2]. Notably, the ventilation resistance component is omitted from this model due to the absence of a ventilation system in the test building.

The model encompasses two state variables: T_{b}, representing the interior temperature of the building, and T_{w}, signifying the temperature of the wall's inner surface. The control input, denoted as $\dot{Q}$, accounts for the heat flow source (e.g., an electric heater). Two sources of uncertainty are inherent in this model. Firstly, model uncertainty, characterized by w_{b} and w_{w}, arises from the stochastic mismatch between model predictions and actual observations. The model mismatch can occur due to various factors such as wind, sunlight and so on. Secondly, external temperature variations and weather forecast scenarios are denoted as T_{∞}.

To capture the building's thermal properties, capacitors C_{b} and C_{w} are integrated into the model, representing thermal energy storage capacities within the interior and the building envelope (comprising walls, floor, and ceiling). Furthermore, the model incorporates three resistance components: R_{b}, symbolizing the thermal resistance between the building interior and the wall; R_{w}, representing the resistance to heat flow through the wall, connecting state T_{w} with the outside temperature; and R_{g}, characterizing heat flow resistance through

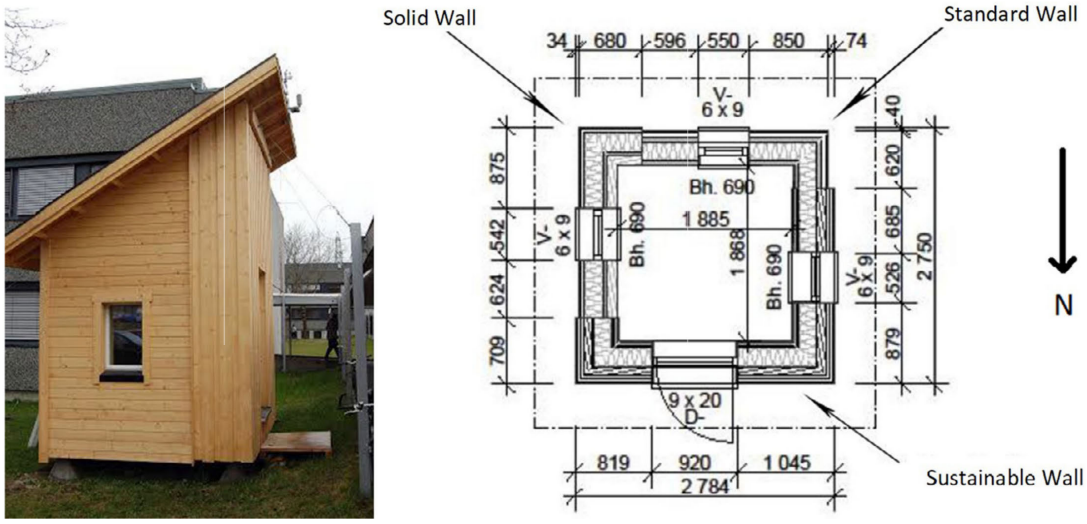

FIGURE 2. The picture of the experimental facility in USN [40].

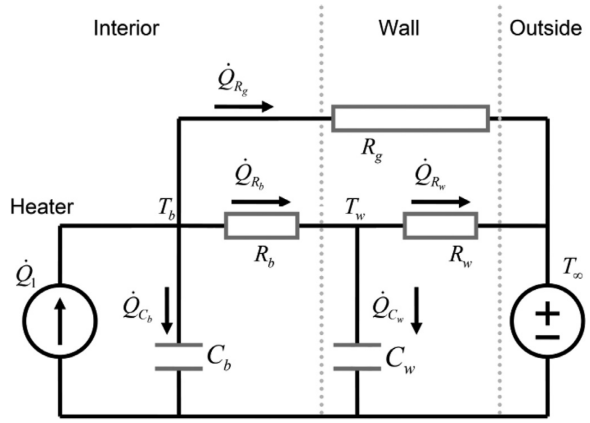

FIGURE 3. RC circuit model of the building [22].

unaccounted components of the building envelope, such as windows and doors.

To derive equations from this thermal network model, Kirchhoff's node potential law is employed. In this approach, each state (T_b and T_w) is assigned to a circuit node, ensuring a balanced flow into and out of each node. Consequently, the stochastic model can be expressed as a set of following ordinary differential equations (ODEs): [21], [22], [39].

$$\frac{dT_b}{dt} = -\left(\frac{1}{C_\mathrm{b}R_\mathrm{b}} + \frac{1}{C_\mathrm{b}R_\mathrm{g}}\right)T_b + \left(\frac{1}{C_\mathrm{b}R_\mathrm{b}}\right)T_w + \left(\frac{1}{C_\mathrm{b}}\right)\dot{Q} + \left(\frac{1}{C_\mathrm{b}R_\mathrm{g}}\right)T_\infty + w_\mathrm{b} \tag{13}$$

$$\frac{dT_w}{dt} = \left(\frac{1}{C_\mathrm{w}R_\mathrm{b}}\right)T_b - \left(\frac{1}{C_\mathrm{w}R_\mathrm{w}}\right)T_w + \left(\frac{1}{C_\mathrm{w}R_\mathrm{w}}\right)T_\infty + w_\mathrm{w} \tag{14}$$

In the context of this analysis, an assumption emerges regarding the determinism of the model under specific conditions. Specifically, assuming constant and unchanging model uncertainties, denoted as w_b and w_w, and further presuming perfect knowledge and precision in the external temperature variable T_∞ as applied in equations (13) and (14), the model takes on a deterministic form.

The deterministic model operates without the presence of randomness or variability associated with the model uncertainties and external temperature fluctuations. This simplification enables a more predictable and precise analysis, which can be advantageous when these assumptions align with the specific research or practical context in question. However, it is crucial to acknowledge that the deterministic model relies on these stringent assumptions and may not fully capture the real-world complexities inherent in many practical scenarios.

B. PARAMETER ESTIMATION

The parameter estimation in this building is previously done in [21] and [22]. The process of parameter estimation involves determining the values of model parameters based on experimental data. In this case study, a nominal parameter vector is employed as an initial approximation for the estimation methods. These nominal values are obtained through trial and error experiments and prior knowledge of the expected parameter range. The physical insight required for these initial approximations is limited to the approximate order of magnitude of the parameters, which can typically be obtained for most practical buildings. The nominal values themselves do not necessarily yield an accurate prediction model for the building, but they serve as normalization constants, allowing parameter estimation to be performed on a unit scale. Moreover, they restrict the search space to a region of interest where reasonable parameter values can be obtained [21], [22].

Table 1 presents a set of nominal parameters obtained through experimental measurements. These values are used as initial guesses for model calibration, and the corresponding minimum and maximum limits define the constrained parameter space [10].

The noise covariance matrix $W = \mathrm{diag}(w_b^2, w_w^2)$ are estimated from the data and assumed to be diagonal. The parameter vector is defined as follows:

$$\theta = [R_g, R_b, R_w, C_b, C_w, w_b, w_w] \tag{15}$$

TABLE 1. Nominal parameter values and min./max. range.

	R_g[K/W]	R_b[K/W]	R_w[K/W]	C_b[J/W]	C_w[J/W]
Nominal value (θ_0)	0.160	0.060	0.100	1200k	1200k
Min value ($\theta_{\min}$)	0.048	0.018	0.03	360k	360k
Max value ($\theta_{\min}$)	0.272	0.102	0.170	2040k	2040k

To prevent over-parameterization, one degree of freedom is removed by fixing the value of R_g to a constant. R_g represents the thermal resistance of windows and doors, which are exposed to both interior and exterior temperatures, and their UA values are specified in [10]. The UA values are calculated as the product of U (the reciprocal of thermal resistance per area) and A (the area). Therefore, knowing R or U for all windows and doors, as well as their areas A, allows for the computation of $R_g = 1/(U_g A_g)$. The specifications for U and A are presented in Table 2, and the value of R_g is set to 0.24 [10], [22].

TABLE 2. Specification of R_g.

	U[W/m^{2}K]	A[m^2]	UA [W/K]	R [K/W]
Door	1.2	1.76	2.1	0.48
Windows	1.3	1.57	2.0	0.50
Total	-	-	4.1	0.24

Using the R3C2 model from Fig. 3, a prior distribution is assigned to the parameter R_g as $\mathcal{N}(0.24, 0.01^2)$, while all other parameters have uniform priors $p(\theta) = 1$. These distributions are employed in optimization calculations with optimization equation (10) [21].

TABLE 3. Values and standard deviations of estimated parameters.

	$\hat{\theta}$	$\sigma/\hat{\theta}$
R_g[K/W]	0.236	6.0%
R_b[K/W]	0.072	5.7%
R_w[K/W]	0.084	5.7%
C_b[J/W]	1444k	4.7%
C_w[J/W]	293k	8.8%
w_b	0.149	3.2%
w_w	0.137	3.7%

The posterior distribution of the parameters is estimated using the Markov Chain Monte Carlo (MCMC) method. Three independent sets of data were collected from the experimental building, including temperature measurements T_b, T_w, and T_∞, as well as one measurement of the input electrical power $\dot{Q}$ supplied to an electric heater. The temperatures T_b and T_w serve as reference data for the model outputs, while T_∞ and $\dot{Q}$ act as the model inputs. Two of the data sets are utilized as training data for parameter estimation and analysis, while the remaining data set is used as a test set solely for evaluating the posterior predictive distribution and assessing the calibrated model's ability to predict future system behaviors. The estimated parameters are presented in Table 3, along with their corresponding standard deviations. The standard deviations are normalized with respect to the maximum a posteriori (MAP) estimates of the parameters, enabling a comparison of different parameters [21], [22].

For a more comprehensive analysis of the parameter estimation in this case study, please refer to [21] and [22].

C. OPTIMAL CONTROL PROBLEM

In this section, the OCPs related to the case study of building temperature control is introduced. The state at time sampling k is denoted as $x_k = [T_{b,k}, T_{w,k}]$. u includes both control input, $\dot{Q}$, and exogenous disturbance, T_∞, as $u_k = [\dot{Q}_k, T_{\infty,k}]$. The model mismatch is described in w_k.

1) DETERMINISTIC MPC WITHOUT CONSIDERING UNCERTAINTIES

In this subsection, the OCP for implementing deterministic MPC is introduced, assuming no model mismatch and perfect forecast in outside temperature. The OCP for deterministic MPC is formulated as follows:

$$\begin{aligned}
\text{minimize} \quad & \sum_{k=0}^{N} J_k && \text{(16a)}\\
\text{subject to} \quad & x_{k+1} = Ax_k + Bu_k && \text{(16b)}\\
& 20^\circ\text{C} \le T_{b,k} + Z_k \le 22^\circ\text{C} && \text{(16c)}\\
& 100\text{W} \le \dot{Q}_k \le 475\text{W} && \text{(16d)}\\
& x_0 = \hat{x} && \text{(16e)}
\end{aligned}$$

In Equation (16a), the cost function is defined, while Equation (16b) represents the system model in deterministic form. The model parameters used are specified in Table 3. The bounds for the building's interior temperature ($T_{b,k}$) and the electricity consumption ($\dot{Q}_k$) are given by Equations (16c) and (16d), respectively. Z_k in (16c) is a slack variable. The minimum electricity consumption in the building is set to 100W due to the use of a computer for data logging. Therefore, when 100W is used, the heater is turned off.

The cost function (16a) is designed in a quadratic form as follows:

$$J_k = T_k W_x T_k^\top + \left(\frac{\dot{Q}_k}{\dot{Q}_{\max}}\right) W_u P_k \left(\frac{\dot{Q}_k}{\dot{Q}_{\max}}\right)^\top + Z_k W_v Z_k^\top \tag{17}$$

In Equation (17), the first term, $T_k W_x T_k^\top$, represents the target temperature term. T_k is the difference between the target temperature and the temperature inside the building at

sampling time k, denoted as $T_{\mathrm{b},k}$. The target temperature is set to 22°C in this work. T_k is mathematically expressed as $T_k = T_{\mathrm{b},k} - 22°\mathrm{C}$.

The second term in Equation (17) represents the power consumption term. $\dot{Q}_k$ denotes the power consumption at time sampling k, and $\dot{Q}_k/\dot{Q}_{\max}$ normalizes the energy usage. P_k is the normalized electricity price over the prediction horizon, expressed as the ratio of the electricity price at sampling time k to the mean price over the prediction horizon.

The last term in Equation (17), $Z_k W_v Z_k^\top$, is a penalty term that allows violations of the constraint (16c) when it cannot be satisfied. Z_k is a slack variable and it is decided by solving optimization. It is encouraged to be zero in most cases.

The parameters W_x, W_u, and W_v are weight parameters for the target temperature term, power consumption term, and penalty for constraint violations, respectively. They are assumed to be positive-definite. By adjusting these parameters, the MPC can control the system differently. For example, if W_x is significantly higher than W_u, the MPC will prioritize controlling the heater to maintain the temperature at the target value with maximum effort. In the opposite case, the MPC will minimize the use of the heater as long as the temperature remains within the constraint (16c). W_v must always be kept significantly higher than the other two parameters for the satisfaction of the constraints.

2) HYBRID MPC: COMBINATION OF MULTISTAGE MPC AND CHANCE-CONSTRAINED MPC

There are two types of uncertainties in the system: exogenous disturbances and model uncertainty. Exogenous disturbances represent uncertainties in weather forecast information. Despite the high accuracy of weather forecasts, deviations between the forecast temperature and the actual temperature are inevitable. Model uncertainty arises from the mismatch between the model and reality, as it is nearly impossible to build a model that precisely represents reality. The uncertainty data can be estimated through experiments, and in this study, the mismatch is shown as w_{b} and w_{w} (refer to Table 3).

The uncertainty in weather forecast information can be mitigated using the multistage MPC framework or scenario-based MPC. The OCP of the multistage MPC framework with the robust horizon set as 1 is formulated as follows:

$$\text{minimize} \quad \sum_{j=1}^{S} w_j \sum_{k=0}^{N} J_k^{(j)} \tag{18a}$$

$$\text{subject to} \quad x_{k+1}^{(j)} = A x_k^{(j)} + B u_k^{(j)} \tag{18b}$$

$$20°\mathrm{C} \le T_{\mathrm{b},k}^{(j)} + Z_k^{(j)} \le 22°\mathrm{C} \tag{18c}$$

$$100\mathrm{W} \le \dot{Q}_k^{(j)} \le 475\mathrm{W} \tag{18d}$$

$$x_0^{(j)} = \hat{x} \tag{18e}$$

$$\dot{Q}_0^{(0)} = \dot{Q}_0^{(1)} = \cdots = \dot{Q}_0^{(S)} \tag{18f}$$

However, in multistage MPC, the uncertainty from model mismatch is not considered. This model uncertainty can be addressed by incorporating the chance-constrained MPC framework. To implement chance constraints, the constraint (16c) can be modified in the OCP (16a) as follows:

$$20°C + e_k \le T_{\mathrm{b},k} + Z_k \le 22°C - e_k \tag{19}$$

To implement the hybrid MPC framework which addresses both uncertainty in model and forecast information, the constraint (18c) can be modified in the OCP (18) as follows:

$$20°C + e_k \le T_{\mathrm{b},k}^{(j)} + Z_k^{(j)} \le 22°C - e_k \tag{20}$$

In the newly proposed constraints (19) and (20), e_k represents the constrained back-off obtained from the inverse cumulative distribution function with the propagated covariance throughout the prediction horizon and pre-defined β. Based on the given w_b and w_w in Table 3 and $\beta \in (0, 0.5]$, the constrained back-off e is defined as shown in Figure 4.

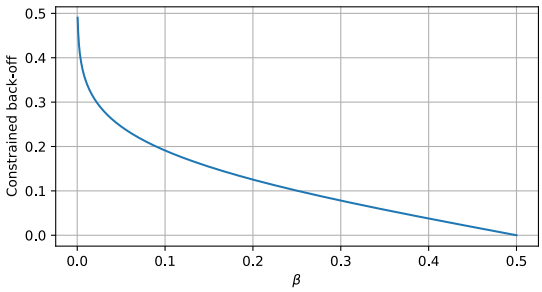

FIGURE 4. The constrained back-off obtained from the inverse CDF for the distribution of $N(0, w_b)$, plotted as a function of the permitted probability of state constraint violation $\beta \in (0, 0.5]$.

V. SIMULATION

A. SIMULATION SETUP

In Norway, the electricity price is determined in advance for the next 24 hours in a deterministic manner and published on the website: **nordpool.no**. Therefore, there is no uncertainty in the electricity price. Figure 5 presents the historical temperature forecast and electricity price.

In simulations, a prediction horizon length is set as 5 hours and a time step is set as 2 minutes. The optimization problem for running MPC is solved using CasADi in Python [41]. In this work, four MPCs are compared, as outlined in Table 4.

TABLE 4. MPCs used in the simulations.

1	Deterministic MPC(D)
2	Multistage MPC(MS)
3	Chance-Constrained MPC(CC)
4	Hybrid MPC(Hybrid)

The simulations are conducted with various sets of weight parameters to demonstrate the effectiveness of each controller. The parameter sets are presented in Table 5 and are selected with trial and error.

To consider the uncertain weather forecast for the implementation of multistage MPC and hybrid MPC, A scenario tree must be built. There are two ways to build a scenario tree. One is to purchase forecast data from third-party companies.

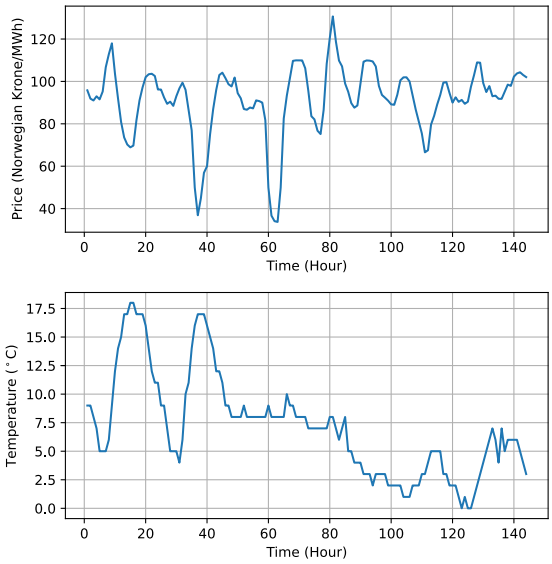

FIGURE 5. Forecast of outside temperature and electricity price.

TABLE 5. Weight parameter sets used in the simulations.

Parameters	A	B	C	D	E
W_x	100	1	0.1	0.05	0.01
W_u	1	1	1	1	1
W_v	10^6	10^6	10^6	10^6	10^6

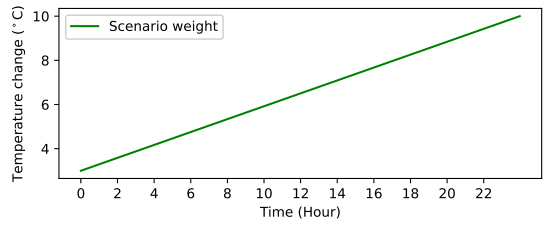

FIGURE 6. The addition and subtraction amounts through the prediction horizon to generate the possible prediction scenarios of the outside temperature.

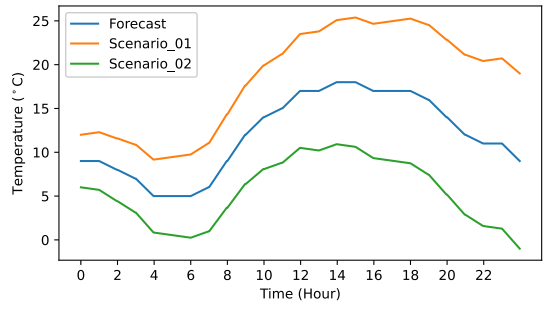

FIGURE 7. The prediction scenario tree of the temperature outside.

The other method is to utilize publicly available weather forecast data and to add or subtract reasonable ranges of temperatures for each time step over the prediction horizon. In this study, the latter method is used in this paper. To generate 2 more possible scenarios from the original forecast data by adding and subtracting the temperature change over the prediction horizon as shown in Figure 6. As a result, three scenario tree of the outside temperature is generated as illustrated in Figure 7 and employed to solve the OCP for multistage MPC.

B. SIMULATION RESULT

This section presents the simulation results through figures comparing and explaining the performance of the four types of MPCs listed in Table 4.

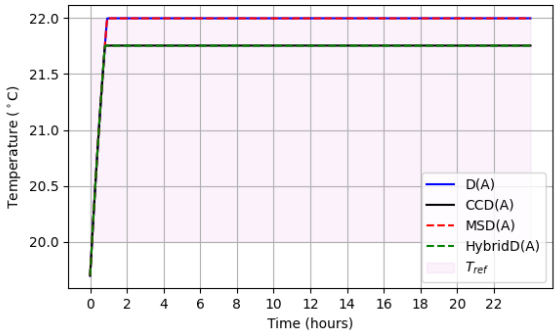

FIGURE 8. Temperature inside of the building (T_b) changes during the simulations of four types of MPCs: Deterministic MPC, Multistage MPC, Chance-constrained MPC, and Hybrid MPC with weight parameters as A in Table. 5, denoted as D(A), MS(A), CC(A), and Hybrid(A) respectively.

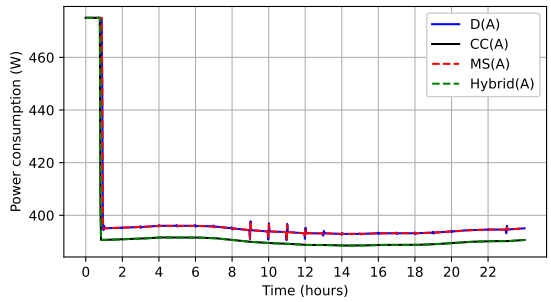

FIGURE 9. Electricity consumption by each type of MPC during the simulation period: Deterministic MPC, Multistage MPC, Chance-constrained MPC, and Hybrid MPC with weight parameters as A in Table. 5, denoted as D(A), MS(A), CC(A), and Hybrid(A) respectively.

Figure 8 and Figure 9 depict the change in the temperature inside the building T_b and the electricity consumption $\dot{Q}$ during the simulations of the Deterministic MPC, Multistage MPC, Chance-Constrained MPC, and Hybrid MPC with weight parameters set as A in Table 5, denoted as **D(A)**, **MS(A)**, **CC(A)**, and **Hybrid(A)**, respectively. Both figures show that all MPCs begin by actively heating the building from the initial temperature until it reaches a certain level. Accordingly, the electricity consumption is at its peak initially and then drops to a certain level to maintain the desired temperature inside the building. **D(A)** and **MS(A)** demonstrate similar performance. **CC(A)** and **Hybrid(A)** exhibit similar performance as well. However, due to the constrained back-off from model uncertainty, **CC(A)** and **Hybrid(A)** show more conservative performance than **D(A)** and **MS(A)**. Also, upon closer inspection in Figure 10, the

differences, between **D(A)** and **MS(A)** or between **CC(A)** and **Hybrid(A)**, become more apparent.

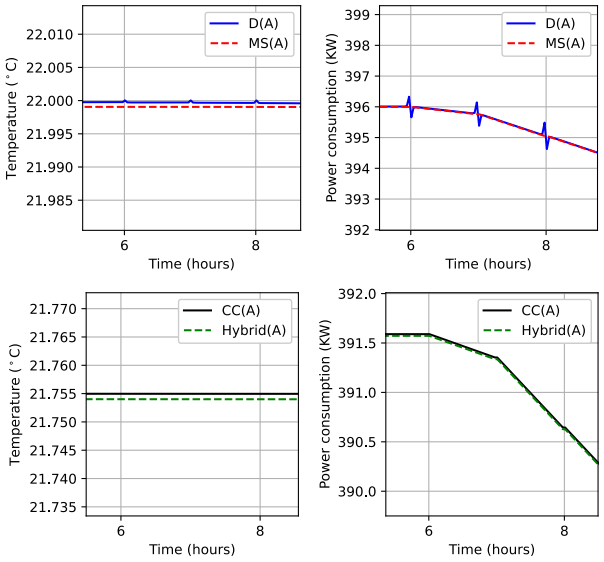

FIGURE 10. Detailed plots of the changes of the temperature inside of the building (T_b) and the electricity consumption in the building between 6 and 8 hours of simulations period: Deterministic MPC(D(A)), Multistage MPC(MS(A)), Chance-constrained MPC(CC(A)), and Hybrid MPC(Hybrid(A)) with weight parameters as A in Table. 5.

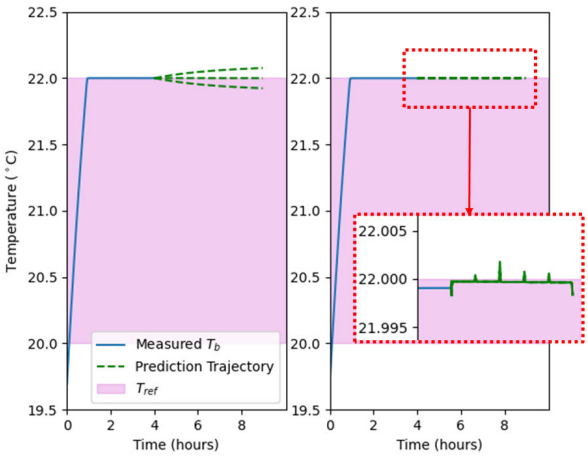

FIGURE 11. Prediction trajectories of T_b with the different realization of the weather forecast scenarios at 4 hours of the simulation period: (Left) Deterministic MPC, (Right) Multistage MPC with weight parameters as A in Table. 5.

Figure 10 provides detailed plots of the temperature changes and electricity consumption between 6 and 8 hours of the simulation period. The **MS(A)** shows a slightly more conservative performance compared to **D(A)**, as it considers the uncertainty of the outside temperature. Similarly, **Hybrid(A)** shows a more conservative performance compared to **CC(A)**. Figure 11 depicts the trajectories of the predicited temperature inside of the building based on three scenarios of the external temperature and control sequences from solving the OCPs during the middle of the simulation. The left plot in Figure 11 is simulated by **D(A)**. When the different scenario of the external temperature is realized, it shows the potential of the violation in the constraint. However, **MS(A)**, in the right plot, mitigate the violations. Upon closer inspection, it shows subtle violations, but it is a numerical error from solving the OCP iteratively. Figure 11 demonstrates the role of multistage MPC framework in both **MS(A)** and **Hybrid(A)** with the robustness of the satisfaction of the constraint against the influence of the uncertainty in the weather forecast information.

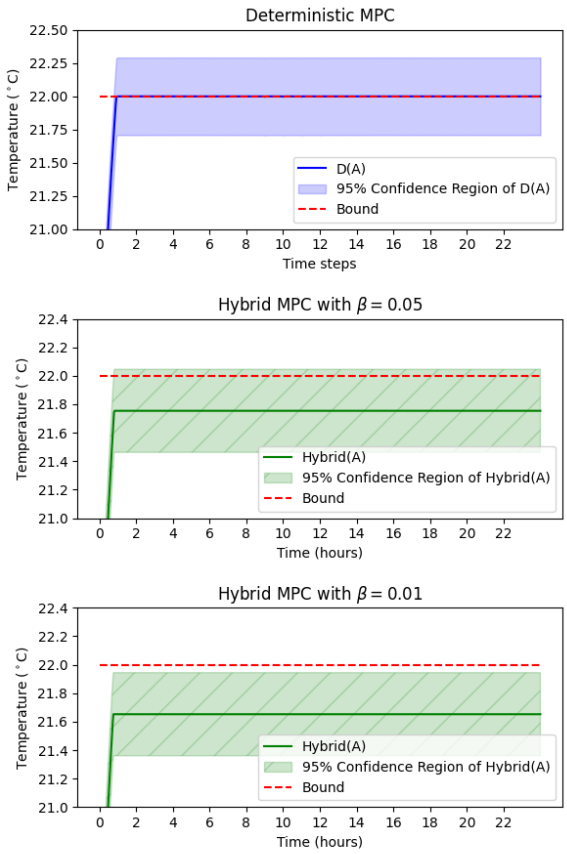

FIGURE 12. Comparison between the 95% confidence regions of Determisitic MPC(D), Hybrid MPC with $\beta = 0.05$, and Hybrid MPC with $\beta = 0.01$. The weight parameters of both MPCs are set as A in Table. 5.

Figure 12 presents a comparison of the 95% confidence regions of the model uncertainty between **D(A)** and **Hybrid(A)** with different values of β. In Figure 12, **D**(A) shows 50% of the 95% confidence region is out of the desired temperature bound. However, in Figure 12, bfHybrid(A) with $\beta = 0.05$ shows some robustness since the constraint is backed-off. When *beta* is set smaller as $\beta = 0.01$, the constraint is more backed off and it shows better robustness in the satisfaction of the constraint.

Table 6 reports the computational time required for solving the optimization problem on each MPC throughout simulations. The Deterministic MPC is the fastest, followed by the Chance-Constrained MPC, the Multistage MPC, and finally, the Hybrid MPC. However, all MPCs demonstrate similar computation times without significant differences in the matter of seconds.

TABLE 6. Computational time [s].

	Mean	Min	Max
Determinic MPC	0.2012	0.1650	0.3944
Multistage MPC	0.2376	0.2040	0.5910
Chance-constrained MPC	0.2185	0.1742	0.4410
Hybrid MPC	0.2637	0.2219	0.5940

By setting the weight parameters differently, the operation can be performed based on a preferred balance between setting the temperature at the set point and considering the electricity price. Figure 13 shows the simulations of the Hybrid MPC over a 5-day period with $\beta = 0.05$ and different sets of weight parameters (B, C, D, and E) from Table 5. As the weight parameter for temperature targeting (W_x) becomes relatively smaller compared to the electricity consumption weight (W_u), the temperature control becomes more influenced by the electricity price. For example, the Hybrid MPC with weight parameter set E (**Hybrid(E)**) displays an increase in temperature at around 40, 60, and 80 hours during the simulation period when the electricity price is relatively lower, as shown in Figure 5.

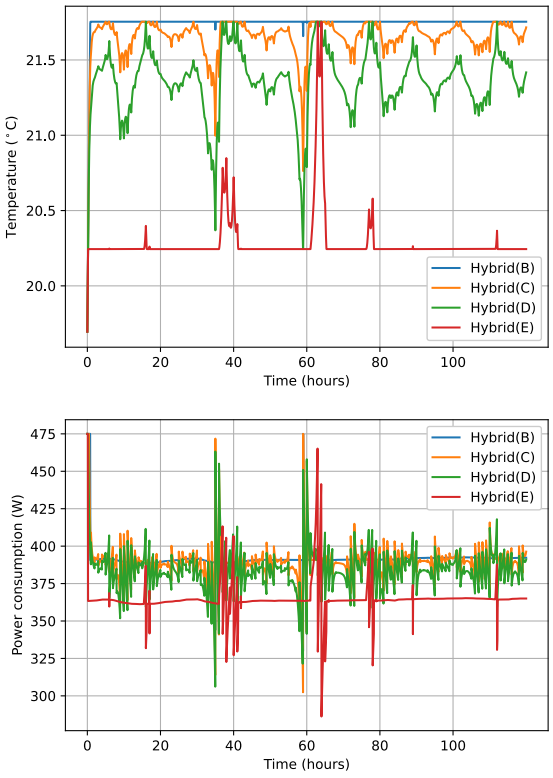

FIGURE 13. Simulations of the Hybrid MPC on the temperature inside of the building (T_b) with $\beta = 0.05$ and different sets of weight parameters: B, C, D, and E in Table.5.

Table.7 shows the total power consumptions and energy costs for the 5 days simulations on hybrid MPCs with different settings as shown in Figure 13. When the weight parameter W_u is relatively larger, less energy is used, and since the objective function (17) reflects the electricity price, it shows even less cost of the energy relatively compared to the reduction of the energy use.

TABLE 7. Power consumption and its cost throughout the 5 days simulations of Hybrid MPCs with different sets of weight parameters: B, C, D, and E in Table.5.

	Power consumption [Wh]	Cost [NOK]
Hybrid(B)	46976.42 (100%)	4.235 (100%)
Hybrid(C)	46777.44 (99.57%)	4.213 (99.46%)
Hybrid(D)	46120.70 (98.17%)	4.148 (97.93%)
Hybrid(E)	43744.33 (93.11%)	3.937 (92.94%)

VI. DISCUSSION

This paper implemented the simulation of various MPCs including the proposed hybrid MPC on a grey-box model of a building system for temperature control. Due to the mismatch between the model and the reality and the uncertainty in weather forecasts, it is not easy to keep the temperature inside the desired range. This may not be a significant concern in a small residential building over short periods, as human may not feel the difference of the temperature by 0.5°C. However, it may become more critical when considering long-term periods or different places such as large public buildings or important laboratories where constraint satisfaction is crucial. The hybrid MPC framework demonstrated a more conservative performance and exhibited higher robustness in satisfying the constraints by considering both uncertainties in the model and the weather forecast.

VII. CONCLUSION

In conclusion, the hybrid MPC, which is the combination of the multistage MPC and chance-constrained MPC frameworks, provides an effective robust approach for temperature control in buildings, particularly in scenarios where constraint satisfaction and robustness are of utmost importance. Further research can explore a method to improve the accuracy of the model by adaptive methods over the running time or additional variations of the hybrid framework and investigate its applicability in different building types and operational contexts.

REFERENCES

[1] IEA. *Buildings*. Paris, France. Accessed: Jun. 24, 2023. [Online]. Available: https://www.iea.org/reports/buildings
[2] T. Berthou, P. Stabat, R. Salvazet, and D. Marchio, "Development and validation of a gray box model to predict thermal behavior of occupied office buildings," *Energy Buildings*, vol. 74, pp. 91–100, May 2014, doi: 10.1016/j.enbuild.2014.01.038.
[3] M. Morari and J. H. Lee, "Model predictive control: Past, present and future," *Comput. Chem. Eng.*, vol. 23, pp. 667–682, Jan. 1999, doi: 10.1016/S0098-1354(98)00301-9.
[4] D. Q. Mayne, J. B. Rawlings, C. V. Rao, and P. O. M. Scokaert, "Constrained model predictive control: Stability and optimality," *Automatica*, vol. 36, no. 6, pp. 789–814, 2000, doi: 10.1016/S0005-1098(99)00214-9.
[5] C. A. Thilker, H. G. Bergsteinsson, P. Bacher, H. Madsen, D. Calì, and R. G. Junker, "Non-linear model predictive control for smart heating of buildings," in *Proc. E3S Web Conf.*, vol. 246, 2021, p. 9005.
[6] C. A. Thilker, H. Madsen, and J. B. Jørgensen, "Advanced forecasting and disturbance modelling for model predictive control of smart energy systems," *Appl. Energy*, vol. 292, Jun. 2021, Art. no. 116889, doi: 10.1016/j.apenergy.2021.116889.

[7] F. Oldewurtel, A. Parisio, C. N. Jones, D. Gyalistras, M. Gwerder, V. Stauch, B. Lehmann, and M. Morari, "Use of model predictive control and weather forecasts for energy efficient building climate control," *Energy Buildings*, vol. 45, pp. 15–27, Feb. 2012, doi: 10.1016/j.enbuild.2011.09.022.

[8] T. Hilliard, L. Swan, and Z. Qin, "Experimental implementation of whole building MPC with zone based thermal comfort adjustments," *Building Environ.*, vol. 125, pp. 326–338, Nov. 2017, doi: 10.1016/j.buildenv.2017.09.003.

[9] S. Prívara, J. Cigler, Z. Váňa, F. Oldewurtel, C. Sagerschnig, and E. Žáčeková, "Building modeling as a crucial part for building predictive control," *Energy Buildings*, vol. 56, pp. 8–22, Jan. 2013, doi: 10.1016/j.enbuild.2012.10.024.

[10] D. W. U. Perera, C. F. Pfeiffer, and N.-O. Skeie, "Modelling the heat dynamics of a residential building unit: Application to Norwegian buildings," *Model., Identificat. Control, Norwegian Res. Bull.*, vol. 35, no. 1, pp. 43–57, 2014, doi: 10.4173/mic.2014.1.4.

[11] L. Ljung, "Prediction error estimation methods," *Circuits, Syst., Signal Process.*, vol. 21, no. 1, pp. 11–21, Jan. 2002, doi: 10.1007/BF01211648.

[12] M. J. Jiménez, H. Madsen, and K. K. Andersen, "Identification of the main thermal characteristics of building components using MATLAB," *Building Environ.*, vol. 43, no. 2, pp. 170–180, Feb. 2008, doi: 10.1016/j.buildenv.2006.10.030.

[13] K. H. Esbensen, D. Guyot, F. Westad, and L. P. Houmller, *Multivariate Data Analysis: In Practice: An Introduction to Multivariate Data Analysis and Experimental Design*, 5th ed. Oslo, Norway: CAMO, 2010, ch. 6, sec. 9, pp. 137–147.

[14] D. W. U. Perera, M. Halstensen, and N.-O. Skeie, "Prediction of space heating energy consumption in cabins based on multivariate regression modelling," *Int. J. Model. Optim.*, vol. 5, no. 6, pp. 385–392, 2015, doi: 10.7763/IJMO.2015.V5.493.

[15] S. F. Fux, A. Ashouri, M. J. Benz, and L. Guzzella, "EKF based self-adaptive thermal model for a passive house," *Energy Buildings*, vol. 68, pp. 811–817, Jan. 2014, doi: 10.1016/j.enbuild.2012.06.016.

[16] A. Afram and F. Janabi-Sharifi, "Gray-box modeling and validation of residential HVAC system for control system design," *Appl. Energy*, vol. 137, pp. 134–150, Jan. 2015, doi: 10.1016/j.apenergy.2014.10.026.

[17] G. Reynders, J. Diriken, and D. Saelens, "Quality of grey-box models and identified parameters as function of the accuracy of input and observation signals," *Energy Buildings*, vol. 82, pp. 263–274, Oct. 2014, doi: 10.1016/j.enbuild.2014.07.025.

[18] N. R. Kristensen, H. Madsen, and S. B. Jørgensen, "Parameter estimation in stochastic grey-box models," *Automatica*, vol. 40, no. 2, pp. 225–237, Feb. 2004, doi: 10.1016/j.automatica.2003.10.001.

[19] *Thermal Network Modelling Handbook*, NASA, Washington, DC, USA, 1972, ch. 2, pp. 3–68.

[20] M. J. Jiménez, H. Madsen, J. J. Bloem, and B. Dammann, "Estimation of non-linear continuous time models for the heat exchange dynamics of building integrated photovoltaic modules," *Energy Buildings*, vol. 40, no. 2, pp. 157–167, Jan. 2008, doi: 10.1016/j.enbuild.2007.02.026.

[21] O. M. Brastein, A. Ghaderi, C. F. Pfeiffer, and N.-O. Skeie, "Analysing uncertainty in parameter estimation and prediction for grey-box building thermal behaviour models," *Energy Buildings*, vol. 224, Oct. 2020, Art. no. 110236, doi: 10.1016/j.enbuild.2020.110236.

[22] O. M. Brastein, D. W. U. Perera, C. Pfeifer, and N.-O. Skeie, "Parameter estimation for grey-box models of building thermal behaviour," *Energy Buildings*, vol. 169, pp. 58–68, Jun. 2018, doi: 10.1016/j.enbuild.2018.03.057.

[23] A. Mesbah, "Stochastic model predictive control: An overview and perspectives for future research," *IEEE Control Syst. Mag.*, vol. 36, no. 6, pp. 30–44, Dec. 2016, doi: 10.1109/MCS.2016.2602087.

[24] Y. Ma, S. Vichik, and F. Borrelli, "Fast stochastic MPC with optimal risk allocation applied to building control systems," in *Proc. IEEE 51st IEEE Conf. Decis. Control (CDC)*, Maui, HI, USA, Dec. 2012, pp. 7559–7564, doi: 10.1109/CDC.2012.6426251.

[25] M. Cannon, B. Kouvaritakis, and X. Wu, "Probabilistic constrained MPC for multiplicative and additive stochastic uncertainty," *IEEE Trans. Autom. Control*, vol. 54, no. 7, pp. 1626–1632, Jul. 2009, doi: 10.1109/TAC.2009.2017970.

[26] P. Li, M. Wendt, and G. Wozny, "Robust model predictive control under chance constraints," *Comput. Chem. Eng.*, vol. 24, no. 2, pp. 829–834, 2000, doi: 10.1016/S0098-1354(00)00398-7.

[27] I. Jurado, P. Millán, D. Quevedo, and F. R. Rubio, "Stochastic MPC with applications to process control," *Int. J. Control*, vol. 88, pp. 792–800, Apr. 2015, doi: 10.1080/00207179.2014.975845.

[28] L. Blackmore, M. Ono, and B. C. Williams, "Chance-constrained optimal path planning with obstacles," *IEEE Trans. Robot.*, vol. 27, no. 6, pp. 1080–1094, Dec. 2011, doi: 10.1109/TRO.2011.2161160.

[29] A. Gray, Y. Gao, T. Lin, J. K. Hedrick, and F. Borrelli, "Stochastic predictive control for semi-autonomous vehicles with an uncertain driver model," in *Proc. 16th Int. IEEE Conf. Intell. Transp. Syst. (ITSC)*, Hague, The Netherlands, Oct. 2013, pp. 2329–2334, doi: 10.1109/ITSC.2013.6728575.

[30] M. Maiworm, T. Bäthge, and R. Findeisen, "Scenario-based model predictive control: Recursive feasibility and stability," *IFAC-PapersOnLine*, vol. 48, no. 8, pp. 50–56, 2015, doi: 10.1016/j.ifacol.2015.08.156.

[31] C. Jeong, B. Furenes, and R. Sharma, "Multistage model predictive control with simplified scenario ensembles for robust control of hydropower station," *Model., Identificat. Control, Norwegian Res. Bull.*, vol. 44, no. 2, pp. 43–54, 2023, doi: 10.4173/mic.2023.2.1.

[32] P. O. M. Scokaert and D. Q. Mayne, "Min-max feedback model predictive control for constrained linear systems," *IEEE Trans. Autom. Control*, vol. 43, no. 8, pp. 1136–1142, Aug. 1998, doi: 10.1109/9.704989.

[33] S. Lucia, T. Finkler, and S. Engell, "Multi-stage nonlinear model predictive control applied to a semi-batch polymerization reactor under uncertainty," *J. Process Control*, vol. 23, no. 9, pp. 1306–1319, Oct. 2013, doi: 10.1016/j.jprocont.2013.08.008.

[34] E. Klintberg, J. Dahl, J. Fredriksson, and S. Gros, "An improved dual Newton strategy for scenario-tree MPC," in *Proc. IEEE 55th Conf. Decis. Control (CDC)*, Las Vegas, NV, USA, Dec. 2016, pp. 3675–3681, doi: 10.1109/CDC.2016.7798822.

[35] A. T. Schwarm and M. Nikolaou, "Chance-constrained model predictive control," *AIChE J.*, vol. 45, no. 8, pp. 1743–1752, Aug. 1999, doi: 10.1002/aic.690450811.

[36] T. A. N. Heirung, J. A. Paulson, J. O'Leary, and A. Mesbah, "Stochastic model predictive control—How does it work?" *Comput. Chem. Eng.*, vol. 114, pp. 158–170, Jun. 2018, doi: 10.1016/j.compchemeng.2017.10.026.

[37] M. J. D. Powell, "A direct search optimization method that models the objective and constraint functions by linear interpolation," in *Advances in Optimization and Numerical Analysis*, vol. 275, 1994, pp. 51–67, doi: 10.1007/978-94-015-8330-5_4.

[38] P. Bacher and H. Madsen, "Identifying suitable models for the heat dynamics of buildings," *Energy Buildings*, vol. 43, no. 7, pp. 1511–1522, Jul. 2011, doi: 10.1016/j.enbuild.2011.02.005.

[39] A. Simpkins, "System identification: Theory for the user, 2nd edition (Ljung, L.; 1999) [on the shelf]," *IEEE Robot. Autom. Mag.*, vol. 19, no. 2, pp. 95–96, Jun. 2012, doi: 10.1109/MRA.2012.2192817.

[40] D. Perera and N.-O. Skeie, "Estimation of the heating time of small-scale buildings using dynamic models," *Buildings*, vol. 6, no. 1, p. 10, Mar. 2016, doi: 10.3390/buildings6010010.

[41] J. A. E. Andersson, J. Gillis, G. Horn, J. B. Rawlings, and M. Diehl, "CasADi: A software framework for nonlinear optimization and optimal control," *Math. Program. Comput.*, vol. 11, no. 1, pp. 1–36, Mar. 2019, doi: 10.1007/s12532-018-0139-4.

CHANGHUN JEONG received the B.S. degree in chemical engineering from the University of Ulsan, South Korea, in 2016, and the M.S. degree in chemical engineering from the Norwegian University of Science and Technology, Norway, in 2020. He is currently pursuing the Ph.D. degree with the University of South-Eastern Norway. His research interests include the applications of the model predictive control on hydropower systems and HVAC systems under the presence of uncertainties.

OLE MAGNUS BRASTEIN received the M.Sc. degree in systems and control engineering and the Ph.D. degree in parameter estimation and machine learning from the University of South-Eastern Norway, in 2016 and 2020, respectively. Industrial research and development background, since 2004, in a wide range of projects, from hardware/instrumentation, to software engineering, and embedded systems. His research interests include software design and development, machine learning, artificial intelligence, estimation algorithms, and creative research and development process.

NILS-OLAV SKEIE received the M.Sc. degree in computer architecture, computer network, and instrumentation and the Ph.D. degree in soft sensors for level estimation from the Norwegian University of Science and Technology, in 1985 and 2008, respectively. With abundant industrial experience, he has been a Professor, since 2006, with the University of South-Eastern Norway (Previously, Telemark University College). His research interests include machine learning, data-driven models, soft sensors, empirical models, digitalization, software engineering, smart buildings, building energy management systems (BEMS), building automation systems (BAS), welfare technology, systems design, level measurement systems, instrumentation technologies, measurement systems (DAQ), process control systems (SCADA/IT/OT), industry 4.0, and smart production.

ROSHAN SHARMA received the Ph.D. degree in process, energy, and automation from the Telemark University College, in 2014. He is currently an Associate Professor with the University of South-Eastern Norway, Norway. He has been a researcher within the energy-related industries, since 2011. His research interests include model-based advanced control, process optimization, and state and parameter estimation.

Model Predictive Control for Energy Systems under Uncertainty
Changhun Jeong

Doctoral dissertations at the University of South-Eastern Norway no. 201

ISBN 978-82-7206-872-0 (print)
ISBN 978-82-7206-873-7 (online)

usn.no